# Structural studies of the corneal stroma with focus on the elastic fibre network in health and disease

Thesis submitted to Cardiff University for the degree of Doctor of Philosophy

November 2016


**Tomas L. White**

Structural Biophysics Research Group

School of Optometry and Vision Sciences

Cardiff University

Supervisors:

Prof. Keith Meek

Dr Philip Lewis

Prof. C. Peter Winlove

# Abstract

The optical and biomechanical properties of the cornea are largely governed by the collagen-rich stroma, a layer that represents approximately 90% of the total thickness. It has been postulated that a novel corneal layer exists in the posterior stroma, immediately above Descemet's membrane, termed 'pre-Descemet's layer'. The main aim of this thesis was to determine if this region has different structural properties to the overlying stroma. A second aim was to examine the elastic fibre distribution throughout the depth of the stroma in healthy and diseased corneas, with focus on pre-Descemet's layer. Techniques used include serial block face scanning electron microscopy, transmission electron microscopy, and X-ray diffraction, amongst various other imaging techniques.

Depth analysis revealed that centre-to-centre interfibrillar spacing was significantly lower in the first ~10μm of stroma distal to Descemet's membrane compared to overlying regions in central cornea. Three-dimensional analysis revealed the presence of long elastic fibres running throughout the stroma, parallel to the surface of the cornea, which were concentrated in pre-Descemet's layer. This elastic material seemed to originate from the limbus as fenestrated sheets before travelling radially into the cornea as small fibres. This data provides evidence for pre-Descemet's layer containing altered biomechanical properties that may contribute to the formation of a variable cleavage plane observed during pneumodissection. Additionally, the elastic fibre network is likely to play an important role in the deformation and recovery of the cornea. Furthermore, the presence of elastic fibres in foetal cornea suggests a potential role in development.

The distribution of elastic fibres was very different in keratoconic buttons. No fibres were located above Descemet's membrane, whereas the elastic fibres appeared concentrated below the epithelium in thinned coned regions, potentially as a biomechanical response to prevent rupture.

Attempts were made to elucidate a functional role for elastic fibres by studying the corneas from a mouse model for Marfan syndrome, where there was a ~50% reduction in elastic fibre quantity. These corneas were significantly thinner and flatter than wild types suggesting that elastic fibres play a role in maintaining the shape of the cornea.

Overall, this thesis has characterised pre-Descemet's layer, demonstrating that structural differences are present. It is likely that the network of elastic fibres described in this thesis play a multi-functional role in the cornea.

# Acknowledgements

First and foremost, I would like to thank my supervisors Professor Keith Meek and Dr Phil Lewis for their continuous support and encouragement throughout the 3 years of my PhD. Keith's enthusiasm and passion for the corneal research field has been inspiring, and has given me further motivation to achieve my targets. Due to Phil's patience, expertise, and willingness to help at all times, I have become confident in performing advanced electron microscopy techniques, which have been used to obtain important results throughout this thesis.

I would also like to thank Dr Sally Hayes for her help and support with all aspects of X-ray diffraction work carried out in this thesis.

Thank you to our collaborators, Professor Shigeru Kinoshita, for providing the keratoconus tissue, and Professor Lygia Pereira, for providing the mouse eyes.

Thank you to the MRC for funding this work.

Finally, I would like to thank all members of the Structural Biophysics Research Group, past and present, for making it a positive and friendly atmosphere to work in.

# List of publications

Lewis PN*****, **White TL***, Young RD, Bell JS, Winlove CP, Meek KM (2016). Three- dimensional arrangement of elastic fibres in the human corneal stroma. *Experimental Eye Research* 146 pp. 43-53.

***equal contribution**

Hayes S, Lewis P, Mirazul Islam M, Doutch J, Sorenson T, **White T**, Griffith M, Meek KM (2015). The structural and optical properties of type III human collagen biosynthetic corneal substitutes. *Acta Biomaterialia* 25 pp. 121-130.

# Table of contents

# List of figures

# Chapter 1 - Introduction

## 1.1 Corneal structure and function

### *1.1.1 Introduction*

The cornea is the outermost layer of the eye that covers the iris, pupil, and anterior chamber. It is a transparent tissue that plays a critically important role in the normal functioning of the eye. Although it appears to lack substance, the cornea is a complex structure where the precise organisation of components is responsible for the crucial part it plays in vision. Like many other tissues, the primary component of the cornea is collagen; however, as well as providing the tissue with mechanical strength, the highly organized arrangement of collagen in the cornea , along with the avascular nature of the tissue, enables light to pass through with minimal scattering, making this unique tissue transparent. The presence of any blood vessels would greatly affect the transparency of the tissue by scattering the light that is passing through, and ultimately reducing the clarity of our vision. Due to the lack of blood supply, the cornea receives nutrients via diffusion from tears and aqueous humour. The intricate structure results in the cornea acting as a structural barrier that protects the eye and prevents pathogens from entering. Additionally, the cornea acts as the eye's outermost lens by refracting the light that enters, and therefore, contributes to approximately two thirds (45 diopters out of the total 60 diopters of unaccommodated ocular power) of the eyes focusing power (Ruberti *et al.*, 2011a) Finally, the cornea protects the lens and retina by filtering out dangerous wavelengths of light, such as ultraviolet.

### *1.1.2. Corneal anatomy*

The cornea is curved centrally, and becomes more flattened at the periphery where it merges with the sclera, making the shape aspheric. At this point, where the cornea reverses its curvature and merges with the sclera, it is termed the limbus. The average horizontal diameter of the cornea is ~11.71mm in normal healthy humans (Rufer *et al.*, 2005). Thickness varies; the central corneal thickness is around 520µm, whereas the peripheral

regions are thicker and may reach 650µm (Ruberti *et al.*, 2011b, Ehlers *et al.*, 2010). The cornea is the first point of contact as light enters the eye; from here it is refracted through the pupil onto the lens that is situated behind. A combination of the lens and cornea are responsible for ensuring that light is focused onto the retina, which subsequently translates the light into impulses that are sent to the brain through the optic nerve. There are currently five distinct layers of the cornea that are arranged from anterior to posterior as follows: the epithelium, Bowman's layer, stroma, Descemet's membrane, and the endothelium. Figure 1.1 shows the structure of the human eye, along with the five layers of the cornea. Each of these layers will now be reviewed individually in the following sections.

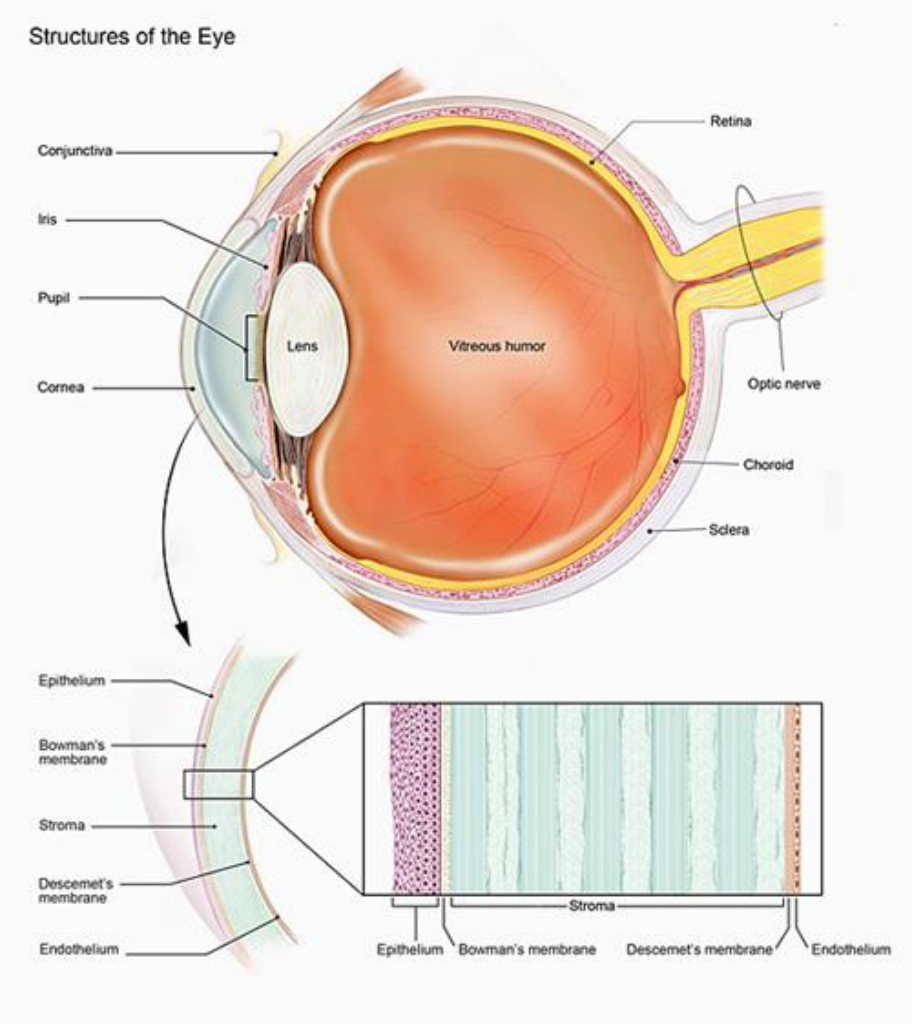


**Figure 1.1. Structure of the eye**. The top image shows the gross anatomy of the eye including all the main structures. Underneath, the magnified image shows the 5 layers of the cornea in order to portray their locations and thickness relative to one another. Taken from (Farjo *et al.*, 2008).

*1.1.3 Epithelium*

In the cornea, the stratified, non-keratinizing squamous epithelium consists of 5-7 layers of cells that combined, measure approximately 36-55µm (Ehlers *et al.*, 2010, Schmoll *et al.*, 2012, Tao *et al.*, 2011). The corneal epithelium plays an important protective role by continuously shedding cells, and preventing pathogens and other harmful matter from reaching the immunological deficient underlying stroma. The lifespan of these cells is around 7-10 days, resulting in a complete turnover of the corneal epithelium layer every week (Delmonte and Kim, 2011). Tight junctional complexes exist between the cells that prevents tears from entering intercellular spaces. The first 2-3 cell layers of the epithelium are superficial cells, which have extensive microvilli apical membrane projections that increase the contact surface area between the overlying tear film and the cell membranes of each individual epithelial cell. Beneath the superficial cells, there are 2-3 layers of wing cells that slightly differ in shape, being less flat than the overlying cells. Basal cells are a single layer of columnar cells that are present beneath the wing cells, and they are the source of both wing and superficial cells, due to their ability to undergo mitosis (Delmonte and Kim, 2011). All three cells layers are shown in Figure 1.2. The three cell types of the epithelium are separated from the stroma by the basement membrane (Fig. 1.3), which is approximately 0.05µm thick and consists of type IV collagen, as well as laminin, both of which are secreted by basal cells. Additionally, the basement membrane contains type VII collagen, which is the primary structural element in anchoring fibrils (Sakai *et al.,* 1986a). Corneal epithelium is firmly attached to the underlying layers due to the presence of adhesion complexes called hemidesmosomes that connect the basal cells to the basement membrane.

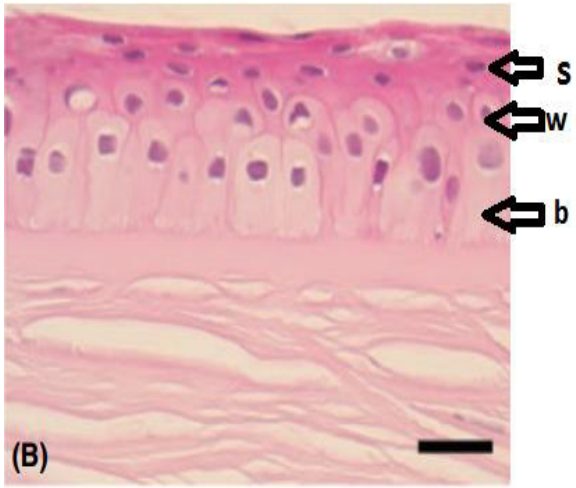


**Figure 1.2. Corneal epithelium stained with haematoxylin-eosin.** The image portrays the three layers of different cell type in the corneal epithelium. From anterior to posterior, these are superficial cells (s), wing cells (w), and basal cells (b). Adapted from (Ehlers *et al.*, 2010).

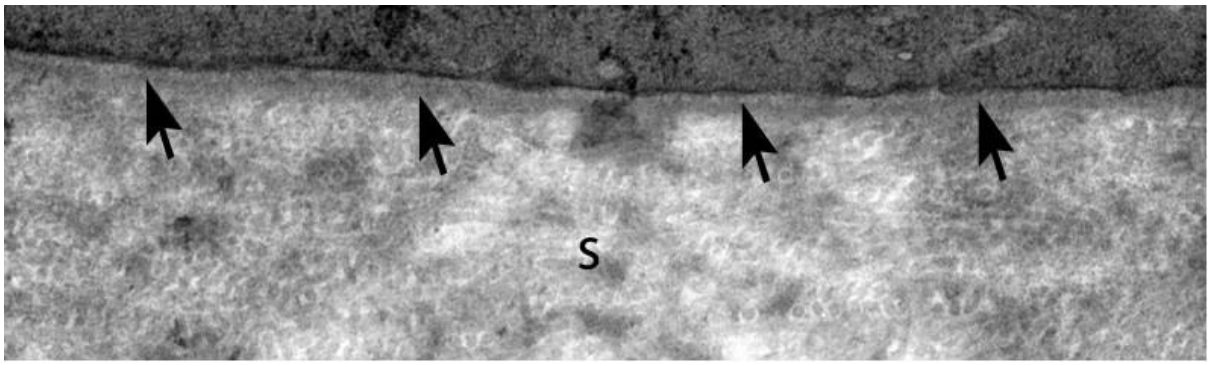


**Figure 1.3. Corneal basement membrane**. Viewing the basement membrane under the transmission electron microscope reveals two adjacent layers: the dark lamina densa (arrow heads) and the overlying lamina lucida. Adapted from (Torricelli *et al*., 2013).

*Epithelial Stem Cells*

Corneal epithelial stem cells are located in the basal layer of the limbus where the cornea and sclera merge. As they migrate to the central cornea, the stem cells differentiate into the progenitor cells, termed transient amplifying cells, and subsequently into basal cells (Fig. 1.4). These stem cells are responsible for producing a continuous supply of basal cells, which in turn, progressively differentiate into wing cells and then superficial cells before undergoing apoptosis; this cycle is then repeated to ensure than there is never a shortage of corneal epithelial cells. This is vitally important as limbal epithelial stem cell deficiency leads to numerous corneal problems such as opacification, inflammation, and vascularisation (Notara *et al.*, 2010), all of which have a devastating impact of the quality of vision. Epithelial stem cells were first identified using immunostaining against corneal-specific keratin (Schermer *et al.*, 1986). One piece of evidence that suggests that these cells are in fact stem cells was provided when the cells were shown to have a higher proliferation rate *in vitro* when compared to more central corneal epithelial cells (Pellegrini *et al.*, 1999). Furthermore, surgically removing the limbal epithelium in rabbits showed a limited ability of epithelium healing following wounding (Huang and Tseng, 1991), indicating that stem cells are present at the limbus as the epithelium fails to heal when it is removed.

A lack of stem cell marker has made it difficult to localise these cells (Schlotzer-Schrehardt and Kruse, 2005). Limbal epithelial stem cells are thought to lie in the limbus between papillae-like structures called the palisades of Vogt, which are thought to provide a protective environment (Notara *et al.*, 2010). Basic histology and immunohistochemistry has identified an anatomically defined stem cell niche in the limbus that extends out from the palisades of Vogt and provides the micro-environment to maintain 'stemness', which the authors named 'limbal epithelial crypt' (Dua *et al.*, 2005, Shanmuganathan *et al.*, 2007). For a much more extensive review of epithelial stem cells see: (Schlotzer-Schrehardt and Kruse, 2005, Notara *et al.*, 2010, Castro-Munozledo, 2013). Cultured autologous epithelial stem cells are now being widely used for regenerative purposes (ocular surface reconstruction) (Tsai *et al.*, 2000), and advances in this field have recently been reviewed by Nakamura *et al.* (2016).

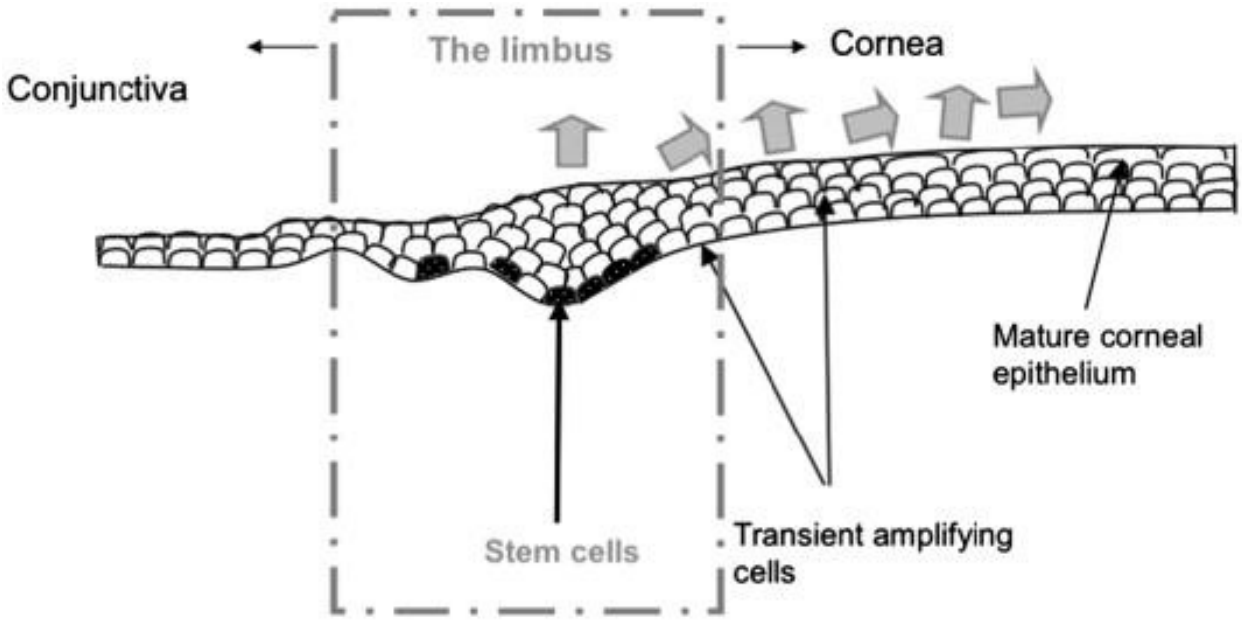


**Figure 1.4**. **Epithelial stem cell differentiation**. The schematic diagram depicts how epithelial stem cells originate in the basal layer of the limbus and gradually travel to the anterior regions of central cornea whilst differentiating into transient amplifying cells, and eventually mature epithelial cells. Taken from (Notara *et al*., 2010).

*1.1.4. Bowman's layer*

Bowman's layer is typically described as an acellular condensation of the anterior stroma and is located directly posterior to the basement membrane of the epithelium. It consists of randomly orientated type I, III and V collagen fibrils that are smaller in diameter and more randomly orientated than those located in the stroma (Komai and Ushiki, 1991, Jacobsen *et al.*, 1984) (Fig. 1.5) because of the greater type V collagen content in Bowman's layer (Gordon *et al.*, 1994). The fibrils have been measured at approximately 25nm in diameter and have been shown to interweave with stromal collagen fibrils in the posterior region of the layer (Komai and Ushiki, 1991). Functionally, the role of Bowman's layer is unclear, although it is thought that it protects the underlying stroma for traumatic injury and helps the cornea maintain its shape (Germundsson *et al.*, 2013). There is currently no evidence to suggest that the Bowman's layer has a critical role within the cornea; this is supported by the fact that there is a lack of adverse complications in eyes that have lost Bowman's layer following excimer laser photorefractive keratecotomy (Wilson and Hong, 2000).

Various techniques have been used to measure the thickness of Bowman's layer in humans, with reported values of 15-19µm (Tao *et al.*, 2011, Schmoll *et al.*, 2012). However, using *in vivo* confocal microscopy, it has been shown that the thickness of Bowman's layer decreases with age, losing one third of its thickness between 20 and 80 years of age (Germundsson *et al.*, 2013). The reason for this is unknown, although it has been hypothesised that gradual cross-linking of collagen with age could result in decreased thickness of Bowman's layer due to the lack of collagen-producing cells, or alternatively, the collagen becomes more compact with age due to a number of possible mechanisms (Germundsson *et al.*, 2013). Shallow-depth phototherapeutic keratectomy can be used to remove approximately half of Bowman's layer or fully remove it. *In vivo* confocal microscopy after both of these treatments indicated that sub-basal nerve regeneration was delayed and sub-epithelial cell density increased after 10 months following total removal of Bowman's layer, compared to half removal (Lagali *et al.*, 2009). This evidence suggests that Bowman's layer may play a role in stromal wound healing and restoration of epithelial innervation after trauma.

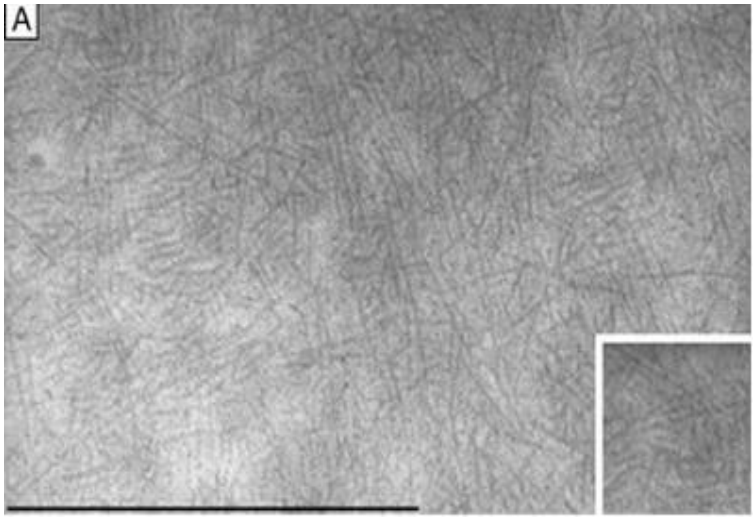


**Figure 1.5. Bowman's layer.** Electron microscope image (x72,500) of Bowman's layer showing the randomly orientated collagen fibrils. Bar = 1µm. Image taken from (Duane *et al.*, 1998).

*1.1.5. Stroma*

The corneal stroma makes up roughly 80% of the cornea's overall thickness, and therefore plays a major role in the transparency and mechanical properties of the tissue. These functions are achieved due to the highly organised arrangement of the stromal extracellular matrix (ECM). The main component of this is type I collagen fibrils, whose parallel arrangement with uniform spacing forms the basis of collagenous stromal layers, termed lamellae. Each lamellae is arranged between 0 and 180 degrees relative to the adjacent layer, and there are between 200 and 300 stacked lamellae in the human corneal stroma (Meek and Boote, 2004, Radner *et al.*, 1998a, Abahussin *et al.*, 2009). This precise organisation provides mechanical strength to the tissue in order to maintain shape and resist tensile forces, as well as providing destructive interference of light scattered in all directions other than the forward direction, subsequently enabling transparency. Besides fibrillar collagen, the stroma contains other components, such as keratocytes, proteoglycans, non-fibril forming collagens, and glycoproteins that also contribute to this highly organised layer. These will be discussed in greater depth in upcoming sections, as will the precise organisation of collagen in the stroma.

*1.1.6. A novel corneal layer?*

It has recently been postulated that an additional corneal layer exists between the stroma and Descemet's membrane (pre-Descemet's layer), that was controversially coined "Dua's layer" by the group that discovered it (Dua *et al.*, 2013). The authors used the big bubble technique (injecting air) to separate the Descemet's membrane from the posterior stroma, and claim the presence of a new well-defined layer (Dua *et al.*, 2013). This technique, first described by Anwar and Teichmann (2002), is often used during deep anterior lamellar keratoplasty (DALK) surgery, which involves removing the anterior region of the cornea and preserving the healthy Descemet's membrane and endothelium in order to reduce the risk of endothelial graft rejection. However, if the patients does not have a healthy functioning endothelium, the more traditional penetrating keratoplasty surgery is performed (full thickness graft.) Using the big bubble technique, Dua *et al.* (2013) revealed that it was possible to peel off Descemet's membrane completely without deflating the bubble, therefore, the authors suggests an additional well-defined, acellular layer in the pre-Descemet's cornea (Fig. 1.6A). Further work by Dua *et al.* (2014) used immuno-labelling to show that type VI collagen is present in the pre-Descemet's layer, and continues into the trabecular meshwork, indicating that the pre-Descemet's layer is continuous with the trabecular meshwork at the periphery of the cornea. Dua *et al.* (2015a) provided further evidence that this layer is 'unique' by demonstrating that by creating a big bubble and excising its posterior wall, further injection on air could not produce another big bubble, suggesting that the bubble is dependent on the existence of pre-Descemet's layer.

These findings have been controversial as previous studies have shown similar findings between the posterior stroma and Descemet's membrane, although they have not implied that this is a distinct corneal layer. Jafarinasab *et al.* (2010) examined corneal stroma and Descemet's membrane tissue obtained from big bubble formation in 3 keratoconic eyes. This tissue became available due to an extensive tear in Descemet's membrane, resulting in the initially intended DALK procedure being converted to penetrating keratoplasty. Interestingly, light and electron microscopy revealed 'residual stroma' attached to the Descemet's membrane, which was constant in thickness in 2 of the samples (6.4 - 12.3µm) (Fig. 1.6B). However, the residual stroma from one of the samples varied from 9.5 - 25.8µm,

indicating that separation may not occur at a single plane. Similarly, Mckee *et al.* (2011) created big bubbles in 30 corneoscleral discs that were deemed unsuitable for transplantation, and carried out histological examination. This showed 'residual stroma' attached to the Descemet's membrane of all 30 corneas, with a mean central thickness of 7µm (range 2.6 - 17.4µm) which concur with the findings by Jafarinasab *et al.* (2010). 'Residual stroma' is also described in a similar study by the same authors (Mckee *et al.*, 2012). In earlier work, electron microscopy demonstrated a network of fibres located at the posterior stroma and Descemet's membrane interface that measured 0.5µm in thickness (Binder *et al.*, 1991). Similarly, when studying the ultrastructure of the posterior stroma, Schlotzer-Schrehardt *et al*. (2015) described the presence of an anchoring zone of interwoven collagen fibrils at the Descemet's-stroma interface. The same study provided counter evident against a new distinct layer, showing that the layer is not acellular, and that the cleavage plane is determined by the variable distance of keratocytes from Descemet's membrane (Schlotzer-Schrehardt *et al.*,2015). Hence, suggestions by Dua and colleagues that a novel layer exists in the corneal stroma has been met with controversy (Jester *et al.*, 2013, Mckee *et al.*, 2014).

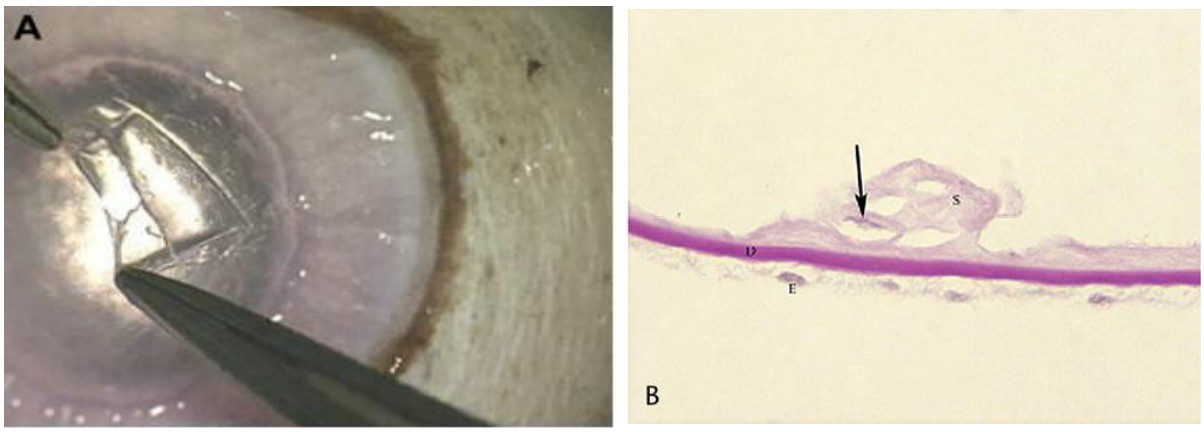


**Figure 1.6. Big bubble technique**. Image A shows a big bubble, viewed from the endothelial side of the cornea. Descemet's membrane is being peeled off whilst the bubble remains inflated. Image B (magnification x400) demonstrates residual stroma (S) attached to Descemet's membrane (D) following the formation of a big bubble. The endothelium (E) and a keratocyte (arrow) can also be seen. Image A taken from (Dua *et al.*, 2013), image B taken from (Jafarinasab *et al.*, 2010).

*1.1.6. Descemet's Membrane*

Descemet's membrane is situated between the stroma and endothelium and consists primarily of type IV collagen (Marshall *et al.*, 1991a), as well as fibronectin (Sabet and Gordon, 1989), laminin (Marshall *et al.*, 1991a), type VIII collagen, and various proteoglycans (Joyce, 2003). The membrane consists of an anterior and posterior layer, which are both structurally distinct (Fig. 1.7).The anterior 3µm layer is secreted before birth and consists of highly organised collagen that appears banded when viewed with electron microscope; conversely, the posterior layer is unorganised with no particular pattern or structure, and is produced after birth. Additionally, the posterior layer gradually increases its thickness with age, from 3µm at birth to approximately 10µm suggesting that the synthesis of components is higher than the degradation, or that there is no degradation occurring (Joyce, 2003, Johnson *et al.*, 1982).

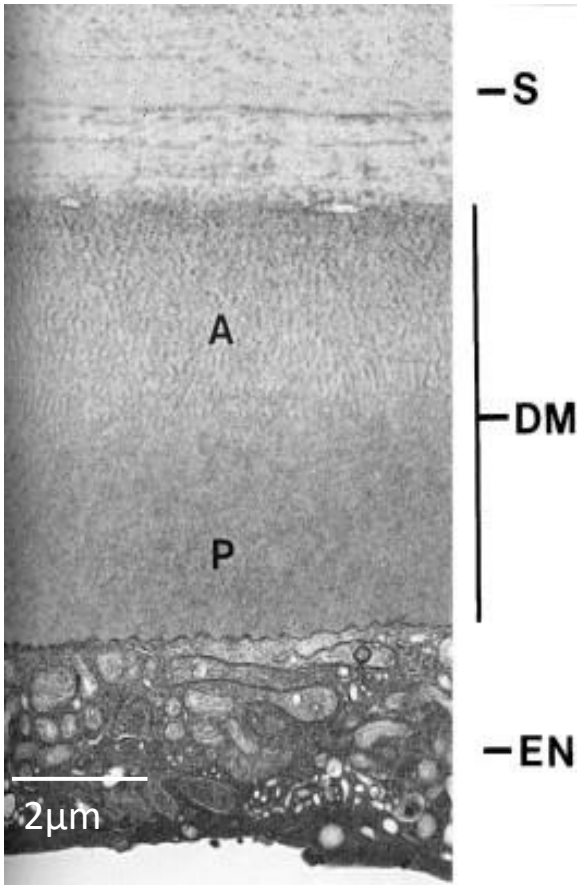


**Figure 1.7. Electron micrograph of Descemet's membrane**. The image shows the location of Descemet's membrane (DM), between the stroma (S) anteriorly, and the endothelium (EN) posteriorly. Within DM, the banded anterior region (A) can be seen, as well as the more unorganised posterior region (P). Taken from **(**Delmonte and Kim, 2011).

*1.1.7. Endothelium*

The corneal endothelium is the innermost layer of the cornea, formed by a monolayer of cells that act as the boundary between the stroma and anterior chamber, and form an irregular polygonal mosaic (Fig. 1.8). These cells are typically hexagonal and contain gap and tight junctions. During adulthood, the thickness is approximately 4µm (Joyce, 2003). Corneal endothelial cell density decreases throughout life – this has been shown in a 10 year study where cell density decreased by around 0.6% per year in adults (Bourne *et al.*, 1997). Furthermore, this decrease in cell density occurs at a faster rate during childhood as specular microscopy has indicated that there is a decrease from 6000 cells/$mm^2$ to 3500 cells/$mm^2$ throughout the first 5 years of life (Nucci *et al.*, 1990). However, a portion of this decrease is due to cornea growth (Bourne, 2003). Adhesion to the overlying Descemet's membrane is achieved due to the presence of hemidesmosomes on one of the endothelial surfaces. Corneal endothelium plays an important role in transparency by the maintenance of deturgescence i.e. keeping the stroma in a relatively dehydrated state, as accumulation of fluid would disturb the uniform spacing of collagen fibres (see section 1.2.5). A second function of the endothelium is to transport nutrients across this barrier from the aqueous humour via facilitated diffusion as there is no blood supply in the cornea.

The endothelium is able to carry out these functions as it acts as a partial barrier to fluid movement into the cornea and also a pump that actively removes water from the stroma to the aqueous humour. The function of controlling hydration is possible as the cells of the endothelium possess gap and tight junctions, and there is interdigitation of lateral membranes from adjacent cells, which contain high densities of NA+, K+-ATPase pumps (Joyce, 2003, Delmonte and Kim, 2011). Endothelium permits 'leaking' of aqueous humour into the cornea through the porous barrier, although the rate of leak is restrained by the tight junctions. Excess fluid is then removed down the osmotic gradient following a net flux of ions from the stroma to aqueous humour due to the active transport mechanism of NA+, K+-ATPase pumps. This has been termed a "pump-leak process" (Bonanno, 2012). Both barrier and pump endothelial functions are critical in maintaining corneal transparency by controlling corneal thickness.

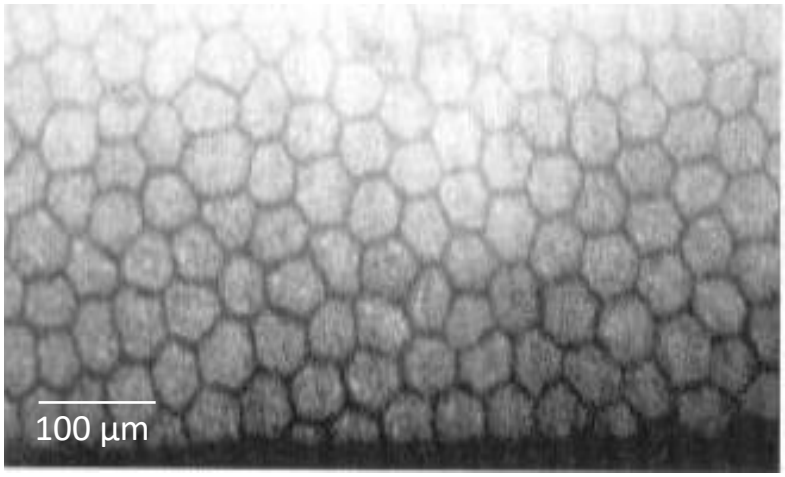


**Figure 1.8. Corneal endothelium.** The image was obtained by specular microscopy from a normal healthy endothelium, where the irregular polygonal array of cells is evident. Taken from (Duane *et al*., 1998).

### 1.2. Corneal collagen nanoscopic structure – fibril organisation

Collagen molecules are made from three polypeptide α chains that combine to form a right handed triple helical structure that is stabilised by hydrogen bonds (Fraser *et al.*, 1979). All members of the collagen family form this structure, however, their size, function and distribution in the ECM varies considerably. Each alpha chain contains the repeating amino acid triplet sequence Gly-X-Y, where X is often proline, and Y is often 4-hydroxyproline; this high glycine content plays an important role in stabilisation of the triple helix as it facilitates hydrogen bonding and intermolecular cross-links. Collagens can be heterotrimeric and consist of different types of alpha chains i.e. two α1 chains, and one α2 chain that differs slightly in chemical composition, or they can be homotrimers, which are built from three of the same type alpha chains. The triple helix may have interruptions or imperfections, depending on the collagen type. Additionally, collagen molecules have N- and C- terminal domains (non-collagenous domains) and assemble in a hierarchical manner into collagen fibrils in the ECM, before further assembling into structures such as sheets or bundles, depending on the tissue type.

The corneal stroma contains a number of different fibril-forming, FACIT, and non-fibril forming collagen types. Fibril-forming collagen of the cornea include types I, III (Davison *et al.*, 1979) and V (Birk *et al.*, 1986) as they are capable of self-assembling into striated fibrils as the name suggests. Corneal non-fibril forming and FACIT collagens include types VI (Zimmermann *et al.*, 1986) and XII (Wessel *et al.*, 1997). There are also various other collagen types found throughout the cornea in minor quantities, including types XIII, XIV and XXIV.

### *1.2.1. Biosynthesis*

Collagen fibril biosynthesis begins in the rough endoplasmic reticulum of stromal keratocytes as three alpha chain are synthesised and assembled as longer precursors called procollagen. Selected proline and lysine residues are then hydroxylated during post translational modification before the three chains form a triple helix, stabilised hydrogen bonding between hydroxyproline residues. Non-collagenous domains flanking the triple helix also play an important structural role in initiating helix formation and regulating primary fibril diameters. Moreover, the globular structure of the C-propeptide is stabilised by intrachain disulphide bonds before the triple helix is formed. After processing and procollagen assembly, molecules are packaged into secretory vesicles in the Golgi before being secreted into the extracellular space, where they are processed into a mature state by removal of the N- and C-terminal propeptides by propeptidase enzymes. This allows the molecules to assemble into parallel arrays to form microfibrils which in turn coil together to form collagen fibrils that subsequently form orthogonal lamellae in the corneal stroma. It is thought that there are about 70 microfibrils within each collagen fibril in the cornea (Holmes and Kadler, 2005). Collagen fibril biosynthesis is represented schematically in Figure 1.9.

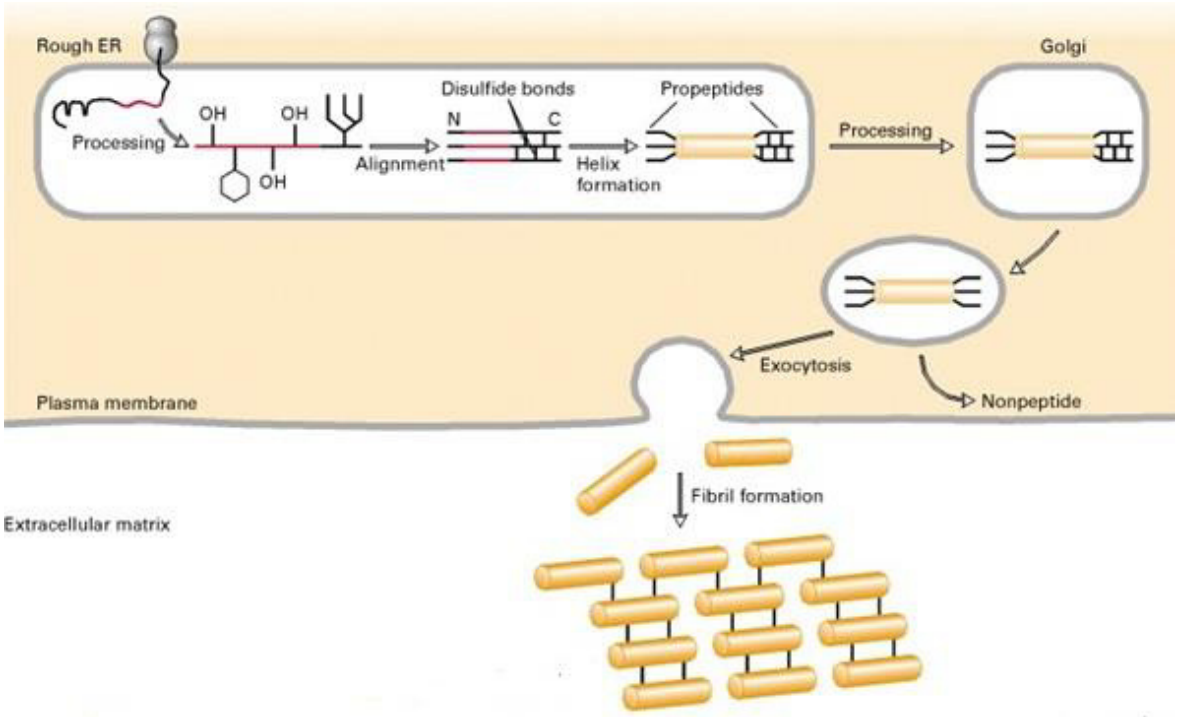


**Figure 1.9. Collagen biosynthesis.** This schematic diagram portrays the major events in the biosynthesis of fibrous collagen. Post-translational modifications occur in the rough endoplasmic reticulum (ER), including hydroxylation and disulphide bond formation before the triple helix forms. Molecules are then secreted into the ECM, where they form fibrils. Adapted from (Lodish *et al.*, 2000).

### *1.2.2. Fibril-forming collagens*

Fibril forming collagens are the most abundant and widespread family of collagens as they are responsible for providing tissues such as cornea and tendon with tensile strength, and are capable of forming striated fibrils with a 65nm repeat (Fig. 1.10). They are synthesised as procollagens containing N- and C- propeptides at each end of the molecule, where the formation of fibrils requires cleavage of the C- propeptide. Stromal collagen is primarily the fibrillar type I collagen in a heterodimeric complex with type V collagen (Fig. 1.11), which is the minor component. Type I collagen is a heterotrimer formed by two α1 chains and one α2 chain that has no imperfections. Type V collagen is responsible for regulating initial fibril assembly in the cornea, is formed by the isoform α1(V)2 α2(V) and it is present where type I collagen is expressed. The molecules are staggered one quarter of their length where a gap

zone and overlap zone between molecules indicates alternating regions of electron density, resulting in the fibril appearing striated. Using electron microscopy this has been demonstrated in the cornea (Meek and Holmes, 1983).

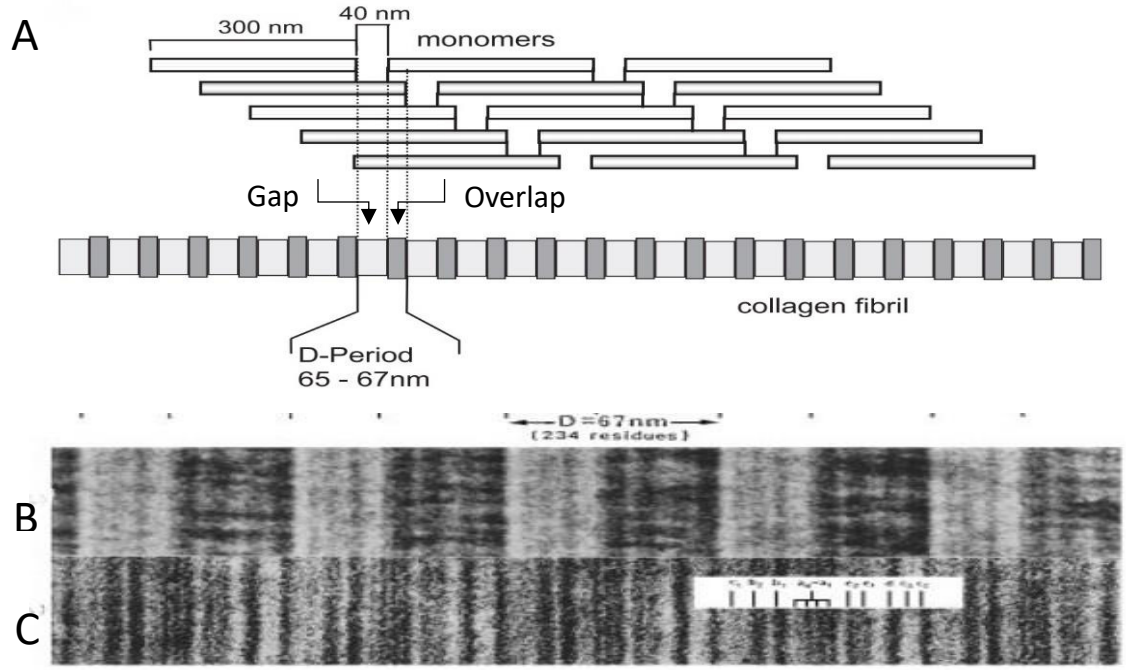


**Figure 1.10. Fibrillar collagen molecule packing.** A: the staggered arrangement of collagen molecules creates 'gap' and 'overlap' zones that produce the 65nm D-periodicity. B: collagen fibril stained with sodium phosphotungstic acid, demonstrating the banding pattern. C: further staining with uranyl acetate reveals transverse bands within the D-period. Top image adapted from (Gelse *et al*., 2003), bottom image (Kadler *et al*., 1996).

Type I and V collagen, along with type III, were identified in the corneal stroma in 1982, with type I shown to be predominant (Newsome *et al.*, 1982), before the discovery that both type I and V collagen are co-distributed within the same fibril (Birk *et al.*, 1988). The interaction between the two collagen types was studied in embryonic chick corneas where monoclonal antibodies where used to visualise type I and V collagen in stromal fibrils (Birk *et al.*, 1986). Results showed that type I collagen was detected at all times, but type V was only seen when the fibril structure was disrupted (Birk *et al.*, 1986). The same author

discovered that the presence of this heterodimeric complex plays an important role in controlling fibril diameter in the cornea. Type I and V collagen interactions were studied using an in vitro self-assembly system where increasing amounts of type V were progressively mixed with type I, resulting in decrease in mean fibril diameter (Birk *et al.*, 1990). Furthermore, Marchant *et al.* (1996) used a dominant-negative retroviral strategy to reduce the production of type V collagen secreted by chick corneal fibroblasts, resulting in the production of abnormally large collagen fibrils being deposited in the matrix. For a more extensive review of type I/V heterotypic collagen fibrils see (Birk, 2001). Type III collagen is a homotrimer of three alpha1 chains and has also been located in the corneal stroma laid down as striated fibrils, in a similar fashion to type I collagen (Marshall *et al.*, 1991a)

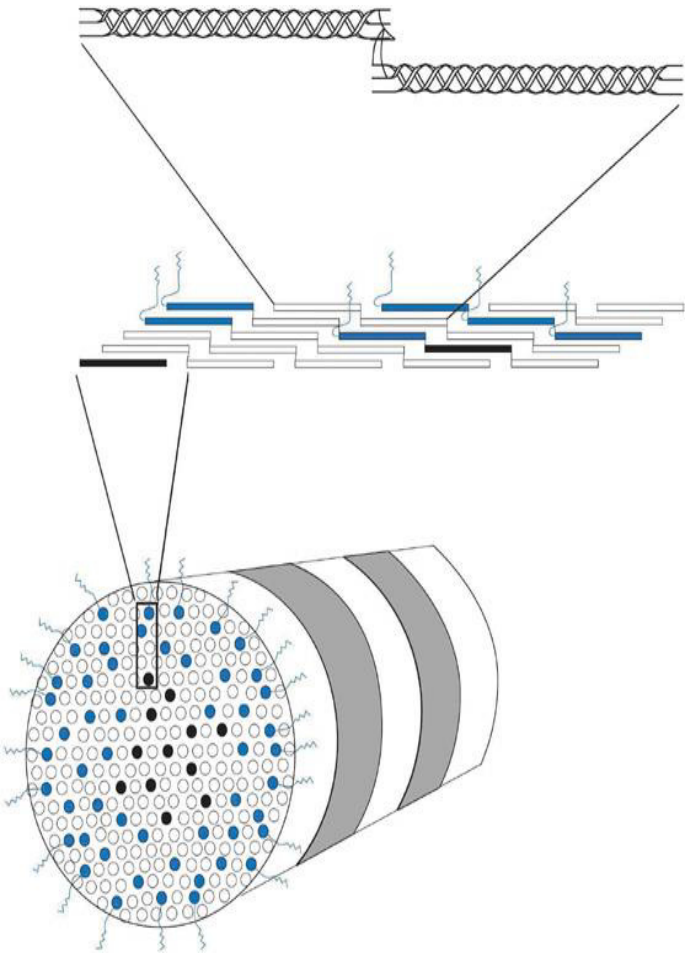

**Figure 1.11. Heterotypic corneal stromal collagen fibril**. This heterotypic fibril (bottom image) is composed of type I collagen (white), type III collagen (black), and type V collagen (blue). The N-pro-peptide domain of type V collagen projects to the fibril surface where it is thought that fibril diameter is regulated. The middle image demonstrated the quarter staggered arrangement of molecules resulting in a striated fibril. Fibrils are further stabilised by the presence of covalent intermolecular cross links between molecules (top image). Taken from (Duane *et al*., 1998).

### *1.2.3. FACIT and non-fibril forming collagens*

Fibril associated collagens with an interrupted triple helix (FACIT) are a group of collagen that have interruptions in the triple helical domain, as the name suggests. They are normally located on the surfaces of fibrillar collagens, as seen by immuno-electron microscopy (Keene *et al.*, 1991a). Type XII collagen is a FACIT that interacts with type I collagen; it was initially identified as cDNA from chick tendon fibroblasts (Gordon *et al.*, 1987). Immunohistochemical analysis identified the presence of type XII collagen in dense connective tissue that contain type I collagen such as tendon and ligament (Sugrue *et al.*, 1989) before it was identified in the corneal stroma using the same techniques (Wessel *et al.*, 1997, Gordon *et al.*, 1996), where it was more localised at 'interfacial regions', i.e. where Bowman's layer and Descemet's membrane meet the stroma (Gordon *et al.*, 1996). Furthermore, corneal type XII collagen as it is present in its long variant, whereas the short variant is present in other tissues (Wessel *et al.*, 1997). Functionally, type XII collagen is thought to be involved in stabilising fibril arrangement by bridging the fibrils (Shaw and Olsen, 1991, Wessel *et al.*, 1997).

Type VI is a beaded-filament-forming collagen found in the interfibrillar matrix of human corneal stroma (Zimmermann *et al.*, 1986) and makes up 17% of the total collagen content in the cornea. Type VI collagen molecules aggregate into repeating tetramers, resulting in a 10-15nm diameter, beaded, non-banded filament (Michelacci, 2003) (Fig. 1.12). These beaded filaments have a 100nm periodicity, they are located between striated collagen fibrils in a meshwork arrangement, and control the arrangement of these fibrils by interactions with proteoglycans, as well as acting as a bridging filaments and binding corneal lamellae together (Nakamura *et al.*, 1993, Nakamura *et al.*, 1997, Hirsch *et al.*, 2001). It has also been suggested that type VI collagen may play a role in increasing cell survival, as demonstrated by *in vivo* and in *vitro* analysis of the avian cornea (Howell and Doane, 1998).

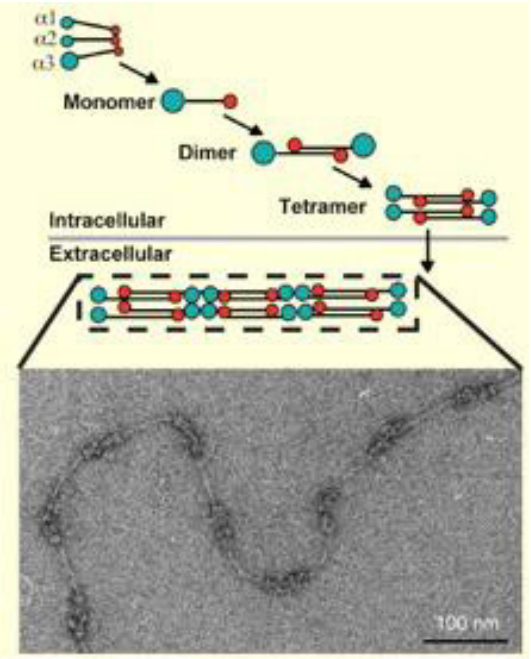


**Figure 1.12. Type VI collagen assembly**. 3 alpha chains combine to form a monomer, which in turn combines with another monomer to form an antiparallel dimer. Two dimers subsequently combine to form a tetramer. End to end aggregates of tetramers result in the beaded appearance of type VI collagen as seen by electron microscopy (Scale bar – 100nm). Taken from (Kadler *et al*., 2007).

### *1.2.4. Corneal collagen fibrils*

Collagen accounts for approximately 70% of the total dry mass in the cornea. The majority of this collagen is found in the corneal stroma, where individual collagen molecules held together by intermolecular bonds combine to form fibrils, which subsequently form lamellae sheets. Corneal transparency is highly dependent on the specific size and spacing of collagen fibrils, hence they are uniform in diameter and are evenly spaced in the cornea (Meek and Quantock, 2001, Maurice, 1957) (Fig. 1.13). The collagen fibrils travel across the whole cornea before merging with collagen in the limbus or continuing to the sclera. In the cornea, the axial periodicity of collagen is 65nm, compared to 67nm in other collagenous tissues such as tendon (Meek and Boote, 2004, Meek *et al.*, 1981). Each individual molecule is roughly 1.6nm apart, although it has been suggested that this spacing increases with age and is governed by fibril hydration (Malik *et al.*, 1992, Daxer *et al.*, 1998, Meek *et al.*, 1991). Conversely, interfibrillar spacing seems to decrease with age due to changes in proteoglycan composition (Malik *et al.*, 1992, Kanai and Kaufman, 1973). Small-angle X-ray diffraction has portrayed that fibril diameter is constant throughout the central cornea at around 31-34nm (Meek and Leonard, 1993, Daxer *et al.*, 1998, Boote *et al.*, 2003, Kanai and Kaufman, 1973), until the fibrils reach the limbus, where there is a 75% increase in diameter (Boote *et al.*, 2003, Boote *et al.*, 2011). Moreover, fibril diameter increases in the periphery where

corneal collagen begins to merge with scleral collagen (Boote *et al.*, 2011). Fibril diameter has also been shown to increase with age (Daxer *et al.*, 1998, Meek and Leonard, 1993), potentially due to increased amount of collagen cross-linking during ageing resulting in molecules being pushed apart. Furthermore, collagen fibril spacing is 5-7% lower in the central third of the cornea, often called the prepupillary layer, compared to the less curved peripheral regions, suggesting that it is more closely packed (Boote *et al.*, 2003). In comparative studies of various species using X-ray diffraction, fibril diameter and interfibrillar spacing varies greatly between different species, whereas the fibril volume fraction (% space occupied by the fibrils) remains constant, indicating that smaller fibrils pack closer together (Meek and Leonard, 1993, Gyi *et al.*, 1988).

Three dimensional reconstructions of corneal collagen molecules have been used to study the organisation of collagen fibrils using automated electron tomography These results have shown that collagen molecules in 36nm fibrils are organised into microfibrils, that are uniform in diameter (~4nm), and are tilted by ~15 degrees right-handed to the long axis of the fibril (Holmes *et al.*, 2001, Baldock *et al.*, 2002). It has been postulated that this tilting may be the reason why the axial periodicity in decreased in the cornea compared to other tissues (Meek and Boote, 2004).

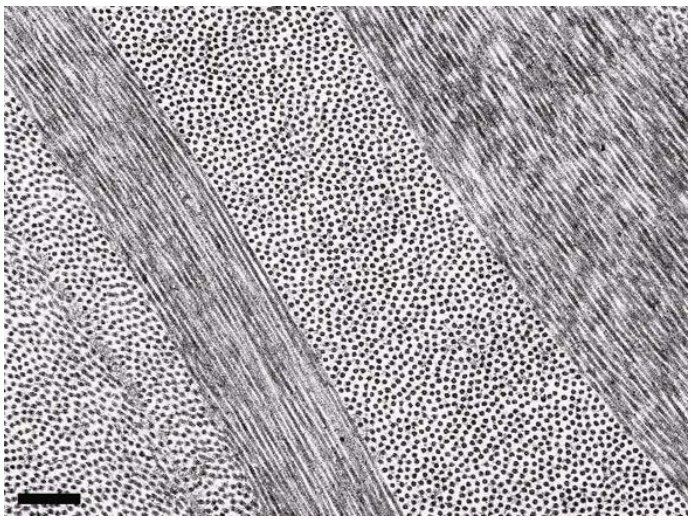

**Figure 1.13. Corneal collagen fibril organisation.** This image, obtained by transmission electron microscopy, shows small diameter collagen fibrils lying within two transverse lamellae. Two longitudinal lamellae can also be seen. Scale bar 1μm. Taken from (Meek and Boote, 2009).

*1.2.5. Corneal transparency*

The precise organisation of collagen fibrils in the stroma provides the cornea with a unique property, transparency, by transmitting and refracting light that passes through the tissue. Maurice (1957) proposed that collagen fibrils, that are uniform in diameter and regularly spaced, are arranged parallel with one another into a defined long range lattice. It is suggested that each fibril scatters a small amount of light due to the difference in refractive index between the fibril and interfibrillar matrix, where the lattice arrangement leads to destructive interference of scattered light in all directions other than the forward, resulting in a transparent cornea. However, this theory is disputed by Hart and Farrell (1969), who propose that only short range order in the position of collagen fibrils is important for transparency. This short range order has been demonstrated with X-ray diffraction (Sayers *et al.*, 1982). Furthermore, Benedek (1971) indicated that scattering does not occur when the distance between collagen fibrils is less than half the wavelength of light in the medium.

Another theory states that transparency is based on consistent refractive index properties of corneal components and regular fibril spacing (Smith, 1969).This theory suggests that the refractive index of collagen fibrils is similar to other matrix components, resulting in minimal scattering of light when passing through the cornea. The theory conflicts with results discovered by Leonard and Meek (1997), where X-ray diffraction showed that the refractive index of collagen fibrils differs to that of the surrounding matrix.

Proteoglycans also play an important role in corneal transparency due to their ability to maintain and develop the unique collagen organisation in the stroma i.e. maintain interfibrillar spacing (Hassell *et al.*, 1980). Furthermore, corneal hydration is thought to have a profound effect on transparency as swelling leads to scattering of significant quantities of light (Meek *et al.*, 2003). In comparison to collagen arrangement, little attention has been paid to the role that stromal cells play in corneal transparency. It is thought that stromal cells contain corneal crystallins that are able to change the refractive index of the cells cytoplasm closer to that of the ECM to eliminate scattering, although when activated during wound healing, there is a mismatch in refractive indices that significantly contributes to light scattering (Jester, 2008, Jester *et al.*, 1999a, Gardner *et al.*, 2015).

### 1.3. Corneal collagen microscopic structure – lamellae orientation

As mentioned previously, the corneal stroma consists of between 200 and 300 stacked lamellae (Fig. 1.14) at the centre, and around 500 at the limbus, each of which is ~2µm thick and contains collagen fibrils that are parallel to each other, and to the corneal surface (Meek and Boote, 2004, Komai and Ushiki, 1991). Furthermore, the fibrils that make up the lamellae are arranged between 0 and 180 degrees relative to the adjacent lamella (Meek and Boote, 2004, Radner *et al.*, 1998a). This specific organisation of the collagen network is responsible for giving the tissue mechanical strength, and hence the ability resist tensile strain. Scanning electron microscopy has demonstrated that lamellae split into branches in two directions; horizontally throughout the stroma, and antero-posteriorly in the anterior third of the stroma, and these branches are interlaced with other lamellae by crossing of fissures (Radner *et al.*, 1998a, Komai and Ushiki, 1991).

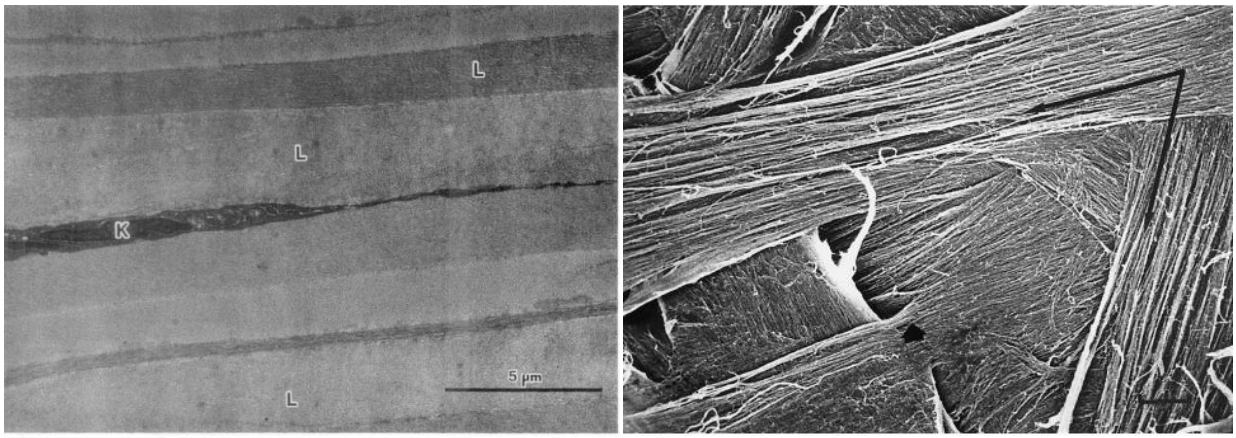


**Figure 1.14. Transmission and scanning electron micrographs of corneal lamellae**. Left image – Layers of lamellae (L) can be observed in the corneal stroma with keratocytes (K) located between layers (x8600). Right image – Interwoven lamellae (arrows) can be seen crossing at an angle in the mid-stroma. Interlacing between lamellae also occurs (Small arrow head) where a lamella splits into 2 branches (Scale bar = 10µm). Images taken from (Komai and Ushiki, 1991) (left) and (Meek and Fullwood, 2001) (right).

*1.3.1. In-plane lamellae organisation*

Lamellae orientation has been studied extensively in recent years using X-ray scattering techniques. Using powerful synchrotron sources, these techniques have been used to map collagen fibril, and subsequent lamellar directions throughout the whole cornea, and allows the tissue to be studied at close to physiological hydration (Meek and Quantock, 2001, Meek and Boote, 2004). Results from using these techniques have shown two preferred orientations of the orthogonal collagen fibrils in the central human corneal stroma, which are as follows; horizontal (nasal-temporal) and vertical (inferior-superior) (Meek *et al.*, 1987, Daxer and Fratzl, 1997, Boote *et al.*, 2006, Abahussin *et al.*, 2009, Aghamohammadzadeh *et al.*, 2004, Meek and Newton, 1999). However, using femtosecond laser technology to study the orientation at different depths of the stroma, these preferred orientations have been shown to be more prevalent in the posterior stroma; conversely, the anterior stroma has shown no preferred lamellae orientation and it is thought that it plays a role in resisting intraocular pressure and maintaining corneal curvature (Abahussin *et al.*, 2009, Aghamohammadzadeh *et al.*, 2004). These preferred orientations are depicted in Figure 1.15.

This preferred orientation occurs at the centre of the cornea and runs to within 2mm of the limbus; from there, the orientation gradually changes to tangential disposition of fibrils occurs (Aghamohammadzadeh *et al.*, 2004, Meek and Newton, 1999), which probably originate from the adjacent sclera, although this has been shown to be restricted to the posterior stroma (Kamma-Lorger *et al.*, 2010). Further studies have discovered that collagen is preferentially aligned outside the central 6mm of stroma, until 1-1.5mm before the limbus (Boote *et al.*, 2011). Additionally, studies have portrayed that roughly 60-66% of the collagen fibrils in the stroma are situated within 45 degree sectors of the superior-inferior direction, and one third in the nasal-temporal preferred direction (Daxer and Fratzl, 1997, Newton and Meek, 1998b); however, some corneas showed significantly high levels of fibrils in one of the two preferred directions (Boote *et al.*, 2005).

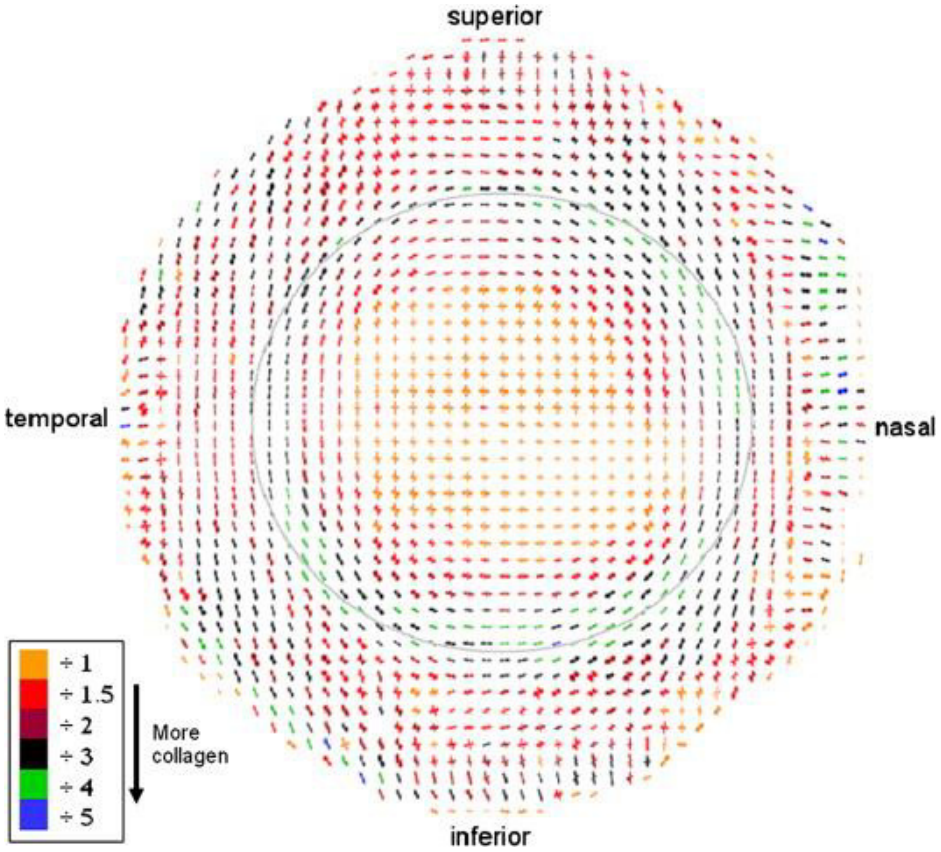


**Figure 1.15. Polar plot map, obtained using wide-angle X-ray scattering.** The above map shows preferred collagen fibril orientation across the human cornea, limbus and sclera at 0.4mm intervals. The gradual change from orthogonal to a more tangential arrangement of collagen can be seen from the centre to the limbus. Taken from (Meek and Boote, 2009).

### *1.3.2. Transverse lamellae organisation – differences between anterior and posterior stroma*

Lamellae orientation is known to differ between the anterior and posterior regions of the corneal stroma. As mentioned previously, the preferred lamellae orientations were more prominent in the middle and posterior layers of the stroma whereas the anterior layer was more isotropic (Aghamohammadzadeh *et al.*, 2004, Abahussin *et al.*, 2009). Furthermore, lamellae in the anterior stroma are thought to be 50% more dense when compared to the posterior stroma (Bergmanson *et al.*, 2005) and also twice as thick (Komai and Ushiki, 1991, Quantock *et al.*, 2007). The middle and posterior regions are orthogonally arranged and more parallel to the surface, whereas the lamellae in the anterior stroma are highly interwoven with branching of fibrils. These patterns of lamellar organisation have been

detected using both electron (Komai and Ushiki, 1991) and more recently confocal (Morishige *et al.*, 2006) and second-harmonic imaging (Morishige *et al.*, 2007, Jester *et al.*, 2010) microscopy. Additionally, these techniques have also shown that lamellae branch and obliquely transverse the anterior cornea, inserting into Bowman's layer, and providing an anchoring function (Morishige *et al.*, 2006, Komai and Ushiki, 1991, Morishige *et al.*, 2007, Jester *et al.*, 2010).

Second harmonic-imaging later showed that the insertion angle into Bowman's layer was ~19 degrees (Morishige *et al.*, 2011). Increased interweaving in the anterior stroma is thought to cause a bigger spread in lamellae inclination angles in comparison to the posterior stroma (Abass *et al.*, 2015, Winkler *et al.*, 2013). Transverse lamellae were not detected in rabbit corneas, indicating that this organisation in human corneas alters the mechanical properties in the anterior stroma, and results in it being more stiff and resistant to tensile forces than the posterior stroma (Morishige *et al.*, 2006). Furthermore, in a study analysing human corneal stroma in extreme hydration, it was found that the anterior 100-120µm of anterior stroma resisted swelling and maintained the corneal curvature (Muller *et al.*, 2001). This provides further evidence that the interwoven and transversely organised lamellae in the anterior stroma contribute to increased rigidity compared to the middle and posterior regions. A high degree of interlacing between lamellae has also been seen in the mid stroma (Radner and Mallinger, 2002). At a fibrillar level, using electron micrographs it has been reported that in the posterior stroma, fibrils are approximately 4% smaller in radius and 1.12 times greater in number density when compared to the anterior stroma (Freund *et al.*, 1995).

### *1.3.3. Corneo-limbal junction*

As mentioned previously, there is a reversal in curvature as the corneal collagen approaches the sclera at the limbus. This change is a result of a different collagen fibril preferred orientation. Using scanning electron microscopy to measure cross angles in the posterior limbus, it was discovered that 68% were less than 30 degrees; it has been suggested that a pseudocircular lamellae orientation is created at the limbus by these small cross angles

(Radner *et al.*, 1998a). In a different study using X-ray diffraction to compare fibril orientation in the cornea and sclera, a circum-corneal annulus of collagen fibrils was discovered at the limbus that ran circumferentially; it is thought that this arrangement assists in maintenance of corneal curvature (Newton and Meek, 1998a, Meek and Newton, 1999). Newton and Meek (1998b) followed up this study in order to determine how the collagen fibrils in the two preferred orientations integrate at the circum-corneal annulus of the limbus and found that the fibrils change direction to run circumferentially (Fig. 1.16). These findings have been consolidated in a separate study using X-ray diffraction, where it has been postulated that this apparent bending of fibrils could be possible by lamellae splitting and fusing with other lamellae that are running in a different angle (Meek and Boote, 2004).

More recent X-ray diffraction work has shown that circum-corneal annulus that surrounds the cornea at the limbus resides predominantly in the posterior region of the cornea (Kamma-Lorger *et al.*, 2010). Furthermore, orthogonally arranged lamellae in the central 6mm of stroma change direction 1-1.5mm before the limbus in order to integrate with circumferential fibrils (Boote *et al.*, 2011). As mentioned previously, as well as a circum-corneal annulus, there are also lamellae with a tangential orientation at the posterior limbus (Aghamohammadzadeh *et al.*, 2004) containing larger diameter fibrils (Boote *et al.*, 2011) that are likely to originate from the adjacent sclera, and have therefore been termed ‘anchoring lamellae’ (Meek and Knupp, 2015), as they may play a role in maintaining the structural integrity of the cornea and sclera.

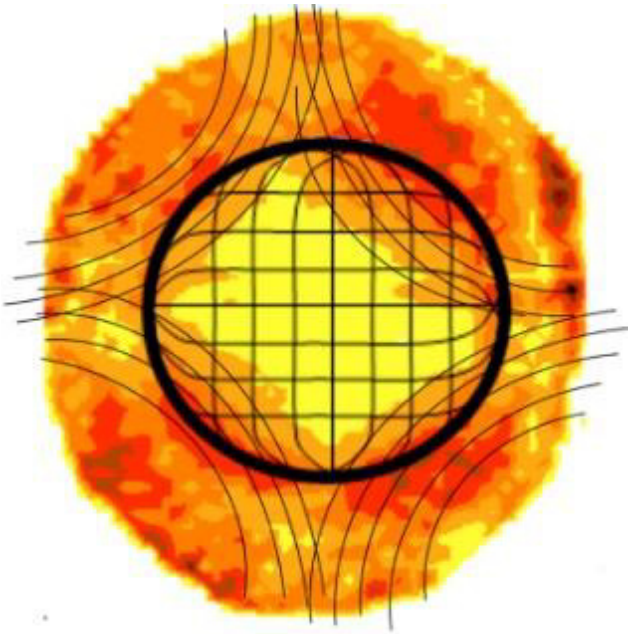

**Figure 1.16. Schematic diagram of fibril orientation.** The diagram portrays the preferred orientations (black lines) of fibrils in the cornea and the proposed orientation change to run circumferentially at the circum-corneal annulus. Anchoring lamellae with larger collagen fibrils can also be seen running tangentially. The colours represent collagen distribution, where total X-ray scatter from fibrillar collagen remains constant (yellow) until an increase is observed (orange) ~1.5 mm from the limbus. Taken from (Meek and Knupp, 2015).

### 1.4. Proteoglycans

Corneal transparency and strength is dependent on other matrix components such as proteoglycans, as these molecules play a role in regulating the precise collagen fibril organization in the cornea. Small, interstitial proteoglycans are the second major constituents of the corneal ECM behind collagen, and by interacting with collagen, they are responsible for controlling the size and arrangement of collagen fibrils in the stroma. Interactions between proteoglycans and collagen fibrils have been demonstrated in three-dimensions (Lewis *et al.*, 2010, Parfitt *et al.*, 2010). These macromolecular structures consist of a leucine-rich protein core that has glycosaminoglycan (GAG) side chains covalently attached to it. GAG's are long unbranched polysaccharides formed from repeating sulphated disaccharide units. The negative charge that these chains carry makes them hydrophilic, therefore, water is attracted which helps the tissue resist compressive forces. There are predominantly three types of GAG's in the cornea; these are keratan sulphate (65%) and

dermatan sulphate/chondroitin sulphate in the same chain (Meek and Boote, 2009). It is thought that proteoglycans control matrix assembly as the protein cores bind to collagen and the GAG's control interfibrillar spacing (Kao and Liu, 2003). In the cornea, the main types of PG's are the dermatan/chondroitin sulphate containing decorin and biglycan (Li *et al.*, 1992), and the keratan sulphate containing lumican (Blochberger *et al.*, 1992), keratocan (Corpuz *et al.*, 1996) and mimecan (also called osteoglycin before it was renamed (Funderburgh *et al.*, 1997)), which differ from each other by the core protein that is present (Michelacci, 2003).

It is believed that keratan sulphate assists in the maintenance of collagen fibril spatial conformation in the cornea. In macular corneal dystrophy, a lack of keratan sulphate results in significantly lower centre-to-centre interfibrillar spacing, ultimately causing thinner corneas (Quantock *et al*., 1990). When lumican-null mice corneas were studied using X-ray diffraction, the results indicated that the stromal collagen organization was in disarray and fibril diameter varied significantly, portraying the structural importance of keratan sulphate (Quantock *et al.*, 2001). In a study looking at bovine corneal stroma in vitro, lumican and decorin were shown to inhibit the rate of fibrillogenesis and subsequently control matrix assemble; additionally, the presence of lumican resulted in the fibrils being significantly thinner in diameter compared to fibrils without the presence of any proteoglycans – the protein core was deemed responsible for this as opposed to the GAG side chains (Rada *et al.*, 1993). Furthermore, homozygous knockout mice lacking derived of lumican demonstrate corneal opacification due to the presence of thick collagen fibrils lack of fibril organization, portraying the crucial role that lumican plays in regulating fibril growth and assembly in the stroma; it should be noted that these findings were more apparent in the posterior stroma (Chakravarti *et al.*, 1998, Chakravarti *et al.*, 2000). Similarly, although keratocan knockout mice maintain transparency, they have thicker collagen fibrils and decreased organization that is less severe than the lumican knockout mice phenotype, it is thought that keratocan is an important regulator of corneal shape (Liu *et al.*, 2003). Keratocan expression has been shown to be regulated by lumican which is thought to explain the difference in phenotype severity between lumican and keratocan deficient mice corneas (Carlson *et al.*, 2005). Interestingly, mimican deficient mice, stromal architecture is normal, suggesting that mimican has a lesser role in corneal collagen fibril organisation (Beecher *et al.,* 2005).

## 1.5. Cell types

### *1.5.1. Keratocytes*

Keratocytes are the predominant cell type in the stromal ECM, where they are located within the lamellae, and are responsible for sectreting the matrix components, collagen and proteoglycans (Fig. 1.17). The dendritic processes protruding from the keratocytes enable them to form an interconnected cellular network (Fig. 1.18) which the cells use to communicate with each other, and various techniques have been used to demonstrate this (Muller *et al.*, 1995, Hahnel *et al.*, 2000, Poole *et al.*, 1993). Keratocyte cell bodies are compact and it has been suggested that a reduced surface area exposed to light decreases the scattering, ultimately aiding transparancy (Hassell and Birk, 2010). As mentioned previously, light scattering is also reduced by the presence of the corneal crystallins transketolase and aldehyde dehydrogenase (Jester *et al.*, 1999a) which match the cells' refractive index to that of the surrounding ECM (Gardner *et al.*, 2015). Quantitative analysis of keratocyte density *in vivo* showed that it was roughly 20,000 cells/mm$^3$, highest in the anterior 10% of stroma, and that it decreases approximately 0.45% a year (Patel *et al.*, 2001).

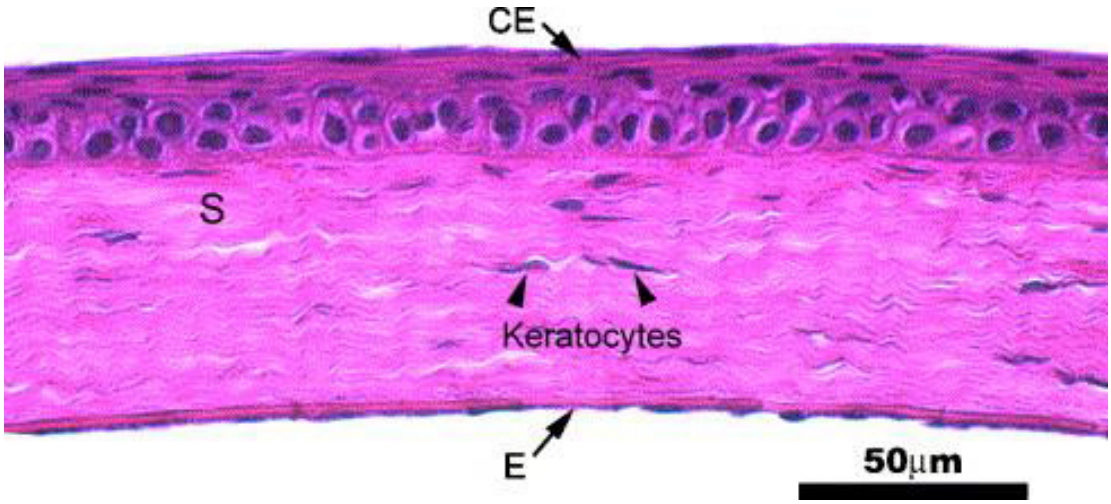


**Figure 1.17. Haematoxylin and eosin staining of mouse cornea.** The cross section shows the location and morphology of keratocytes in the corneal stroma (S), situated between the corneal epithelium (CE) and endothelium (E). Taken from (West-Mays and Dwivedi, 2006).

Keratocytes lie quiescent in the cornea until injury occurs, resulting in two possible outcomes depending on the environmental signals present. Firstly, the keratocytes may be stimulated to undergo apoptosis, which was discovered by microinjecting Interleukin-1 into the mouse stroma (Wilson *et al.*, 1996). The extent of apoptosis is thought to differ depending on the type of injury (West-Mays and Dwivedi, 2006). For example, keratocyte apoptosis following PRK is seen in the superficial stroma, whereas LASIK results in apoptosis occurring deeper in the stroma (Wilson *et al.*, 2003). Additionally, the cells may be activated to become repair phenotypes; this option promotes regeneration or induces fibrotic scar formation due to the trans-differentiation of keratocytes into fibroblasts distal to the wound, unlike the corneal epithelium, which is capable of healing without scar formation (Pinnamaneni and Funderburgh, 2012). The formation of fibrotic scars following healing has catastrophic effects on the originally transparent cornea.

Keratocytes are activated and migrate to the site of injury following the initial wave of cell death. At this stage, the cells begin to show morphological changes such as increased cell size into a fusiform shape and multiple nucleoli, which are characteristics of fibroblasts (West-Mays and Dwivedi, 2006). Myofibroblasts are an additional keratocyte phenotype that are seen in the stroma following injury. They are larger in appearance and express alpha smooth muscle actin, which differentiates them from normal fibroblasts. It is thought that myofibroblasts secret and organize the ECM during repair (West-Mays and Dwivedi, 2006).

Various tissue culture techniques have been used to study keratocyte activation. It has been discovered that when culturing keratocytes in media without the presence of serum, they display a similar phenotype to that of a quiescent keratocyte in vivo, such as dendritic morphology and keratocan secretion (Beales *et al.*, 1999). Conversely, when cultured in media containing serum and various growth factors such as transforming growth factor beta (TGF-β), the keratocytes show characteristics of activation such as alpha smooth muscle actin expression (Jester *et al.*, 1996), as well as the decrease in the expression of keratan sulphate PG's (Funderburgh *et al.*, 2003, Funderburgh *et al.*, 2001) and decreased expression of corneal crystalins (Jester *et al.*, 1999a). TGFB-β is secreted by corneal

epithelial cells. When keratocytes are cultured without serum and exposed to TGF-β, they transform into myofibroblasts, and this can be inhibited by antibodies that block TGF-β (Jester *et al.*, 1999b). However, keratocytes cultured with serum in vitro with fibroblast growth factor 2 (FGF-2) added stimulated keratan sulphate PG expression as the keratocytes maintained their characteristic phenotype, indicating that keratocyte fate is dependent on the growth factors that they are exposed to (Long *et al.*, 2000).

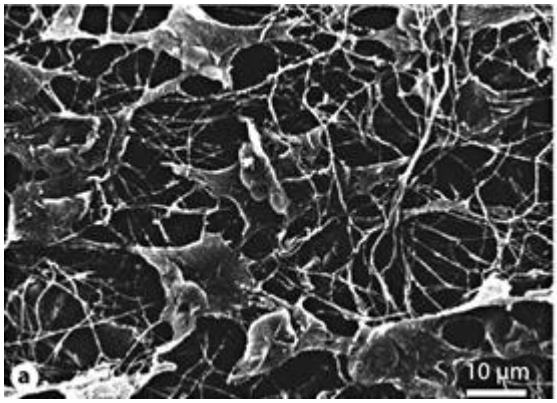


**Figure 1.18. Electron micrograph of corneal keratocyte network.** The image shows how dendritic processes extend from the keratocyte cell bodies are for interconnected networks throughout the tissue. Image taken from (Knappe *et al.*, 2011).

*1.5.2. Stromal stem cells*

In addition to keratocytes, it is thought that the stroma may contain a small population of corneal stromal stem cells that display properties of mesenchymal stem cells (Pinnamaneni and Funderburgh, 2012, Branch *et al.*, 2012). As mentioned previously, keratocytes proliferate during wound healing and in vitro into fibroblasts. In a study using bovine stromal cells *in vitro*, 3% exhibited clonal growth, expressed a number of mesenchymal stem cell markers, and were able to maintain keratocyte phenotype following proliferation (Funderburgh *et al.*, 2005). Yoshida *et al*. (2006) demonstrated multipotency in the mouse stroma of cells that they termed 'neural crest-derived corneal precursors'. These cells expressed various stem cell markers and had the ability to differentiate into adipocytes and chondrocytes (Yoshida *et al.*, 2006). A population of cells that had stem cell characteristics such as, multipotent differentiation potential and clonal growth have also been isolated in the human corneal stroma near the limbus; these cells were also able to produce stromal matrix following expansion in vitro (Du *et al.*, 2005, Wu *et al.*, 2014, Wu *et al.*, 2013). The ability of these corneal stromal cells to replicate in vitro whilst maintaining the potential to

differentiate and lay down stromal matrix could have profound potential in corneal bioengineering. An example of this has been demonstrated in vivo, where human corneal stem cells were injected into opaque mouse corneas where they began to lay down human ECM components and corneal transparency was restored (Du *et al.*, 2009). More recently, human limbal biopsy-derived stromal stem cells prevented scarring in mouse corneal wounds (Basu *et al.*, 2014). Stromal stem cells have recently been reviewed by (Funderburgh *et al.*, 2016).

### 1.6. Trabecular meshwork

The trabecular meshwork is a tissue located in the anterior chamber angle of the eye, in the posterior region of the corneo-scleral limbus, where it is anchored into the base of the cornea anteriorly, near the termination of Descemet's membrane (Schwalbe's line), extending posteriorly to the ciliary body and scleral spur, and plays a critical role in aqueous humor outflow (Fig. 1.19). Aqueous humor fills the anterior and posterior chambers of the eye and is responsible for providing nutrients to avascular structures in the eye such as the cornea and lens, as well as maintaining intraocular pressure, both of which are critical for normal vision. Aqueous inflow occurs via the cilliary processes of the cilliary body, whereas aqueous humor is recycled via two different outflow pathways (Fig. 1.19): the uveoscleral pathway (non-conventional)(reviewed by Alm and Nilsson (2009)), by diffusion through intercellular spaces among ciliary muscles (Bill, 1975), or the trabecular pathway (conventional)(reviewed by Tamm (2009)), where aqueous humor exits the eye through the trabecular meshwork and into Schlemm's canal before finally draining into aqueous veins.

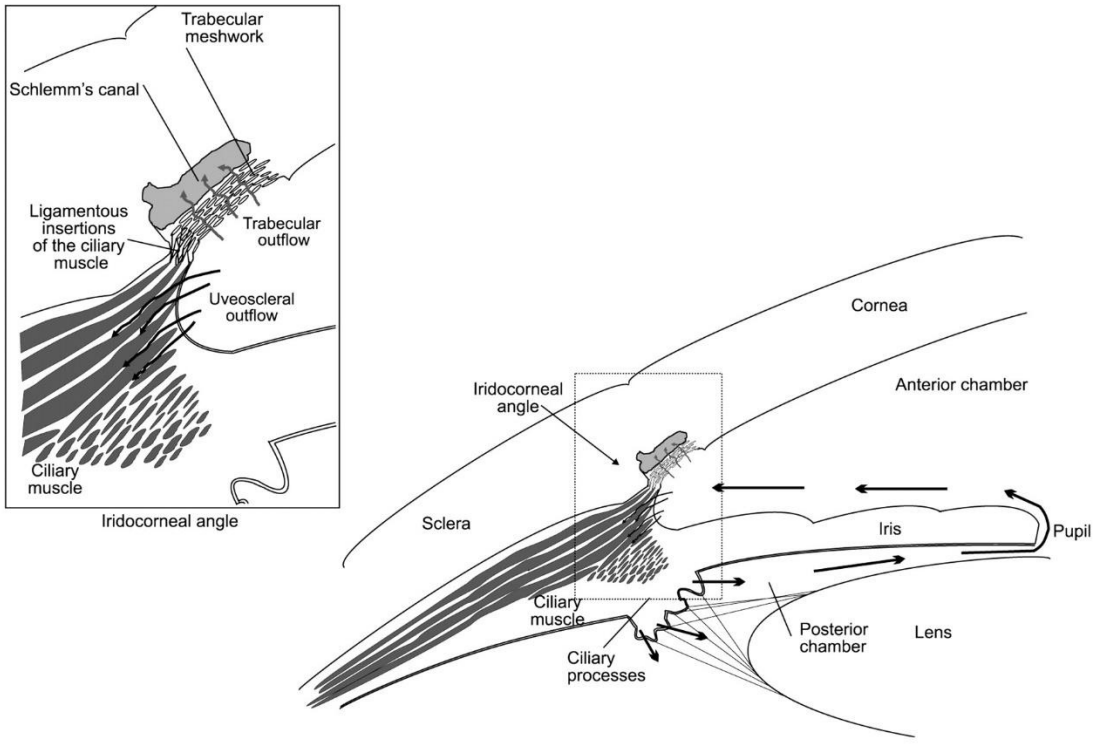


**Figure 1.19. Schematic diagram of aqueous humour cycle**. Aqueous inflow occurs via the ciliary processes and enters the anterior chamber of the eye (black arrows). The inset shows the two outflow pathways: uveoscleral and trabecular. Most of the aqueous humour exists via the trabecular pathway, consisting of the trabecular meshwork and Schlemm's canal. Taken from (Llobet *et al*., 2003).

Trabecular meshwork is divided into three distinct regions: uveal meshwork, corneoscleral meshwork, and juxtacanalicular tissue (Fig. 1.20). The uveal meshwork is most posterior layer, and is composed of one to three layers of trabecular beams or lamellae that attach to one another to form a porous structure. Large number and size of intercellular spaces in this layer mean that it does not offer much resistance to aqueous humor outflow (Llobet *et al.*, 2003). Corneo-scleral meshwork is situated above the uveal meshwork, contains 8-15 thicker trabecular layers that originate from the scleral spur, with trabecular beams covered in endothelial-like cells, resting on basal lamina. Trabecular beams contain a core of type I and III collagen (Marshall *et al.*, 1991b), in addition to true elastic fibres, containing abundant amounts of electron-dense amorphous material (Gong *et al.*, 1989, Lutjendrecoll *et al.*, 1981). Moreover, type VI collagen has also been immunolocalised between the elastic fibre cores and basal lamina (Lutjendrecoll *et al.*, 1989). Juxtacanalicular tissue is the smallest part of the trabecular meshwork, is in direct contact with endothelial lining of

Schlemm's canal. This layer does not form beams, but is formed by cells embedded in a dense ECM. An elastic fibre system has been identified in the juxtacanalicular tissue, appearing to play a role in support and distensibility (Hann and Fautsch, 2011). Increased resistance to aqueous humor outflow subsequently leads to elevated intraocular pressure, increasing the risk of glaucoma by excess pressure on the optic nerve head, conveying the importance of the trabecular meshwork.

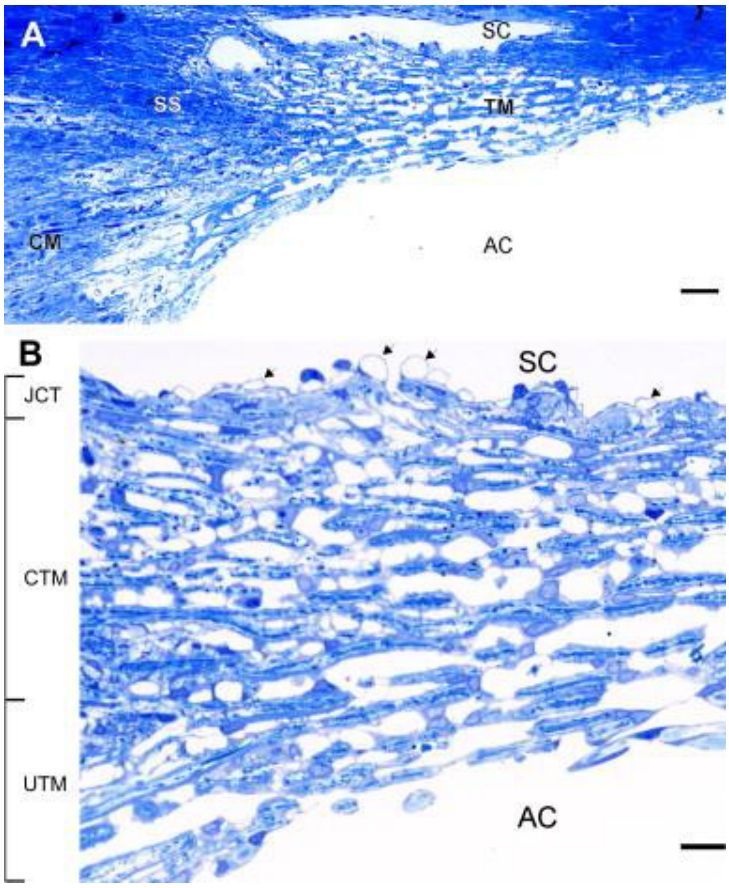


**Figure 1.20. Trabecular meshwork anatomy.** A: Schlemm's canal (SC) has two lumens separated by a septum. Trabecular meshwork (TM) is situated below SC, bound posteriorly by the scleral spur (SS) and ciliary muscle (CM). Below the TM is the anterior chamber (AC). B: higher magnification image shows the three regions of TM – uveal meshwork (UTM), corneoscleral meshwork (CTM) and juxtacanalicular tissue (JCT). Scale bar = 5µm. Taken from (Tamm, 2009).

### 1.7. Serial block face scanning electron microscopy

Transmission electron microscopy (TEM) is the most common technique used to study extracellular fibres such as collagen and elastic. Although this technique is useful to assess the formation of the fibres/fibrils, predominantly by measuring fibril diameter and viewing lamellae organisation, it has limitations such as being unable to measure fibril length, as well as an inability to view 3D organisation and tracking of long-range fibrils, which all determine tissue function (Starborg *et al.*, 2013). The use of serial-section TEM and electron tomography (rotating the angle of the sample and taking multiple images) enables 3D organisation to be viewed. Although these techniques have many advantages, they are technically challenging and time-consuming.

Denk and Horstmann (2004) developed a more time-efficient serial block-face scanning electron microscope (SBF SEM) (commercialised with the name Gatan 3view) that enables automated serial section electron microscopy. Specimens are stained with heavy metals, embedded into resin blocks and placed into the microscope – the block face is imaged by detection of back-scattered electrons before the built-in ultramictrotome removes that section and repeats to obtain a stack of up to 1000 aligned images. This technique has many advantages, with the main one being the ability to examine tissue/structures over substantial spatial volume, often hundreds of microns, whereas other 3D imaging techniques like tomography are limited to 300nm sections. Furthermore, SBF SEM was initially developed to study complex neuronal networks in the nervous system (Denk and Horstmann, 2004), making it ideal to examine fibrous networks in the cornea. Stacks of images obtained from the machine are analysed and reconstructed to form 3D model using imaging software.

This technique has currently been used to obtain 3D data from various tissues such as neuronal (Andres *et al.*, 2012), vascular (Rezakhaniha *et al.*, 2011) and more recently in the chick cornea to gain insights into development (Young *et al.*, 2014). Using this technique to study the cornea will enable a better understanding of the intricate architecture of the stroma as well as increasing our understanding of cell-matrix interaction and cell-cell communication. SBF SEM was the most frequently used technique in this thesis, obtaining important results for chapters 4, 5 and 6.

### 1.8. Aims and objectives

The overall hypothesis is that the corneal stroma immediately above Descemet's membrane (the "pre-Descemet layer") has different structural properties to the rest of the stroma. The aims of this thesis are therefore:

1. To use X-ray scattering to examine the hydrodynamic behaviour of the collagen within the corneal stroma in order to relate water distribution to structural changes.
2. To use the same methods to examine the collagen structure of the cornea as a function of depth, particularly focusing on the pre-Descemet layer.
3. To carry out an in-depth study of the elastic fibre distribution as a function of depth in the whole cornea, but focusing on the pre-Descemet layer.
4. To extend the above study to examine the distribution of elastic fibres in keratoconus.
5. To elucidate a functional role of the elastic fibre system using a mouse model for Marfan syndrome.

# Chapter 2 – General methods

## 2.1. SBF SEM

The following protocol was used to process samples of tissue for SBF SEM in all chapters, with the exception of chapter 5, where an additional processing protocol was developed and will be described at a later stage. All human tissue, other than the keratoconus buttons in chapter 5, was obtained from Bristol Eye Bank. Institutional Ethics Committee approval was obtained for these studies and the research followed the Tenets of the Declaration of Helsinki.

### *2.1.1. Fixation and staining*

Corneas were dissected into thin segments and immediately fixed in modified Karnovsky's fixative (2.5% glutaraldehyde and 2% paraformaldehyde (PFA) in 0.1M cacodylate buffer at 7.2 pH) for 3 hours (Morris, 1965). The use of glutaraldehyde as well as PFA ensures rapid and complete penetration of the fixative into the tissue. Initial fixation is halted by washing the tissue in sodium cacodylate buffer for 3 x10mins. Secondary fixation was carried out with 1% osmium tetroxide for 1 hour, a heavy metal that primarily reacts with lipid moieties, specifically oxidising unsaturated bonds of fatty acids: as well as being a fixative, osmium tetroxide provides additional contrast to the tissue and acts as a mordant, enhancing lead staining that occurs later in the protocol. After a wash in distilled water to remove all of the fixative, samples were stained with 0.5% tannic acid in distilled water for 2 hours due to slow penetration into the tissue. Tannic acid is a polyphenol, primarily used to enhance collagen staining contrast, in combination with uranyl acetate. Following a further wash in distilled water for 30 mins, samples were placed into 2% aqueous uranyl acetate in the dark overnight. Uranyl acetate provides images contrast as uranyl ions bind to proteins and lipids with sialic acid carboxyl groups.

The following day, corneal samples were dehydrated in a graded ethanol series: 70%, 90%, 100% x2 ethanol concentration for 20 minutes each. Further tissue contrast was provided with the use of 2% uranyl acetate in 100% ethanol for 1 hour, before being thoroughly

washed with 100% ethanol for 20 minutes and placed into a 1:1 mixture of ethanol and acetone for 30 minutes with multiple changes. The tissue was stained with filtered lead acetate* for 2 hours (Kushida, 1966), finishing with a final 30 minutes wash in 100% acetone.

*Preparation of lead acetate – lead acetate added in excess to 25ml of 100 ethyl alcohol. The mixture is shaken for ~10minutes and an equal volume of 100% acetone in then added. Mixture is shaken for another 10 minutes, filtered and used immediately.

Heavy metal staining is a vital part of the staining process as it provides images contrast. This works because scattering of electrons is dependent on the charge of the atomic nucleus, therefore, backscattered electron signal is stronger from structures stained with heavy metals, providing a clear distinction from unstained structures. Moreover, a lot of heavy metal staining is needed as SBF SEM does not allow contrast enhancement after cutting, a process that is carried out with TEM samples, meaning that all of the staining must occur *en bloc*. The tannic acid-based staining method used throughout this thesis was developed in order to stain elastic fibres as well as collagen, and was based on previous TEM protocols (Simmons and Avery, 1980, Kageyama *et al.*, 1985).

### *2.1.2. Embedding in resin*

120ml of araldite CY 212 epoxy resin was mixed with 132ml of DDSA. 30ml of this mixture was added to 30ml of acetone and the rest was set aside. The samples were left in the 1:1 resin acetone mixture overnight. The following morning, 3.3ml of BDMA hardener was added to the remaining resin mixture. Samples were left in this all day, with 6 resin changes spaced out throughout the day. On the final day, specimens were embedded into a mould using fresh resin, where they were aligned before being polymerised in an oven at 60°C for around 48hours.

*2.1.3. 3view SEM (data acquisition)*

Once polymerised (Fig. 2.1A), a block of choice is removed from the mould and cut to form a ~1-2mm cube from a region of interest, which is subsequently super-glued onto a Gatan specimen pin (Fig. 2.1B) for 2 hours, before being further stabilised by applying adhesive conductive silver epoxy resin that is left to set overnight. The block is then trimmed using a razor blade on the upper surface to reveal the specimen and create a cutting surface (polished using a glass knife), and also trimmed around the side faces at ~90 degrees to reduce the size of the block. Semi-thin sections (0.25µm) are often cut, picked up using a glass slide, and visualized under the light microscope (stained with toluidine blue) in order to determine the orientation of the specimen. The specimen block is then cut down even further with a razor blade, leaving the area of interest. All of the above procedures are carried out on a Leica Ultracut5 ultra-microtome.

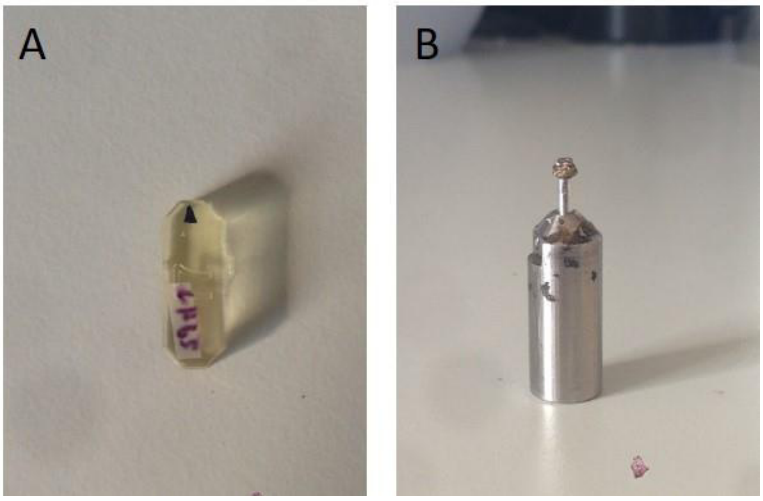


**Figure 2.1. SBF SEM sample preparation**. Processed corneal sample embedded in resin (left). Samples are triangular in shape, where the tip represents central cornea, and the base is peripheral cornea. A small area of interest is cut away and trimmed down using a hacksaw and a razor blade before being super glued onto a Gatan specimen pin (right), which is further stabilised with application of conductive resin around the edges.

Before entering the SEM, the specimen block is given a 5nm thick gold coat (Leica EM ACE 200) to give it a conductive surface and prevent charging of electrons around the edge of the block. The block is placed into the microscope (Zeiss Sigma VP FEG SEM equipped with Gatan 3view2 system), the diamond knife is aligned with block surface and cutting ranges are set before 200 micron thick sections are cut from the imaging surface to remove the gold. Gatan Digital Micrograph software is used to visualize the surface of the block and focus on a region of interest before the system is set to scan and cut. Data sets of up to 1000 images (.dm4 format) were obtained every 50nm of tissue, with each image usually acquired using ~5.16k magnification, 4k x 4k pixels, 4nm pixel resolution, 8microsecond dwell time, and using an accelerated voltage of 3.4 keV in low vacuum variable pressure mode (~28 Pa), unless stated otherwise. By maintaining a low charge of gas in the chamber, ions are provided to neutralise charge on the sample. It was found that 3.2 – 3.4 keV accelerated voltage was optimal to provide good backscattered electron signal with no heating effects such as burning of the resin and shrinkage. SBF SEM setup up and a schematic representation of how the system work is shown in Figure 2.2.

## *2.2.* Data Analysis

### *2.2.1. 3D reconstruction*

All 3D reconstructions were generated using Amira 6 software (FEI, Mérignac, France). Data sets were first converted to .TIF format from .dm4 (Gatan digital micrograph software) before being resampled from 4k x 4k resolution (Fig. 2.3a) to 512 x 512 pixels (Fig. 2.3b) to better match the resolution of the PC monitor. Further noise reduction could be provided by using a non-local means filter (Fig. 2.3c) to enhance contrast and enable a smoother rendering process.

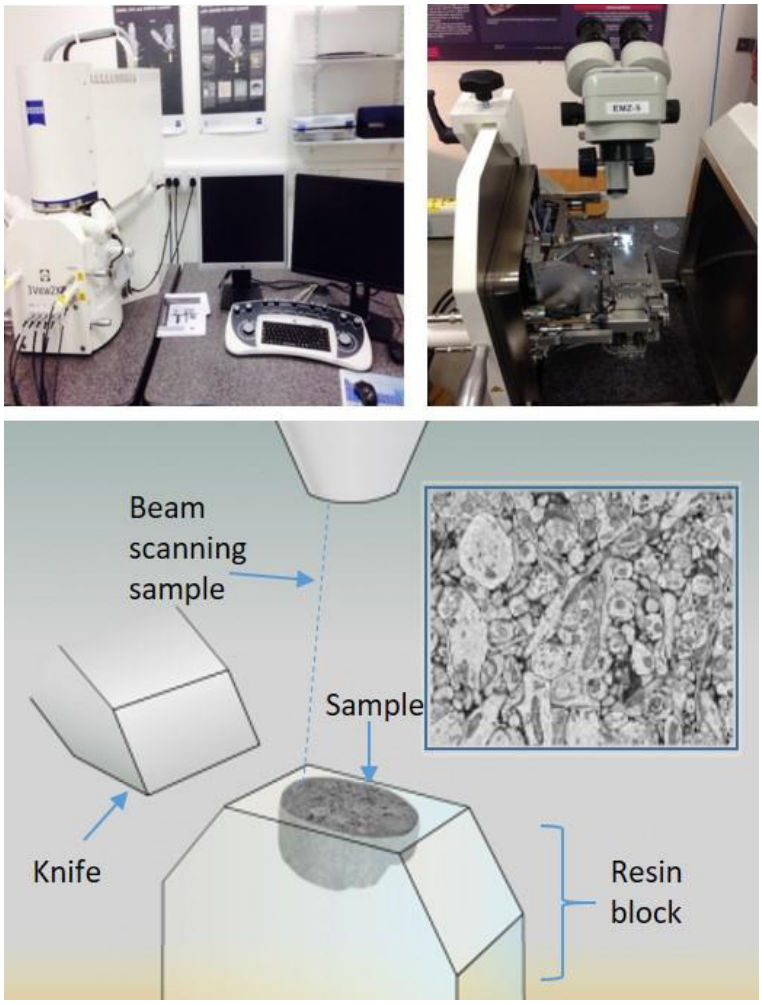


**Figure 2.2.SBF SEM setup.** The top two images show the Gatan 3view SBF SEM setup from outside and inside the machine. The bottom schematic diagram illustrates how the system works: stained samples are embedded into a resin block with the imaging surface polished before entering the machine. An electron beam then scans the surface, resulting in the formation of an image (blue inset) by back scatter of electrons, before the diamond knife cuts away the surface and the process is repeated to obtain a stack of images. Bottom image obtained from a video found at: *http://www.gatan.com/products/sem-imaging-spectroscopy/3view-system– accessed 20/10/2016*

Elastic fibres were rendered using a mixture of automated, semi-automated, and manual segmentation threshold segmentation. Structures that back scattered more electrons when the surface of the block was scanned with the beam are seen as darker features. An iso-surface automated rendering tool is used on the data set to show these dark structures in three-dimensions, where the threshold is manually adjusted to an appropriate level that segments the fibres with little background noise (Fig. 2.4a). As well as segmenting elastic fibres, the iso-surface tool segments other structures with the same contrast levels such as Descemet's membrane and keratocytes. Therefore, the next step is to create a label field (Fig. 2.4b), where the pixels that these structures consist of are highlighted and labelled with different colours using semi-automated segmentation, as unwanted pixels are removed. By using the surface generator tool, the highlighted pixels are transformed into 3D structures that are subsequently overlaid onto the original iso-surface (Fig. 2.4c). In data sets that produced poor contrast, certain structures were segmented by manually tracing around their edges. A consistent colour theme for each structure has been maintained throughout: gold = elastic fibres, blue = Descemet's membrane, pink/purple = keratocytes, green = trabecular meshwork.

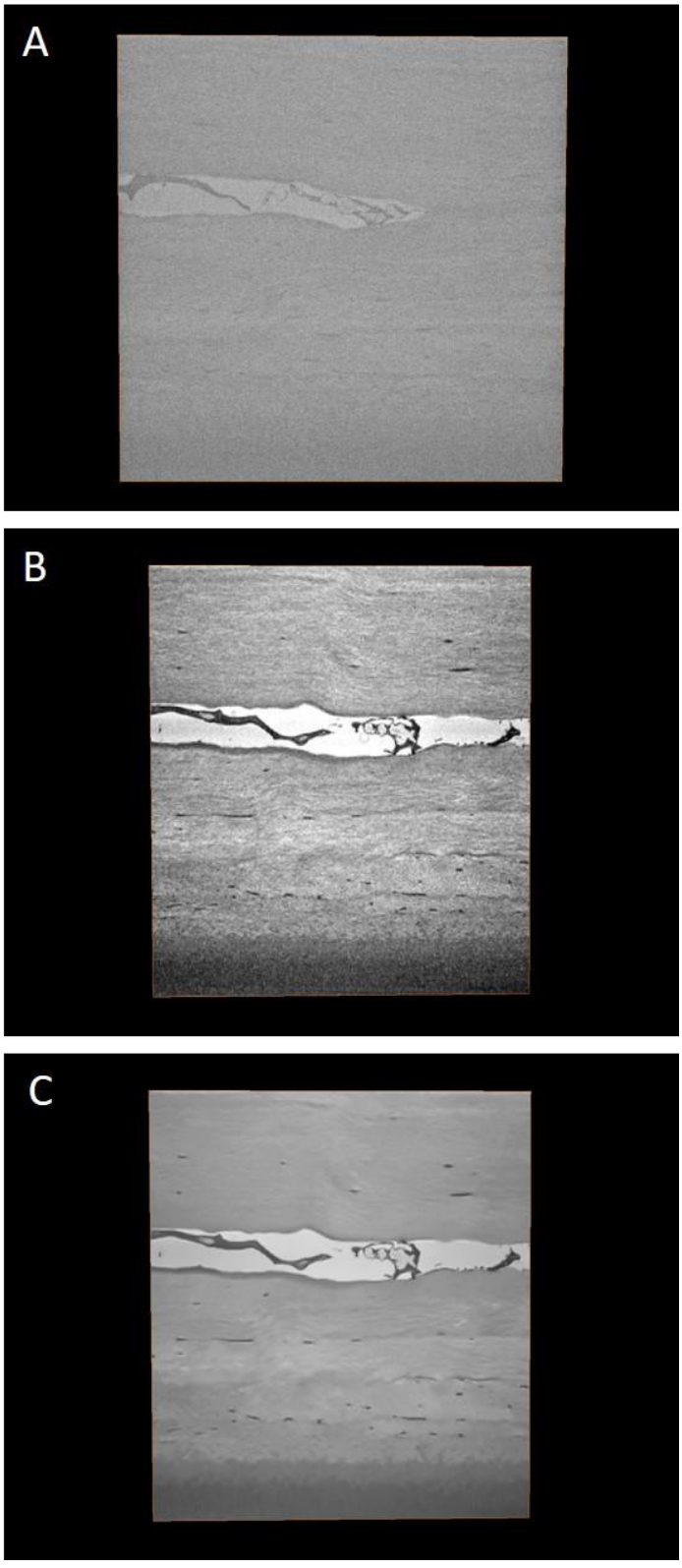


**Figure 2.3. Re-sampling and filtering of SBF SEM data.** All images in this figure represent one image from a large data set. 3view images are initially collected at 4k x 4k pixel resolution (A) before being re-sampled to 512 x 512 resolution, making the images a lot clearer (B). Darkly stained structures caused by higher backscattered electron signal can be further highlighted by using a non-local means filter to reduce background noise caused by other features such as lamellae (C). Although image B provides better resolution, using the filter provides a better quality reconstruction of the dark structures of interest.

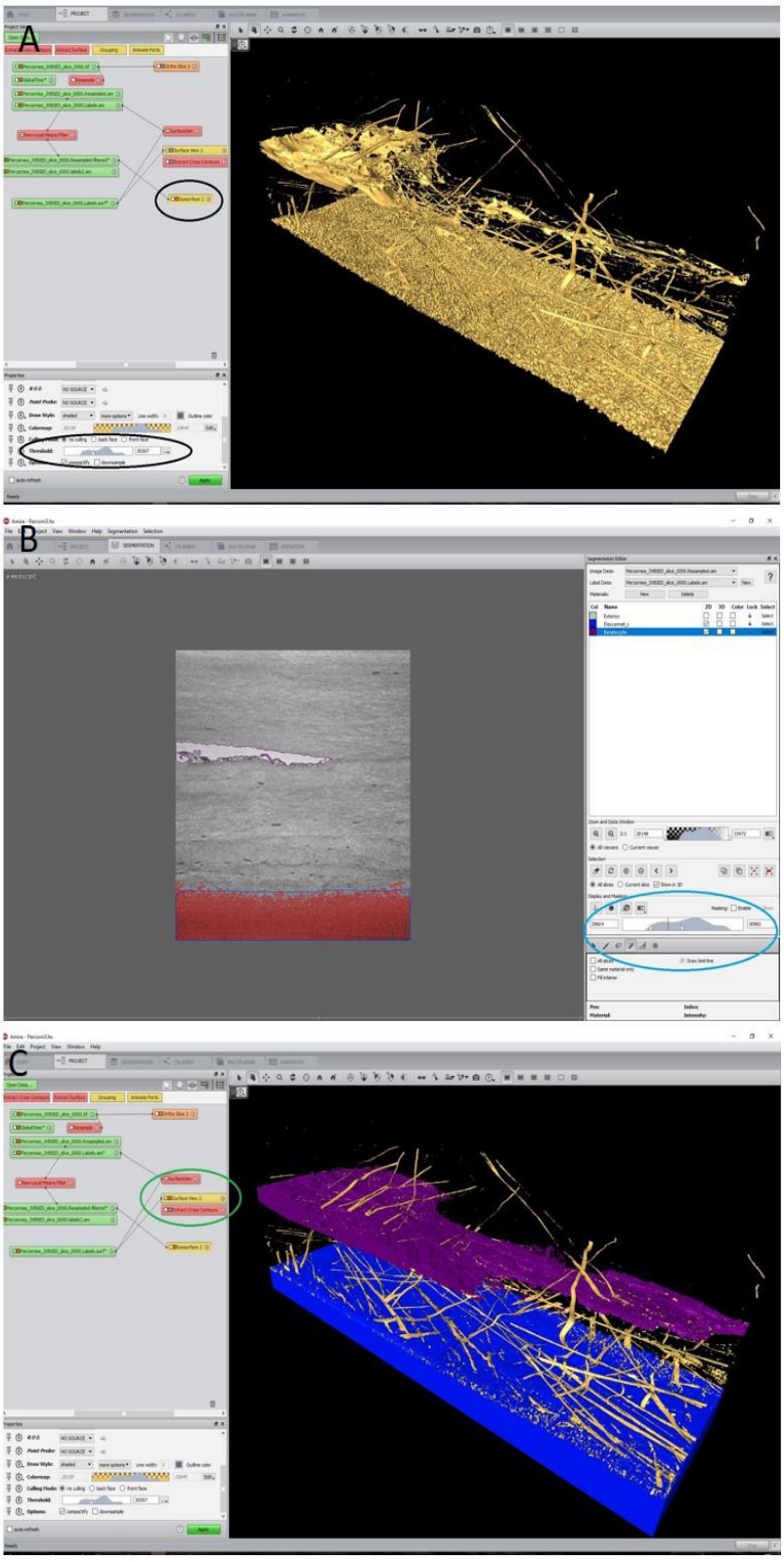


**Figure 2.4. Automated and semi-automated thresholding using Amira 6**. Dark features are automatically rendered using the iso-surface tool (A) manually selecting an appropriate threshold levels (black oval). Different features can be separately labelled with different colours using a label field (B) based on automated thresholding (blue oval) as well as manual selection of pixels. A surface generator (C) (green oval) reconstructs these selected pixels, which are subsequently overlaid onto the original iso-surface.

*2.2.2. Elastic fibre quantification*

Full thickness elastic fibres quantification was carried out on central and peripheral human cornea in chapter 4, and central mouse cornea in chapter 6. Each cornea was imaged (30 x 30 µm area) en face every 50nm from epithelium to Descemet's membrane, at 2k x 2k resolution, obtaining ~20,000 images for the human cornea, and ~2,600 from the significantly thinner mouse cornea. Human data was split into sets of 1000 images, and mouse split into sets of 250 images, before being analysed using Amira6 with XImagePAQ extension. For each set of images, elastic fibres were selected using interactive top-hat segmentation tool, where the selected number of voxels were subsequently converted to percentage elastic fibres using the total volume voxel count. A more detailed quantification was carried out in the human cornea for the first 1000 images (50µm of tissue) above Descemet's membrane, by measuring fibre volume every 200 images. When analysing the data, it was evident that the cornea samples were not being cut directly parallel to the surface resulting in an oblique cutting angle. Theoretically, when scrolling through a series of images, the transition from Descemet's membrane to stroma should occur instantly, however, this was not the case. The actual number of images taken for this transition were counted and used to make a geometrical calculation of the offset angle (appendix 1), given that slice thickness and imaging area are known parameters. This subsequently led to a correction of the depth measurements when plotted against percentage of fibres, with an uncertainty of ± 5 µm in each depth measurement.

**2.3. TEM**

As cornea samples processed for SBF SEM were en bloc stained with heavy metals, ultra-thin sections cut from these blocks could also be used for TEM. 90nm gold sections were cut using on a Leica UC6 ultra-microtome with a diamond knife, floated on distilled water, stretched out using chloroform, and picked up with copper hex grids. Sections were left to dry for 24 hours before being viewed with a JEOL 1010 TEM with a 80kv voltage. Images were acquired with a Gatan Orius camera.

## 2.4. X-ray diffraction analysis

Small-angle X-ray scattering (SAXS) patterns relate to the arrangement of the regularly spaced and uniform diameter collagen fibrils within lamellae, whereas wide-angle X-ray scattering (WAXS) patterns give us information on the orientation and distribution of individual molecules that make up the fibrils. Collection of both SAXS and WAXS data is described in Chapter 3. X-ray All SAXS patterns were analysed using MATLAB (MathsWork, UK) with integrated SAXS4COLL software. Firstly, the images are centred using the diffraction pattern obtained from powdered silver behanate. This is done by manually selecting 7 points around the circumference of one of the diffraction rings (Fig. 2.5a), after which, the X and Y coordinates are recorded. Patterns are then calibrated against the known 67nm D-periodicity of hydrated rat tail tendon. To do this, the peak of the first order meridional reflection is selected (Fig. 2.5B), obtaining a pixel value, which is input into the calibration input box alongside the 67nm first order.

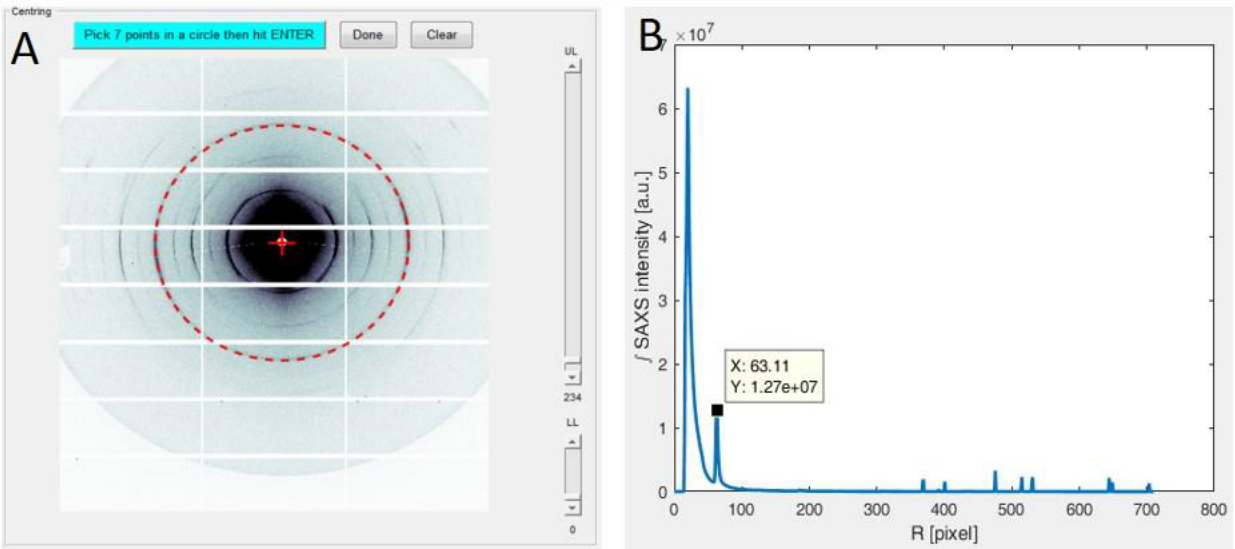


**Figure 2.5. SAXS4COLL image centring and calibration**. Diffraction rings of silver behenate are used to find the centre point by selecting seven points around one of the rings (A). Images are calibrated by selecting the peak arising from the first order of collagen in rat tail tendon (B).

The software calibrates the image by converting radial distance in pixels into reciprocal space with the use of Bragg's law:

$$n\lambda = 2dsin\theta$$ Equation 1

Where,

n = order of reflection

λ = wavelength of radiation

θ = half the angle between incident X-ray beam and reflection

d = Bragg spacing

In order to find Bragg spacing (d), a value for θ must be calculated. This is done by firstly determining the distance from the specimen to the detector (detector distance) (Fig. 2.6). For example, using the third order meridional reflection from rat tail tendon, the following parameters are known: D-periodicity = 67nm, n = 3, λ = 0.1nm, which are used in equation 1 to find θ. This is then used to calculate detector distance using equation 2. As the detector distance is now known, θ can be calculated from unknown X-ray scatter patterns and subsequently used to determine Bragg spacing using equation 1.

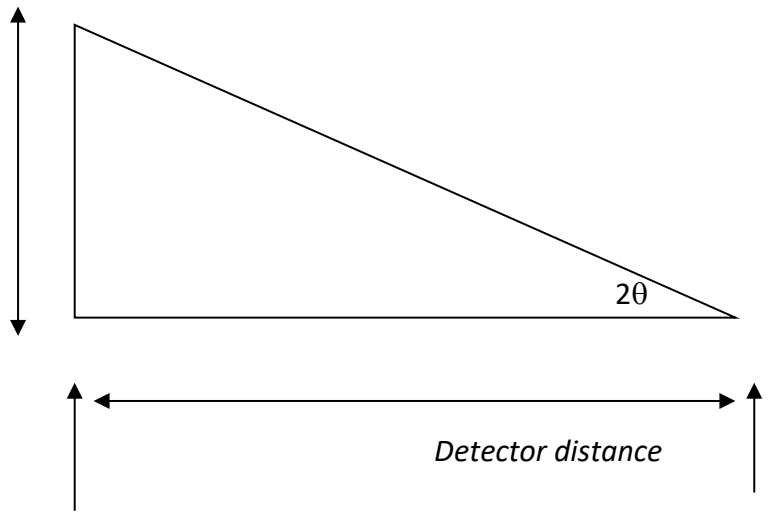


**Figure 2.6. Calculation of detector distance.**

$$\text{Detector distance} = \frac{\text{radius of calibrated reflection (r)}}{\tan 2\theta}$$ Equation 2

The intensity of the SAXS pattern from the cornea is the product of an interference function (arising from the ordering of the collagen fibrils) and a so-called "fibril transform" represented by a Bessel function (which is the scatter form each uniform diameter collagen fibril), all superimposed on background scatter from non-collagenous components of the cornea (Meek and Quantock, 2001). The software allows removal of the background scatter followed by separation of the interference function and the fibril transform, from which the average interfibrillar spacing and fibril diameter can be respectively calculated as follows

After calibration, a SAXS pattern is loaded up and is automatically radially integrated before being presented as a double logarithmic plot (Fig. 2.7a). Residual background scatter is then removed by interactively fitting a power function to the data as accurately as possible selecting 3 points (Fig 2.7a). From the background subtracted SAXS signal, the collagen equatorial interference function peak is manually identified by clicking close to the peak (Fig 2.7b), after which the closest peak is automatically detected by the software. This is then used to calculate the lattice spacing d, which here represents the interfibrillar Bragg spacing. Following this, the fibril transform, which produces a low, broad peak near the third order of collagen, needs to be manually fitted with the Bessel function using the slider bars (Fig 2.7c), in order to calculate average collagen fibril diameter. Finally, selecting the third order meridional peak (Fig. 2.7c) results in calculation of D-periodicity.

The WAXS pattern from the intermolecular ordering within each fibril is shown in Figure 2.8A. The analysis of the pattern involved calibration of the system using calcite, a linear background removal (Fig. 2.8B) and then the application of Bragg's Law (equation 1) to determine the lattice spacing (in this case the intermolecular Bragg spacing).

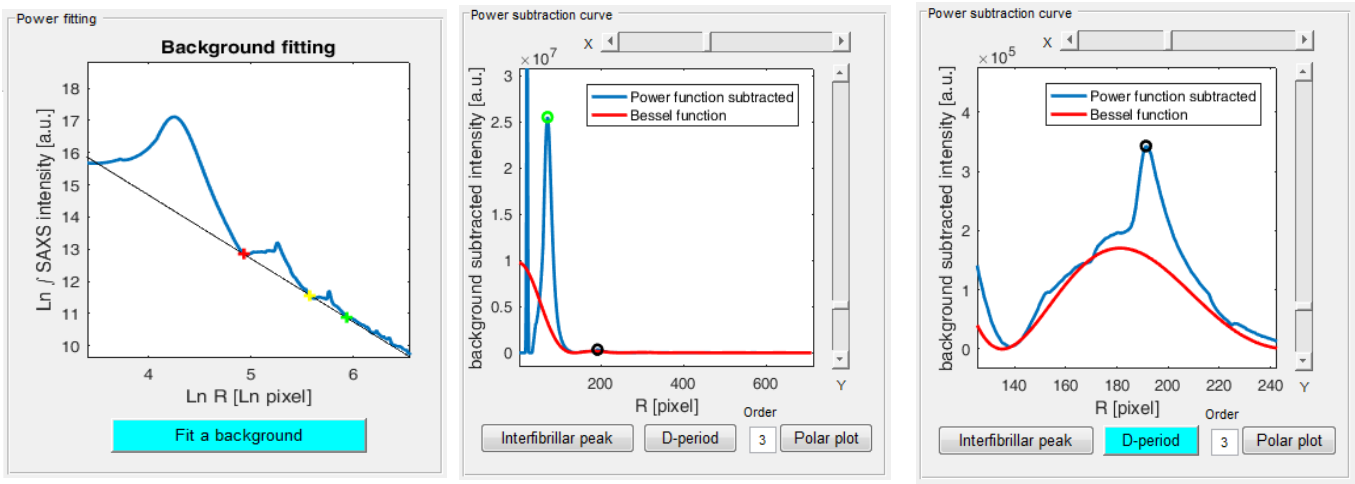


**Figure 2.7. SAXS pattern analysis**. Three points are manually selected to fit a power function (A). Once background scatter is subtracted (B), interfibrillar peak is selected to calculate IFS (green circle) before zooming in to select the peak arising from the third order of collagen for D-periodicity calculation (C) (black circle). Fitting of the Bessel function (C) (red line) gives fibril diameter readings. R = radial distance from the centre of the pattern

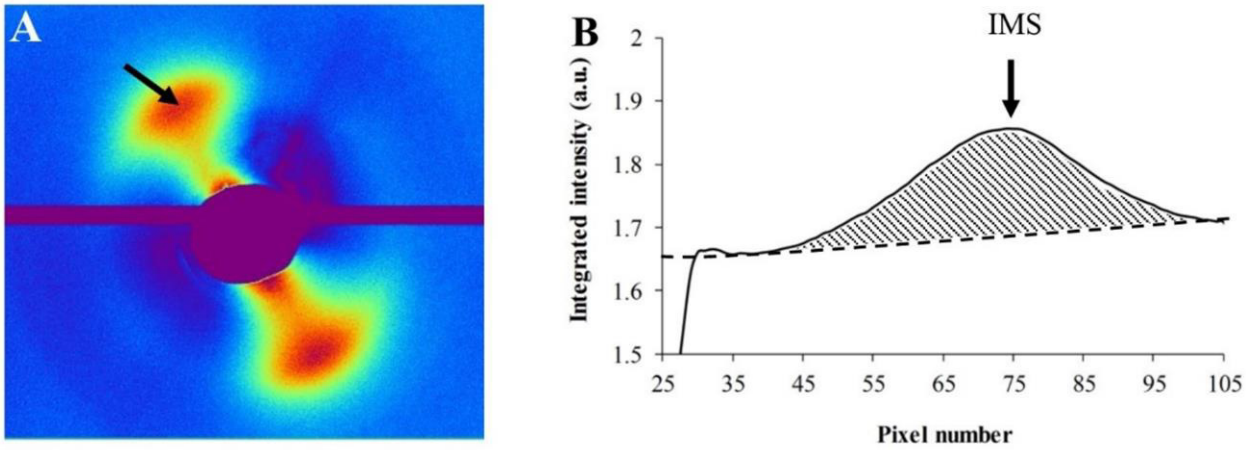


**Figure 2.8. WAXS analysis**. A: corneal WAXS pattern with collagen intermolecular peak (arrow). B: Circumferentially-integrated radial profile (solid line) with background function (broken line) fitted. The shaded region represents scatter from molecular collagen within fibrils. Once calibrated, the background-subtracted peak position (arrow) gives a measure of the average collagen IMS.

# Chapter 3 - X-ray diffraction studies of the corneal stroma

## 3.1. Introduction

The intrinsic properties of the cornea are largely governed by the unique architecture of the stroma, occupying 90% of the total corneal thickness and comprising of approximately 200-300 stacked lamellae. It is the precise organisation of collagen fibrils within the lamellae that imbues the cornea with strength and resiliency to resist external forces whilst simultaneously maintaining transparency. Electron microscopy has been invaluable in increasing our understanding of stromal ultrastructure (Komai and Ushiki, 1991, Radner *et al.*, 1998a), however, this technique only provides qualitative and localised information. X-ray diffraction is a non-invasive technique that can give us quantitative data regarding the organisation of collagen fibrils in the cornea. When X-rays pass through the cornea, the high degree of regularity in the spatial distribution of collagen leads to interference of scattered waves in certain directions; the resulting scatter pattern is recorded on a detector behind the specimen. SAXS patterns relate to the arrangement of the regularly spaced and uniform diameter collagen fibrils within lamellae, whereas WAXS patterns give us information on the orientation and distribution of individual molecules that make up the fibrils. Furthermore, X-ray diffraction provides quantitative data throughout the whole thickness of the cornea, so numerical values obtained represent an average across the full thickness of stroma, without the need of any prior tissue processing (chemical fixation and dehydration) that may ultimately disrupt the native structure of the tissue.

WAXS patterns, consisting of a single pair of equatorial reflections (perpendicular to the collagen fibril axis), arise from the average lateral spacing between adjacent collagen molecules within fibrils. Analysis of WAXS patterns has told us that, in the hydrated cornea, the spacing between these molecules is about 1.6 nm (Meek *et al.*, 1991), and that collagen molecules, and hence fibrils, and therefore lamellae, are predominantly aligned in the superior-inferior and nasal-temporal directions in the central and posterior stroma (Aghamohammadzadeh *et al.*, 2004, Meek and Newton, 1999, Abahussin *et al.*, 2009), with the orientation becoming circumferential in the corneo-limbal region (Newton and Meek, 1998a, Meek and Newton, 1999, Newton and Meek, 1998b). SAXS patterns consist of

equatorial and meridional (parallel to the fibrillar axis) reflections. Analysis of SAXS equatorial patterns, arising from regular lateral spacing of collagen fibrils, yields information on diameter and the centre-centre separation of collagen fibrils, whereas meridional patterns consist of a series of reflections, produced from the 65 nm D-periodic repeat along the fibril axis (Meek *et al.*, 1981). The interfibrillar spacing in human hydrated cornea is ~ 65 nm (Meek *et al.*, 1991), whereas collagen fibril diameter is around 31-34nm in the central cornea, varying with age (Daxer *et al.*, 1998, Meek and Leonard, 1993) and increasing at the limbus (Boote *et al.*, 2011). Small-angle and wide-angle X-ray scattering in the cornea is schematically represented in Figure 3.1.

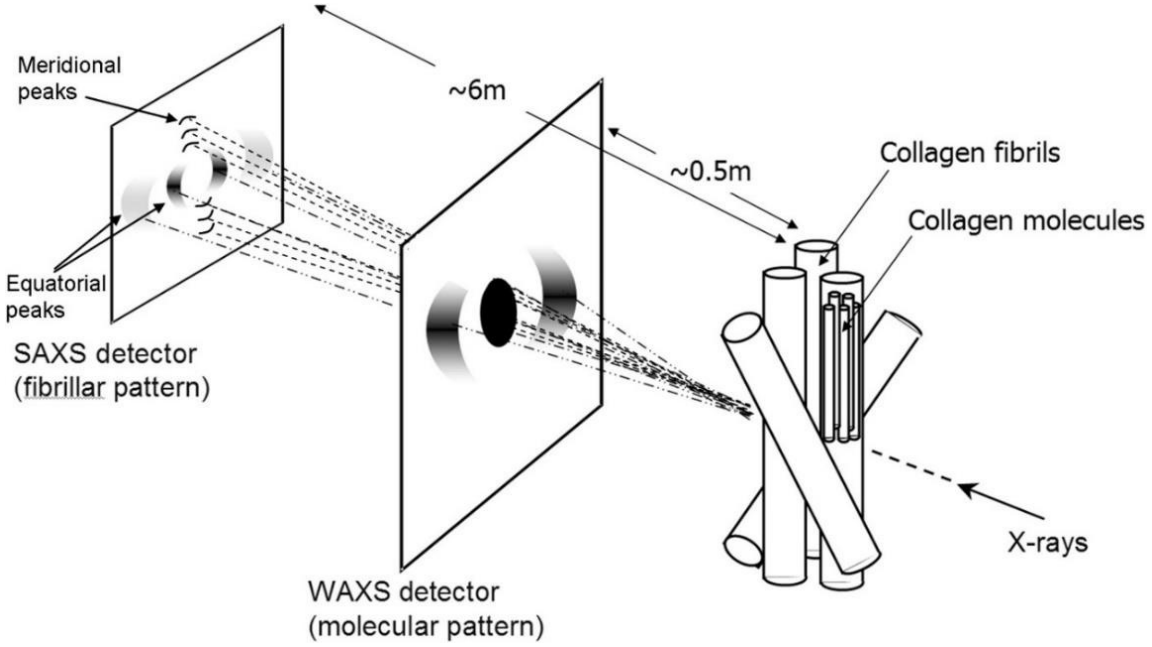


**Figure 3.1. X-ray scattering in the cornea**. When X-rays pass through the cornea, the lateral spacing between collagen molecules within the fibril produce WAXS patterns. On the other hand, the regularly spaced collagen fibrils produce a SAXS equatorial pattern, yielding information on the centre-centre spacing and fibril diameter, in addition to a series of meridional reflections arising from the 65nm D-periodicity along the axis of corneal fibrils. SAXS and WAXS patters are produced simultaneously, with the position of the detector determining which is recorded. Figure taken from (Quantock *et al*., 2015).

Normal physiological and biophysical function of the cornea depends on appropriate hydration levels within the stromal extrafibrillar matrix and within the collagen fibrils themselves, because as the cornea swells, transparency is lost and light scattering increases, subsequently impairing vision (Hodson, 1997, Elliott and Hodson, 1998). SAXS and neutron diffraction has previously been used to demonstrate that when the cornea swells, interfibrillar space increases, hence fibrils and molecules are moving apart laterally, and that there is a linear relationship between the square of collagen interfibrillar spacing (IFS) and hydration, as fibrils can only move apart in a plane perpendicular to the fibril axis (Goodfellow *et al.*, 1978, Sayers *et al.*, 1982, Elliott *et al.*, 1982). Furthermore, when the cornea swells, the D-period remains constant, indicating that the fibres do not swell along their axis (Huang and Meek, 1999). Using neutron diffraction on highly hydrated corneas, Elliott *et al.* (1982) suggested that the swollen cornea is a system of mutually repelling cylinders, expanding uniformly to fill the space made available by water.

Meek *et al.* (1991) carried out a more in depth X-ray diffraction study to measure the effect of hydration on intermolecular and interfibrillar spacings of collagen in bovine cornea. Inter-molecular spacing (IMS) (and therefore fibril diameter) increased with hydration in the dry cornea, up to physiological hydration (H = 3.2) (hydration is defined as the weight of water/ dry weight of the cornea), with very little change after. On the other hand, SAXS measurements showed that IFS continued to rise with increasing hydrations above physiological value, confirming the linear relationship between the two variables. At H=0, the IFS would have been 34nm, which is less than the diameter of hydrated bovine cornea fibrils (38nm) (Meek and Leonard, 1993), indicating that the collagen fibrils may reduce in diameter during drying. Additionally, the surfaces of fibrils remained in contact until hydration was reduced to H=1, suggesting that initially water is distributed between and within fibrils equally, and then after that absorbed by the surrounding matrix, potentially because intermolecular bonds are fully extended when the cornea is at 50% hydration (Meek et al., 1991). A similar two-stage process was described by Fratzl and Daxer (1993) where air drying of human cornea resulted in only IFS dehydrating at physiological hydration, whilst maintaining constant fibril diameter, followed by water being lost from the fibrils themselves at H=1.

Fullwood *et al.* (1992) used X-ray diffraction to compare collagen interfibrillar and intermolecular spacings in normal and keratoconus corneas, at a range of different hydrations (H 1-11). It was discovered that there was no difference in IFS, but intermolecular spacing was significantly lower in keratoconus corneas at normal physiological hydration and over a range of hydrations. Overall, results from these hydration studies has enabled the effects of swelling on refractive indices, and therefore light scattering, of collagen fibrils and interfibrillar matrix to be calculated (Meek *et al.*, 2003).

The primary aim of the first part of this study were to quantify and compare the relationship between corneal structure and hydration in human and porcine eyes with the use of X-ray diffraction, in order to further understand the effects of hydration on collagen organisation and hence tissue function. Both human and pig corneas were used because the original aim was to examine the whole stroma, whilst concentrating on the pre-Descemet layer in both species. X-ray diffraction has shown that significant collagen structural changes occur in the corneal stroma after processing tissue for TEM (Fullwood and Meek, 1993). These changes primarily occur as the tissue is dehydrated, therefore, as future chapters in this thesis will involve a substantial amount of electron microscopy to study corneal ultrastructure, it was deemed important to characterise the effects of dehydration, and therefore, this was a secondary aim of part 1 of the study. In the second part of this study, SAXS was used to calculate the IFS and fibril diameter throughout the entire depth of the human corneal stroma, specifically looking for differences in the pre-Descemet's layer (see 1.1.6). Findings from part 1 of the study may also be applied to this, as the parameters being measured are dependent on stromal hydration, which varies between tissue samples. Pig corneas were not used for this part of the study because, during the course of the work, it was found that a pre-Descemet layer could not easily be separated in this species (A. Mukherjee and D. O'Brart, personal communications).

## 3.2. Methods

### *3.2.1. Sample preparation*

*Part 1*

A total of 28 post-mortem human corneo-scleral discs were obtained from Bristol Eye Bank, and 50 porcine eyes from a local abattoir. The epithelium and endothelium were removed from each human cornea before a 6mm button was taken from the centre. The anterior segment of the porcine eyes was dissected using a razor blade, followed by removal of the lens and iris, and 6mm corneal button taken. Each corneal button was weighed before being placed into dialysis tubing (12-14kDA molecular cut off), which had been prepared by soaking in 1% acetic acid for 1 hour, rinsed in $dH_2O$, soaked in 1% sodium carbonate solution with 10mM EDTA for 30 minutes at 75°C, and heated in $dH_2O$ at 75°C for 30 minutes. All air bubbles were removed from the dialysis tubing containing corneal buttons before being placed into a solution of poly-ethylene glycol (PEG) (20,000 molecular weight) in 0.9% saline (made up using sodium chloride and HEPES (N-2-hydroxyethylpiperazine-N'-2-ethanesulfonic acid) adjusted to pH 7.4 using sodium hydroxide) at various concentrations ranging from 1-30% PEG to obtain a range of different hydration levels. The samples were left to equilibrate for 2 days at 4°C.

*Part 2*

Three whole eye globes were perfusion fixed with 4% PFA for three hours. By using this method to inflate the globes to intraocular pressure before fixation, the corneas should closer to physiological hydration. Globe 1 was from an 85 year old male (left eye), globe 2 was from an 88 year old female (right eye), and globe 3 was from a 78 year old male (right eye). Corneas were dissected from each globe and cut into thin strips of tissue that were about 1.5cm in width. All of the strips were cut simultaneously using a device consisting of a series of razor blades, each separated by ~1.5cm intervals. The edges of strips were cut using a Microm HM 440 E sliding microtome to obtain transverse sections. Strips of tissue were placed onto the cutting block, covered with distilled water and left to freeze. Transverse sections 160µm and 250µm in thickness were cut from strips obtained from all 3 corneas, placed into a tube containing 4% PFA and stored at 4°C.

*3.2.2. Data collection*

*Part 1*

SAXS patterns were recorded on beamline I22 (Diamond Light Source, UK) from the centre of 26 of the porcine and 14 of the human pre-equilibrated corneal buttons. Corneal samples were removed from the dialysis tubing, weighed, and to prevent drying, immediately tightly wrapped in cling film and placed into an airtight Perspex sample holder enclosed between two sheets of Mylar, before exposure to X-rays. Samples were subjected to a 2 second exposure to an X-ray beam measuring 200 x 200 µm with a wavelength of 1Å.

The remaining 24 porcine and 14 human corneas were examined with WAXS, using beamline I02 (Diamond Light Source, UK). These samples were prepared in the same way as described above for SAXS data collection. A single diffraction pattern was obtained from the centre of each corneal button, with 0.5 - 1second exposure to an X-ray beam measuring 80 µm vertically by 100 µm horizontally, with a wavelength of 1Å.

Following the collection of scatter patterns, samples were wrapped in tinfoil, placed in a 60°C oven for 72 hours to completely dry, and then weighed for a final time. Hydration was specified by the parameter H, which was calculated by using the following:

$$\text{Hydration (H)} = \left(\frac{Wet\ weight - Dry\ Weight}{Dry\ Weight}\right)$$

*Part 2*

SAXS patterns were recorded at the ESRF (Grenoble, France), with an X-ray micro beam measuring 8 x 8µm and a wavelength of 0.94Å. Corneal strips were placed inside an airtight Perspex sample holder enclosed between two sheets of Mylar (Fig. 3.2). The strips were orientated vertically, with the cut edge perpendicular to the incident beam direction, meaning that the full thickness of the tissue (i.e. all layers) was visible for data collection. A series of 8 scans were obtained through central corneal strips at 0.5 µm intervals, with each

line of the scan running anterior to posterior at 10 µm sequential steps with 0.03 second exposure, traversing the entire thickness. In peripheral regions, a series of 6 scans were obtained at 0.5 µm intervals, starting at the limbus and ending 3mm into the cornea, at 10 µm sequential steps and 0.04 second exposure within each scan running from the anterior to the posterior edge.

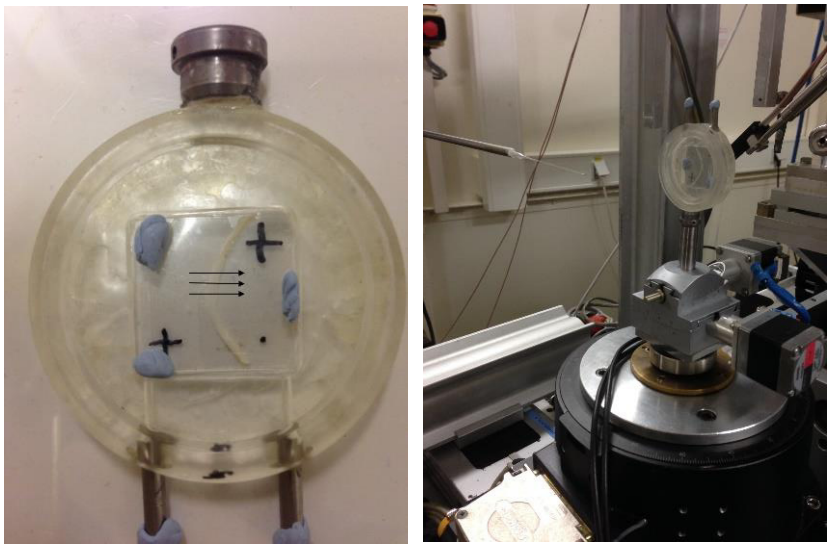

**Figure 3.2. SAXS setup**. A corneal strip inside the sample holder (left) where the black lines indicate the scan direction from anterior to posterior. 6-8 scans were obtained from each strip when the sample holder was positioned in front of the beam (right).

### *3.2.3. Data analysis*

*SAXS*

SAXS patterns were obtained at the Diamond synchrotron Didcot, Oxfordshire (Part 1) or at the ESRF synchrotron, Grenoble (Part 2). The patterns were analysed using MATLAB (MathsWorks, UK) with an integrated software tool designed for analysing fibrous collagen-based tissues (SAXS4COLL) as described in section 2.4. SAXS patterns from part 1 of the study were calibrated against hydrated rat tail tendon (67 nm D-periodicity), whereas patterns from part 2 were calibrated against the 5.8nm lattice reflection from silver behenate. All IFS results in this study will be reported as Bragg spacings. This can be

converted to actual IFS using a multiplication factor of 1.12, based on the assumption that the cornea has a liquid-like packing arrangement (Worthington and Inouye, 1985).

*WAXS*

Bragg intermolecular spacing of collagen was calculated with MATLAB software by measuring the distance from the centre of the scattering pattern to the intermolecular reflection and calibrating it against the 0.304nm reflection of powdered calcite.

## ***3.3.*** **Results**

### *3.3.1. Part 1*

The relationship between $IFS^2$ and hydration for both porcine and human cornea can be seen in Figure 3.3. $IFS^2$ increased linearly with hydration for both human and porcine corneas (Fig. 3.3). The lowest hydration reached was H= 0.5 - 0.6. Using the linear trend line equation displayed on the graph, the centre-to-centre fibril spacing when the cornea is dry at H=0 is estimated as 37.8 nm for porcine, and 26.8nm for human corneas. It is assumed that when H = 0, all water is removed from the tissue and therefore, IFS corresponds to the dry fibril diameter as the fibril surfaces are in contact (Sayers *et al.*, 1982). However, taking into account the coating of proteoglycans surrounding fibrils (Fratzl and Daxer, 1993), the true dry fibril diameter value is likely to be lower. It is necessary to extrapolate the trend line back to 0 as, when the fibrils touch (which is above the point when the tissue is dry), the interference pattern disappears, meaning it is not possible to measure IFS.

In contrast, fibril diameter versus hydration, seen in Figure 3.4, showed a non-linear, bi-phasic trend, increasing up to hydration in the region of H = 2, with minimal change thereafter (Fig. 3.4). There are critical gaps in the human data from hydrations 1.9 – 2.5, making it difficult to determine exactly where fibril diameter stops increasing. Porcine corneas reached a greater final fibril diameter compared to human. Diameters in the dry human cornea were around 25-26nm, which is consistent with TEM measurements (Komai and Ushiki, 1991, Akhtar *et al.*, 2008), where the cornea is almost in a dry state.

IMS also varied with hydration showing a similar bi phasic trend, but reaching maximum values at lower hydration (H = 1.5) than fibril diameter (H = 2), with most of the increase occurring between H=0.5 and H=1.5, before remaining constant at H>1.5, where cross links between adjacent collagen molecules reach their maximum extension (Fig. 3.5). Human corneas displayed a significantly higher IMS at all hydration levels, measuring 1.70nm at physiological hydration (H = 3.2) compared to 1.47nm for porcine specimens, suggesting that human cornea fibril store more water between the molecules.

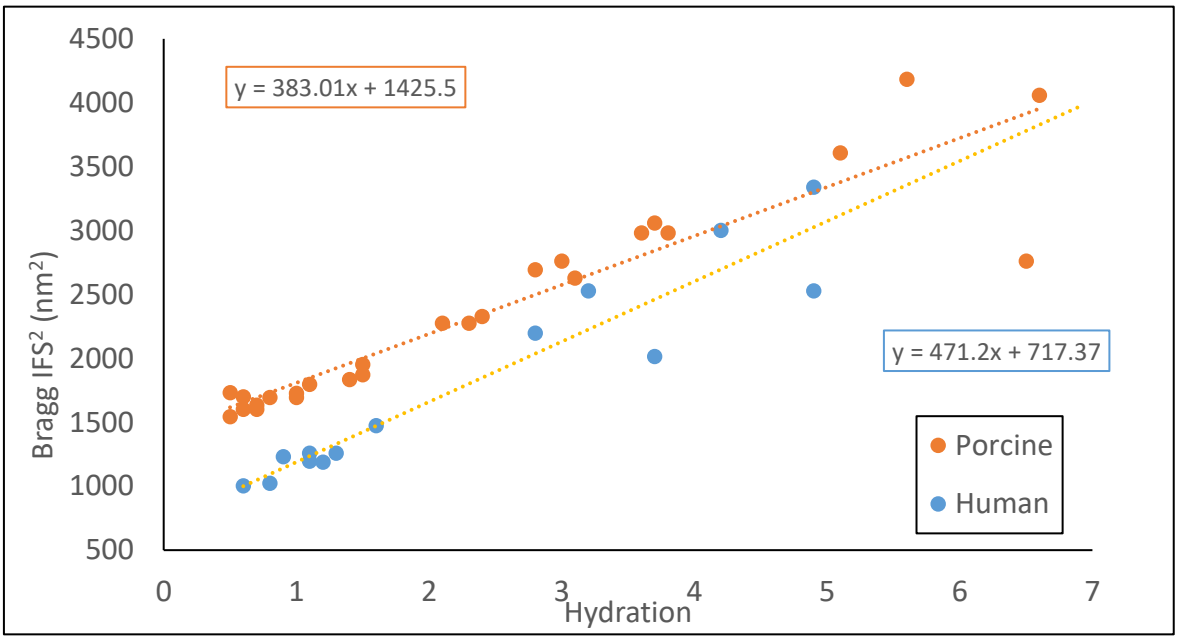


**Figure 3.3. IFS² as a function of hydration in human and porcine cornea.** The graph displays the linear relationship between hydration and IFS² in both human and porcine corneas. Dashed lines represent linear trend lines. Equations for each line are also shown.

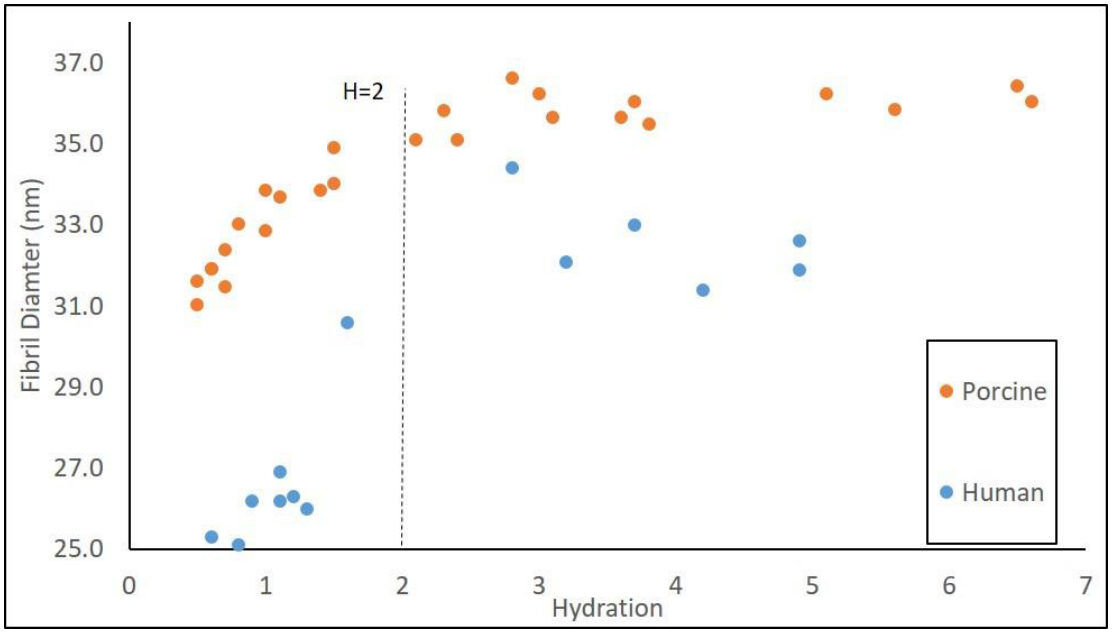


**Figure 3.4. Fibril diameter as a function of hydration in human and porcine cornea.** The graph shows variation is fibril diameter with hydration for human and porcine corneas. Fibril diameter increases with hydration until about H = 2 with minimal change thereafter. There is a clear gap in human data points between hydrations 1.9 – 2.5.

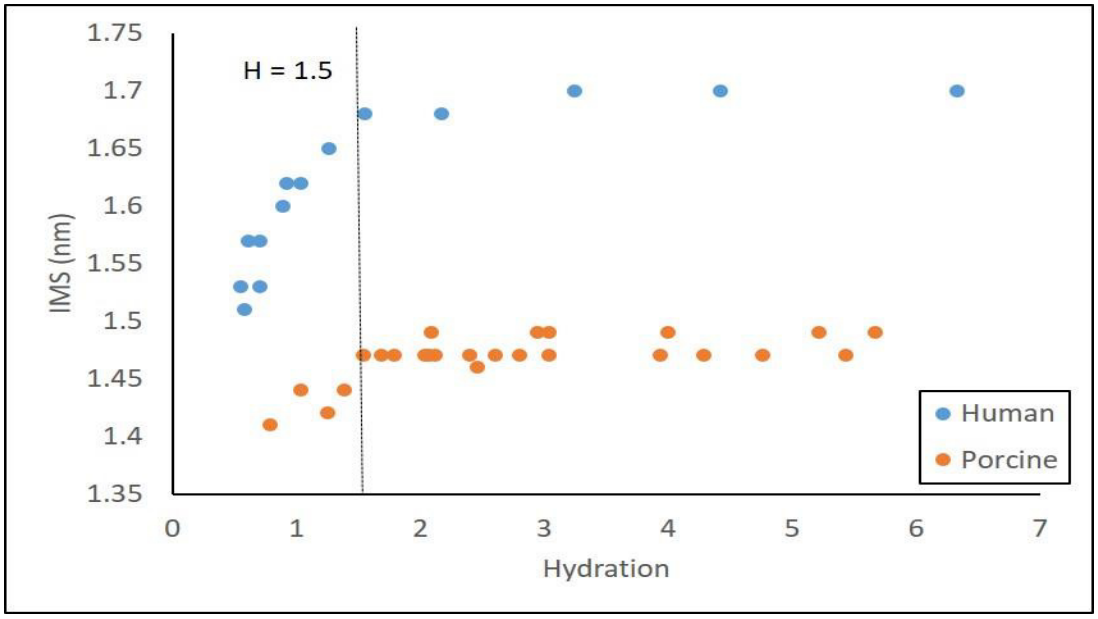


**Figure 3.5. Variation of collagen IMS with hydration for human and porcine corneas**. IMS increased with hydration until H= 1.5, remaining constant thereafter. In humans, IMS is higher at all hydration levels.

*3.3.2. Part 2*

Using one scan from each strip, the thickness of the tissue was calculated by firstly detecting the initial SAXS pattern on the anterior edge, and the final pattern at the posterior edge in order to discover the number of images containing scatter patterns, as each scan started and finished beyond the edge of the tissue. This number was then multiplied by the space between each shot, which was 10 µm, to reveal the thickness of the cornea. However, the thickness measurements should be regarded as maximum values, as they depend on the orientation and curvature of each individual strip within the sample holder. For example, in areas with a higher degree of curvature, the X-ray beam would scan at an oblique angle, resulting in more scatter patterns and therefore higher thickness calculations.

Three scans of data were analysed from the central region of a strip from corneas 1 and 3, with each line containing patterns from the full thickness of the cornea, at 10 µm intervals. The central stromal thickness of cornea 1 was about 600 µm, whereas cornea 3 was thicker at about 750 µm. Two lines of data were analysed from the peripheral region of cornea 2, which measured about 900 µm in thickness. The known linear relationship between human central corneal thickness and hydration (Hedbys and Mishima, 1966) was used to calculate hydration using the following equation, where q = the thickness of the cornea in mm:

$H = 7q – 0.64$

The centre of cornea 1 was at H = 3.6, close to physiological hydration, whereas cornea 3 was more hydrated at H =4.6

Intensity scan across the SAXS patters showed a clear interference function arising from the regular arrangement and spacing of collagen fibrils, enabling calculation of Bragg IFS. However, the fibril transform peak was very weak, making it difficult to fit the Bessel function in order to calculate fibril diameter. IFS and fibril diameter were calculated every 50 µm (5 images) in the central cornea, and every 100 µm in the periphery, from anterior to posterior. The most posterior region of stroma was analysed in more detail (every 10 µm), in the central region of corneas 1 and 2, and the periphery of cornea 3, in an attempt to detect any structural differences in the pre-Descemet's layer, with the assumption that Descemet's

membrane does not produce a scatter pattern. Scatter patterns across the entire depth of the central region of cornea 1 can be seen in Figure 3.6.

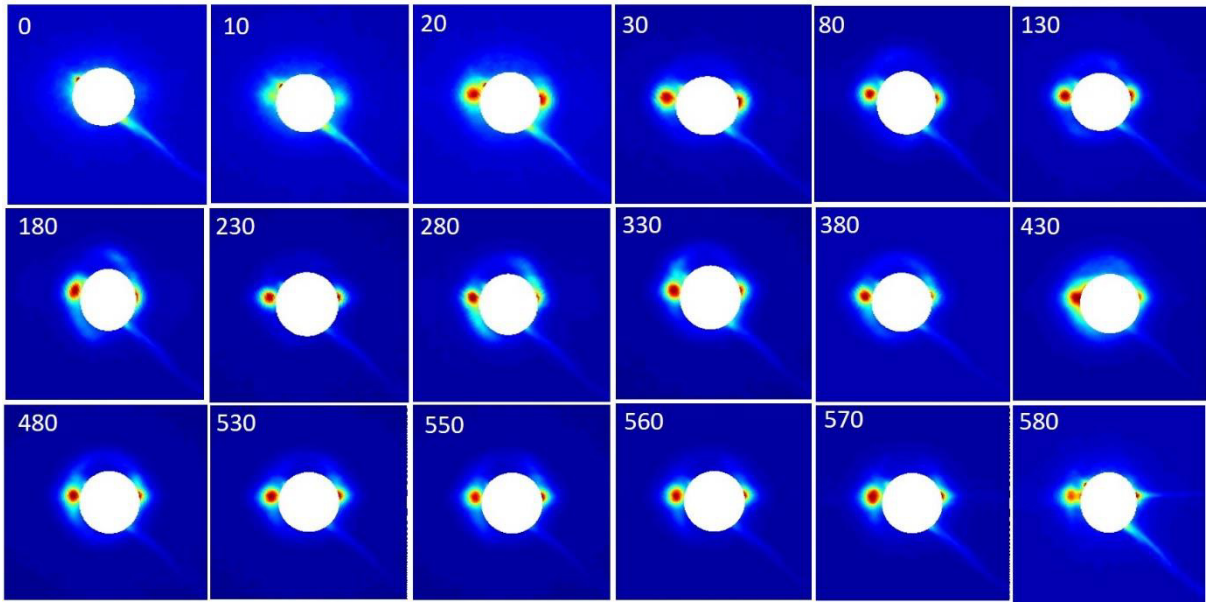


**Figure 3.6. A series of SAXS patterns across the entire thickness of central cornea.** The images start from the anterior edge of the cornea and end at the very edge of the posterior stroma. Each number represents the depth in the cornea in microns (from the anterior edge). Equatorial reflections are evident in horizontal directions, either side of the white beam stop. The last image at 580 µm depth should theoretically be the pre-Descemet's layer. No clear difference in scatter intensity is evident throughout the cornea.

Analysis of SAXS patterns revealed that centre-to-centre IFS remained fairly constant at all depths in the central and peripheral stroma in all corneas analysed, potentially showing a slight increase in the posterior stroma (Fig. 3.7), with most lying between 50 – 55nm at all depths. Conversely, fibril diameter appeared to decrease in size from the anterior to the posterior stroma in both central and peripheral cornea (Fig. 3.8). In the two central corneal strips analysed, this change was more pronounced in cornea 3 (Fig. 3.8B) with a 13% decrease in fibril diameter in the posterior. The first two scans in the peripheral cornea showed a similar decrease in fibril diameter of about 12%. Moreover, fibril diameters were highest in scan 1, which was taken in a region close to the limbus, and decreased in subsequent scans as the beam moves towards the centre.

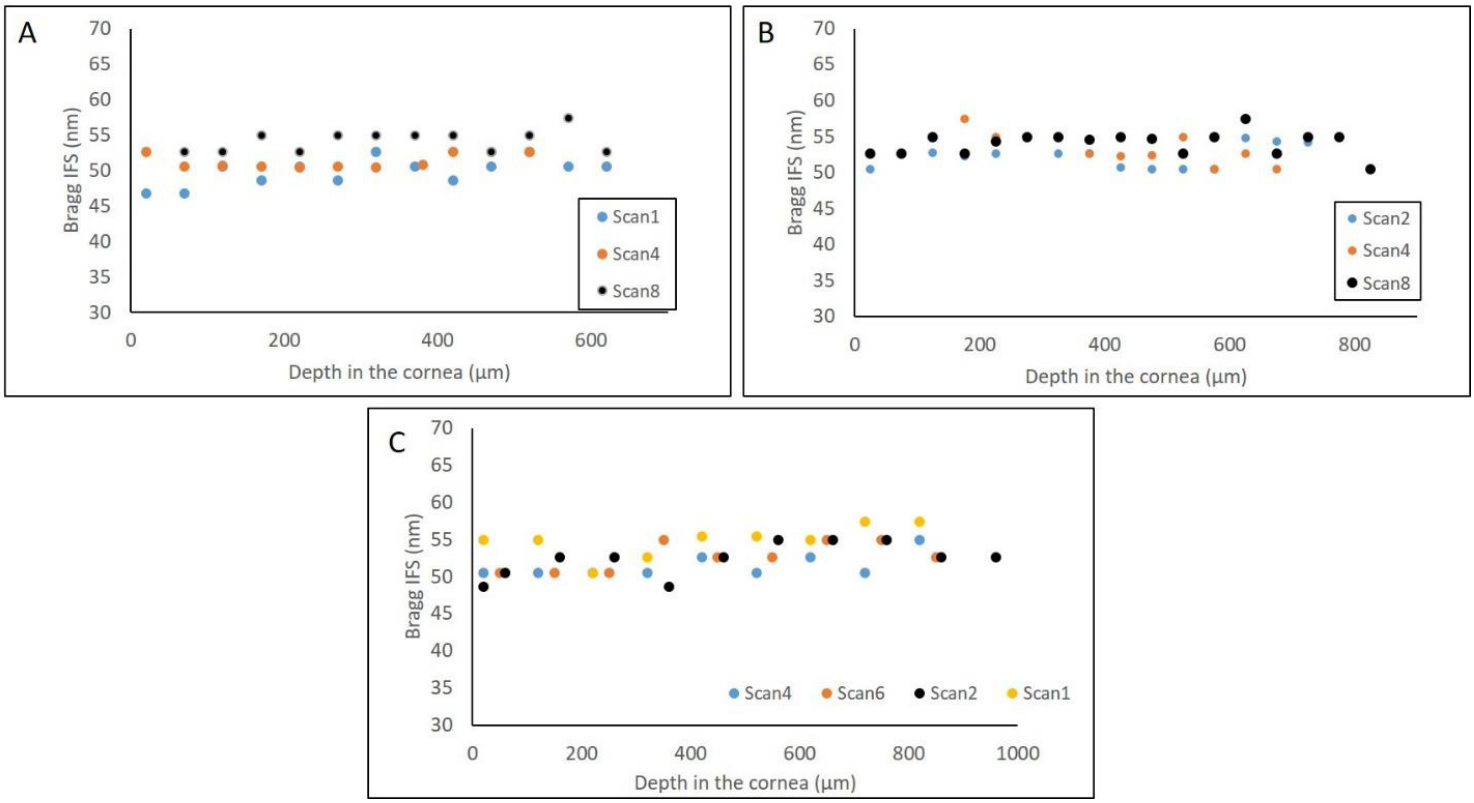


**Figure 3.7. IFS throughout the depth of central and peripheral cornea**. IFS increased very slightly moving from the anterior to the posterior stroma in central (A – cornea 1, B – cornea 3) and peripheral (C – cornea 2) cornea. The majority of centre-to-centre spacings measured between 50-55nm at all depths.

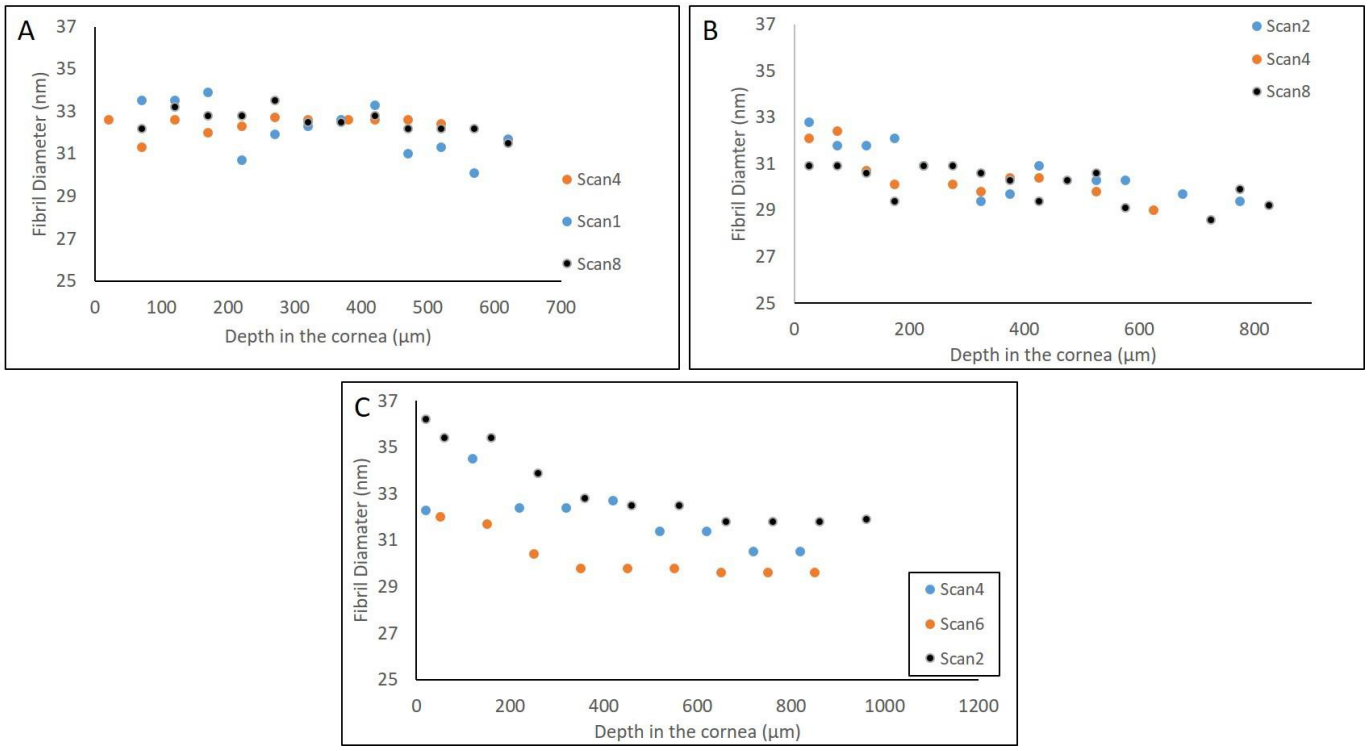


**Figure 3.8. Fibril diameter throughout depth of central and peripheral cornea**. Fibril diameter appeared to decrease as a function of depth in the central (A – cornea 1, B, cornea 3) and peripheral (C – cornea 2) stroma. This decrease was clearer in the peripheral cornea (C), although there was more variation between individual scans.

Pre-Descemet's layer is thought to exist in the posterior stroma, specifically the first 10- 20 µm of corneal stroma lying immediately adjacent to Descemet's membrane (Dua *et al.*, 2013). The first three scatter patterns from the posterior edge of strips of tissue from all three corneas were analysed, equating to ~ 30 µm of stroma, on the assumption that Descemet's membrane does not produce a scatter pattern. IFS was calculated in the pre-Descemet's layer from 6 central scans of data (3 of each from corneas 1 and 2), and 3 lines of data from the periphery of cornea 3. Mean values from each 10 µm step above Descemet's membrane are plotted in Figure 3.9. Very weak fibril transform peaks meant that it was not possible to calculate fibril diameters in this area. Spacing in the first 10 microns of central stroma averaged 48.7nm, which was significantly lower than the IFS present in overlying regions, which averaged 52.3nm ($p = 0.04$). This difference was not

observed in the peripheral cornea, where centre-centre spacing average remained constant in the first 30 microns of stroma adjacent to Descemet's membrane. However, peripheral data contained a higher standard deviation than the centre, indicating that the there is greater variation from the mean values calculated.

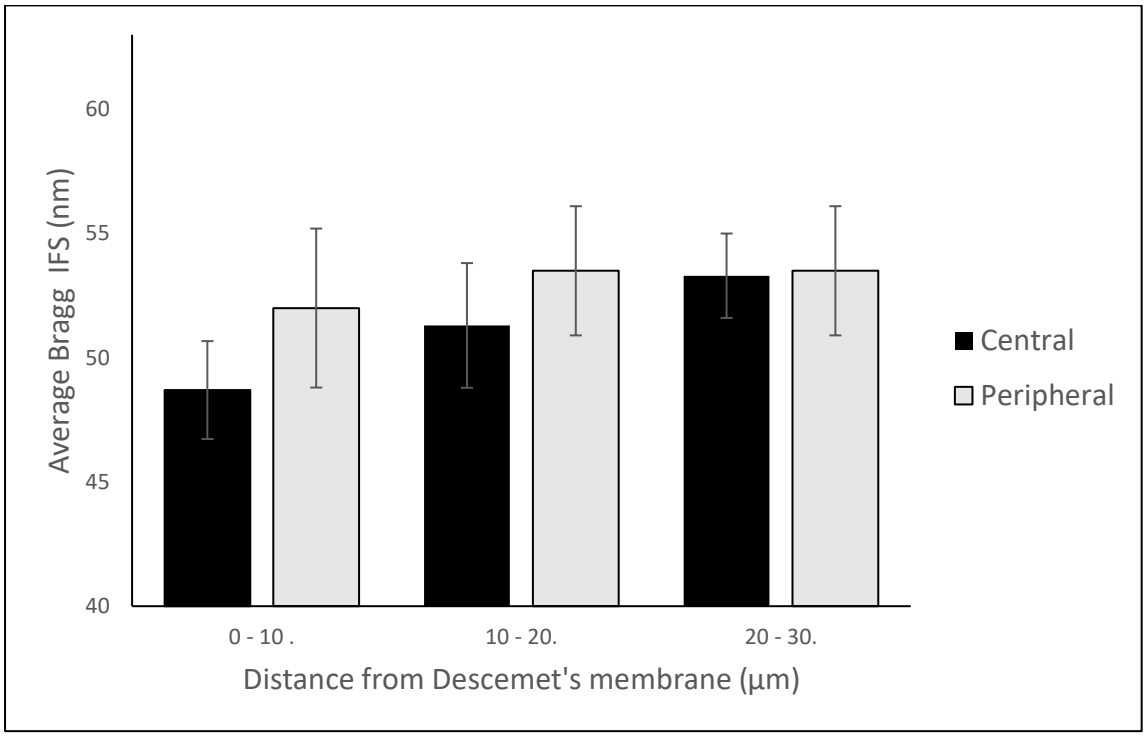


**Figure 3.9. IFS in the pre-Descemet's layer of posterior stroma.** IFS was lower in the first 10-20 microns of stroma above Descemet's membrane in central stroma, however, this was not observed in the same region of peripheral stroma. Bars represent standard deviation.

### 3.4. Discussion

*Part 1*

Part 1 of this study aimed to further understand how variations in hydration levels in the corneal stroma effect collagen fibril organisation, using pre-equilibrated porcine and human corneas. $IFS^2$ increased as a function of hydration in both human and porcine cornea, which is consistent with findings from previous X-ray and neutron scattering studies on bovine corneas (Sayers *et al.*, 1982, Meek *et al.*, 1991, Elliott *et al.*, 1982, Goodfellow *et al.*, 1978). Additionally, the current study compares the hydrodynamic behaviour between two different species, where interesting differences in collagen organisation were observed. Analysis of WAXS patterns also produced similar results to previous studies, showing an increase in IMS from dry cornea to ~ H = 1.5, with little change at higher hydrations (Meek *et al.*, 1991, Fratzl and Daxer, 1993), corresponding with fibril diameter measurements. It should be noted that fibril diameters measured by X-ray diffraction include the collagen fibril itself and any proteoglycan coating in the fibril surface (Cheng and Pinsky, 2013). The IMS results show that the collagen fibril itself ceases swelling close H = 1.5. The diameter measurements suggest that the fibril coating continues to absorb water, thus increasing the measured diameter, up to a hydration of close to H=2. At H>2, fibril diameter was constant at around 32nm in human, as opposed to the critical transition point of H = 1 as reported by Fratzl and Daxer (1993), although the authors results are questionable due to the lack of data points collected (4), which were normalised against data points collected from bovine cornea by Meek et al. (1991). These results suggest that initially the water is taken up within and between the collagen fibrils, and therefore their surfaces remain close together until about H=1.5, where water is then absorbed preferentially into the interfibrillar spaces. Therefore, structural changes to the fibril do not occur until the interfibrillar substance has released all of its water, suggesting that collagen fibrils have a much stronger affinity for water. It is interesting to examine the behaviour of the molecules within the fibrils as this fibrillar water is gradually removed. Figure 3.10 shows the data in Figure 6 plotted during the final stages of drying (<H=2). The data are plotted as $IMS^2$ because, just as for interfibrillar spacings, the molecules expand or contract in two dimensions, not one, so this plot should be linear.

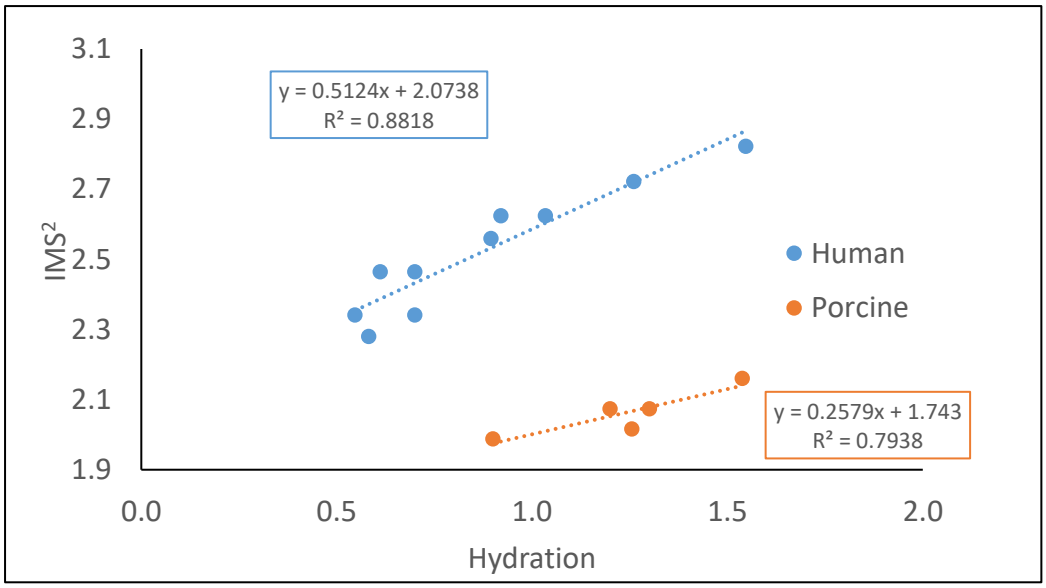


**Figure 3.10. IMS² at low hydration.** The graph shows IMS² at hydration values < 1.5. This was deemed to be the critical transition point for IMS (see Fig. 3.6).

Projecting the best fit lines to H=0 allows us to estimate the spacing between the dry collagen molecules in each species. This turns out to be 1.44nm (± 0.02) in human and 1.32nm (± 0.04) pig. Additionally, the inter-molecular spacing at a given tissue water content is greater in human corneas during the drying process. These observations may be explained by the age of the tissue samples used. Whereas the porcine corneas were obtained from relatively young animals (<1 year of age and equivalent to 18 human years), the human corneas used in this study were often from older donors (mean age 68 ± 10 years). IMS has been shown to increase with age in human corneas (Daxer *et al.*, 1998, Malik *et al.*, 1992) as a result of increased cross-linking between the molecules, pushing them apart (Malik *et al.*, 1992, Malik and Meek, 1994). When dry, it could be that the cross-links in the human corneal collagen brace the molecules and limit their lateral collapse, compared with the less cross-linked porcine collagen.

The swelling behaviour of porcine corneas has been reported to be similar to humans (Hatami-Marbini *et al.*, 2013). Although porcine cornea showed broadly similar changes in collagen organisation compared to human cornea as a function of tissue hydration, such as a linear relationship between IFS² and hydration, and similar critical transition points for IMS and fibril diameter, the individual values differed between the two species. IFS in the dry

human cornea was 26.8nm, calculated from the IFS at H = 0, assuming the collagen fibrils are in contact. This value is lower than porcine (37.8nm) and previous reported fibril diameters in dry bovine cornea (34-40nm) (Meek *et al.*, 1991, Sayers *et al.*, 1982, Fratzl and Daxer, 1993). IFS was higher at all hydration levels in porcine cornea. Furthermore, porcine cornea contained a significantly lower (~14%) average IMS at physiological hydration, and larger fibril diameter compared to human cornea. Meek and Leonard (1993) used X-ray diffraction to calculate a number of different parameters for a wide range of species and, unlike the current work, reported fairly constant IMS between all species analysed. Diameter and interfibrillar spacing varied greatly between different species, whereas the fibril area fraction (% space occupied by the fibrils) remained constant, indicating that smaller fibrils pack closer together (Meek and Leonard, 1993, Gyi *et al.*, 1988). Additionally, discrepancies in intrafibrillar swelling behaviour between human and porcine corneas may reflect differences in the specific local axial and azimuthal relationships of collagen molecules within their respective fibrils, as suggested by studies in other collagen-rich connective tissues such as articular cartilage (Wachtel and Maroudas, 1998).

IFS is higher in porcine cornea than in the human (Fig. 3.4), suggesting that there may be a difference in the proteoglycan-rich matrix surrounding the collagen fibrils (Fratzl and Daxer, 1993). The water-binding capacity of negatively charged sulphate groups on GAG's in the stroma play a vital role in maintaining corneal hydration, attracting water molecules and causing osmotic flow into the tissue, a mechanism that is counteracted by an active ion transport pump in the endothelium to maintain hydration *in vivo*. Keratan sulphate is present in high quantities in the central cornea (Borcherding *et al.*, 1975) and contains a large hydration capacity (Bettelheim and Plessy, 1975). Furthermore, mice that lack lumican, a proteoglycan with keratan sulphate side chains, develop bilateral corneal opacification (Chakravarti *et al.*, 1998) and a 40% decrease in stroma thickness (Chakravarti *et al.*, 2000) as a result of an alteration in stromal hydration. SAXS analysis on lumican deficient mice has also shown that collagen organisation is significantly altered in these animals (Quantock *et al.*, 2001). Differences in this GAG content may be responsible for the discrepancies in interfibrillar swelling that are observed between the two species, as increased keratan sulphate levels in porcine cornea would result in higher hydration levels in the interfibrillar space, and therefore higher centre-to-centre interfibrillar spacing. However, human corneas

were stored in organ culture media before use. Keratan sulphate leakage has be shown to occur when corneas are stored in this media (Moller-Pedersen and Moller, 1996, Moller-Pedersen *et al.*, 2001) and therefore may account for the differences seen between the two species, if a substantial amount of GAG's have been lost via leakage. IFS spacing is also subject to changes with ageing, showing an 8% decrease between 20 and 90 years of age in humans, potentially related to changes in proteoglycan composition (Malik *et al.*, 1992), meaning further loss of GAG's in the older human corneas.

The first part of this study adds to our current knowledge of the effects of stromal hydration on the intra and interfibrillar organisation of collagen in the cornea. An in depth comparison in these changes between human and porcine corneas suggests that the differential swelling behaviour is likely due to a combination of inter-species differences in collagen molecule organisation within the fibrils, and potentially variations in proteoglycan composition in the extracellular space.

Part 2

The first part of this study looked at the average IFS and fibril diameter throughout the entire depth of the cornea in relation to changes in hydration. Leading on from this, the second part of the study used SAXS to analyse collagen organisation in detail at each depth in the corneal stroma, from anterior to posterior, using an X-ray microbeam. Corneas used in this study were perfusion fixed with the entire globe in an attempt to maintain their physiological state. The study was designed to compare measurements of structural parameters at different depths in the tissue, and it was assumed that any effects of fixation would be uniform throughout the tissue.

Ultrastructural differences between the anterior and posterior stroma are known to exist in the cornea, with many previous studies focusing on the lamellae orientation. The middle and posterior regions are orthogonally arranged and more parallel to the surface, whereas the lamellae in the anterior stroma is highly interwoven with branching of fibrils (Komai and Ushiki, 1991, Morishige *et al.*, 2006). Furthermore, preferred lamellae orientations are more prominent in the middle and posterior layers of the stroma whereas the anterior layer was more isotropic (Aghamohammadzadeh *et al.*, 2004, Abahussin *et al.*, 2009). Few studies

have examined the differences in centre-to-centre spacing and fibril diameter as a function of depth in the human cornea.

IFS remained fairly constant at all depths in both the central and peripheral stroma. This finding disagrees with results obtained in a similar study by Quantock *et al.* (2007), who show that IFS decreases in the anterior stroma of human cornea. It should be noted that the corneas used in this study were highly swollen, measuring 850 and 925 μm, which when converted to hydration using the previously described equation (Hedbys and Mishima, 1966), these equate to H = 5.3 and 5.8. The differences in this current study may be due to these high levels of hydration that are known to alter collagen organisation as discussed in part 1. Earlier image analysis studies of electron micrographs have reported no variation in IFS from anterior to posterior stroma in human cornea (Freund *et al.*, 1995, Patey *et al.*, 1984), although a difference was observed in rabbit cornea due to a 40% increase in fibril number density in the posterior stroma (Freund *et al.*, 1995). In an X-ray diffraction depth study on bovine cornea, IFS increased until it reached the mid stroma before decreasing again in the posterior, a pattern seen at all radial positions (Ho *et al.*, 2014). There was no difference in IFS in this current study between the central (average 52.6 nm ±2) and peripheral (average 52.2 nm ± 2.2) cornea, which contradicts previous SAXS results by Boote *et al.* (2003), although data was collected at 1mm radial intervals from a number of corneas, with each pattern obtained from the entire depth of the tissue, resulting in stronger patterns. In porcine cornea, hydration remains relatively constant from central to peripheral regions (L. Lawrence, 2014 unpublished results), and therefore supports a constant IFS radially across the cornea, as hydration levels are known to directly affect centre-to-centre spacing (Meek *et al.*, 1991, Fratzl and Daxer, 1993).

Fibril diameter decreased with depth in the cornea in peripheral regions. These changes were not observed in the SAXS study on eye bank human corneas (Quantock *et al.*, 2007), however, they are consistent with findings in the bovine corneal stroma, where fibril diameter decrease as a function of depth at all radial position along the cornea (Ho *et al.*, 2014). Fibril diameters were fairly constant from centre (average 31.4nm ± 1.3) and periphery (average 32nm ± 1.8), consistent with previous findings (Boote *et al.*, 2003, Daxer *et al.*, 1998). However, in the periphery, scans closer to the limbus revealed higher fibril diameters. It is known that fibrils are significantly larger at the limbus (Boote *et al.*, 2003,

Borcherding *et al.*, 1975, Boote *et al.*, 2011) where corneal collagen begins to merge with the sclera. Analysis of transmission electron micrographs in swollen human cornea has shown that posterior collagen fibrils were 4% smaller than those in the anterior and 1.12 times greater in fibril number density, whilst being 15% smaller in rabbit cornea (Freund *et al.*, 1995).

Studies on rabbit and bovine cornea have demonstrated that the posterior stroma has a larger swelling capacity and is more hydrated (Lee and Wilson, 1981, Kikkawa and Hirayama, 1970). Muller *et al.* (2001) elaborated on these earlier findings, showing that in extreme hydration, the anterior 100-120µm of human anterior stroma resisted swelling and maintained the corneal curvature, a property attributed to the interweaving of lamellae in this region. Differences in swelling behaviour may be a result of variations in GAG composition throughout the stroma, with higher levels of keratan sulphate in the posterior, resulting in a greater affinity for water in the interfibrillar space in comparison to anterior stroma (Bettelheim and Plessy, 1975, Castoro *et al.*, 1988). This swelling behaviour may explain the discrepancies between the current results and the similar study carried out in swollen eye bank corneas where the authors reported smaller IFS in the anterior stroma and constant fibril diameter throughout the depth of the cornea (Quantock *et al.*, 2007). With lower hydration levels in the cornea, IFS would be expected to be decreased in comparison to the IFS reported by Quantock and colleagues as there would be less water present in the interfibrillar space, however, this was not the case.

Dua *et al.* (2013) postulated that an additional structurally distinct layer exists in the posterior stroma, located adjacent to Descemet's membrane, that is variable in thickness (~15 µm), 5-8 lamellae thick, and rich in type VI collagen (Dua *et al.*, 2014). SAXS analysis in this area of stroma revealed a significant difference (about 4nm) in the average centre-to-centre collagen fibril spacing compared to the overlying ~20 µm of stroma, although this difference was only present in the central cornea. A reduction in centre-to-centre spacing in the pre-Descemet's region would subsequently result in closer packing of collagen fibrils and increased biomechanical strength (Boote *et al.*, 2003), potentially contributing to the production of the cleavage plane created during pneumodissection, which led to Dua and colleagues suggesting that a new layer in the cornea exists. Interestingly, Dua *et al*. (2013) described two types of big bubble; the first enlarged centrally, where it was possible to peel

away Descemet's membrane without deflating the bubble, whereas type 2 enlarged from the periphery, where removal of Descemet's membrane deflated the bubble. Decreased IFS in pre-Descemet's layer of central cornea, with no change in the peripheral, correspond with these findings, where increased biomechanical strength in the first ~10 microns of stroma adjacent to Descemet's membrane may contribute to the type 1 bubble formation. The lack of fibril transform peak in these patterns at the edge of the stroma meant that it was not possible to measure fibril diameter. However, in a recent ultrastructural study of the posterior stroma, Schlotzer-Schrehardt *et al.* (2015) reported no change in fibril diameter or IFS in the posterior stroma with the authors suggesting that the cleavage plane is non reproducibly determined by the variability of keratocytes from Descemet's membrane (Schlotzer-Schrehardt *et al.*, 2015).

### 3.5. Conclusion

The first part of this study has shown that both human and porcine cornea contain similar critical transition points in response to variations in hydration. However, there are distinct differences in collagen organisation between the two species. The second part of this study has demonstrated that IFS in constant as a function of depth in the human cornea, whereas fibril diameter decreases from anterior to posterior in the periphery. Analyses of pre-Descemet's layer revealed a lower IFS in the centre of the cornea, potentially altering the biomechanical properties due to closer packing of collagen fibrils.

# Chapter 4 – Three-dimensional arrangement of elastic fibres in the human corneal stroma

## 4.1. Introduction

The cornea is the main refracting lens in the eye. As part of the outer tunic, it must combine transparency with toughness. In particular it must be flexible enough to withstand external insult and intraocular pressure variation, but elastic enough to regain its precise shape afterwards, in order not to affect the focussing of light on the retina. The optical and biomechanical properties of the human cornea are largely governed by the specific arrangement of lamellae throughout the stroma (Aghamohammadzadeh *et al.*, 2004, Whitford *et al.*, 2015). Moreover, other dynamic tissues that expand and contract in response to variations in blood pressure, for example lungs and blood vessels, contain a system of elastic tissue, in addition to collagen, in order to provide further strength and resiliency to withstand mechanical forces (Sherratt, 2009). Additionally, the sclera contains an elastic system that allows the eye to deform slightly and regain its original shape (Alexander and Garner, 1983b, Marshall, 1995). Despite the importance of elastic tissue in these force bearing tissues, our knowledge of its presence and distribution in the human cornea is limited.

Elastic tissue was, remarkably accurately, initially observed in the cornea as far back as the mid-19$^{th}$ century, described as fibres that commence on Descemet's membrane and continue to the wall of Schlemm's canal ,and are said to be "closely allied to the to the elements of the zonule of Zinn" (Kolliker, 1860). Interestingly, this refers to the ciliary zonules in the eye, which hold the lens in dynamic suspension, and are known to contain elastic fibres (Ashworth *et al.*, 2000, Keene *et al.*, 1991b). Almost 50 years later, M'ilroy (1906) used Weigert's and orcein elastic stains on calf, foal, and human foetal cornea, to demonstrate the presence of elastic fibres, after removing the collagen with acetic acid. These fibres were reported chiefly in the posterior stroma, near Descemet's membrane, and confined to the peripheral portion of the cornea. Fullmer and Lillie (1958) then went on to describe a novel connective tissue fibre in periodontal membranes that was significantly

different to collagen, elastic, and reticular fibres. These fibres were named ‘oxytalan’ as they were resistant to acid hydrolysis.

The advancement of electron microscopy in the 1960’s enabled connective tissue fibres to be studied in more detail, leading to many new studies in this field. Chapman (1961), showed microfibrils with a periodicity of about 50nm in the extracellular space, although it was believed that they were collagenous in nature. Low (1962), described the presence of bundles of microfibrils in the ECM that were structurally distinct from collagen and elastic fibres, with a varying diameter of 4-12nm. Furthermore, the microfibrils were reported near basement membrane, and in close association with elastic fibres, where they form the ‘electron dense margin’ (Low, 1962). Similar findings were revealed by Haust (1965), where-as Haust *et al.* (1965) went on to suggest that these microfibrils participate in the organisation of elastic units during elastogenesis in the aorta.

Further advancement in elastic fibre knowledge occurred when Greenlee *et al.* (1966) described the fibres as containing two distinct morphologic components: 10nm fibrils, staining with uranyl acetate and lead, and an amorphous core, which only stains with phosphotungstic acid. The authors also proposed that microfibrils are an immature form of elastic fibres (Greenlee *et al.*, 1966). Elastic fibre components were further characterised by Ross and Bornstein (1969), who used selective digestion to show that the central amorphous component was elastin, and microfibrils consist of proteins that are neither collagen nor elastin. Light and electron microscopy revealed that the ‘oxytalan’ fibres described by Fullmer and Lillie (1958), are in fact bundles of 10-12nm microfibrils (Cottapereira *et al.*, 1976). When these bundles of microfibrils contain a central amorphous component, they were classified as ‘true’ elastic fibres, although they may also exist as intermediate fibres, where the central amorphous component is sparse, and these were termed elaunin fibres (Cottapereira *et al.*, 1976, Gawlik, 1965), all of which are visible with light microscopy following differential staining protocols i.e. aldehyde fuschin with or without prior oxidation (Alexander *et al.*, 1981a). 10-12nm microfibrils were shown to consist of a novel 350kDA protein called ‘fibrillin’ (Sakai *et al.*, 1986b).

After the early studies by Kolliker (1860) and M'ilroy (1906), there was little interest in the presence of elastic fibres in the cornea, until it re-surfaced in the 1980’s. Oxytalan fibres were identified in the deep stroma of young human cornea, but none were found in the

mature healthy adult cornea (Alexander and Garner, 1983b, Hirano *et al.*, 1991). Electron microscopy then identified oxytalan fibres in embryonic and chick corneas, running parallel to the corneal surface (Bruns *et al.*, 1987) and increasing in density from the centre to the periphery (Daga Gordini *et al.*, 1990). These fibres have also been reported in various other species (Carrington *et al.*, 1984, Bruns *et al.*, 1987, Carlson and Waring, 1988), but not in mature, healthy, human cornea. That is until 2010, when Kamma-Lorger *et al.* (2010) reported a network of fibres using two photon fluorescence microscopy. These fibres were shown to run roughly parallel to the collagen lamellae in the circumcorneal annulus (Newton and Meek, 1998a), a deep limbal structure that is supposed to help maintain the change in curvature between the cornea and sclera (Boote *et al.*, 2009). The advancement in imaging techniques, such as SBF SEM, has enabled these structures to be studied in three-dimensions. For example, Hanlon *et al.* (2015) used SBF SEM to describe the presence of oxytalan fibres in murine cornea, which they have termed 'elastin-free microfibril bundles' (EFMB's). Despite this, the presence or absence of elastic fibres in the human cornea remains unclear, highlighting the need to re-visit this area with more advanced techniques. There is no consistency in the literature in terms of nomenclature, with oxytalan fibres often called 'microfbril bundles', 'EFMB's', and fibrillin-containing microfibrils'. For simplicity, these fibres will be referred to as 'elastic fibres' throughout this thesis, whereas fibres containing a central amorphous elastin component are referred to as 'true elastic fibres.'

As discussed previously, Dua *et al.* (2013) have controversially postulated that the stroma that lies directly adjacent to Descemet's membrane is a distinct corneal layer, termed pre-Descemet's layer, which contains different biomechanical properties to the rest of the stroma. Dua and colleagues used the big bubble technique to demonstrate that when injecting air to separate Descemet's membrane from the stroma, the cleavage plane resulted in a thin layer of stroma remaining attached to Descemet's membrane (Dua *et al.*, 2013). Although this had previously been observed (Jafarinasab *et al.*, 2010, Mckee *et al.*, 2011), and despite the suggestion that the cleavage plane was non-reproducibly determined by the variable distances of keratocytes to Descemet's membrane (Schlotzer-Schrehardt *et al.*, 2015), Dua and colleagues insisted that it was a structurally distinct layer, following up the initial study by showing that there is a concentration of type VI collagen within the layer of tissue (Dua *et al.*, 2014). These recent developments have highlighted the importance of

studying the structure of the corneal stroma at all depths, with new techniques, paying more attention to elastic fibres, as well as collagen lamellae, as these too influence the biomechanical properties of the cornea.

The aims of this chapter are to examine the structure of the human corneal stroma using a range of techniques, with particular focus on pre-Descemet's layer, in order to determine if there are any structural differences present in comparison to the overlying stroma. The techniques used include SBF SEM, conventional TEM, non-linear microscopy and immune-fluorescence microscopy.

## 4.2. Methods

### *4.2.1. Human corneas*

Five human corneas were obtained from the CTS Eye Bank, Bristol, UK. Cornea 1 was from a 69-year–old female. The whole enucleated eye was fixed in 4% paraformaldehyde. The cornea was removed with a scleral rim and placed in modified Karnovsky's fixative (2.5% glutaraldehyde and 2% paraformaldehyde in 0.1M cacodylate buffer at pH 7.2) for 30 minutes, dissected and processed for electron microscopy (SBF SEM and TEM). Cornea 2 was from a 50-year-old male and was received from the Eye Bank in Eagle's minimum essential medium as a cornea with about 2 mm of the adjacent sclera. It was de-swelled with 8% dextran overnight, mounted in a Barron artificial anterior chamber to maintain a trans-corneal pressure and was fixed using the same modified Karnovsky's fixative for 3 hours. It was then dissected and used for SBF SEM and TEM. Cornea 3 was from a 72-year old female. It was fixed in 4% paraformaldehyde then wax embedded for histology. Cornea 4 from a 67-year-old male was processed for non-linear microscopy as described below. Cornea 5 was from a 63 year old male which was collected and fixed in 0.5% PFA in Sorenson's buffer within two days of death and used for immuno-labelling. Cornea 6 was from a 13-week old foetus obtained from the Human Developmental Biology Resource (HDBR). The whole globe was fixed in modified Karnovsky's fixative and was then processed for SBF SEM as below.

*4.2.2. SBF SEM and TEM*

The protocol for processing tissue for SBF SEM and TEM is described in chapter 2, along with the full-thickness quantification methods and 3D rendering using Amira6.

*4.2.3. Non-linear microscopy*

Corneal buttons 8 mm in diameter were dissected from the centre of Cornea 4, placed into dialysis tubing (molecular cut-off 14 kDa), and brought to physiological hydration by immersion in 2.5% polyethylene glycol overnight. The buttons were then mounted on Superfrost glass slides, in 1:1 phosphate buffered saline – glycerol solution, protected by a 0.16mm thick glass coverslip. Non-linear microscopy was carried out at the Physics department, Exeter University. A modified confocal microscope (FluoView IX71 and F300, Olympus) was used to obtain two-photon fluorescence (TFP) and second harmonic generation (SHG) images simultaneously (see Bell *et al.* (2014) for a complete description of the system configuration). As well as single images, stacks of aligned images at 1µm intervals were also obtained throughout the depth of the stroma. TPF and SHG images from the same area of cornea were overlaid using ImageJ software, resulting in composite images.

*4.2.4. Immunofluorescence labelling*

One half of cornea 5 was transferred to PBS for 24 hours, involving three changes. The tissue was then embedded in OCT and snap frozen in isopentane cooled in liquid nitrogen before being stored at -20°C. 10µm thick frozen sections were cut using a cryostat (Leica CM3050 S) and collected on lysine coated glass slides. Sections were rehydrated with PBS for 15 minutes at room temperature before being blocked with 2% BSA (bovine serum albumin) in PBS for 30 minutes. Mouse monoclonal anti-fibrillin 1, rabbit polyclonal anti-type VI collagen and anti-elastin antibodies (Abcam, Cambridge) were applied at 1/100 and 1/1000 dilutions overnight in a dark humid chamber at 4°C, with PBS applied to negative controls. After a wash with PBS, sections were transferred to secondary antibodies goat anti-mouse or rabbit (as appropriate) conjugated with Alexafluor 488, at a 1/200 dilution. During the staining

process, all slides were kept in a dark humid chamber with wet paper towels used at the base to prevent drying out. Finally, sections were washed with PBS (5 x 2minutes) and coverslips mounted using vectashield hardset with DAPI (4',6-diamidino-2-phenylindole). The mounting medium was allowed to air dry for 2 hours before sections were examined using fluorescence microscopy (Leica DM6000B) with appropriate wavelength filters. Images were collected using Leica application suite: Advanced fluorescence, and analysed using ImageJ software.

## 4.3 Results

### *Central and peripheral cornea*

#### *4.3.1. TEM*

Initial TEM examination of the area of stroma anterior to Descemet's membrane in the centre and peripheral cornea revealed the presence of elastic fibres that were clearly distinct from collagen fibrils (Fig. 4.1). Corneas used for TEM and SBF SEM were processed using the tannic-acid based staining method, which heavily stains elastic fibres as well as collagen (Simmons and Avery, 1980, Kageyama *et al.*, 1985). It was evident that these structures were not 'true' elastic fibres as they were heavily stained throughout, lacking the central amorphous component. When viewed longitudinally, the fibres exhibited banding with a pseudo-periodicity of 56.5 ± 4.8nm (Fig. 4.1A). Also, when viewing transversely orientated elastic fibres, the 10-12nm individual microfibrils that make up the fibre could be seen be seen (Fig. 4.1B), as well as a textured substructure in longitudinal sections (Fig. 4.1C). The diameter of the elastic fibres varied, with most lying between 100-200nm. At low magnification, the fibres appeared to be concentrated in the most posterior 10µm of stroma (Fig. 4.1D).

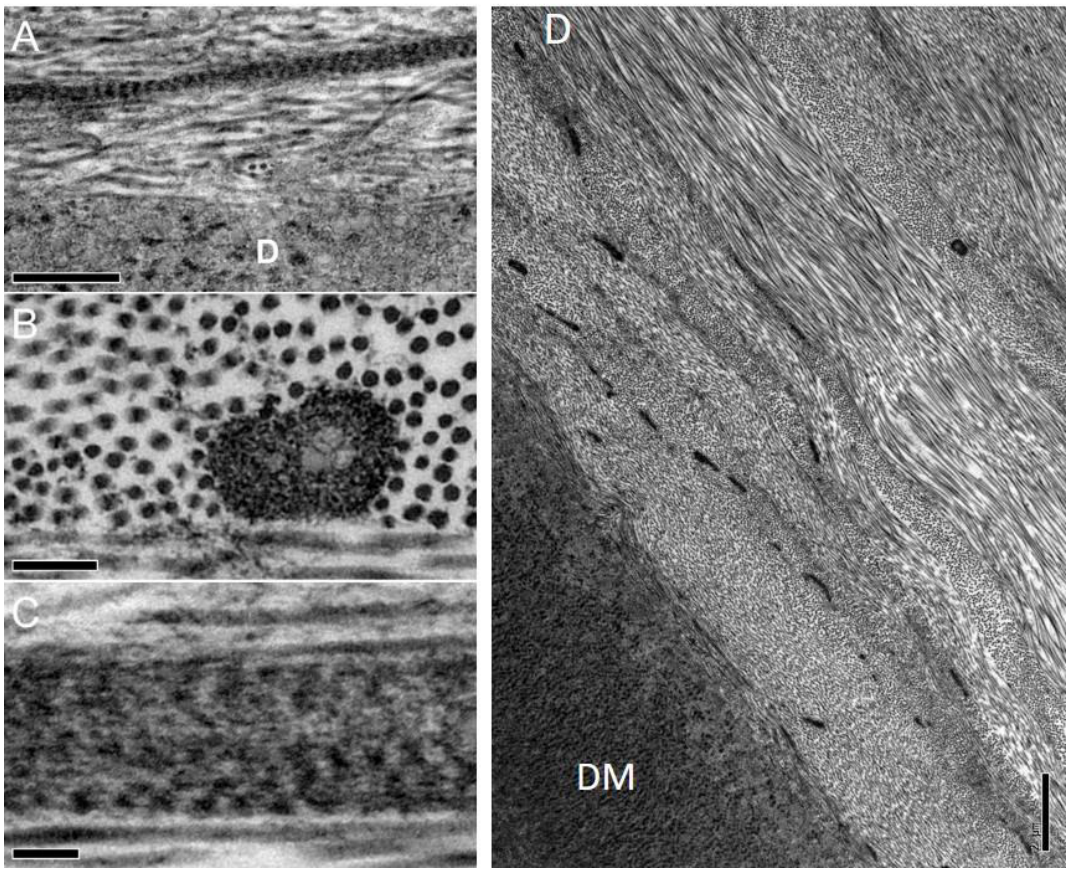


**Figure 4.1. TEM images of elastic fibres from the central and peripheral cornea stained with tannic acid.** Fig. 4.1A: A banded fibre running longitudinally above Descemet's membrane (D) (bar = 500 nm). Fig. 4.1B: In cross-section, individual microfibrils are visible, (bar = 200 nm). Fig. 4.1C: At high magnification some elastic fibres show less distinct banding and longitudinal texture suggesting a microfibrillar substructure (bar = 100 nm). Fig. 4.1D: At low magnification, fibres are concentrated anterior to Descemet's membrane (DM) (bar = 2µm). A-C taken from (Lewis *et al*., 2016).

### *4.3.2. Non-linear microscopy*

Non-linear microscopy confirmed that the structures visualised with TEM were indeed elastic fibres. Initially, fixed corneal buttons were used, resulting in the tissue displaying high amounts of auto-fluorescence, potentially due to the age of the specimens. Unfixed corneal buttons were then used as described in the methods above, producing a slightly better image quality. TFP images, revealing elastic fibres, and SHG images, revealing collagen, were superimposed to create composite images (Fig. 4.2). Long fibres were seen running along

the plane of the cornea before branching into two, a characteristic features of elastic fibres. By analysing stacks of images taken throughout the full depth of the stroma, it was evident that the fibres were only present in the posterior stroma (particularly concentrated in the final ~80µm), in both the centre and at the edge of the button. As 8mm corneal buttons were used, it was not possible to visualise fibres at the very periphery/limbus of the cornea.

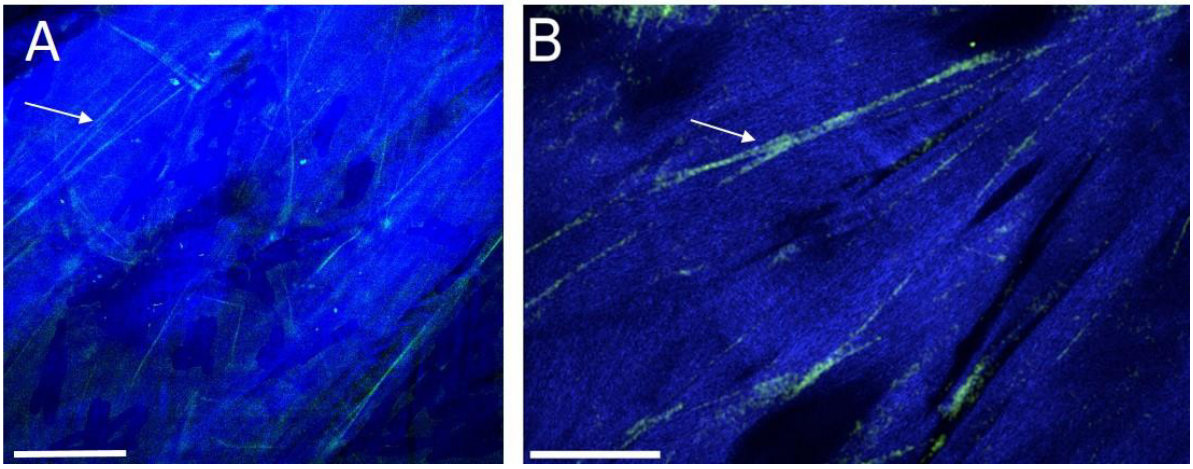


**Figure 4.2. TPF and SHG composite images.** These images show the presence of elastic fibres (green) amidst collagenous material (blue) in the posterior stroma at the periphery (A) and centre (B) of 8mm buttons. Elastic fibres show evidence of characteristic branching (arrows). High levels of noise in the form of auto fluorescence made it difficult to produce composite images. Bar = 50µm. Image B adapted from (Lewis *et al*., 2016).

### *4.3.3. SBF SEM*

The area of stroma lying directly above Descemet's membrane was further investigated using SBF SEM. A 16 x 16 x 50 µm data set was obtained in this region from peripheral (4-5mm from the optical axis) cornea. Individual images from the data set displayed many darkly stained structures that appeared as black dots (Fig. 4.3A). Converting this stack of images into a 3D model using automated 3D rendering revealed that these dark structures were in fact long elastic fibres running throughout the entire length of the volume (Fig. 4.3B

and E). These fibres were concentrated in the first 8µm of stroma above Descemet's membrane, below the last keratocyte, although fibres were also visible in areas anterior to this. Furthermore, the elastic fibres ran approximately parallel to the surface of the cornea, along the plane of the stromal lamellae, and were seen to birfurcate and trifurcate (Fig. 4.3C). Fibre orientation appeared random, with some orientated at an oblique angle to the direction of limbus and others arranged circumferentially around the cornea. Anterior to the concentrated zone, elastic fibres generally appeared to trace within and between collagen lamellae (Fig. 4.3D).

The same region of posterior stroma was examined in the central cornea. Elastic fibres were visible between stromal lamellae above Descemet's membrane, however, they were smaller and sparsely distributed when compared to the same region of peripheral cornea (Fig. 4.4A), ultimately resulting in a difficult 3D reconstruction, with more manual rendering. Additionally, the fibres appeared thinner than those observed in the peripheral cornea, with no branching evident either. Elastic fibres were orientated radially and obliquely towards the limbus, again running parallel to the plane of the cornea, with many appearing to lie on the anterior surface of Descemet's membrane (Fig. 4.4B and C).

### *4.3.4. Full-thickness quantification*

After discovering the presence of an elastic fibre system in the posterior stroma of both central and peripheral cornea, the next step was to quantify the distribution of fibres throughout the entire depth of the stroma, therefore, over 20,000 *en* face images were acquired every 50nm from epithelium to Descemet's membrane in the peripheral cornea. Due to the large amount of data collected, it was divided into groups of 1000 images, representing 50µm of stroma. Within each group, the percentage volume occupied by elastic fibres was calculated and plotted as a function of depth within the tissue (Fig. 4.5A). Results indicated that elastic fibres density was highest in the posterior stroma, remained uniform at a lower density in the mid-stroma, before falling to zero in the anterior stroma. The first point on the graph (representing the first 50µm of stroma above Descemet's membrane) contained almost double the density of elastic fibres compared to the second point on the graph.

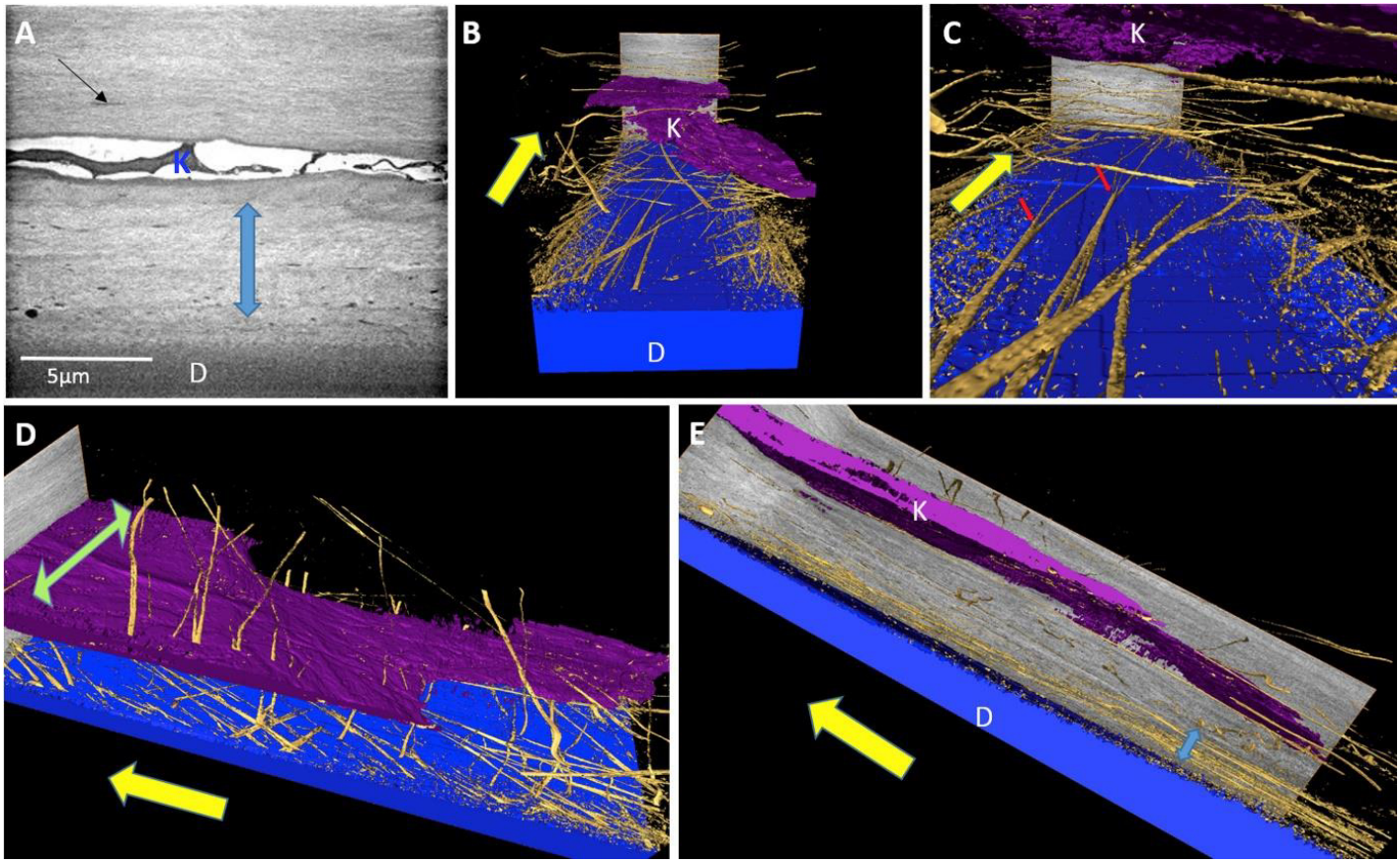


**Figure 4.3. 3D reconstruction of elastic fibres in the peripheral cornea.** The yellow arrows indicate the radial direction towards the limbus. Fig. 4.3A: SBF SEM image of posterior peripheral cornea reveals the presence of numerous elastic fibres, which appear highly concentrated within a zone containing 4–5 lamellae (blue arrow) next to Descemet's membrane (D). Elastic fibres are also evident above this zone (black arrow) above a keratocyte (K). Fig. 4.3B: 3D volume rendering of the posterior peripheral cornea reveals the distribution of elastic fibres (gold) above and below a keratocyte (K, coloured purple) running parallel to Descemet's membrane (coloured blue). Fig. 4.3C: Fibres exhibit bifurcated and trifurcated branching (red arrows). Fig. 4.3D: The elastic fibres appear randomly orientated. Some are orientated at an oblique angle toward the limbus while others appear to be orientated more circumferentially (green arrow) with respect to the cornea. Fig. 4.3E: Side plane view of 3D volume reveals the elastic fibres to be concentrated just above Descemet's membrane (blue arrow). Images taken from (Lewis *et al.*, 2016).

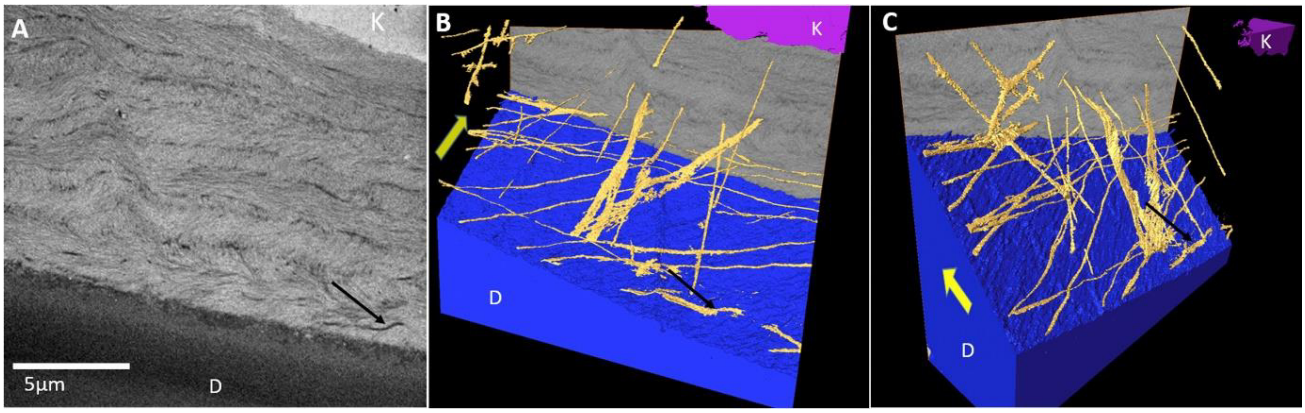


**Figure 4.4. 3D reconstruction of elastic fibres in the central cornea.** Fig. 4.4A: SBF SEM image of posterior central cornea. The black arrow highlights a single elastic fibre running longitudinally within the stroma. (D = Descemet's membrane; K = keratocyte). Fig. 4.4B and C: Three-dimensional volume rendering of the same region shown in A reveals that most fibres run radially toward the limbus (yellow arrow). Taken from (Lewis *et al.*, 2016).

Furthermore, when analysing the first data set, it was evident that the majority of these fibres were concentrated directly above Descemet's membrane, therefore, this 1000 image data set was analysed in greater detail, with fibre percentage calculated every 200 images (8µm of tissue)(Fig. 4.5B). As expected, these results showed that elastic fibre concentration was significantly higher in the first 8µm of stroma above Descemet's membrane before falling rapidly as you move anteriorly. The same analysis was carried out on the central stroma (Fig. 4.5C). This showed the same density pattern as the peripheral cornea, with a significantly higher concentration of fibres directly above Descemet's membrane compared to stroma outside this region. However, the density of elastic fibres in this zone was almost 8 times lower (0.5%) than the same area in the peripheral cornea (4%).

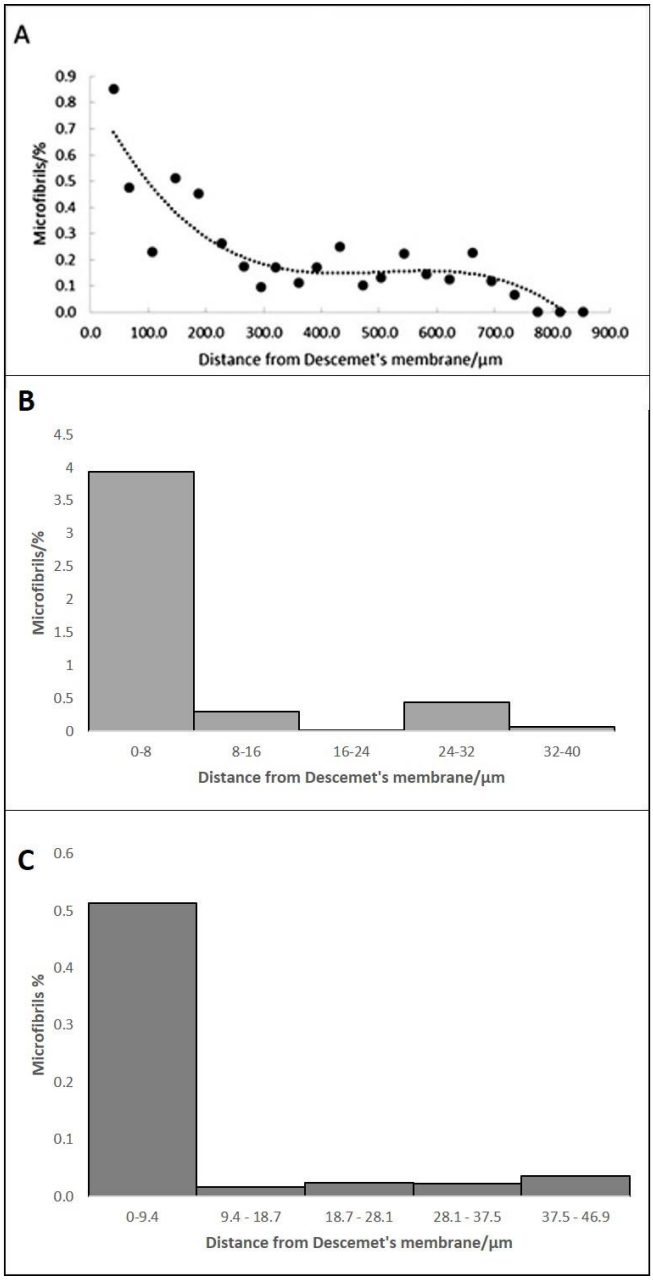


**Figure 4.5. Distribution of elastic fibres as a function of depth in the peripheral and central cornea.** Fig.4.5A: the percentage of the peripheral tissue volume occupied by elastic fibres from 0 µm (top of Descemet's layer) to about 800 µm (bottom of epithelium). Each point represents data from about 1000 en face serial images summed between that depth and the one before it in the graph. The number of elastic fibres falls rapidly after about 200 µm from Descemet's membrane. No fibres were observed in the anterior ~100 µm of the stroma). The histograms shows the volume percentage of elastic fibres in the first ~50µm of stroma anterior to Descemet's membrane in the peripheral (Fig. 4.5B) and central (Fig. 4.5C) cornea. This shows that the majority of the fibres are located in the ~8 µm region immediately above Descemet's membrane. A and B taken from (Lewis *et al*., 2016).

*4.3.5. Corneo-limbal region*

After studying elastic fibres in the central and peripheral cornea, it was important to discover the organisation of these fibres at the posterior limbus and adjacent cornea. Low magnification SBF SEM examination of this area in transverse section revealed the presence of numerous electron-dense elastic fibres within the posterior limbus which extended into the posterior cornea (Fig. 4.6). The trabecular meshwork extended into the posterior cornea, where it anchored via a wedge-like insertion between Descemet's membrane and the overlying stroma. Trabecular meshwork is often described as anchoring in the corneo-limbal junction where Descemet's membrane terminates; however, in this instance the trabecular meshwork extended approximately 250µm beyond this region and inserted into the peripheral cornea. Elastic fibres were visible above the insertion point as well as anterior to the trabecular meshwork in the limbus, where they were concentrated within a 40-50µm region.

Furthermore, a 3D reconstruction of this region revealed that these fibres appeared densely packed, appeared broader than fibres observed in the peripheral cornea, and were generally found to be aligned parallel to the limbal stroma (Fig. 4.7A). Viewing the same region with TEM showed that these structures are actually 'true elastic fibres, containing an amorphous central component that can be distinguished from the electron dense microfibrils surrounding the core (Figs. 4.10B-C).

SBF SEM data further revealed that the trabecular meshwork terminates in the posterior cornea, and that the insertion is bordered by 2-4 layers of elastic sheets (Fig. 4.8). Anterior to the trabecular meshwork insertion, elastic tissue appeared to form fenestrated sheets. These elastic sheets extended just beyond the posterior corneolimbal junction, where they appeared to transform into fibre-like extensions, which continued into the posterior corneal stroma.

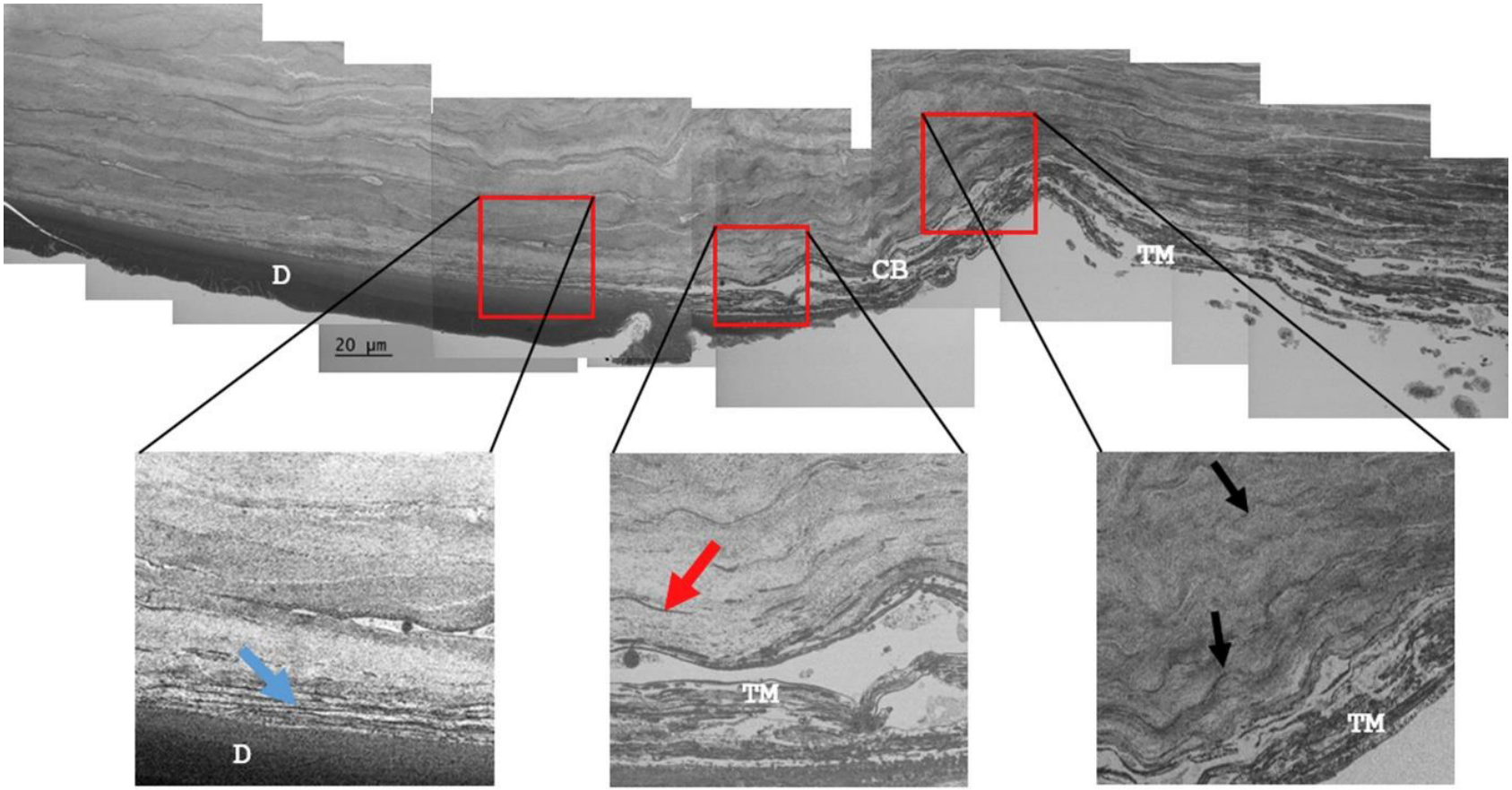


**Figure 4.6. Low magnification montage of SEM images showing a transverse section through the corneo-limbal region**. Numerous elastic structures are evident within the corneolimbal region (black arrows). The trabecular meshwork (TM) appears to have a “wedge like” insertion into the adjacent posterior cornea above Descemet's membrane (D) (blue arrow) which tapers to a terminal point some 250 µm in from the corneolimbal boundary (CB). The elastic fibres are visible above this insertion (red arrows). Taken from (Lewis *et al*., 2016).

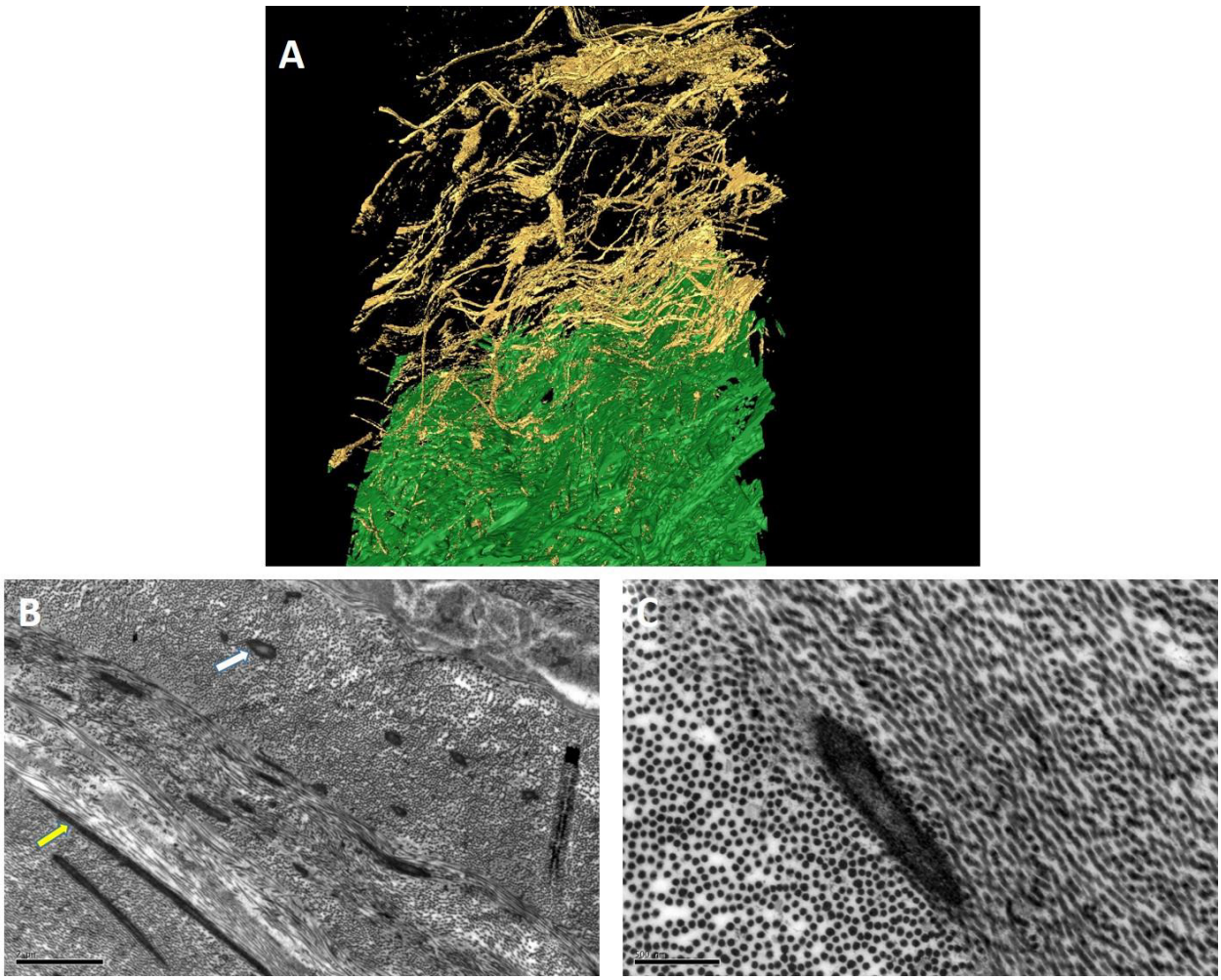


**Figure 4.7. Elastic fibres at the limbus**. Fig. 4.7A: 3D reconstruction of the limbal area anterior to the trabecular meshwork revealed a mass of elastic tissue, including long fibres and broad elastic sheet-like material. Fig.4.7B: TEM micrograph of this region demonstrates the longitudinal elastic sheets (yellow arrow) and thick transverse fibres (white arrow) (Bar = 2µm). Fig. 4.7C: Higher magnification shows that the fibres contain an amorphous central core surrounding by darkly stained bundles of microfibrils (Bar = 500nm).

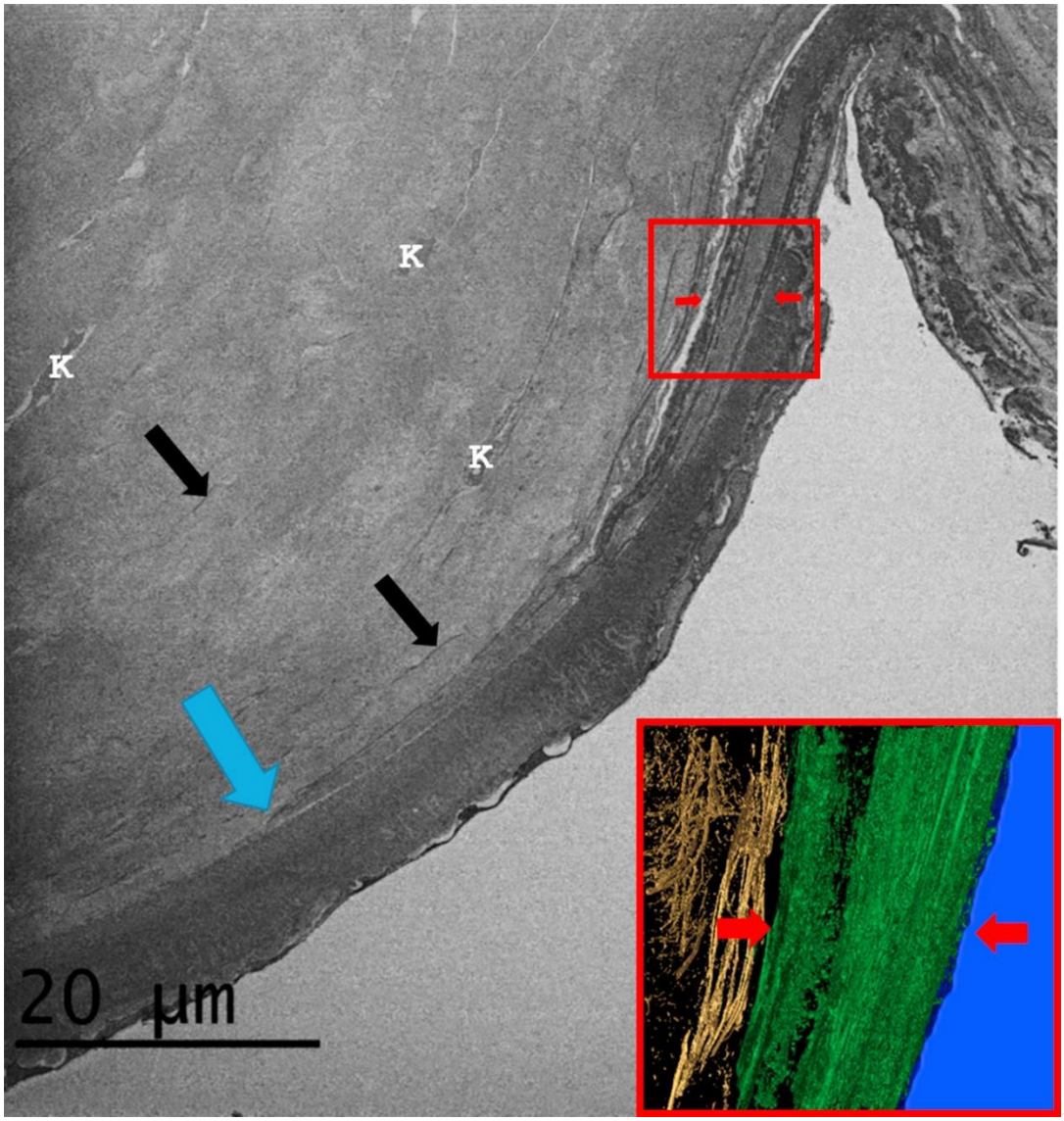


**Figure 4.8. The corneo-limbal region**. The main SEM image shows the trabecular meshwork insertion between Descemet's membrane and the posterior corneal stroma. The trabecular meshwork insertion is separated from the stroma and Descemet's membrane by sheets of elastic-like tissue (red arrows), which appear to terminate at a point (blue arrow) within the posterior stroma next to Descemet's membrane. Elastic fibres and elastic sheets are evident (black arrows) within the posterior stroma to a depth of about 25 µm distal to Descemet's membrane. Keratocytes (K) are also visible within the posterior stroma. Inset: A 3D image slice through the trabecular meshwork insertion highlighting the presence of elastic sheets (coloured green and indicated by red arrows) and fenestrated elastic sheets present within the posterior stroma above it (coloured gold). Taken from (Lewis *et al*., 2016).

*4.3.6. Foetal cornea*

In order to discover if elastic fibres are present in the developing human cornea, a 13-week old foetal cornea was examined with SBF SEM. Interestingly, elastic fibres were present, even at this early developmental stage. The fibres were visible above the endothelium and developing Descemet's membrane (Fig. 4.9).

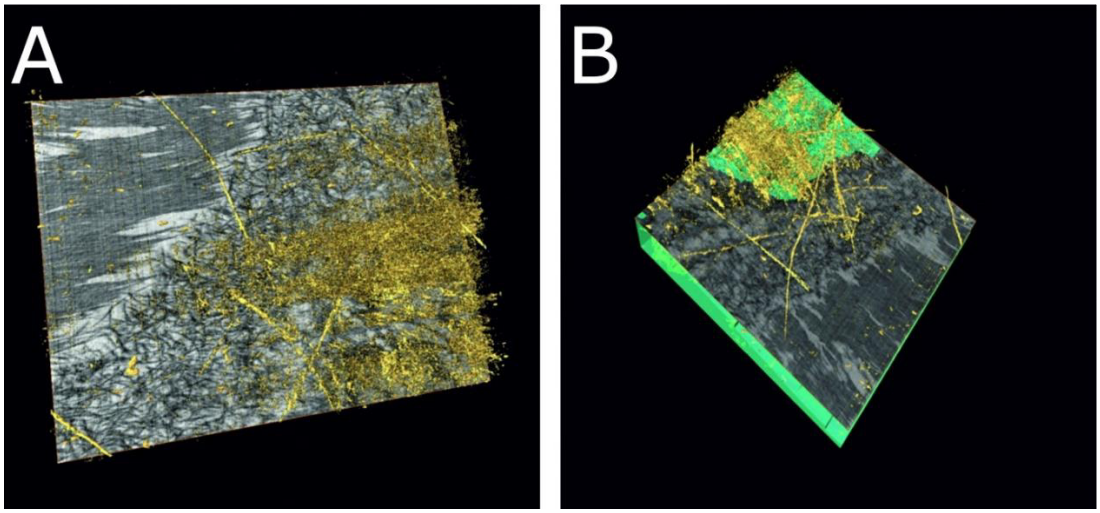


**Figure 4.9. 3D reconstruction from the central posterior cornea of a 13-week-old human foetus**. Fig. 4.9A shows the presence of elastic fibres (gold) above a meshwork of dark filaments which will later become Descemet's membrane. Because of the oblique imaging plane, some stroma above the fibres is seen at the top left of the image. Fig. 4.9B, acquired from a different orientation shows elastic fibres (gold) immediately above the endothelium (light green). Taken from (Lewis *et al*., 2016).

*4.3.7. Immuno-fluorescence microscopy*

Immuno-labelling revealed that type VI collagen was concentrated in the posterior stroma, in a thin layer of tissue above Descemet's membrane (Fig. 4.10A), and was continuous with the trabecular meshwork (Figs. 4.10B-C). No elastin was detected in the corneal stroma (Fig4.10D), although it was prominent throughout the trabecular meshwork (Fig. 4.10E). Fibrillin failed to label in both the stroma and trabecular meshwork (Fig. 4.10F). Controls with no primary antibody did not reveal any labelling (data not shown).

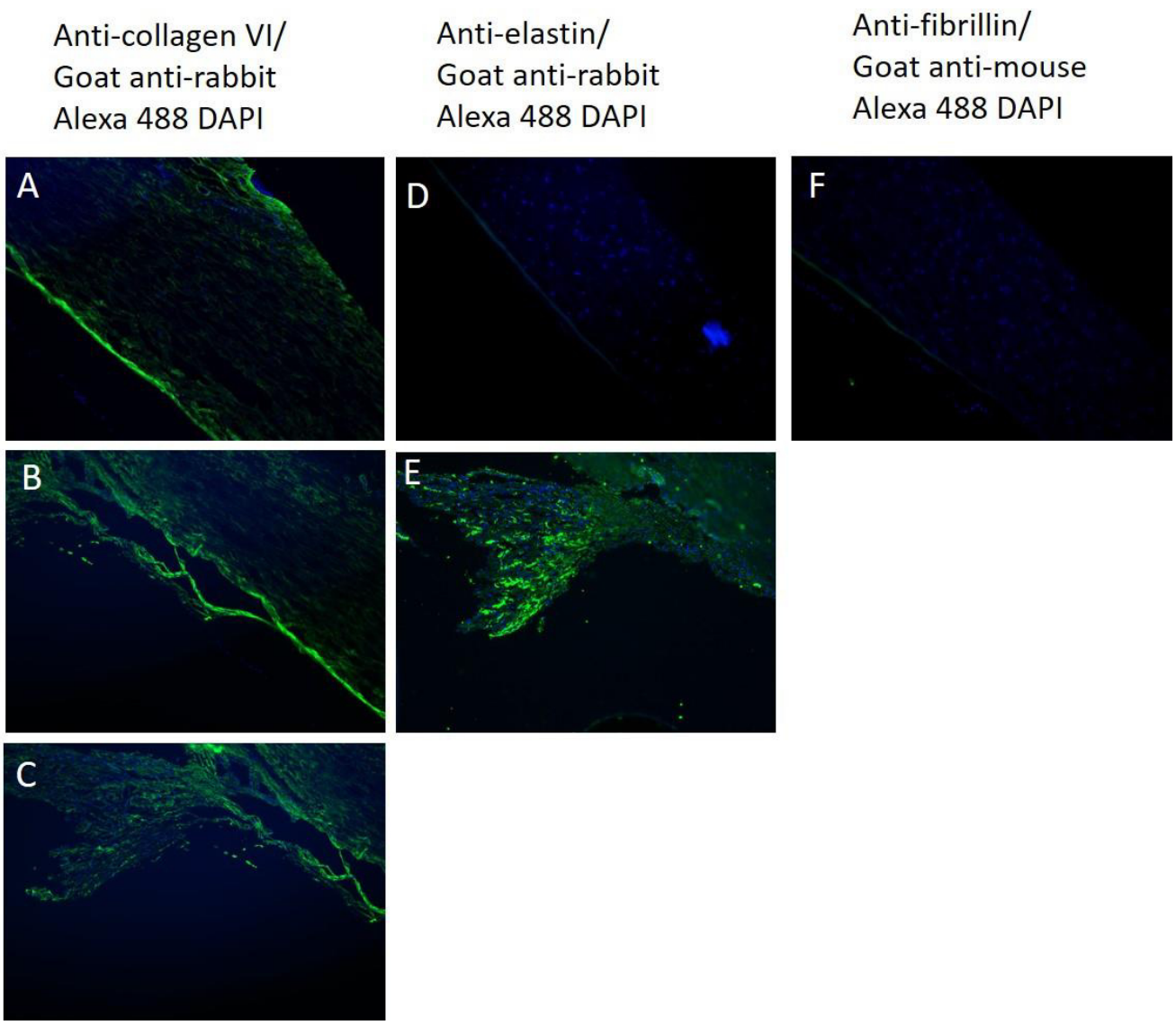


**Figure 4.10. Immuno-fluorescence microscopy**. Figs. 4.10A-C: Type VI collagen was concentrated in a thin layer of tissue in the posterior stroma, anterior to Descemet's membrane (A), and continued into the trabecular meshwork (B, C). No elastin was present in the stroma (Fig. 4.10D), but was ubiquitous in the trabecular meshwork (Fig. 4.10E). Fibrillin failed to label in the corneal stroma (Fig. 4.10F).

**4.4. Discussion**

This study has revealed the presence of a complex elastic fibre system in the human cornea. The tannic acid-based en bloc staining protocol is known to stain the microfibrillar and amorphous components of elastic fibres (Kageyama *et al.*, 1985, Simmons and Avery, 1980), enabling them to be viewed using both TEM and SBF SEM. Viewing these structures in the central and peripheral cornea with TEM showed that they lack the central amorphous component, and are therefore not 'true elastic fibres, but bundles of fibrillin-containing microfibrils (Sakai *et al.*, 1986b), also termed oxytalan fibres (Fullmer and Lillie, 1958). Additionally, these fibres exhibited a periodicity of ~56nm, which is typical of elastic fibres (Keene *et al.*, 1991b, Kielty *et al.*, 1992). Further evidence was provided by two-photon fluorescence microscopy, tuned close to the elastin two photon excitation peak, highlighting the existence of elastic fibres in the posterior stroma, as seen by Kamma-Lorger *et al.* (2010). Fibres identified by TFP would almost certainly be elastic, as the signal from collagen is not fluorescent, but almost entirely SHG .This technique is often used to visualise elastic fibres in tissues such as articular cartilage (Mansfield *et al.*, 2009, Yeh *et al.*, 2005), arteries (Boulesteix *et al.*, 2006), and more recently, the trabecular meshwork (Park *et al.*, 2016). These findings contradict previous studies that failed to detect elastic fibres in the mature healthy human cornea (Alexander and Garner, 1983a, Hirano *et al.*, 1991).

These structures have also been stained with orcein and Millers stain (Lewis *et al.*, 2016), both of which are elastic fibre specific stains. However, the elastic fibres failed to label with commercially available fibrillin-1 antibodies, whereas type VI collagen labelled above Descemet's membrane, and continued into the trabecular meshwork, consistent with findings from Dua *et al.* (2014). In the mouse cornea, elastic fibres have been immuno-gold labelled with non-commercially available fibrillin-1 antibodies (Hanlon *et al.*, 2015). An association between type VI collagen and elastic microfibrils has previous been shown (Finnis and Gibson, 1997, Everts *et al.*, 1998): this close association may potentially masks the fibrillin antigenic sites in the human cornea. The precise composition of elastic fibres in the cornea is unclear, although as in other tissues, it is likely that individual microfibrils that make up the fibres contain other glycoprotein components in smaller quantities, such as fibrillin-2 (Charbonneau *et al*., 2003), which may be involved in elastic fibre formation as Fbn2 mRNA is predominantly expressed during the embryonic period in mice (Zhang *et al*.,

1995), and microfibril-associated glycoprotein 1 (MAGP-1), that is thought to provide structural integrity (Trask *et al.*, 2000, Kielty *et al.*, 2002a).

SBF SEM enabled the elastic fibres to be viewed in three-dimensions, revealing an extensive network in the posterior stroma of central and peripheral cornea, appearing to be concentrated immediately above Descemet's membrane. This was confirmed with full thickness quantification, showing that the density of elastic fibres was significantly higher in the first 8µm of stroma above Descemet's membrane, in both central and peripheral cornea. Elastic fibres in the peripheral cornea made up 4% of the volume in this 8µm layer of tissue; it should be noted, however, that the threshold value chosen to highlight the elastic fibres was such as to avoid staining other tissue components, so no weakly stained elastic fibres would have been included; the quantitative data presented should therefore be regarded as minimum values.

At the posterior corneo-limbal junction, elastic fibres are broader or form fenestrated sheets anterior to the TM. It appears as though the elastic fibres seen in the peripheral and central stroma are continuous with this region, the TM, and possibly the adjacent posterior sclera, potentially travelling throughout the entire width of the cornea, limbus to limbus, as no termination points were evident. It is likely that the presence of this elastic tissue in the posterior limbus acts in conjunction with the anchoring lamellae, providing further biomechanical stability in this transition zone (Boote *et al.*, 2011, Meek and Knupp, 2015).

Elastic fibres were concentrated in an 8-10micron layer of tissue above Descemet's membrane, a region that Dua *et al* suggest is structurally distinct. However, the elastic fibres were not limited to this area, as they were distributed in lower quantities throughout the stroma. The fibres in the pre-Descemet's layer may play a mechanical role in big bubble surgical technique. If the cleavage plane is created by air pressure splitting the posterior stroma along the last layer of keratocytes nearest Descemet's membrane, the elastic fibre network would support this thin separated layer of tissue, and may even contribute to the cleavage plane location by biomechanically strengthening the layer, making it difficult to detach from Descemet's membrane. Dua *et al.* (2013) described a "type 1 big bubble", formed in the central cornea and expanding up to 8mm in diameter that was able to

withstand high strains without bursting. Furthermore, the toughness of the layer has been shown by performing deep anterior lamellar keratoplasty and phacoemulsification at the same time, as the layer maintains a stable anterior chamber for cataract surgery following the removal of scarred corneal stroma (Zaki *et al.*, 2015). Elastic fibres would enable this by providing extensibility, whereas collagen fibrils alone may slip or break under excessive tension. Following stretching, the pre-Descemet's layer reverts to its original dimensions on deflation of the bubble, conveying how the elastic system provides elasticity as well as biomechanical strength (Dua *et al.*, 2015a). Dua and colleagues also described a "type 2 bubble," where air travelling around the periphery of the cornea before the bubble enlarged centrally (Dua *et al.*, 2013). At the corneo-limbal region, elastic fibres became broader and formed fenestrated sheet-like structures in the posterior stroma, resulting in an elastic annulus. These sheets may be responsible for the circumferential air flow seen during type 2 bubble formation, by initially containing and restricting the airflow around the corneal perimeter.

The elastic fibre system seems to be continuous with the TM. During penetrating keratoplasty surgery, this system would be severed and the tension released. As elastic fibres cannot be replaced during normal matrix turnover, this would permanently alter the mechanical properties of the cornea. As well as potentially affecting the shape of the cornea, the release of tension could also have negative implication on trabecular outflow, subsequently playing a role in the development of glaucoma, which has been associated with penetrating keratoplasty surgery (Al-Mahmood *et al.*, 2012, Dada *et al.*, 2008). Recently, two photon fluorescence microscopy has revealed the intricate connections between elastic fibres in the trabecular meshwork and ciliary muscle tendons (Park *et al.*, 2016). These connections suggests that ciliary muscle tone can therefore directly influence the trabecular beams and alter aqueous outflow. In the other direction, elastic fibres in the posterior cornea and limbus that are continuous with the TM may play a similar role, with the tension in the fibres involved in keeping trabecular outflow channels open to facilitate aqueous drainage.

This study has revealed that the TM projects about 250 µm into the peripheral cornea between the Descemet's membrane and the posterior stroma. This result confirms a recent

observation by Dua *et al.* (2014) in which the TM was also identified to extend into the peripheral cornea, although these authors did not describe the anatomy of the TM insertion in any detail. The anatomical description of the TM in this study is very different from the currently accepted description of TM anatomy in terms of its anterior fixation. Hogan (1971) describe the TM joining the limbus at a point where Descemet's membrane terminates, referring to this as the posterior corneolimbal junction. The TM is regarded as a "toned" tissue, which is required to be under tension in order to function normally. The aqueous outflow is regulated by the contraction and relaxation of the trabecular meshwork, through the action of ciliary muscles attached to the meshwork at its posterior fixation point deep within the sclera (Llobet *et al.*, 2003, Tamm, 2009). The TM insertion would appear to be closely associated anteriorly with the concentrated elastic fibre zone identified in this study, which spanned the limbus and the peripheral cornea. It is possible that this elastic system helps maintain the tone by fixing the TM anteriorly to the peripheral cornea and limbus.

To maintain focus in vision, the cornea must be resistant to deformation from external forces, and when it is deformed it must regain its original shape quickly. *In vivo*, and in the absence of external forces, a force balance exists between the collagen network, which resists only tension, the proteoglycan interfibrillar gel, which exerts an internal swelling pressure on the collagen network, and the IOP, which exerts an outward force on the cornea that acts evenly across all layers of the stroma (McPhee *et al.*, 1984), keeping them taut. The response to changes in IOP, either over the cardiac cycle or as a symptom of disease, has been shown to be complex. Boyce *et al.* (2008) showed that in bovine cornea, when increasing the IOP from 3.6 to 8 mmHg using an *ex vivo* pressure cell, 90% of the outward corneal distension at the optic axis was accounted for by deformation in the peripheral cornea. The corresponding marked difference in material parameters across the cornea (Elsheikh et al., 2013) enables the eye to maintain focus with minimal compensation over significant variations in IOP. Given that the IOP can change due to a number of factors, it appears that there is a need for an efficient, long range elastic structure in the peripheral cornea/limbus.

While corneal collagen is known to be crimped (Liu *et al.*, 2014), it is unlikely that straightening of this crimp alone will provide the range of deformation in the periphery

required to maintain central corneal shape. The collagen arrangement in the periphery is predominantly circumferential (Aghamohammadzadeh et al., 2004), meaning radial deformation is likely to give rise to collagen realignment through the proteoglycan gel (Lewis *et al.*, 2010), which suggests the requirement of further mediating force to maintain internal structure. In other collagenous tissues that incur significant and repetitive strains, such as arteries, chordae tendinae and cartilage, this mediating force is a network of elastic fibres (Green *et al.*, 2014). The properties of high extensibility would suit the elastic fibre's proposed role of supporting the collagen network in deformation. It is possible that elastic fibres in the peripheral cornea fulfil a similar role.

Elastic fibres were identified in human foetal cornea, before Descemet's membrane has formed, conveying that these structures are not a result of age-related changes in the stroma. Elastic microfibrils were identified in a 13-week embryonic cornea within four very thin lamellae of the posterior stroma, forming an 8μm thick region anterior to the endothelium. Their presence at this early stage of development, before Descemet's membrane has formed, indicates that elastic microfibrils in the cornea are not the result of degenerative age-related changes, but presumably fulfil instead some basic function in the presumptive stroma. Calcium binding by the elastic fibres of most tissues makes them resistant to proteolysis (Reinhardt et al., 1997), so it is also unlikely that they undergo any significant breakdown and remodelling as a function of age. Secreted by the earliest invading mesenchymal cells, it is tempting to speculate that they might provide mechanical stability (Shawky and Davidson, 2015) and elasticity (Wingate *et al.*, 2012) to the expanding posterior lamellae prior to deposition of Descemet's membrane, and the assumption of a functional role by the maturing stroma. In a mechanism akin to that in which the primary stroma is believed to form a template for cell migration and matrix synthesis in the embryonic chick cornea, elastic microfibrils may additionally serve some function in guidance of inwardly migrating cells, and so have an influence upon posterior lamellar organisation. Microfibrils would become separated spatially from one another as the lamellae expand with further collagen synthesis during development. This could explain why microfibrils situated at sites increasingly anterior to their greatest concentration distal to Descemet's are distributed between lamellae and appear to fan out towards the limbal region. If this hypothesis is correct, the elastic microfibrils would represent a residual

primary structure of the developing cornea, with no function in the adult tissue. However, based on the important role fulfilled by elastic microfibrils in other tissues, their presence in the cornea and limbus does suggest other possible functions.

### 4.5. Conclusion

In conclusion, this study describes a complex elastic system in the posterior human cornea and limbus. This takes the form of elastic sheets in the limbus from which protrude elastic fibres into the peripheral cornea. As these fibres extend into the cornea they bifurcate and trifurcate, forming a layer of thin elastic fibres that is concentrated within the posterior 8 µm. This elastic system may have a number of developmental and structural roles. Its presence is likely to influence the biomechanical behaviour of the cornea and may provide explanations for the effects of a number of surgical interventions.

# Chapter 5 - Elastic fibres in the cornea: differences between normal and keratoconic stroma

## 5.1. Introduction

The transparency and strength of the cornea arise from the highly organised arrangement of the stromal ECM. The main component of this matrix is type I collagen fibrils that are arranged parallel to each other within lamellae. Corneal transparency is maintained by the uniform diameter and quasi-regular spacing between these collagen fibrils (Maurice, 1957), which itself is controlled by the presence of interfibrillar proteoglycans (Kao and Liu, 2003, Lewis *et al.*, 2010). Lamellae are highly interlaced (Radner *et al.*, 1998a) and randomly orientated (Komai and Ushiki, 1991) in the anterior stroma when viewed *en face*, whereas they are more organised in the posterior stroma, showing two preferred orientations (Abahussin *et al.*, 2009, Meek *et al.*, 1987, Aghamohammadzadeh *et al.*, 2004), and form a circum-corneal annulus at the limbus (Newton and Meek, 1998a). This specific arrangement of collagenous lamellae throughout the stroma provides the cornea with biomechanical strength and the ability to resist tensile strain (Abahussin *et al.*, 2009).

Keratoconus is a pathological condition that is characterised by bilateral progressive stromal thinning and ectasia of the cornea that results in irregular astigmatism and eventual conical shaped cornea as the tissue bows under the influence of intraocular pressure. In more advanced forms of the disease, axial corneal scarring may develop which further reduces the quality of vision. However, the aetiology of keratoconus is currently unclear, as it is likely to involve many different factors including biochemical, genetic and environmental. In advanced stages of keratoconus, the organisation of the collagen lamellae is severely disrupted, resulting in a loss of tensile strength and the progression of ectasia (Daxer and Fratzl, 1997, Radner *et al.*, 1998b, Meek *et al.*, 2005).

As well as collagen, elastic tissue plays a vitally important biomechanical role in many dynamic tissues, for example lungs and blood vessels, allowing them to expand and contract in response to variations in blood pressure (Sherratt, 2009). In similar fashion, the sclera contains an elastic fibre system (Marshall, 1995, Alexander and Garner, 1983) allowing the eye to deform slightly and regain its original shape following the pull of external extraocular

muscle and changes in intraocular pressure. Despite the cornea being part of the outer tunic of the eye, along with the sclera, the presence of elastic tissue in the corneal stroma has been overlooked in recent years. Elastic fibres are often grouped into three categories: 'True' elastic fibres (amorphous core of elastin surrounded by a layer of microfibrils), elaunin (intermediate fibres with less amorphous component), and oxytalan (bundles of elastin-free microfibrils) (Alexander and Garner, 1983, Fullmer and Lillie, 1958). Previous studies using histological stains for elastic fibres have concluded that there was no form of elastic tissue present in mature human corneas (Alexander and Garner, 1983, Hirano *et al.*, 1991), with the exception being Kamma-Lorger *et al.* (2010), who reported a network of elastic fibres using two-photon fluorescence microscopy.

The development of more advanced imaging techniques, such as SBF SEM, has enabled this area to be re-visited. Hanlon *et al.* (2015) used this technique to demonstrate the presence of 'elastin-free microfibril bundles' throughout the murine corneal stroma. These microfibrils were shown to contain fibrillin, a major component of elastic fibres (Sakai *et al.*, 1986b). Furthermore, we have recently characterised a complex network of elastic fibres in human cornea using SBF SEM (chapter 4) (Lewis *et al.*, 2016). These appear as elastic sheet at the limbus before becoming narrower fibres in the peripheral and central stroma that run parallel to the surface of the cornea, and are highly concentrated immediately above Descemet's membrane. Elastic fibres have previously been reported in various corneal pathologies including bullous keratopathy and Fuchs endothelial dystrophy (Ljubimov *et al.*, 1998b, Akhtar *et al.*, 2001, Alexander *et al.*, 1981b). In the only study of elastic fibres in keratoconus, elastic fibres have been reported below the epithelium in thinned central regions of the conical cornea (Jefferies and Alexander, 1995). The loss of biomechanical strength and the progression of ectasia in the stroma of keratoconic corneas, as well as the demonstration of an extensive elastic network in normal corneal stroma, highlights the importance of further investigating the presence and distribution of elastic tissue in this disease.

The aims of this study were to use SBF SEM, conventional TEM, and immunofluorescence microscopy to examine elastic tissue throughout the stroma of keratoconic corneal buttons in comparison to normal cornea, focussing in particular on areas directly above Descemet's membrane, and below the epithelium.

## 5.2. Methods

### *5.2.1. Tissue specimens*

Three human keratoconic buttons (7mm diameter) were obtained from the Department of Ophthalmology, Kyoto Prefectural University, Japan, following penetrating keratoplasty surgery. Button 1, from the right eye of a 47 year old female, had a minor apical scar inferior to the pupil (Fig. 5.1B). Button 2, obtained from the right eye of a 57 year old male was more severely scarred in the same region, and was at the most advanced stage of keratoconus out of the three samples used (Fig. 5.1D). Button 3, from the right eye of a 68 year old female, was scarred superiorly (no image). All thinned cone regions were located para-centrally. Following surgery, buttons were immediately fixed in 4% paraformaldehyde before being transported to Cardiff on dry ice. Normal human corneas with scleral rim were obtained from Bristol Eye bank and stored in 4% paraformaldehyde until use.

### *5.2.2. SBF SEM*

Thin segments were dissected from each sample and fixed in modified Karnovsky's fixative (2.5% glutaraldehyde and 2% paraformaldehyde in 0.1M cacodylate buffer at pH 7.2) at room temperature before being stored in buffer at 4°C overnight. Button 1 was processed *en bloc* using a tannic-acid based protocol, whereas button 2 and 3 were processed with a novel *en bloc* orcein staining protocol. Normal corneas were processed using both protocols. Sclera control was processed with the orcein protocol only.

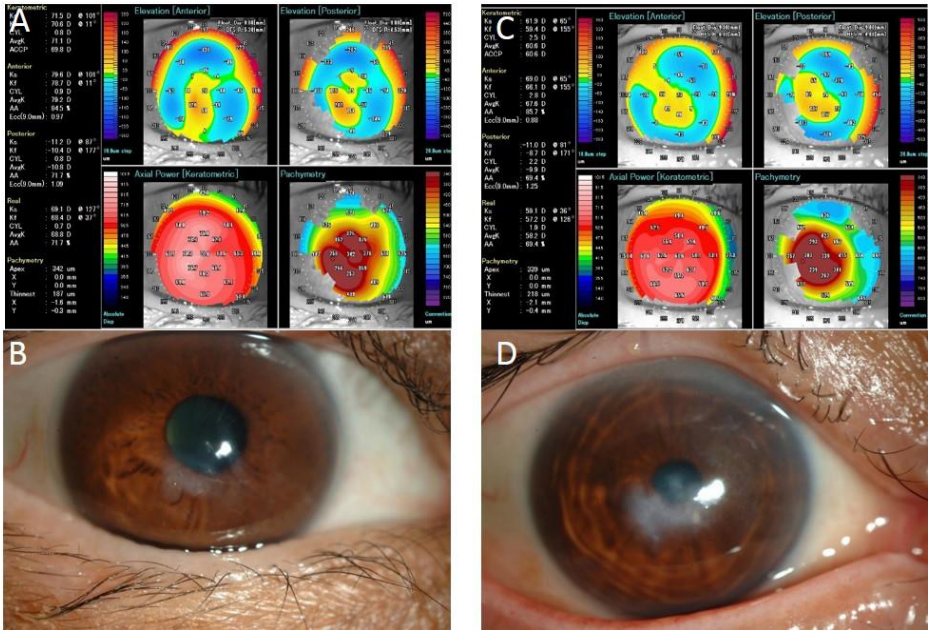


**Figure 5.1. OCT corneal shape analysis and images of keratoconic corneas**. Images show cornea 1 (A,B) and 2 (C,D) before surgery. Cornea 1 has mild scarring inferior to the pupil (B) whilst the scarring in cornea 2 is more severe (D). Elevation and pachymetry measurements reveal that both cone regions are located para-centrally.

*Tannic acid-uranyl acetate based protocol*: Initially, the standard protocol described in chapter 2 was used to process button 1. This method resulted in dark staining throughout the tissue, with little contrast. Therefore, additional tissue was processed using a modified version of this protocol, where 1% uranyl acetate was used instead of 2%, or ethanoic uranyl acetate was removed. Specimens stained with the modified protocols also appeared very dark with little contrast, compared to normal controls.

*Orcein based protocol:* Orcein staining has been used to visualise elastic fibres in the cornea using TEM (Lewis et al., 2016), with a protocol based on earlier work (Nakamura et al., 1977). A novel en bloc orcein staining protocol was developed in an attempt to enhance contrast of keratoconic samples using SBF SEM. Samples were fixed with 1% osmium tetroxide before washed in $dH_2O$ for 20 mins and transferred to 70% ethanol for 10 mins. Samples were stained with 0.3% orcein in 70% ethanol for 2 hours. After a 30 minute wash with 70% ethanol, specimens were dehydrated in 90% ethanol for 20 mins, followed by

100% ethanol x 2 for 20 mins. Following dehydration, the tissue was subjected to the same remaining steps described in the tannic acid based protocol (chapter 2).

### *5.2.3. Transmission electron microscopy*

All 3 buttons and the normal cornea that were *en bloc* stained for SBF SEM were also used for TEM. 90nm gold sections were cut using a Leica UC6 ultramicrotome, floated on distilled water and collected on copper grids. All section were visualised using a JEOL 1010 TEM.

### *5.2.4. Immunofluorescence labelling*

One half of the normal cornea and one quarter of button 2 were transferred to PBS for 24 hours, with multiple changes during this time. As the specimens were fixed, it is thought that washing in PBS enhances labelling. The tissue was then embedded in OCT (optimal cutting temperature) compound and snap frozen in isopentane cooled in liquid nitrogen, before being stored at -20°C. 10um thick frozen sections were cut using with a cryostat (Leica CM3050 S) and collected on lysine coated glass slides. Sections were rehydrated with PBS for 15 minutes at room temperature before being blocked with 2% BSA in PBS for 30 minutes. Mouse monoclonal anti-fibrillin 1, rabbit polyclonal anti-type VI collagen and anti-elastin antibodies (Abcam, Cambridge) were applied at 1/100 and 1/1000 dilutions overnight in a dark humid chamber at 4°C, with PBS applied to negative controls. After a wash with PBS, sections were transferred to secondary antibodies goat anti-mouse or rabbit (as appropriate) conjugated with Alexafluor 488, at a 1/200 dilution. Finally, sections were washed with PBS (5 x 2minutes) and coverslips mounted using vectashield hardset with DAPI. Sections were examined using fluorescence microscopy (Leica DM6000B) with appropriate wavelength filters. Images were collected using Leica application suite: Advanced fluorescence, and analysed using ImageJ software.

## 5.3. Results

### *5.3.1. Tannic acid stain*

Normal cornea stained with tannic acid displayed an extensive elastic fibre system in the central and peripheral cornea, concentrated immediately above Descemet's membrane (Figs. 5.2 A-C). These fibres ran transversely and longitudinally, parallel to the plane of the cornea, from limbus to limbus, and were seen to bifurcate and trifurcate. SBF SEM data sets obtained from above Descemet's membrane in keratoconic button 1 appeared very dark with little contrast, so it appeared that no elastic fibres were present, and therefore, it was difficult to produce 3D reconstructions. However, one data set produced visible elastic fibres that were segmented out to produce a 3D reconstruction (Figs. 5.2 D-F). The lack of contrast is evident as it is difficult to distinguish between Descemet's membrane and posterior stroma, something which is clear in normal cornea using the same staining protocol. Image reconstruction of the keratoconic data set produced 4 elastic fibres laying above the last keratocyte, running in the same direction, parallel to the surface of the cornea and towards the limbus. No fibres are visible in the stromal space between the keratocyte and Descemet's membrane. The difference in elastic fibreconcentration between normal and keratoconic cornea is clearly evident. Virtually no elastic fibre stain is present in the ~10 micron region of stroma directly above Descemet's membrane in keratoconic cornea, compared to the extensive network of fibres normal cornea. In the SEM data set obtained below the epithelium, a ~5micron band of dark staining was observed. The fibres appeared very small, so they were difficult to clearly distinguish with the lower resolution imaging of SEM. This, in combination with poor contrast made it extremely difficult to transform the data set into a 3D reconstruction. A single image from the data set has been incorporated into Figure 5.4(E).

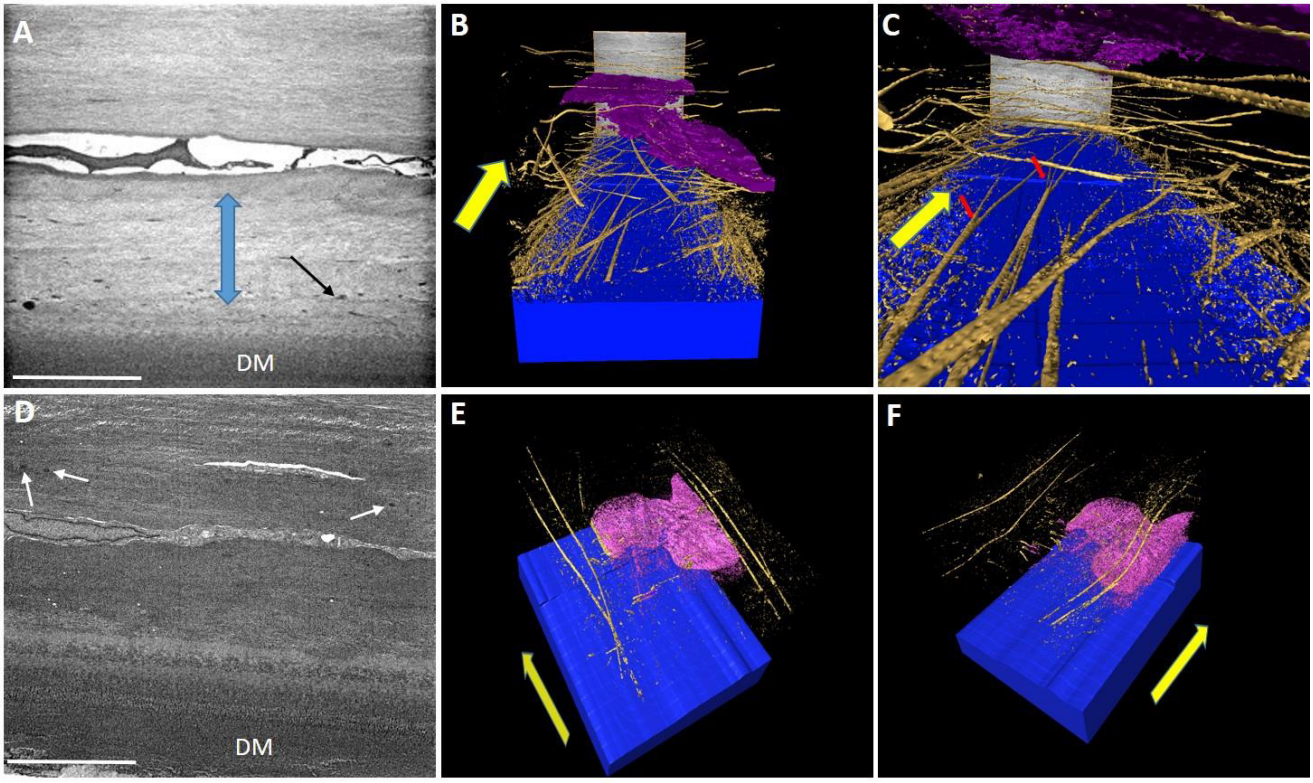


**Figure 5.2. Distribution of elastic fibres above Descemet's membrane (DM) in normal (A-C) and keratoconic button 1 (D-F) cornea using tannic acid staining.** Blue = DM, Gold = elastic fibres, Pink/Purple = Keratocyte**.** A mass of darkly stained fibres (black arrow) are present in a region between the DM and keratocyte (blue arrow) (A). 3D reconstruction of this data portrayed an extensive elastic fibre network concentrated above DM, running towards the limbus (yellow arrow), parallel to the surface of the cornea (B,C); these fibres were seen to bifurcate (red arrows). Elastic fibres were visible in one keratoconic data set in the same region (D-F). In a single image from the data set, a small number of elastic fibres are visible above the cell (white arrows), with no staining directly above DM (D). The rendered data set shows fibres running longitudinally towards the limbus (yellow arrows) (E,F)**.** Scale bar = 5µm. Images A-C taken from (Lewis *et al.*, 2016).

TEM provided clearer images of keratoconic cornea with better contrast compared to SEM. When viewing the area of stroma above Descemet's membrane, it was difficult to detect many elastic fibres in the centre or periphery of the button (Fig. 5.3), compared to the concentration of elastic fibres seen in the same area of normal cornea (Fig. 5.4A) (also refer back to Fig. 4.1D for a control image showing a concentration of elastic fibres above Descemet's membrane). Viewing these structures in the normal cornea at high

magnification revealed a periodic banding pattern repeating every 50-60nm. A very small number of fibres could be seen after an extensive search of the area in both keratoconic buttons 2 and 3; these fibres were orientated transversely, with a diameter of ~250nm (Fig. 5.4B). Many vacuoles were seen protruding from some areas of epithelium in keratoconic cornea, with the absence of basal lamina and Bowman's layer (Fig. 5.4C). Furthermore, an abundance of electron dense elastic fibres were discovered between the basal epithelium and stroma (Figs. 5.4D-F). These fibres were orientated both transversely and longitudinally, running along the plane of the cornea. In the same area, breaks in the stroma were evident.

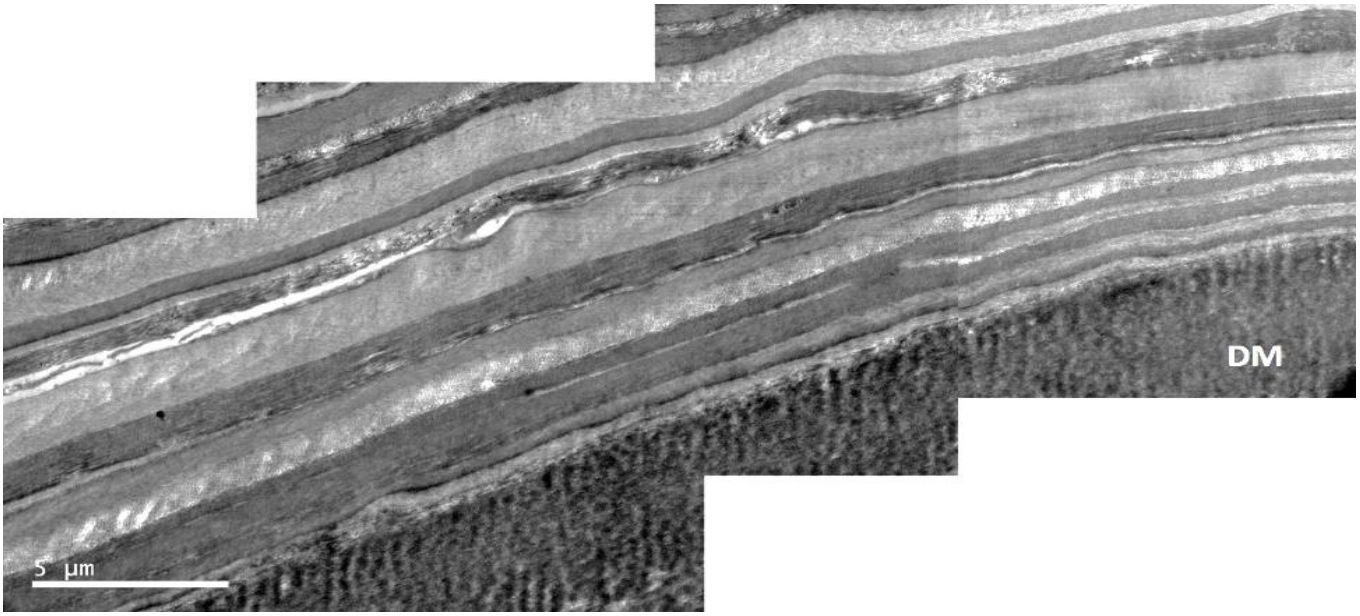


**Figure 5.3. TEM montage of Descemet's membrane and overlying stroma.** The TEM montage displays the absence of darkly stained elastic fibres in a ~20micron region above DM in the stroma of keratoconic button 1, stained with tannic acid.

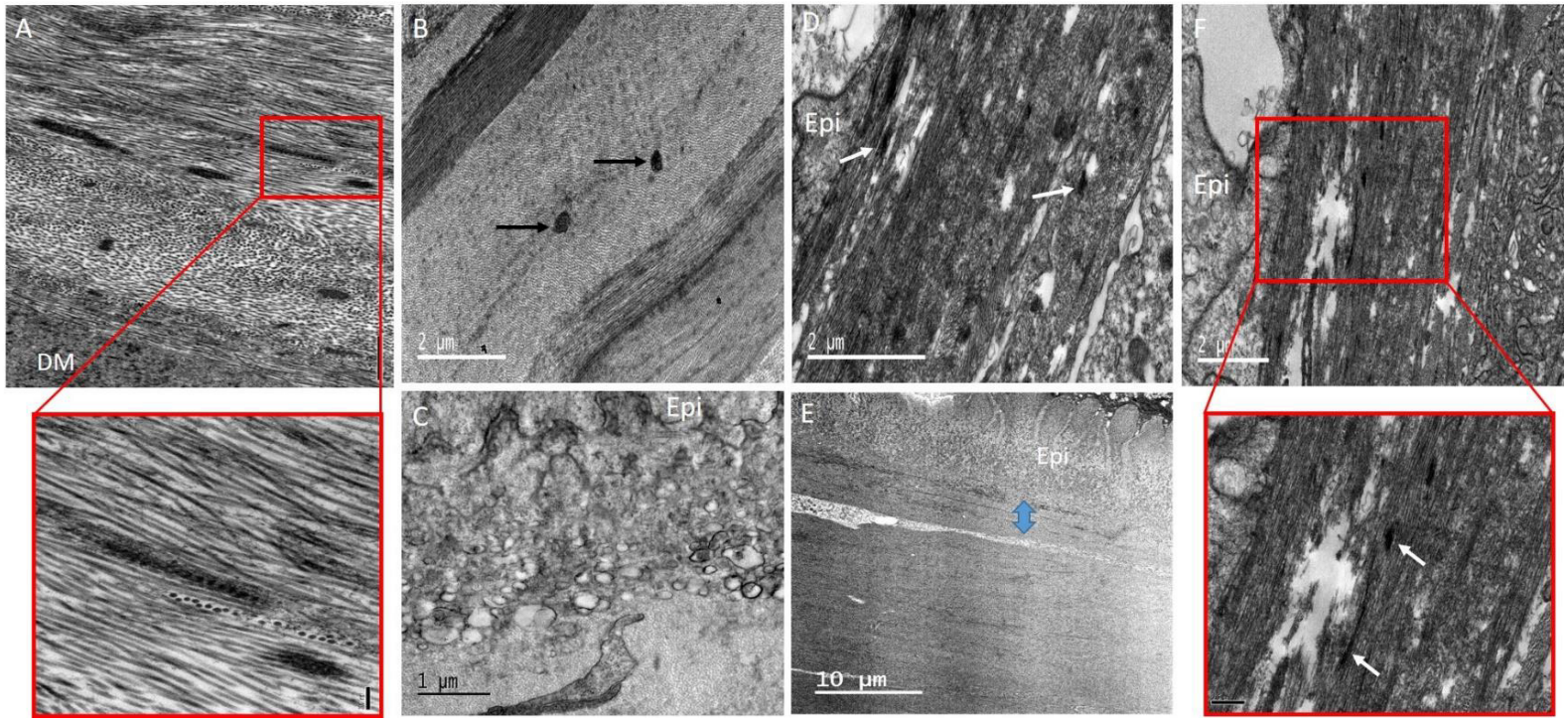


**Figure 5.4. TEM images of normal (A) and KC (B-F) cornea using tannic acid staining**. Normal cornea contains a concentration of elastic fibres above DM (A), with transversely orientated fibres having a ~60nm periodicity (inset – scale bar 200nm). A small number of elastic fibres were located in the posterior and middle stroma of keratoconic button1 after extensive searching (black arrows) (B). Many vacuoles were discovered at the border between basal epithelium (Epi) and stroma (C) with the absence of basal lamina and Bowman's layer. Many elastic fibres were seen directly below the basal epithelium (white arrows) (D-F), concentrated in a 5micron region (blue arrow). These fibres were oriented longitudinally and transversely (inset – scale bar 0.5µm).

*5.3.2. Orcein stain*

The orcein based staining protocol was implemented in an attempt to improve image contrast by removing uranyl acetate, which predominately stains collagen, and replacing it with a well-known elastic fibre stain, orcein. Despite this change, data sets obtained from keratoconic buttons 2 and 3 still appeared to lack contrast, making it difficult to produce 3D reconstructions. A single image from the normal cornea stained with orcein data set shows good contrast between Descemet's membrane and overlying stroma (Fig. 5.5A), and dark fibres can easily be identified in this region. Reconstructing this data set portrayed a concentration of electron dense elastic fibres lying directly above Descemet's membrane (Figs. 5.5 B-C). These fibres were very similar in concentration and orientation as those seen using the tannic acid stain, providing evidence that both protocols are staining the same structures. The majority of these fibres ran longitudinally towards the limbus, with some travelling transversely. No elastic fibres were identified in the 3D reconstructions above Descemet's membrane in KC cornea (Figs. 5.5 D-F), although this may have been due to the poor contrast and image quality, as mentioned previously. Throughout many KC data sets, keratocytes were seen lying directly on top of Descemet's membrane (Figs. 5.5 5E-F) something rarely observed in normal cornea.

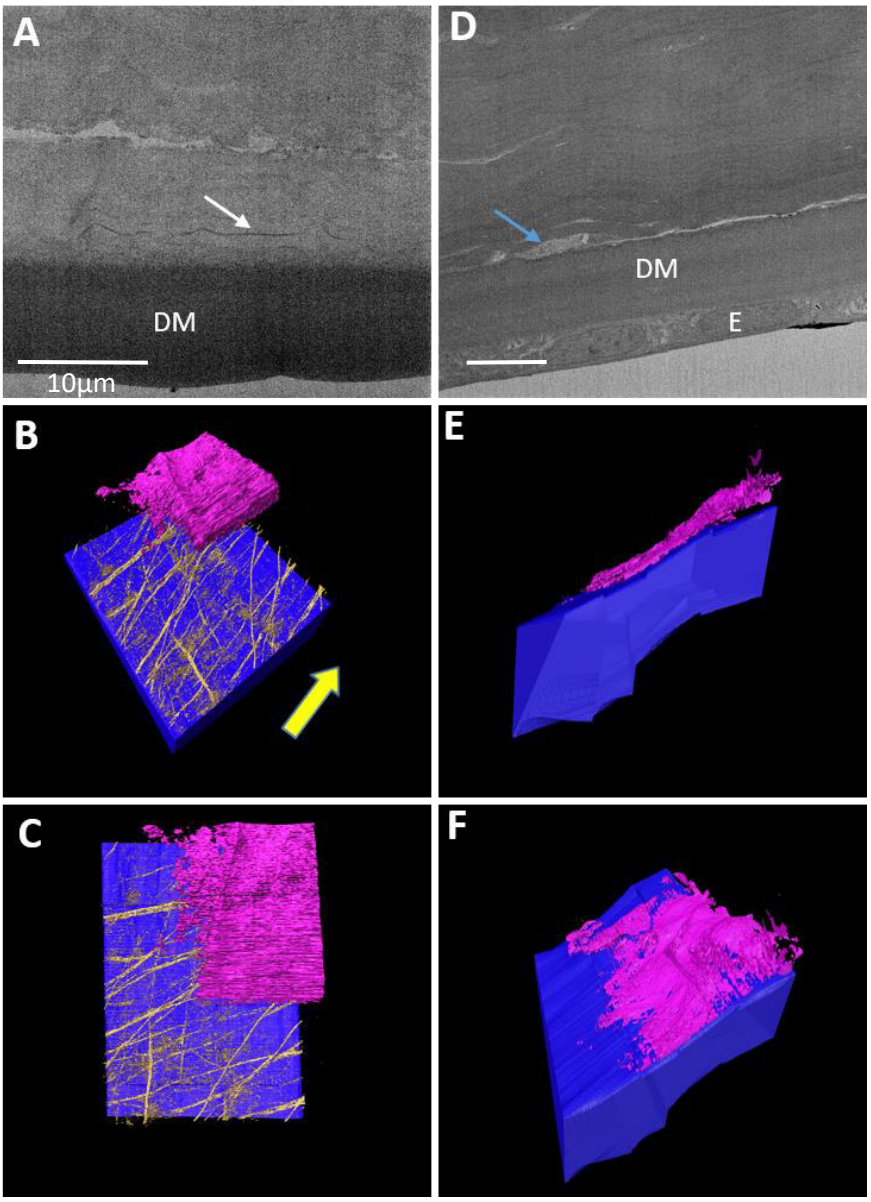


**Figure 5.5. Distribution of elastic fibres above Descemet's membrane (DM) in normal (A-C) and keratoconic button 2 (D-F) cornea using orcein staining.** Blue = DM, Gold = elastic fibres, Pink/Purple = Keratocyte. Dark elastic fibres (white arrow) seen above DM in normal cornea (A) were reconstructed, resulting in a 3D model where the elastic fibres were similar in number and orientation to those we have previously described in tannic acid stained cornea (B-C), with the majority travelling towards the limbus (yellow arrow). No fibres were identified in the keratoconic cornea data set, with poor contrast between DM and stroma (D). A keratocyte (blue arrow) was seen lying directly on top of DM (E-F), a finding that was seen frequently in other keratoconus data sets.

As with SEM, TEM results from keratoconic buttons 2 and 3 stained with orcein were consistent with those from the tannic acid staining protocol. Fibres were sparsely populated above Descemet's membrane (Fig. 5.6A), with the occasional fibre seen, portraying the characteristic 50-60nm periodicity of elastic fibres (Fig. 5.6B). Similarly to the tannic acid stained keratoconic button 1, electron dense fibres were visualised in abundance below the epithelium, with diameters ranging from 100-200nm (Fig. 5.6C). These structures were seen both between the basal lamina and the intact Bowman's layer, and also directly below Bowman's layer. By viewing these structures at a high magnification, the individual microfibrils making up the bundles could be seen (Fig. 5.6D). The diameter of these individual microfibrils appeared to be between the range of 7-13nm.

The scar tissue seen in keratoconic button 2 was also examined using TEM. Electron-dense material surrounded fibroblasts throughout the entire stroma of the scarred tissue (Fig. 5.6E). In some areas of scar tissue, vast amounts of densely-stained elastic fibres were seen, with diameters ranging from 70-300nm (Fig. 5.6F). Normal cornea and sclera were used as controls for the orcein stain, with both demonstrating the presence of elastic fibres (Figs. 5.6G-H).

### *5.3.3. Immunofluorescence microscopy*

Normal cornea labelling for type VI collagen showed a clear concentration in the posterior stroma, above Descemet's membrane that was continuous from centre to periphery, and into the trabecular meshwork at the limbus (Fig. 5.7A),with no stain present throughout the rest of the stroma. This differed in keratoconic cornea, with strong type VI collagen labelling throughout the whole thickness of the stroma (Fig. 5.7B). No labelling of elastin was seen in normal cornea (Fig. 5.7C), whereas the epithelium of KC cornea positively stained for elastin, which appeared to be present inside the epithelial cells (Fig. 5.7D). Fibrillin (Figs. 5.7E-F) labelling failed in both normal and KC corneas, and no fluorescence was observed in negative controls.

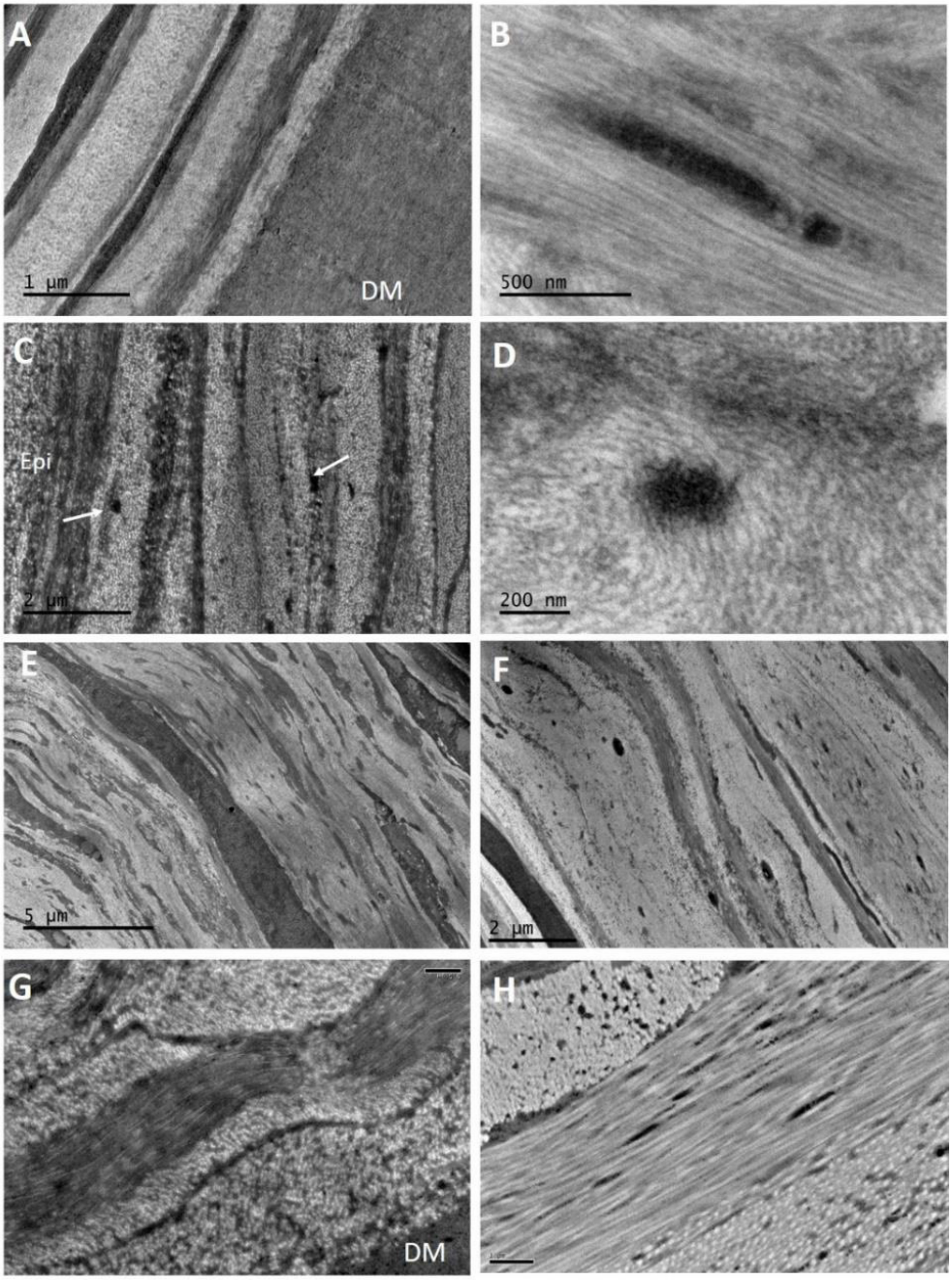


**Figure 5.6. TEM images of orcein stained cornea.** No fibres seen above DM (A). Fibres were occasionally seen in the posterior and mid stroma, with longitudinally orientated fibres displaying a faint ~50-60nm periodicity that was difficult to measure (B). More elastic fibres (white arrows) were located in the anterior stroma, below the epithelium (C). High magnification images of transverse fibres portrayed the presence of individual microfibrils within the bundle, although these were difficult to visualise (D). Scarred areas of stroma contained a mass of electron dense material (E) and an abundance of elastic fibres (F). Elastic fibres were seen in normal control tissue – cornea (G) and sclera (H).

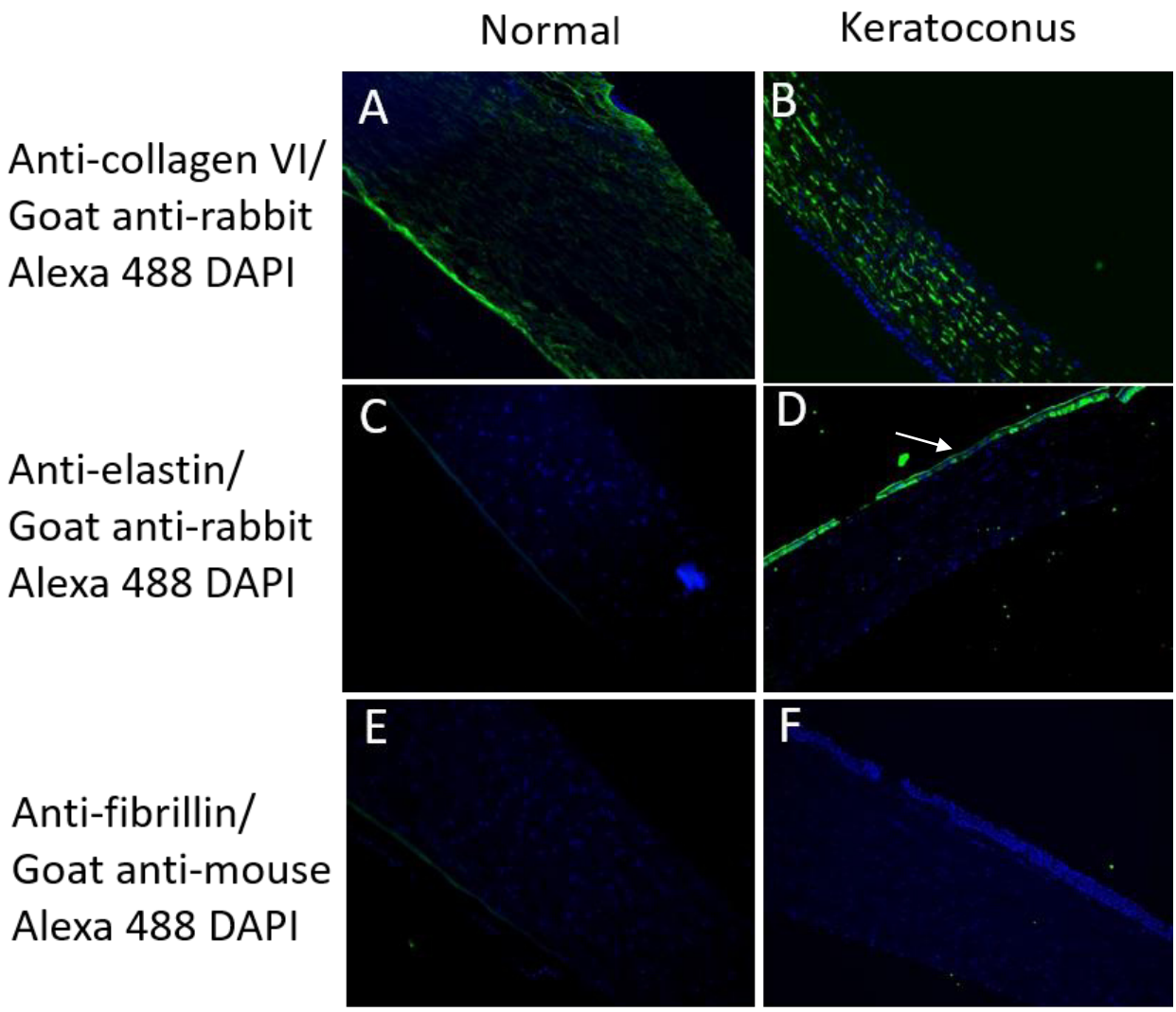


**Figure 5.7. Immuno- fluorescence labelling of normal and KC button 2**. Type VI collagen was concentrated directly above DM in normal cornea and was continuous with the trabecular meshwork (A), whereas type VI collagen was present throughout the whole keratoconic button 2 stroma (B). No elastin labelling was present in normal cornea (C), whilst the epithelium (white arrow) of KC produced a clear positive stain (D)**.** Commercial fibrillin antibodies showed no staining in normal or KC cornea (E,F).

## 5.4. Discussion

Using two different elastic specific staining protocols, this study has shown that the presence of elastic fibres in the stroma of keratoconic cornea is very different to the normal healthy cornea. Both the tannic acid-uranyl acetate (Simmons and Avery, 1980, Kageyama *et al.*, 1985) and orcein based (Nakamura *et al.*, 1977) protocols are known to stain the microfibrillar and amorphous components of elastic fibres. When applied to keratoconic corneas, the techniques revealed poor contrast in the images, although it was still possible to identify elastic fibres where present. It is not clear why processed keratoconic buttons produced poor contrast, as the same protocol worked very well for human (Lewis *et al.*, 2016), porcine, and murine cornea (see chapter 6).

SBF SEM volume reconstructions in the area of stroma immediately above Descemet's membrane showed a significant difference in elastic fibre concentration in keratoconic cornea compared to normal cornea. Both staining protocols clearly demonstrated the presence of an extensive network of elastic fibres above Descemet's membrane in normal cornea, as we have previously described (Lewis *et al.*, 2016). Many data sets were obtained from the same area, in thinned coned regions, from both tannic acid and orcein stained keratoconic buttons, with fibres present in only one reconstruction. The lack of fibres in this region was confirmed with TEM, where an extensive search was required to identify any fibres in this area. Transversely orientated fibres displayed a banding pattern with periodicity of 50-60nm, characteristic of fibrillin containing microfibrils (Sherratt *et al.*, 2003, Jensen *et al.*, 2012). Frequently, keratocytes were seen lying directly on top on Descemet's membrane, in a 'layer' of stroma that Dua *et al.* (2013) described as acellular in normal cornea, although this has been disputed (Jester *et al.*, 2013, Schlotzer-Schrehardt *et al.*, 2015). As the samples are 7mm corneal buttons, it is unknown if there is a lack of elastic tissue at the very periphery and limbus of the keratoconic cornea.

Elastic fibres are present in foetal cornea (Lewis *et al.*, 2016) and the posterior stroma of young infants (Alexander and Garner, 1983), therefore, patients with keratoconic corneas are either born with a lack of fibres in this region, or they are degraded throughout life. Fibrillin microfibrils are important in the development of tissues containing 'true' elastic fibres, as they provide a scaffold for the deposition of elastin during elastogenesis (Jones *et*

*al.*, 1980, Kewley *et al.*, 1978, Kielty *et al.*, 2002a). They also link elastic fibres to each other and to other components of the ECM, and thus play a role in tissue homeostasis by engaging in various cell-matrix interactions (Kielty and Shuttleworth, 1995, Jensen and Handford, 2016). However, the normal cornea only contains these true elastic fibres at the limbus, therefore, the role of these elastin-free microfibril bundles in more central areas of the cornea remains unclear, so it is unknown if their absence throughout life would cause any structural or functional issues. In other tissues, the importance of fibrillin microfibrils in maintaining tissue function is highlighted in Marfan's syndrome, an autosomal dominant disease caused by defects in the fibrillin-1 gene, leading to a lack of/disorganised fibrillin microfibrils in the ECM, resulting in cardiovascular, skeletal, and ocular manifestations. This disease often leads to features that overlap with keratoconus including astigmatism and corneal thinning (Konradsen *et al.*, 2012, Heur *et al.*, 2008), as well as a flattened cornea (Sultan *et al.*, 2002). Despite this, keratoconus is rarely detected in Marfan's syndrome corneas (Maumenee, 1981). In terms of degradation, it is thought that collagen is broken down by proteolytic enzymes in keratoconus, resulting in corneal thinning (Balasubramanian *et al.*, 2010). Fibrillin domain structure is dominated by cbEGF domains (calcium binding epidermal growth factor) (Jensen *et al.*, 2012), where calcium binding to these domains is thought to rigidify the microfibrils and protect them from proteolysis (Reinhardt *et al*., 1997). Lysyl oxidase activity, an enzyme involved in cross linking, is decreased in the stroma of keratoconus corneas (Dudakova *et al.*, 2012). Furthermore, lower levels of lysinonorleucine, a lysl oxidase-derived crosslink found in collagen and elastic fibres, are reported in the stroma of keratoconus cornea (Takaoka *et al.*, 2016), meaning a loss of strength and stability of elastic fibres, which could make them more susceptible to degradation.

In contrast to the posterior stroma above Descemet's, elastic fibres were seen concentrated in a ~5 micron band in the anterior stroma below the epithelium in thinned central regions of keratoconus buttons, as seen by Jefferies and Alexander (1995) with light microscopy. This is a finding that was not seen in full thickness quantification analysis of normal cornea, where no fibres were detected below the epithelium (Lewis *et al.*, 2016). These fibres were smaller (130nm average) in diameter compared to fibres seen in the middle and posterior stroma; this, along with poor contrast, made it difficult to create a 3D reconstruction from

the data set that they were observed in. TEM confirmed that these fibres consisted of 10-12nm microfibrils, characteristic of fibrillin-containing microfibrils (Sakai *et al.*, 1986b). Whereas the elastin component of elastic fibres provides tissue with elasticity, fibrillin microfibrils primarily provide rigidity and act to reinforce the elastic fibre, as they have been shown to be two orders of magnitude stiffer than elastin (Sherratt, 2009, Sherratt *et al.*, 2003). However, tensile testing has demonstrated that elastic fibres in hydrated ciliary zonules are reversibly extensible, and therefore have an element of elasticity (Wess *et al.*, 1998). The importance of this biomechanical strength is evident in ciliary zonules, where an abundance of fibrillin microfibrils are responsible for holding the lens in dynamic suspension, with a loss of this structural anchorage in Marfan's syndrome leading to ectopia lentis (Ashworth *et al.*, 2000). The central anterior cornea is a weak area in keratoconus, forming the apex of the cone, and likely in need of additional biomechanical strength to that provided by collagen. Furthermore, abnormalities in Bowman's layer were observed, along with the presence of vacuoles, suggesting that proteases are being released from a degenerating basal epithelium. In an early electron microscopy study, Tseng (1963) suggested that one of the earliest microscopical changes observed in keratoconus is degeneration of epithelial cells, with simultaneous release of unspecified enzymes, disrupting Bowman's layer and ultimately resulting in anterior stroma scarring. This may occurring in button 1, although scarring did not reach the severity as that seen in button 2, which was at a more advanced stage of the disease.

It is thought that the corneal thinning observed in keratoconus is a result of a loss of stromal tissue (Morishige *et al*., 2007, Mathew *et al*., 2011), although the precise mechanisms leading to this are currently unknown. In the normal cornea, anterior stroma is thought to be biomechanically stronger than the posterior stroma due to a high degree of lamellar interweaving (Komai and Ushiki, 1991, Morishige *et al*., 2006), however, numerous studies have shown that lamellar interweaving is significantly reduced in the anterior stroma of keratoconus corneas, as well as a loss of collagen lamellae inserting into Bowman's layer (Morishige *et al*., 2007, Morishige *et al*., 2014, Radner *et al*., 1998b, Meek *et al*., 2005). Further electron microscopy studies have postulated that ectasia and corneal thinning in keratoconus is associated with the loss of and splitting anterior lamellae, ultimately as a result of weakened anterior stroma (Mathew *et al*., 2011, Mathew *et al*., 2015).

Furthermore, a loss of lamellae interweaving and insertion into Bowman's layer may facilitate lamellar "slippage" (Meek *et al*., 2005). An increased concentration of elastic fibres below the epithelium/Bowman's layer in keratoconus corneas may be a biomechanical response to strengthen this weakened area to prevent rupture. If this is correct, the presence of fibres in this area, which were not observed in normal cornea (Lewis *et al*., 2016), may also have an effect on the shape of the cornea and could potentially contribute to cone formation.

The areas of stroma with scarring present were very different, with the majority consisting of disorganised collagen and an abundance of electron dense material, as previously observed in the stroma of keratoconus tissue (Pouliquen, 1987) In addition to this, a concentration of structures with a very similar appearance to elastic fibres were identified throughout the scarred stroma. The diameter of individual fibres was variable but most were found to be between 130-230nm. Newly synthesised elastic fibres have been reported in scar tissue of skin (Roten *et al.*, 1996, Tsuji and Sawabe, 1987), but little work has been carried out in the cornea. Kenney *et al.* (1997) discovered fibrillin-1 in fibrotic regions of keratoconic corneas, whereas Ljubimov *et al.* (1998a) described abnormal deposits of fibrillin-1 in stromal scars after radial keratotomy. Fibrillin-1 labelling in these scars is likely to be caused from the elastic fibres we describe in this study. It is likely that these fibres are laid down by fibroblasts, along with collagen and other extracellular material, in order to strengthen the repairing stroma.

Immuno-labelling of type VI collagen showed strong staining in normal cornea in a 10-20µm band of stroma above Descemet's membrane that was continuous with the trabecular meshwork, consistent with findings by Dua *et al.* (2014), who termed the layer pre-Descemet's layer. The tissue used to label type VI collagen in keratoconus was likely scarred, and showed staining throughout the stroma. The distribution of type VI collagen in normal and scarred keratoconic corneas correlates with the distribution of elastic fibres, suggesting an association between the two, a finding that has been previously observed in various other tissues (Everts *et al.*, 1998). Further support for a close physical relationship between fibrillin containing microfibrils and type VI collagen microfibrils was provided by Finnis and Gibson (1997), where microfibril associated glycoprotein-1, an ECM component frequently co-localised with microfibrils, interacts with type VI collagen microfibrils, potentially

providing indirect anchorage of the two microfibrils. Similarly, Jefferies and Alexander (1995) propose that elastic fibres express a type VI collagen epitope, which could explain why it is difficult to see fibrillin-1 staining with commercial antibodies in both normal and keratoconic corneas. This makes it difficult to determine the true extent of elastic microfibril concentration, as type VI collagen antibodies are potentially labelling elastic fibres, but not all positively labelled fibres are elastic (Jefferies and Alexander, 1995). Labelling for fibrillin-1 was unsuccessful with several commercially available antibodies; however, these microfibril bundles have been successfully immunogold labelled with non-commercially produced anti-fibrillin antibodies in murine cornea (Hanlon *et al.*, 2015). Anti-elastin antibodies produced a strange result by distinctively labelling the entire epithelium, a finding that was not observed in the normal control.

### 5.5. Conclusion

In conclusion, the distribution of elastic fibres in the stroma of keratoconus is very different to normal cornea. The stroma of normal cornea contains an extensive network of elastic fibres above Descemet's membrane, becoming progressively less abundant anteriorly, with none detected below the epithelium. This finding is reversed in non-scarred regions of keratoconus, with a concentration of fibres below the basal epithelium in thinned central regions, and very few above Descemet's membrane and throughout the rest of the stroma. It is likely that these fibres are produced to provide additional biomechanical strength to the anterior stroma in order to prevent tissue rupture at the apex of the cone. A lack of elastic fibre system above Descemet's membrane in keratoconus would render this area biomechanically weaker than normal cornea, with a loss of other cell signalling mechanics involved in tissue homeostasis, potentially contributing to the pathogenesis of the disease.

# Chapter 6 – Corneal elastic fibres in a mouse model for Marfan syndrome

## 6.1. Introduction

Marfan syndrome is an autosomal dominant disease of connective tissue caused by mutations in the FBN1 gene encoding the fibrillin-1 protein (Dietz *et al.*, 1991), the main component of elastic microfibrils, discovered by the detection of immunohistologic abnormalities of elastic fibres in the skin and cultured fibroblasts in patients with the disease (Hollister *et al.*, 1990). The prevalence of the disease is approximately 1 in 10,000 (Gray *et al.*, 1998), and results in primarily ocular, skeletal, and cardiovascular manifestations, with the leading cause of premature death caused by aortic incompetence. Elastic fibres are responsible for providing elasticity and tensile strength, therefore, abnormal production/reduction in quantity affects the functional ability of force bearing tissues. The most common symptom seen in the eye is ectopia lentis (dislocation of the lens), occurring in around 60% of patients with the disease (Maumenee, 1982), due to biomechanically weak ciliary zonules (fibrillin rich strands of tissue connecting the lens to the ciliary body), and is almost always bilateral (Robinson and Godfrey, 2000). Other ocular symptoms include abnormally flat cornea and increased axial length of the globe, although this is not used as part of the diagnostic criteria (Judge and Dietz, 2005). The majority of Marfan syndrome research has been carried out on the cardiovascular system as a result of the severe and life threatening symptoms it produces, with little focus on the cornea.

The FBN1 gene contains 65 exons spanning 235kb of genomic DNA (Corson *et al.*, 1993, Biery *et al.*, 1999). This is translated to form the 350 kDa multidomain glycoprotein fibrillin-1, a major component of 10-12nm microfibrils (Sakai *et al.*, 1986b). These fibrillin rich microfibrils forms sheaths around the central amorphous components of true elastic fibres, playing a key role in the production of the fibres by acting as a scaffold for the deposition of tropoelastin, an elastin precursor, whilst also occurring independently in many tissues, such as the cornea and periodontal ligament, as elastin-free bundles, providing tissue with additional strength and resiliency. A schematic representation of a fibrillin-1 monomer can be seen in Figure 6.1. There is a repetition of two disulphide-rich domains; 47 epidermal growth factor-like (EGF) domains, and 7 transforming growth factor β binding protein-like

(TB) domains. 43 of the 47 EGF domains are calcium binding (cbEGF domains). It is thought that the presence of calcium ions protects fibrillin-1 from proteolysis (Handford, 2000, Reinhardt *et al.*, 1997). Other minor domains present are two hybrid domains and a proline-rich region. Elastic microfibrils also contain smaller quantities of other glycoproteins such as fibrillin-2, MAGP-1, and MAGP-2. Fibrillin-2 has a similar domain organisation where the proline-rich region is replaced by a glycine-rich sequence (Zhang *et al.*, 1994). Mutations in the FBN-2 gene lead to the connective tissue disease congenital contractural arachnodactyly (Putnam *et al.*, 1995), a disease phenotypically similar to Marfan syndrome, although ocular manifestations are rare. It is thought that elastic microfibrils may form fibrillin-1 homopolymers, or fibrillin-1/2 heteropolymers (Charbonneau *et al.*, 2003).

The cysteine-rich fibrillin-1 monomer is approximately 148nm long and assembles into microfibrils with a head-to-tail orientation, resulting in a beads on a string-like appearance (Sakai *et al.*, 1991, Keene *et al.*, 1991b). The method in which these 148nm molecules are packaged into fibrils with an average, but variable, bead to bead periodicity of 56nm remains unclear, with two proposed models: 1) a pleated model, where one fibrillin monomer is folded per interbead distance (Baldock *et al.*, 2006, Kielty *et al.*, 2002b), or 2) the extended model, where fibrillin monomers are extended and span two or more interbead distances, with overlaps occurring at the beads (Kuo *et al.*, 2007). This arrangement results in 1/3 staggering of the microfibril that can subsequently be extended 2-3 fold (Baldock *et al.*, 2001, Keene *et al.*, 1991b). X-ray diffraction and tensile testing have demonstrated that the elastic microfibrils in hydrated ciliary zonules are reversibly extensible (Wright *et al.*, 1999, Wess *et al.*, 1998). Although fibrillin microfibrils provide an element of elasticity to elastin-free tissues such as ciliary zonules, they have been shown to be 2 orders of magnitude stiffer than elastin (Sherratt *et al.*, 2003), with calcium binding to cEGF domains thought to produce microfibril rigidity (Eriksen *et al.*, 2001).

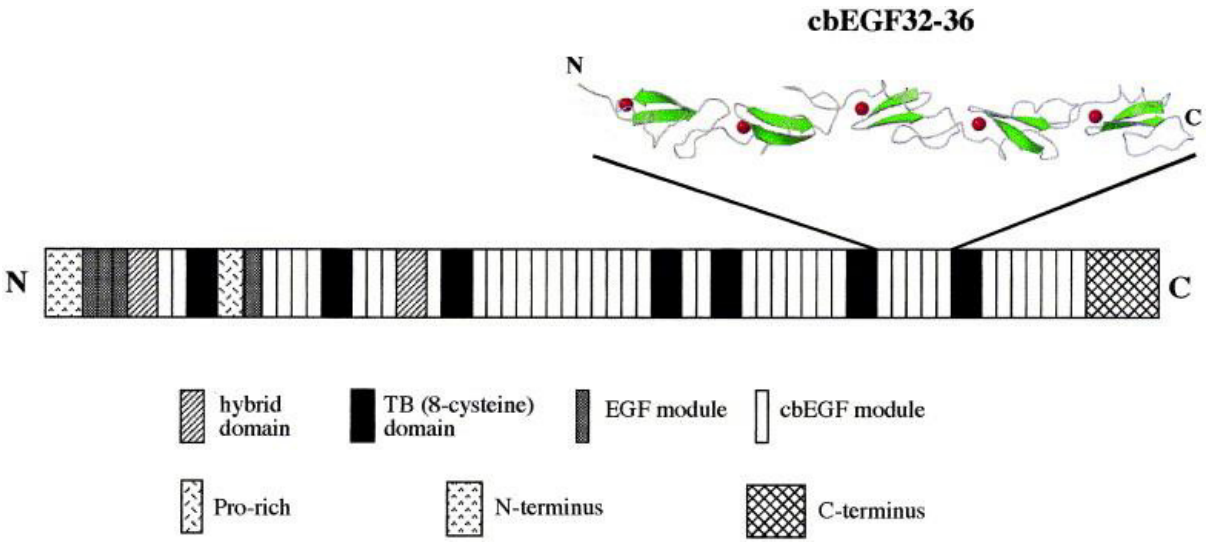


**Figure 6.1. The structure of fibrillin-1 monomer**. This schematic representation of a fibrillin-1 monomer portrays the various domains that are present. cbEGF domains 32-36 are represented in three dimensions, where the red balls indicate calcium binding to the domains. Image taken from Handford (2000).

The pathogenic mechanisms underlying Marfan syndrome have been studied following the development of mouse models. Pereira *et al.* (1997) developed a mouse model to mimic the dominant-negative effect of fibrillin-1 mutations seen in Marfan syndrome patients, where mutant fibrillin-1 production adversely affects normal production and function of normal fibrillin-1. The mgΔ mouse model was created by deleting exons 19-24 of the FBN1 gene and replacing them with a neomycin-resistance expression cassette. Homozygous mgΔ mice produced 10 times less of the fibrillin-1 protein compared to wild types (WT), however, they suddenly died after severe cardiovascular problems 3 weeks after birth. Heterozygous (HT) mice producing very low levels of mutant product were histologically indistinguishable from WT mice. A second model was generated by Pereira *et al.* (1999), called mgR, where the neomycin-casette was inserted between exon 18 and 19. Homozygous mgR mice produce around 25% of the normal amount of fibrillin-1 and display similar phenotypic features in the aorta and skeleton as Marfan syndrome patients, however, the mice die at around 4 months of age from pulmonary and vascular insufficiency. Finally, Lima *et al.* (2010) generated a novel variant of the mgΔ mouse model by replacing the deleted exons with a

neomycin-resistance expression cassette flanked by lox-P sequences (mgΔ$^{loxPneo}$), resulting in HT mice that present some aspects of Marfan syndrome as a result of defective microfibrillar deposition, including skeletal and cardiovascular manifestations, whereas homozygous mice die during gestation. The level of expression by the mutant allele was shown to be 47% less than the WT. HT mice also live a normal lifespan, making this mouse model the closest to mimicking Marfan syndrome.

A collaboration was formed with the Pereira laboratory in Sao Paulo, Brazil. As their group use the mouse models to study the skeletal and cardiovascular manifestations of Marfan syndrome, they kindly agreed to send us the eyes from the mgΔ$^{loxPneo}$ mice for corneal studies. Having shown the 3D organisation of elastic fibres in human cornea (chapter 4), the aim of this study is to attempt to further elucidate the functional role that elastic fibres are playing in the cornea. An obvious way to discover what role a protein is playing in a tissue is to take it out. Therefore, corneas from HT mgΔ$^{loxPneo}$ mice containing defective/reduced levels of fibrillin-1 were studied and compared to WT corneas. A range of techniques including SBF SEM, optical coherence tomography (OCT), TEM, and X-ray diffraction were used to compare mutant cornea to normal controls.

## 6.2. Methods

### *6.2.1. Mouse eyes*

Heterozygous mgΔ$^{loxPneo}$ mouse eyes were obtained from Professor Lygia Pereira at the Department of Genetics, Sao Paulo University, Brazil. Mice were sacrificed at 3 and 7 months of age. Whole eye globes were removed and fixed in 0.5% PFA immediately, before being transported to the UK in a box cooled with ice packs. A 0.5% concentration of PFA was used, as opposed the standard 4% solution, as it is thought that this fixes the tissue whilst better preserving the shape of the globe (S. Campbell, J. Ferguson, personal communication). 20 pairs of eyes were sent – 12 male (8 heterozygotes, 4 wild types) and 8 female (4 heterozygotes, 4 wild types). Following arrival, the eyes were split into 3 groups that either: remained in 0.5% PFA, were transferred to 4% PFA, or were fixed in Karnovsky's fixative for 3 hours and transferred to 0.1M cacodylate buffer.

*6.2.2. SBF SEM and TEM*

Corneas were dissected from eyes that had been fixed in Karnovsky's fixative before being processed using the standard protocol described in chapter 2.1. Full thickness quantification was carried out on the central stroma of HT and WT corneas, and is described in chapter 2.2, with the only difference being that the images were split into groups of 250, as opposed to groups of 1000 in the human cornea, due to differences in corneal thickness between the two species. Full thickness data sets were also used to create 3D reconstructions. Additionally, higher resolution (4k x 4k) data sets were obtained from a region above Descemet's membrane. All 3D analysis was carried out using Amira6 software (chapter 2.2). Blocks of tissue processed for SBF SEM were used to obtain 90nm sections that were observed using a JEOL 1010 TEM (chapter 2.3).

*6.2.3. Cupromeronic blue stain*

Corneas were dissected from eye globes fixed in Karnovsky's fixative and further cut down into small segments. Tissue was washed in 25mM sodium acetate buffer containing 0.1M $MgCl_2$ (pH 5.7) for 3 hours at room temperature on a rotator. Segments then stained with the 25mM sodium acetate buffer containing 0.1M $MgCl_2$ and 0.05% cupromeronic blue at room temperature overnight. Tissue was rinsed (3 x 5 mins) with the sodium acetate buffer (without cupromeronic blue) before being exposed to 0.5% aqueous sodium tungstate (3 x 10 mins) and 50% etOH + 0.5% sodium tungstate for 15 minutes; this enhances the electron density of the PG-cupromeronic blue complex (Scott and Haigh, 1985, Scott and Bosworth, 1990). This was followed by dehydration:, 70% etOH, 90% etOH, 100% etOH x 2, propylene oxide x 2 – each step for 15 minutes. 1:1 mixture of propylene oxide and araldite resin mixture (araldite monomer CY212, DDSA hardener, BDMA accelerator) used for 1 hour before 100% araldite resin infiltration for 1.5 days (6 changes). Cornea segments were placed into plastic moulds with fresh araldite resin and polymerised at 60°C for 36hours.

90nm gold section were cut, collected on copper grids and allowed to dry overnight. Sections were counter stained with 1% aqueous uranyl acetate for 15 minutes, washed with distilled water for 5 minutes and visualised using a JEOL 1010 TEM.

*6.2.4. OCT*

Mouse eyes fixed in 0.5% PFA were used for OCT imaging; a low concentration of PFA was used in an attempt to preserve the true shape of the globes (i.e. no shrinkage). A small well made from Blue Tack was created on a glass slides in order to hold the eye in position (Fig. 6.2). Each eye was placed into the well (cornea facing upwards) and kept hydrated with drops of 0.5% PFA before being imaged. Data sets of 1000 images at 1k x 1k resolution (axial scaling of 2.66 µm, lateral scaling 3.09 µm per pixel in air) were obtained from the axial plane of the eye globe, focused on the cornea and anterior chamber. Data set were reconstructed into 3D models using Amira6 software.

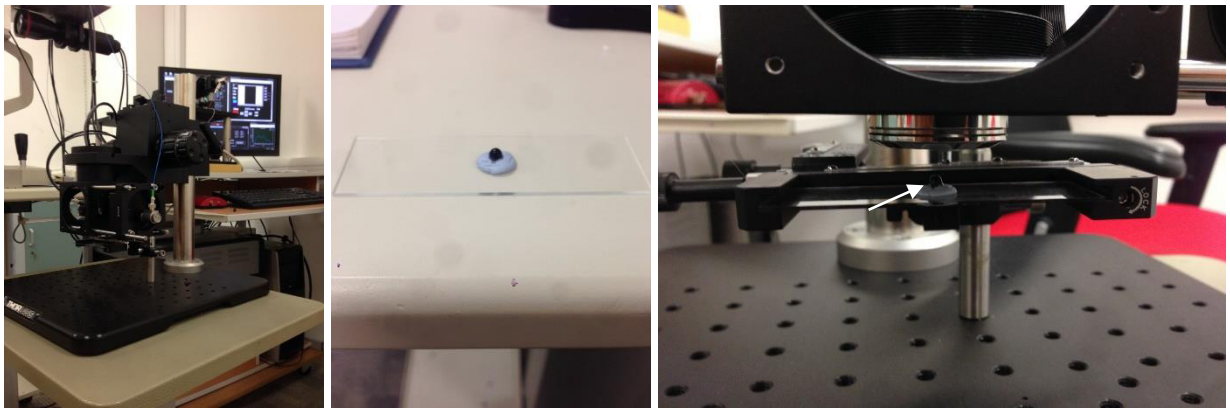

**Figure 6.2. OCT setup.** From left to right: OCT setup, mouse eye (white arrow) sitting in Blue Tak well on glass slide, mouse eye inside the machine ready for imaging.

Central corneal thickness was calculated by firstly taking the average intensity of ~10 images from the centre of each data set. The images have an axial scaling of 2.66µm per pixel in air, therefore, for any part of the image that is in the tissue, the scaling is reduced by the refractive index of the material. The number of pixels from the anterior to the posterior surface at the centre of the cornea was measured and converted to actually thickness using the following formula:

$$\text{Actual thickness (µm)} = \frac{\text{number of pixels} \times \text{axial scaling (2.66µm)}}{\text{Refractive index of the cornea (1.376)}}$$

The radius of curvature was measured from the arc formed at the anterior surface (see schematic diagram below) of the cornea using the following equation:

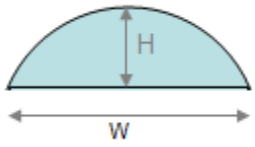


$$r = \frac{H}{2} + \frac{W^2}{8H}$$

The height (H) of the arc being measured for each sample was consistent at ~300µm to ensure that similar size arcs were being measured, with the width (W) varying. All thickness and radius of curvature measurements were carried out using ImageJ software.

### *6.2.5. Statistical analysis*

Tests for normality and equal variance were carried out before an Independent t-test was used in order to determine any differences between HT and WT corneas for central corneal thickness, radius of curvature, and interfibrillar spacing. Correlation between the two variables was tested using Pearson's correlation test. $p < 0.05$ was determined as statistically significant. All statistical testing was carried out using SPSS software.

### *6.2.6. X-ray diffraction*

4 WT and 4 HT corneas were dissected from whole globes that had been fixed and stored in 4% PFA. Dissected corneas were transferred to beamline I22 (Diamond Light source, Oxfordshire) in small tubes containing 4 % PFA, cooled with ice packs. At the beamline, each cornea was prepared for X-ray exposure by being wrapped in cling film to prevent dehydration, and placed inside an airtight Perspex sample holder containing to two transparent Mylar sheet windows. Samples were exposed to an X-ray beam measuring 200 x 200 µm for 0.4s per point to obtain SAXS patterns. For each cornea, a scan along the x-axis

was carried out in order to locate the edges of the sample, followed by a vertical scan along the y-axis at centre of the specimen, from edge to edge, at 0.2 or 0.3mm intervals.

SAXS patterns were analysed using SAXCOLL4 software described in chapter 2. Diffraction patterns were centred using the pattern of powdered silver behanate, and calibrated against the 67nm meridional spacing of hydrated rat tail tendon. Vertical scans ran beyond each edge of the samples, therefore, each edge was found by detecting the first and last SAXS patterns containing an interference function, which arise from cornea and not sclera. IFS was calculated from each pattern along the vertical axis of the cornea, where the middle point of the scan was deemed to be the centre of the sample. Weak/ lack of fibril transform peak meant that is was not possible to measure fibril diameter.

## 6.3. Results

### *6.3.1. Full thickness quantification*

The first experiment carried out was elastic fibre quantification throughout the entire central stroma of both HT and WT mouse corneas, as done with normal human cornea in chapter 4. The reasons for this were: 1) to determine the amount of elastic tissue in normal mouse cornea, and 2) discover the extent of elastic fibre reduction in the fibrillin-1 knock out corneas. Additionally, obtaining this data provided three-dimensional information throughout the entire depth of the cornea. Approximately 2300 images were obtained from epithelium to Descemet's membrane in each corneal stroma, equating to a depth of 115 µm (before geometrical corrections). The percentage of volume that elastic fibres occupied for each group of 250 images (12.5 µm) of data was calculated for HT and WT corneas, and plotted in Figure 6.3. Elastic fibre density was highest in the posterior HT cornea before gradually decreasing to very low levels in the anterior stroma. Density of elastic fibres in the WT cornea show a similar trend, but reach their highest point in the mid stroma before gradually decreasing towards the anterior. When comparing the two groups, the overall levels of elastic fibres are ~50% lower in HT cornea (HT mean 0.33% (± 0.16), WT mean 0.64% (± 0.27), with the most dramatic difference seen in the mid stroma, where WT cornea

had about 5 times more fibres. Moreover, in comparison to the human data obtained in chapter 4, mouse cornea on average contains significantly higher levels of elastic fibres.

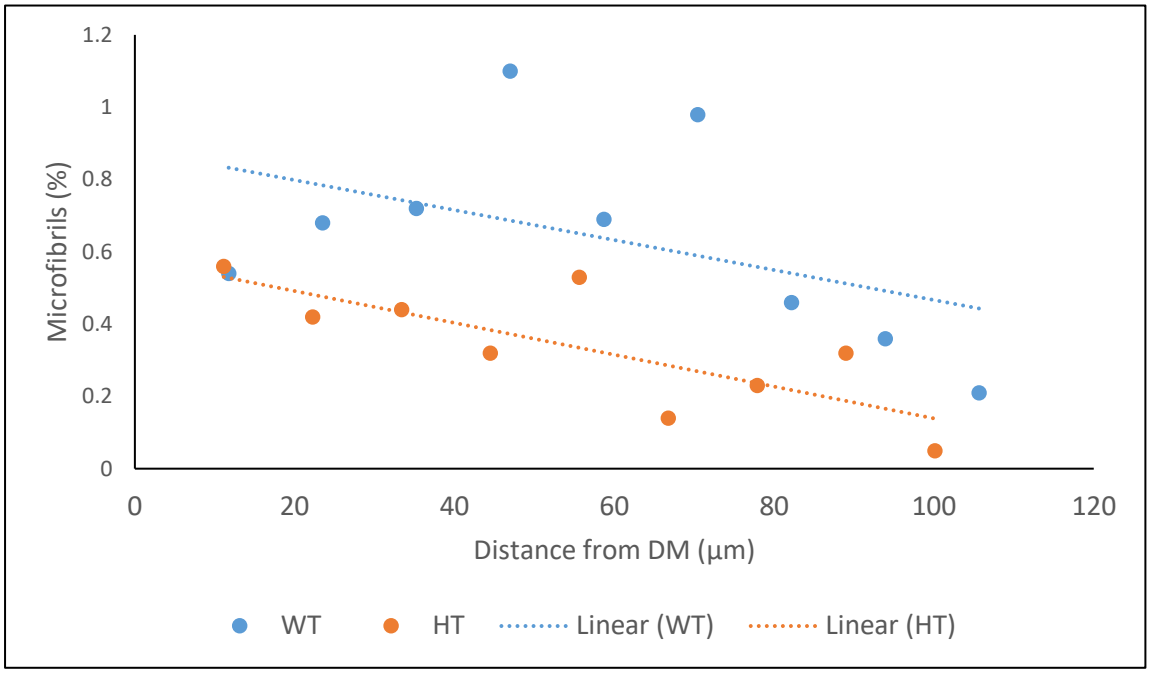


**Figure 6.3. Quantification of elastic fibres as a function of depth in the mouse corneal stroma**. The graph conveys the difference in elastic fibre density throughout the stroma of WT and HT mouse cornea, starting at Descemet's membrane, and ending in the anterior stroma. HT cornea contained on average ~50% less elastic fibres, although this varied from at different regions of the stroma, with a 5 fold difference seen in the mid-stroma.

*6.3.2. TEM*

Elastic fibres in the mouse cornea were clearly visible in TEM micrographs after using the standard tannic acid based staining protocol (Fig. 6.4). Similarly to the human cornea, fibres were orientated both transversely and longitudinally, with individual 10-12nm microfibrils visible within transverse fibres, however, the pseudo-periodicity seen in human elastic fibres was not visible in the mouse elastic fibres. Fibre diameter varied between 100-270nm; the average diameter was ~187nm in WT, and slightly lower in HT corneas at ~145nm. No differences were apparent when comparing the anterior, middle and posterior stroma of WT and HT corneas (Fig. 6.5). The stroma of the knock-out mouse cornea was structurally organised, with comparable lamellae thickness, collagen fibril diameter and collagen interfibrillar spacing to the normal mouse cornea. Descemet's membrane varied between

2.5-2.9 µm in thickness in the WT corneas, and slightly thinner in HT cornea measuring 2.1-2.5 µm.

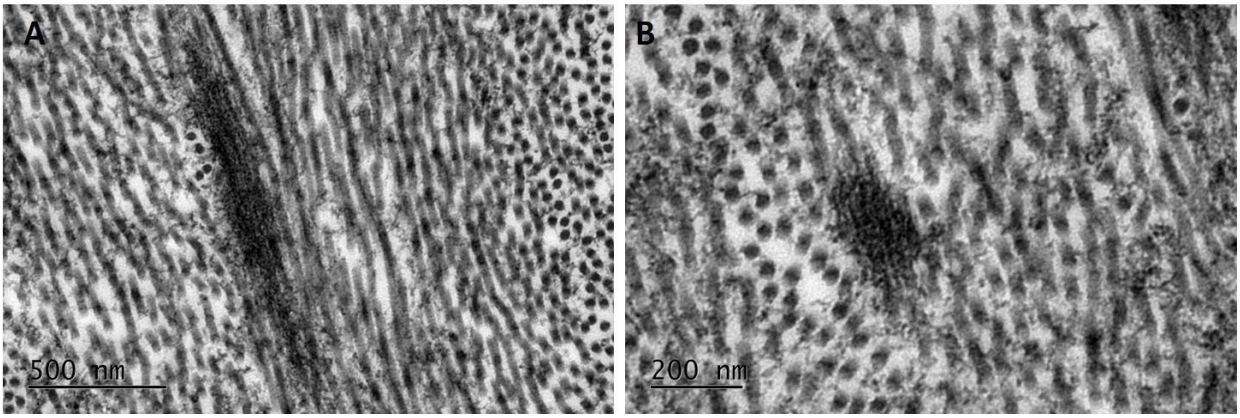


**Figure 6.4. Longitudinal (A) and transverse (B) elastic fibres in mouse cornea stained with tannic acid**. Individual 10-12nm microfibrils can be seen in transversely orientated fibres, whereas the pseudo-periodicity seen in human fibres is not visible in mouse longitudinal fibres

*6.3.3. Cupromeronic blue stain*

Cupromeronic blue staining was carried out to compare proteoglycan levels/distribution between the two groups (Fig. 6.6). Comparing the two sets of micrographs by eye seemed to suggest that there were no obvious differences in the quantity or spatial arrangement of proteoglycans between the two groups. Proteoglycan filaments were observed in the interfibrillar spaces, in association with collagen fibrils. These filaments formed bridges between both transversely and longitudinally arranged collagen fibrils. Transverse elastic fibres were observed as circular blank spaces in the micrographs due to the omission of tannic acid from the staining protocol (Fig. 6.7). This assumption is based on the fact that both the size and shape of the spaces closely match those of elastic fibres. Observing the fibre spaces at high magnification indicated that there is a potential association between proteoglycan filaments and fibrillin, as long CS/DS chains seemed to travel into the fibre.

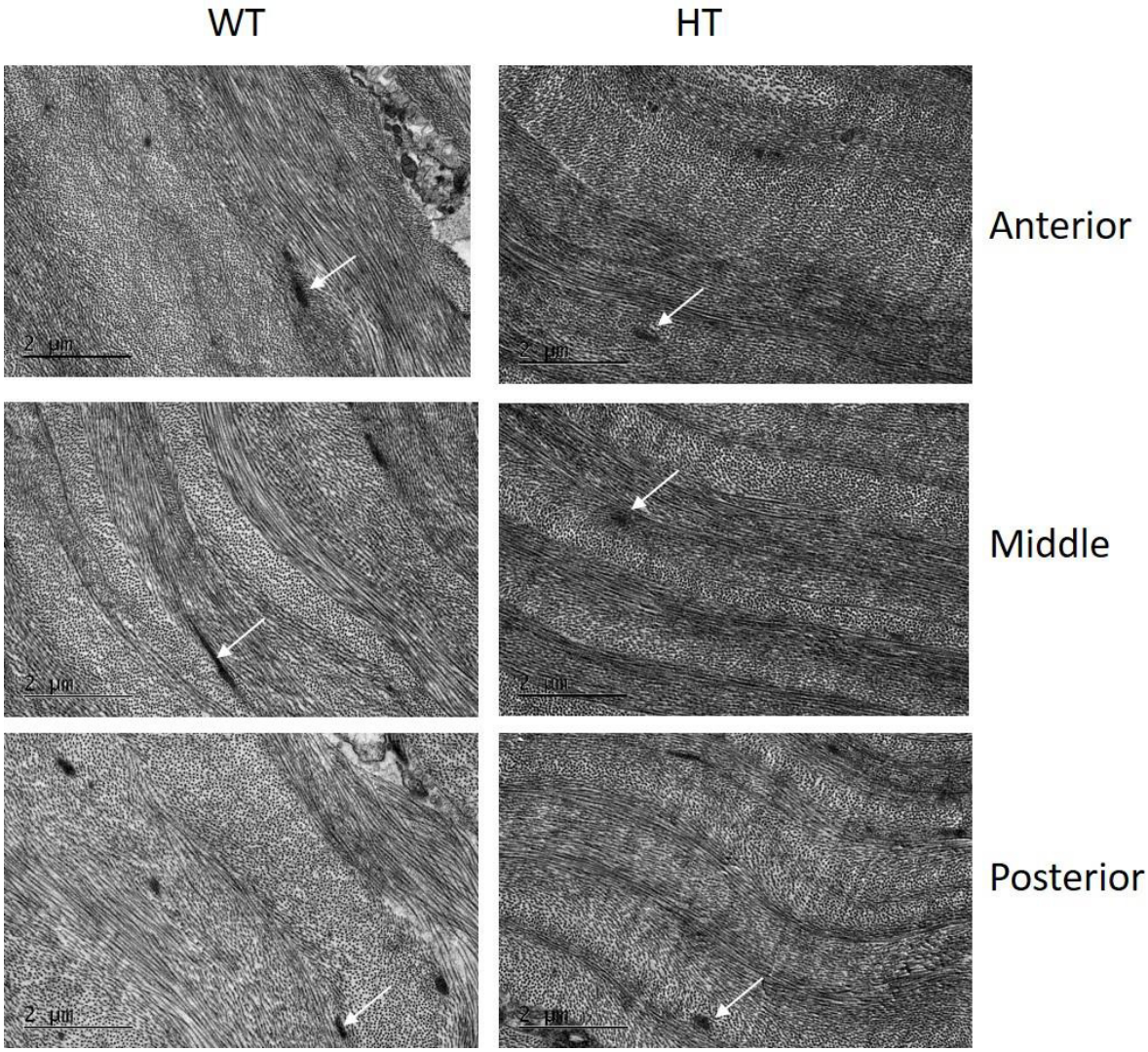


**Figure 6.5. TEM images at various depths of stroma**. Comparing anterior, middle and posterior stroma of WT (left) and HT (right) shows no obvious differences in ultrastructure. Both cornea appear well organised with comparable lamellae thickness and collagen interfibrillar spacing. Elastic fibres are visible in each image (white arrows).

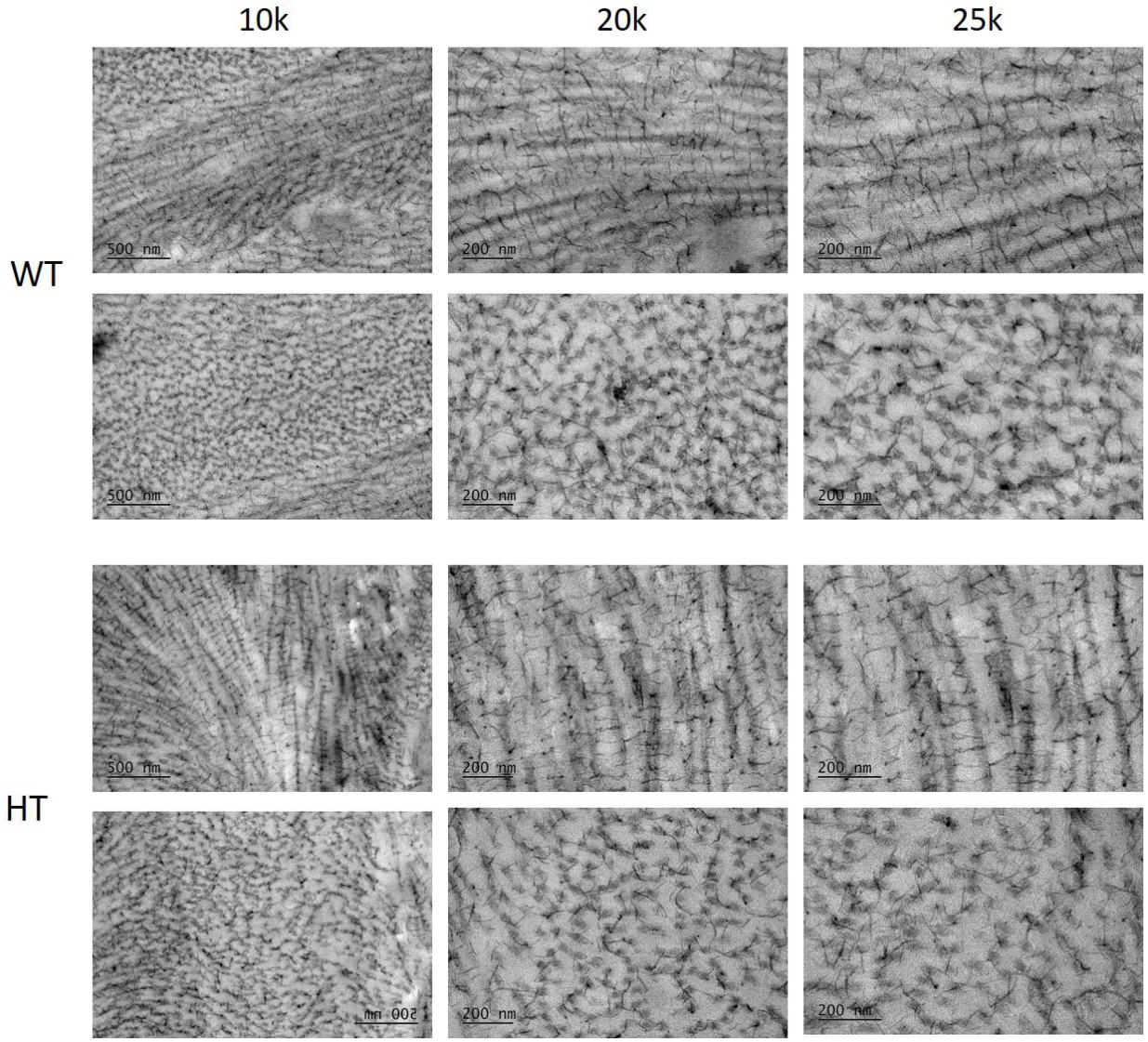


**Figure 6.6. Cupromeronic blue staining of proteoglycans.** WT (top panel) and HT (bottom panel) cornea, at 10, 20 and 25k magnification, showing both transversely and longitudinally oriented collagen fibrils with associated GAG's. No differences were apparent between the two groups.

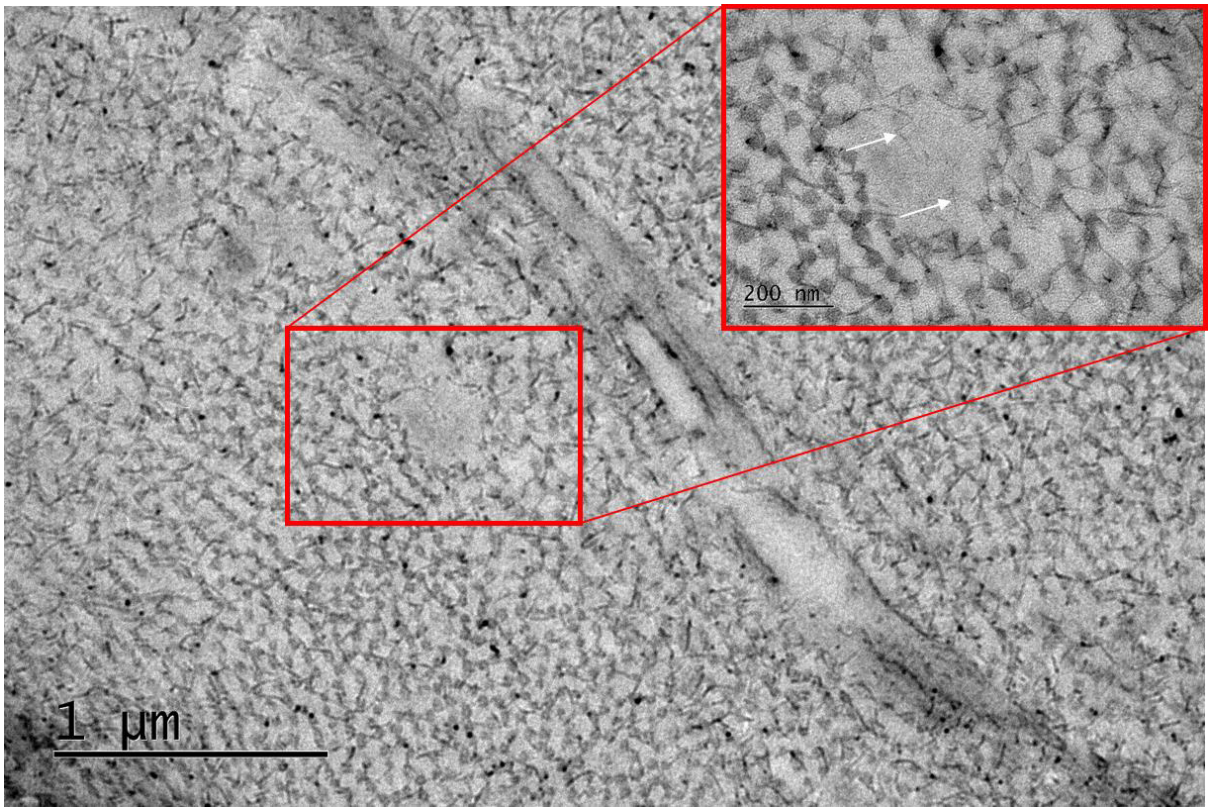


**Figure 6.7. Proteoglycan-elastic fibre interaction**. An elastic fibre space in the stroma viewed at high magnification (inset) appeared to show proteoglycan filaments (white arrows) travelling into the space and associating with fibrillin microfibrils.

### *6.3.4. 3D reconstructions*

The data obtained from the full thickness fibre quantification was used to create 3D reconstructions of WT and HT cornea stroma (Fig. 6.8). These models represent the first ~50 µm of stroma above Descemet's membrane. The reconstructions also portray how the block was not cut perfectly parallel to the surface, resulting in stroma that runs obliquely from Descemet's membrane. An abundance of gold elastic fibres can be seen running throughout the stroma of both groups. At first glance, there does not seem to be much difference between WT and HT corneas, however, zooming into a ~12.5 µm region of stroma (Fig. 6.8 insets), and viewing from above, shows a clear difference in the concentration of elastic fibres, with WT cornea being more densely populated (as seen from the quantification results). Fibres from both groups run in all directions, parallel to the surface of the cornea.

Further data sets were obtaining above Descemet's membrane at a higher resolution (4k x 4k) than the full-thickness data sets (2k x 2k) (Fig. 6.9). Moreover, the higher resolution data sets were collected by cutting the cornea in a radial direction, as opposed to being cut en face for the full thickness data sets. Elastic fibres in the normal WT cornea were structurally organised, running in straight lines with uniform thickness, and occasionally bifurcating, with the two new fibres continuing to run in the same direction following the division. Fibres in the HT knock-out cornea appeared disorganised, running in random directions when compared to the preferred orientation seen in WT cornea fibres. 5 or 6 individual fibres were seen to originate from a broader region of elastic material at the centre of the data set before travelling in several different directions. Furthermore, the elastic fibre in HT cornea formed more extensive connections, with ~10 individual fibres seen sprouting from a thicker fibre.

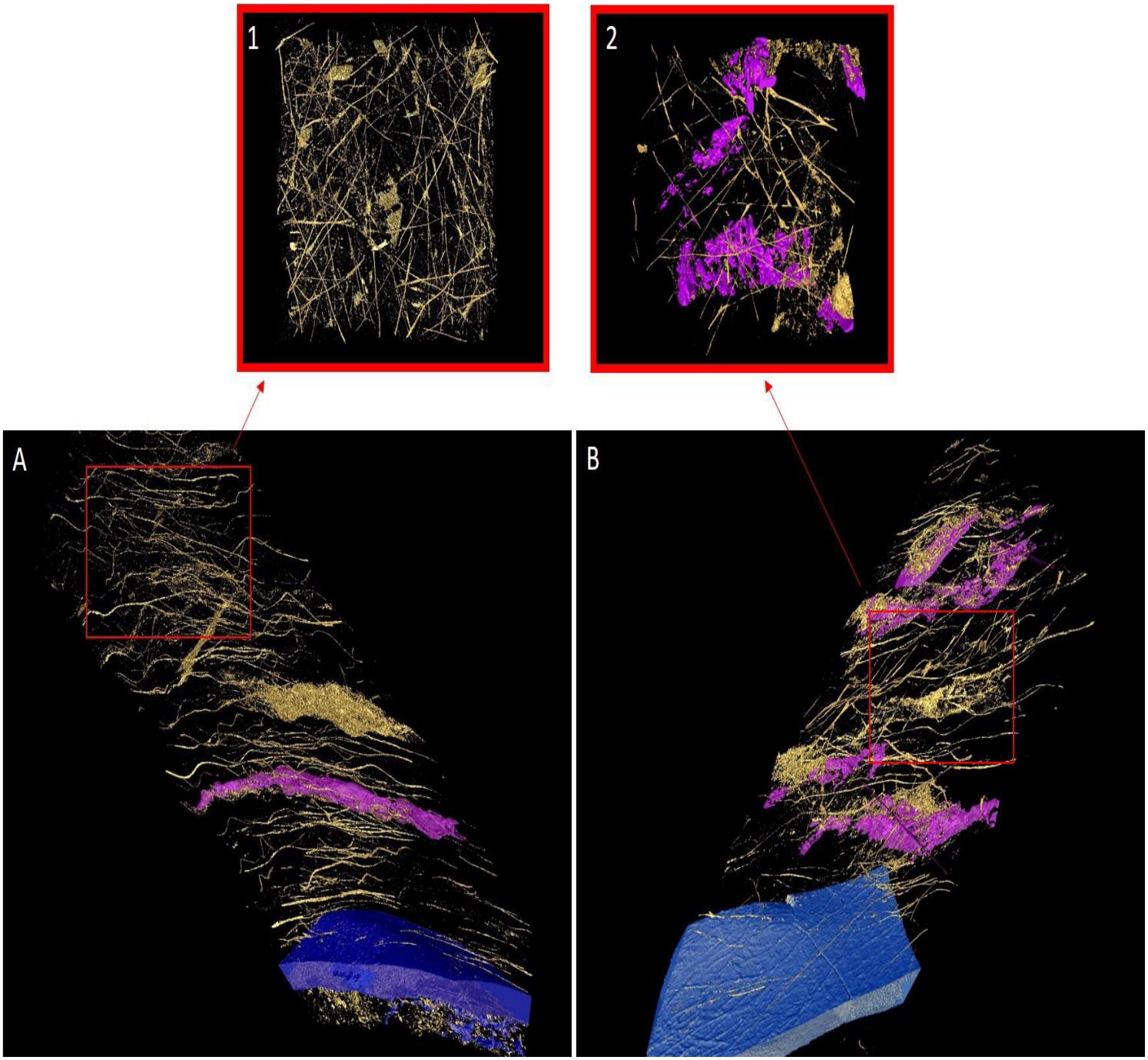


**Figure 6.8. 3D reconstruction of WT and HT cornea.** The 3D arrangement of elastic fibres (gold) in the first ~50 µm of stroma above Descemet's membrane (blue) in WT (A) and HT (B) mouse cornea. Some of the keratocytes have been segmented out (purple). About 12.5 µm of stroma from each group was focused on and viewed from above (insets) portraying the difference in fibre density.

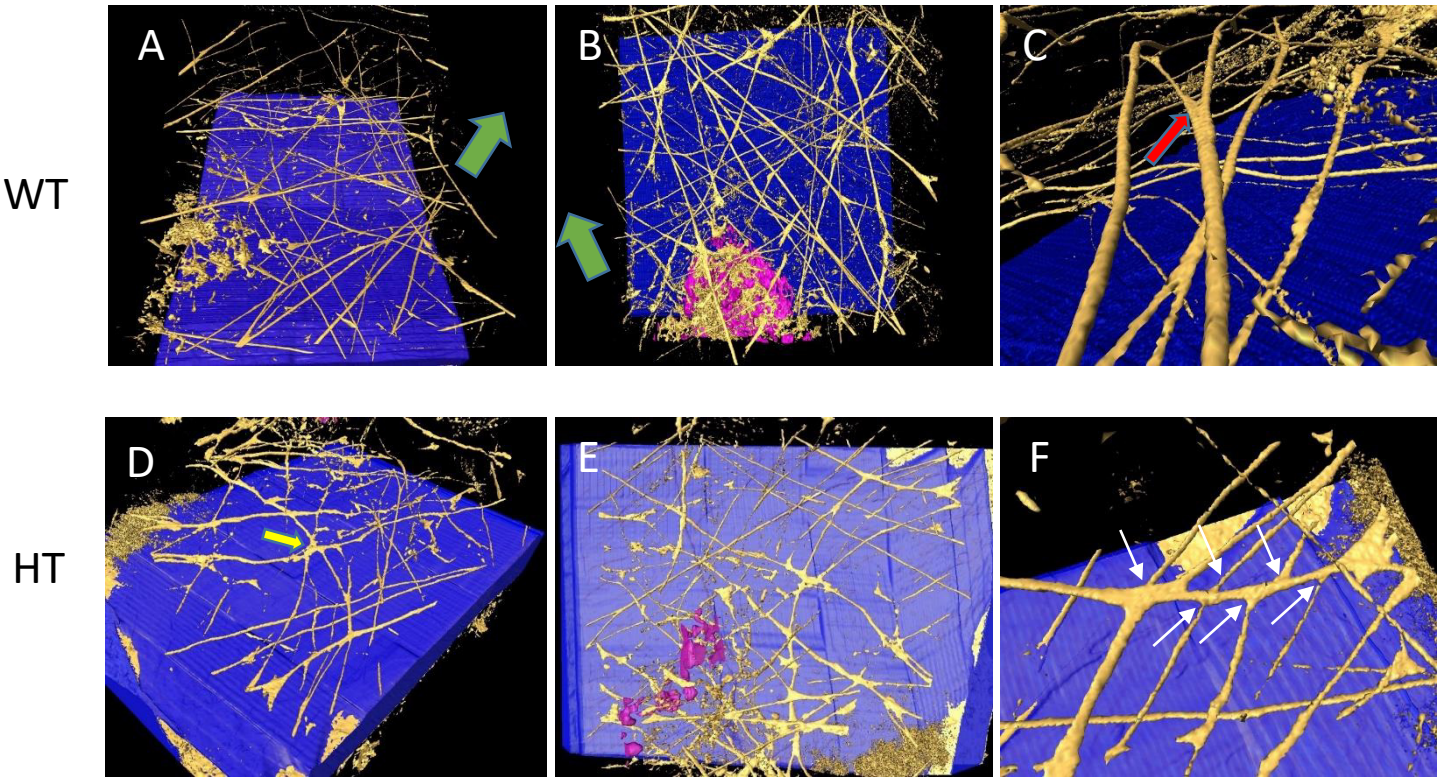


**Figure 6.9. High resolution 3D reconstructions above Descemet's membrane.** WT (A-C) cornea shows an organised elastic fibre network (gold) running in a preferred direction (green arrows), and occasionally bifurcating (red arrow). In contrast, fibres from HT cornea (D-F) appear disorganised, originating from a thickened area of tissue (yellow arrow) before travelling in many directions. Fibres were seen to divide into many branches (white arrows).

*6.3.5. 3D OCT*

OCT data sets containing 1000 images were then used to create 3D reconstructions of one eye from each group (Fig. 6.10). Individual images taken from the centre of each data set clearly portray the difference in central corneal thickness between WT and HT corneas. Additionally, HT cornea appeared to be flatter compared to the more curved WT. The centre-mid corneas were segmented, along with the iris and pupil. As a result of poor contrast, the peripheral cornea was omitted from the 3D reconstructions. Other than corneal thickness, no obvious differences were apparent between the two 3D eyes.

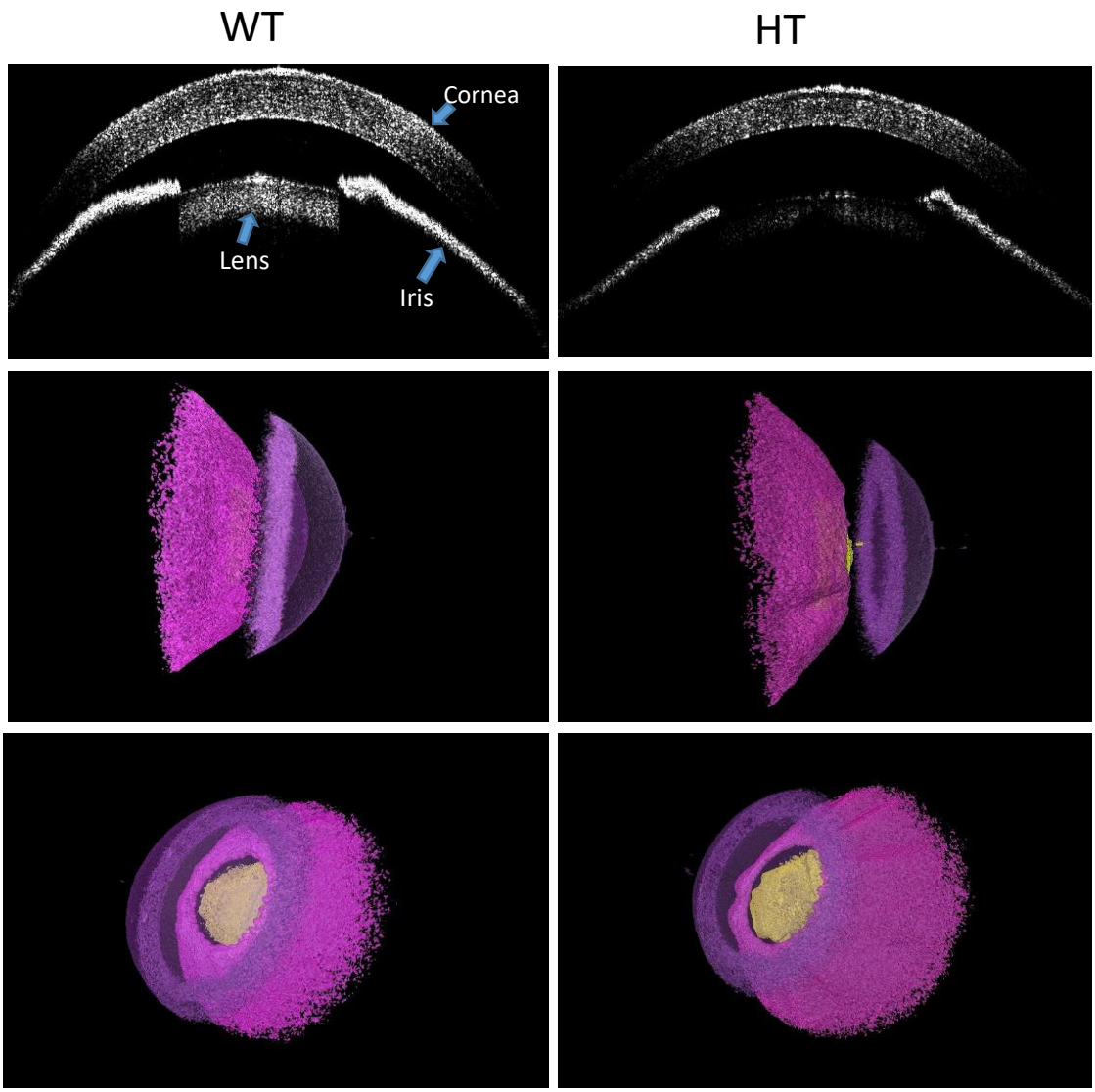


**Figure 6.10. 3D reconstruction of OCT data sets.** The top two images portray differences in central corneal thickness between WT and HT. Data sets were reconstructed to form a 3D model showing the cornea (transparent purple), iris (pink) and lens (yellow). No differences were detected between the two groups.

### *6.3.6. OCT measurements*

Central corneal thickness and radius of curvature were measured for WT and HT corneas using the OCT images (Fig. 6.11). Independent t-tests showed that WT corneas were significantly thicker than HT corneas ($p < 0.001$), with an average thickness of 186.8 µm (±15.5), compared to 158.6 µm (±9.4) in HT. This is evident in the graph, where WT corneal

thickness reached >200 µm, whereas HT corneas were often <160 µm, meaning a difference of ~40µm (almost 1/3 of the stromal thickness in mice). Radius of curvature was also significantly different between the two groups ($p = 0.035$), with an average radius of 1.460mm (±0.035) in WT, and 1.502mm (±0.039) in HT corneas. This was less convincing, with many radii lying between 1.46 and 1.49mm. Additionally, the method of measuring a small segment of the corneal arc to obtain radius of curvature may produce results that are not entirely accurate. Pearson's correlation coefficient was calculated in order to determine if there is any correlation, and if so, how strong this is, between the radius of curvature and corneal thickness variables. The coefficient indicated a weak negative correlation between the two variables ($r = -0.321$), indicating that as radius of curvature is increased, central corneal thickness decreases, although this correlation was not statistically significant ($p = 0.209$). However, p value for this test is affected by sample size, and due to the small number of corneas sampled, moderate correlations may not reach significance.

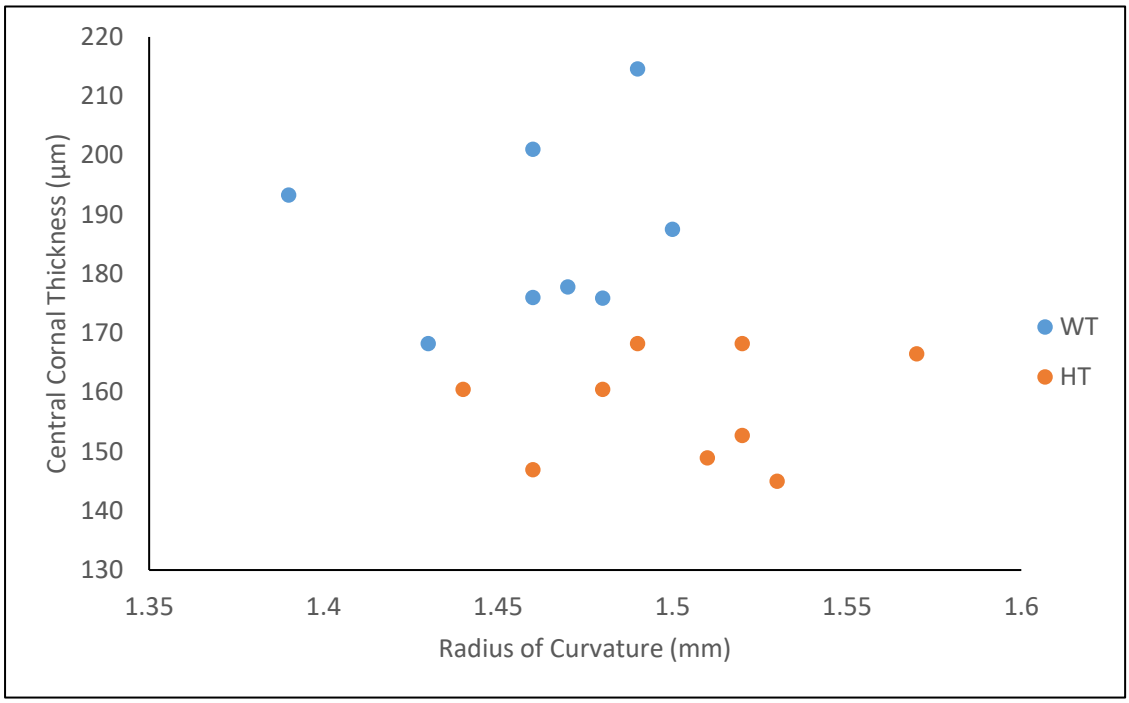


**Figure 6.11. Central corneal thickness plotted against radius of curvature**. From the graph, a significant difference in thickness between WT and HT corneas is evident, as is the less convincing difference in radius of curvature. A weak negative correlation exists between the two variables.

*6.3.7. X-ray diffraction*

Average centre-centre fibril spacings for WT and HT corneas are shown in Figure 6.12. In all specimens, IFS in the centre of the cornea was clearly reduced in comparison to peripheral regions, where IFS increased by about 25-40%. This 'U' shaped distribution is also seen when measuring mouse corneal fibril diameters (Boote *et al*., 2012). Most corneal samples measured ~3mm in diameter, indicating that each vertical scan was taken through the centre, with the only exception being the one vertical scan that recorded patterns at 0.3mm intervals, as opposed to 0.2mm intervals, meaning that each edge of the sample may have been missed. However, the technical difficulties involved in this study mean that it is not possible to know for certain if the vertical transect is perfectly through the centre of each specimen, with any deviation likely to affect IFS measurements. As the samples were fixed with 4% PFA before being analysed, it is unlikely that hydration would vary between each cornea. D-periodicity at the centre of each sample was consistent at 64-65nm. Interestingly, the IFS at the centre of HT corneas was higher (average 71.9 nm ± 5.6) than WT equivalents (average 63.7 nm ± 5.8) (Figure 6.13), although an independent sample t-test revealed that this difference was not statistically significant ($p = 0.09$), potentially because of the low sample number ($n = 4$ for each group).

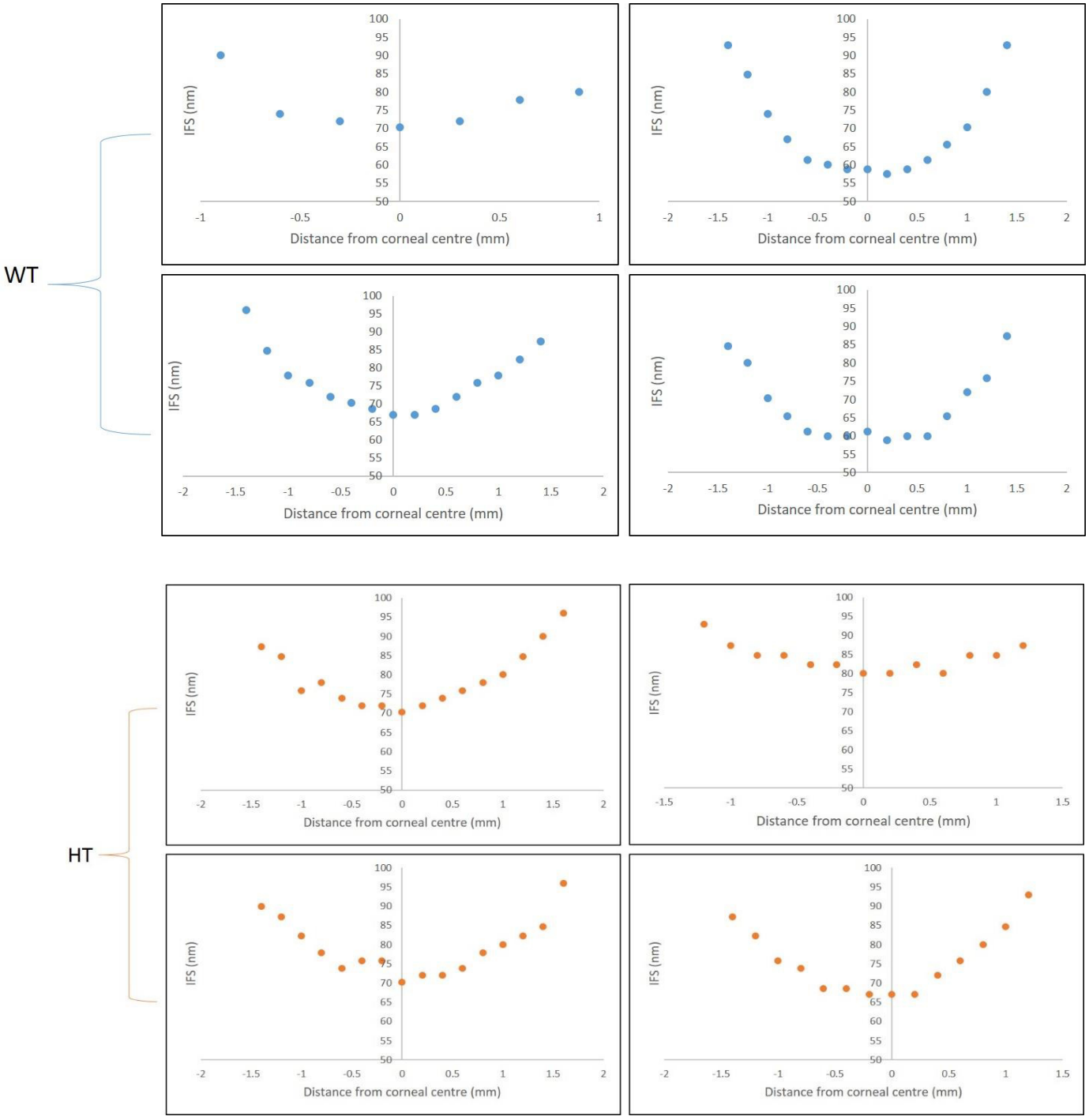


**Figure 6.12. Radial plots of IFS in WT and HT mouse cornea**. These graphs portray the centre-centre average IFS in the central and peripheral cornea of WT and HT corneas. Each plot shows a 'U' shaped distribution, with higher IFS at the periphery.

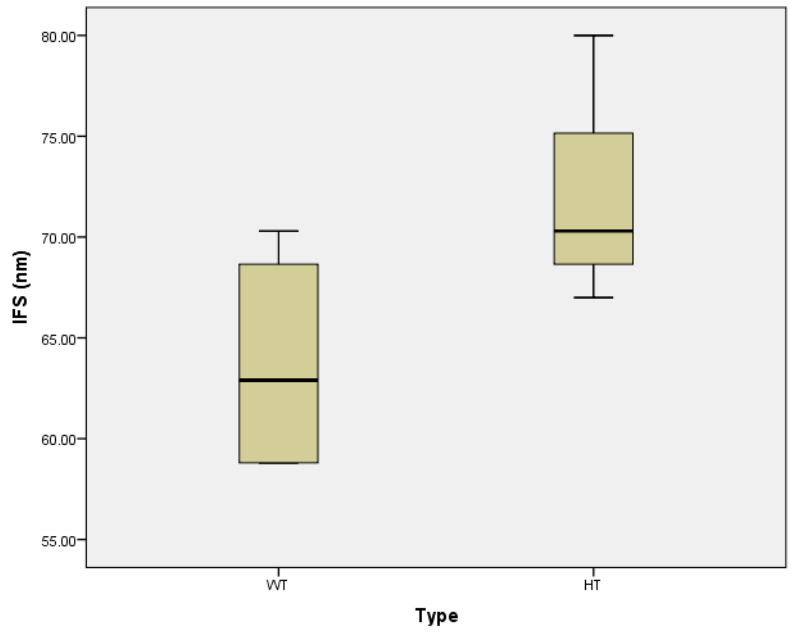


**Figure 6.13. Boxplot comparing IFS at the centre of WT and HT corneas.** The boxplot visually demonstrates how IFS was higher in the centre of HT corneas, compared to WT equivalents. The line inside each box represents the median value.

## 6.4. Discussion

This preliminary study has provided evidence that using the mg$\Delta^{loxPneo}$ mouse model for Marfan syndrome is a valuable way of studying the ocular pathogenesis of the disease and the functional role of fibrillin-1 in the cornea. Importantly, quantification of elastic fibres in knock-out corneas showed a significant reduction (~50%) in overall levels of fibrillin-1 containing elastic fibres throughout the entire thickness of the stroma in comparison to WT controls. These findings are consistent with studies from Lima *et al.* (2010), who showed that the expression of the mutant FBN1 allele is ~50% less compared to the WT allele in cultured foetal fibroblasts. Similar findings were observed in human Marfan syndrome patients, where decreased extracellular deposition of fibrillin by fibroblasts has been reported (Raghunath *et al.*, 1993, Milewicz *et al.*, 1992, Hollister *et al.*, 1990). By using SBF SEM to quantify elastic fibres, we are limited to analysing a ~30 x 30 µm area of tissue throughout the stroma, with only 1 cornea from each group being analysed due to the

technical difficulty and time consuming nature of the technique. It is likely that the elastic fibre content varies slightly between each HT cornea given the nature of the disease, where gene mutations are dominant-negative, ultimately resulting in a variable ratio of elastic fibre loss and fibre disorganisation. The issue is complicated further by the fact that fibrillin-2 microfibrils may be produced to replace the mutated fibrillin-1 proteins, as shown in mouse ciliary zonule (Beene *et al*., 2013). In comparison to human, elastic fibres are more densely populated in the mouse cornea, where they may be responsible for accommodating the increase in curvature.

Elastic fibres in the mouse cornea are highly concentrated throughout the stroma, in comparison to elastic fibres in human cornea, which are highly concentrated in the first ~10 µm of stroma immediately above Descemet's membrane (Lewis *et al.*, 2016). 3D volume rendering revealed that the elastic fibres are also similar in appearance to those in human cornea, and to those demonstrated in mouse cornea by Hanlon *et al.* (2015), running in many directions parallel to the surface of the cornea, often bifurcating. Comparisons of 3D reconstructions above Descemet's membrane indicated that elastic fibres in the HT cornea were structurally different, appearing less organised than the WT. Fibres in knock-out cornea had a meshwork-like appearance, with many connections originating from a broader region of material, whereas normal fibres travelled in relatively straight lines in a preferred direction, occasionally bifurcating. Lima *et al.* (2010) reported qualitative differences in fibres produced by cultured foetal fibroblasts between WT and mutant animals, whilst also observing the deposition of mutant protein in fibroblasts of HT animals. Furthermore, histological examination of the lens capsule in human Marfan patients revealed both qualitative and quantitative differences, with significantly less fibrillin-containing microfibrils as well as the presence of misshapen, irregular and fragmented bundles (Traboulsi et al., 2000). Similar finding have been observed in the skin of different mouse models for Marfan syndrome, where non-invasive multiphoton microscopy demonstrated elastic fibre fragmentation, disorganisation and reduction in density (Cui *et al.*, 2014), as well as in lumbosacral dura tissue using light microscopy (Jones *et al.*, 2005). Rotary shadowing electron microscopy has shown disorganization in individual fibrillin microfibrils from Marfan dermal fibroblasts (Kielty and Shuttleworth, 1994, Kielty *et al.*, 1994, Handford, 2000). This is the first study to present reduction in elastic fibre density and microfibril

disorganisation in the cornea. In Marfan syndrome, it is thought that the mutant protein that is produced has a dominant-negative effect, where it causes adverse activity on the deposition, stability or function of the protein encoded by the normal copy of the FBN1 gene (Judge and Dietz, 2005). Therefore, it is likely that the disorganized elastic fibres that are laid down in the mutant mouse cornea are either mutant protein, or their deposition has been affected as the mutant protein has attempted to assemble with normal fibrillin monomers, resulting in a structurally altered elastic system. A reduction in number and disorganisation of elastic fibres would ultimately result in a biomechanically weaker cornea, as the tissue relies more heavily on the collagen to deform reversibly under stress following the pull of extraocular muscles and changes in intraocular pressure.

The reduced number/disorganisation of fibres did not seem to have an adverse effect on overall structure of the cornea when comparing TEM micrographs of the two groups. Fibres were similar in appearance to those previously reported in mouse cornea, with some fibres seen in close association with keratocytes (data not shown), suggesting a possible mechanotransduction role in the stroma (Hanlon *et al.*, 2015). The slight reduction in mean fibre diameter in HT cornea may be caused by less individual microfibrils making up the bundles. Reviewing the literature revealed that ultrastructural changes in the cornea in Marfan eyes has received little attention, with the majority of studies being based on discovering new diagnostic techniques. One structural study using *in vivo* confocal microscopy reported no difference in epithelium or keratocyte morphology/density in Marfan corneas, with 'highly reflective interconnected lines' present between keratocoytes (Iordanidou *et al.*, 2007). The lack of publications, together with the results from this study, imply that no structural differences are present.

OCT image measurements revealed that central corneal thickness was significantly reduced in HT mice compared to normal WT, with a difference of ~30 µm in mean values. Radius of curvature was also significantly different between the two groups, with a weak negative correlation between the two variables (increase in thickness causing decrease in curvature). A significant reduction in central corneal thickness has been reported in human patients with Marfan syndrome (Sultan *et al.*, 2002, Heur *et al.*, 2008, Konradsen *et al.*, 2012). The difference in mean thickness between Marfan patients and controls was ~50 µm; taking into account the difference in human and mouse corneal thickness, it is evident that the ~30 µm

mean difference between mouse HT and WT groups is more profound compared to the human studies. A significant difference in keratometry readings has also been reported, suggesting a flattened cornea in Marfan syndrome (Drolsum *et al.*, 2015, Sultan *et al.*, 2002, Maumenee, 1982, Konradsen *et al.*, 2012). The weak negative correlation between thickness and curvature in this study may be caused by variable phenotypes often seen in Marfan syndrome, or due to the eyes being fixed in PFA, despite using a lower concentration (0.5%) of PFA than is normally used to fix tissue in an attempt to preserve topography. Increased radius of curvature and increase in axial globe length in Marfan syndrome cornea has been observed in previous studies (Maumenee, 1982, Drolsum *et al.*, 2015, Konradsen and Zetterstrom, 2013). Therefore, it seems that the elastic fibre system plays an important role in maintaining the curvature of the cornea. A reduction/malformation of elastic fibres in Marfan syndrome would result in the cornea being pulled outwards at the periphery by an expanding globe following an increase in intraocular pressure, leading to a thin and flattened cornea. However, Beene *et al.* (2016) have recently reported significant difference in corneal curvature in Marfan patients, with no significant difference in axial length, which again portrays the phenotypic variability in Marfan syndrome.

Glycosaminoglycan side chains of the protein core provide hydration and swelling pressure to tissues, enabling them to withstand compressional forces, in addition to mediating collagen diameter and interfibrillar spacing. Therefore, it was thought that differences in proteoglycan levels/distribution may contribute to the differences in cornea thickness. No differences in proteoglycans were evident throughout the stroma of WT and HT cornea. High levels of CS/DS GAG's and low levels of KS GAG's have previously been reported in mouse cornea (Scott and Bosworth, 1990), where the synthesis is thought to be influence by higher levels of oxygen in the thin mouse cornea (Scott and Haigh, 1988). Electron dense filaments passing into an elastic fibre space suggest an association between CS/DS GAG's and fibrillin. Baccaranicontri *et al.* (1990) used antipeptide antibodies to demonstrate that the CS proteoglycan decorin was localised to fibrillin-microfibrils in the skin. It has been suggested that CS containing proteoglycans associate with fibrillin and contribute to microfibril organisation, as treatment of microfibrils with chondroitinase ABC resulted in disruption of the beaded filament architecture (Kielty *et al.*, 1996). Furthermore, fibrillin-1

and MAGP-1 (another protein component of elastic microfibrils) were shown to interact with decorin in cultured foetal bovine chondrocytes (Trask *et al.*, 2000). In the rat eye, CS GAG's are associated with ciliary zonules (Chan and Choi, 1995). This is the first study to demonstrate GAG's co-locating with fibrillin in the cornea. Further work could be carried out with the use of GAG specific degrading enzymes to enable clear distinction between different GAG's e.g. KS and CD/DS. Overall, it is likely that proteoglycans play an important role in the assembly and maintenance of elastic fibres.

X-ray diffraction revealed that IFS was lowest at the central region of all specimens, increasing at the periphery, as previously observed in human corneas (Borcherding *et al.*, 1975, Boote *et al.*, 2003). IFS was on average ~8nm higher in the central region of HT corneas, an unexpected result given that these corneas were significantly thinner than the WT's. These results should be interpreted with caution, given that a slight deviation away from the central of each sample would subsequently effect IFS measurements, and that the corneas were fixed, meaning that the specific arrangement of collagen fibrils may have been altered (Quantock et al 2001), and that a low sample number were analysed. Centre-to-centre fibril spacing in the cornea is governed by several factors, mainly stromal hydration (Meek *et al*., 1991), proteoglycan composition and abundance (Chakravarti *et al*., 2000), and composition of collagen types within the fibril (Birk *et al*., 1998). Thinner corneas accompanied by higher average IFS in the centre indicates that HT samples containing reduced levels of fibrillin contain fewer lamellae compared to WT's. This has similarities to keratoconic cornea, where X-ray diffraction showed normal fibril spacings, conveying that the thin cornea in keratoconus is a result of reduced collagen levels (Fullwood *et al*., 1992). On the other hand, thin corneas are a result of lower IFS in macular corneal dystrophy (Quantock *et al*., 1990). Interestingly, earlier work by Patey *et al*. (1984) discovered a significant increase in collagen diameter and IFS in keratoconus as the disease progresses in severity, particularly in the middle and central stroma, leading to Pouliquen (1987) stating that this is the reason for stromal thinning and ectasia, since there are fewer lamellae. Therefore, findings from this current study showing increased IFS and thinner corneas in fibrillin knock-out animals are consistent with findings observed in keratoconus. As well as having a structural role, microfibrils forming elastic fibres are known to have a regulatory role in the ECM by binding cytokines (e.g. bone morphogenetic proteins (BMP's) (Sengle *et*

*al*., 2008). It may be possible that elastic fibres play a role in collagen biosynthesis, which could be negatively impacted when fibrillin-1 levels are reduced.

Overall, it is likely that elastic fibres have a multi-functional role in the cornea. The difference in corneal thickness and radius of curvature in the mouse cornea containing ~50% less fibrillin suggests that the fibres play an important role in maintaining the shape of the cornea. These findings are often reported in studies on human Marfan patients, and have previously been proposed to be due to increased dimensions of the eye globe as a whole, resulting in the cornea stretching outwards. Furthermore, true elastic fibres, as well as fibrillin-containing microfibrils are located in the sclera (Wheatley *et al.*, 1995, Marshall, 1995). This would imply a reduction in biomechanical properties in the sclera, as well in the cornea, in Marfan patients' eyes. With one of the main functions of the sclera being to maintain fixed axial dimensions in order to ensure a stable retinal image (Mcbrien and Gentle, 2003), and with quantities of elastic tissue in the sclera unknown, it is unclear whether the increased globe dimensions and subsequent flattened cornea are a result of biomechanically weaker cornea or sclera, or a combination of both. Biomechanical behaviours of Marfan syndrome corneas have recently been assessed *in vivo* using an ocular response analyser, revealing a greater maximal deformation of the Marfan cornea compared to control, indicating decreased resistance to bending (Beene *et al.*, 2016). This evidence supports the proposal of elastic fibres playing a pivotal role in providing the cornea with mechanical strength/elastic recoil, and maintaining corneal curvature.

Weak negative correlation between radius of curvature changes and the drastic changes in central corneal thickness between HT and WT mice indicates that corneal stretching alone is not responsible changes in thickness. However, with no apparent difference in lamellae organisation and proteoglycan levels between the two groups, it appears as though fibrillin-1 mutation does not affect the normal ultrastructure of the stroma other than reducing thickness. Given that IFS is higher in HT corneas, it is likely that thinning is a result of a reduced number of lamellae, as seen in keratoconus, potentially indicating that fibrillin plays a role in collagen biosynthesis. It is probable that the elastic fibres carry out functions that are not apparent from ultrastructural observation, such as cell signalling and mechanotransduction in the ECM. Fibrillin is thought to play an important role in controlling TGF-β activation and signalling in the ECM, with studies showing dysregulation of TGF-β

activity contributing to the pathogenesis of Marfan syndrome, with excessive levels of TGF-β in the matrix (Neptune *et al.*, 2003, Chaudhry *et al.*, 2007, Benke *et al.*, 2013). TGF-β is involved in many processes in the cornea, including keratocyte activation, myofibroblast transformation and proliferation, and wound healing (Tandon *et al.*, 2010). Hanlon *et al.* (2015) have stated that microfibrils are associated with arteries and lymphatic vessels, implying a mechanotransductional role whereby microfibrils detect mechanical force caused by stroma swelling that is in turn transferred to lymphatics pulling them open to facilitate tissue oedema clearance. With the conformation that elastic fibres form an extensive network in the normal human cornea (chapter 4) (Lewis et al., 2016), and that this organisation is very different in keratoconus (chapter 5), further work in needed to discover their precise role/roles in the cornea, as this is relevant for corneal biomechanics, surgery, Marfan syndrome pathogenesis, and potentially other area such as ECM homeostasis.

### 6.5. Conclusion

Central corneal thickness, radius of curvature, fibre disorganisation and increased IFS were the differences detected between HT and WT corneas. This preliminary study demonstrates that this knock-out mouse is a good model for studying elastic fibres in the cornea. Future studies should focus on testing differences in mechanical strength between the two groups. Furthermore, Pereira and colleagues also have the MgR models, where the mice produce a more severe phenotype. Studying this model would give us further insights into the functional roles of elastic fibres in the cornea. There is a clear lack of research carried out on the cornea in Marfan syndrome as it is widely believed that there are very few/no elastic fibres in the human cornea. Our published findings from the human cornea should encourage more interest in studying the tissue.

## 7. Concluding discussion

The general aim of this thesis was to examine the three-dimensional organisation of the corneal stroma using SBF SEM, focusing on pre-Descemet's layer. Previously, electron tomography, an extension of traditional TEM, has been used to examine the stroma in three-dimensions, with particular focus of collagen-proteoglycan interactions (Lewis *et al*., 2010, Parfitt *et al*., 2010). Despite the advantages of electron tomography, it is technically challenging and time consuming, requiring a lot of manual labour. SBF SEM was developed to enable more time-efficient automated serial section electron microscopy (Denk and Horstmann, 2004), allowing the collection of large sets of data through a volume of tissue that is subsequently rendered into a 3D model. This provides a much bigger picture than two-dimensional techniques, as the interactions between various stromal components can be examined, which is particularly important during development, as shown in embryonic chick cornea (Young *et al*., 2014), in addition to viewing the 3D structure of fibrous material.

Coincidentally, back in 2013, Dua and colleagues described the presence of a novel corneal layer deep in the posterior stroma, directly adjacent to Descemet's membrane, which was initially termed 'Dua's layer' (Dua *et al*., 2013). This discovery was based on a cleavage plane created by injection of air (big bubble technique) into the stroma to separate the layer from the underlying Descemet's membrane, a process that is used during DALK transplant surgery. Dua *et al* (2013) claimed that an acellular layer of stroma that varied in thickness (7-20μm) remained attached to Descemet's membrane following the separation, in which the authors described as a novel structurally distinct layer of the cornea. This caused an adverse reaction in the scientific community (McKee *et al*., 2014, Jester *et al*., 20134) as a result of the naming of the 'layer' (subsequently renamed 'pre-Descemet's layer'), and the lack of evidence to support these claims. As a result of this controversy, the aims of this project were orientated towards characterising this area of stroma, in an attempt to discover if any structural differences are present in comparison to the overlying tissue.

The first experimental chapter (3) of this thesis involved X-ray diffraction, before electron microscopy based chapters 4-6. X-ray diffraction provides quantitative data on collagen organisation in the stroma, as an average throughout the bulk of tissue in its natural state, with no prior processing required. Electron microscopy involves chemical fixation and

dehydration of the tissue before it can be visualised. The first X-ray diffraction study in chapter 3 provides further information of the effects of varying hydration on the human corneal stroma by comparing it to porcine cornea, building on previous studies (Meek *et al*., 1991, Fratzl and Daxer, 1993), as the original aim of the thesis was to examine both human and porcine stroma. Inter-species differences, as well as similarities, in the way in which water is distributed within corneas were discovered, potentially due to changes in the proteoglycan gel surrounding collagen fibrils, affecting the fixed charge density. Furthermore, this information tells us how the structure of the stroma is changed following dehydration during electron microscopy processing, which should be considered when interpreting electron micrographs.

Following on from this, the second X-ray diffraction study aimed to examine collagen organisation at each depth in the physiologically hydrated human stroma, from anterior to posterior, with detailed analysis on the pre-Descemet's layer, to discoverer if any differences are detectable in the final 30µm of stroma. Despite the technical difficulties, average centre-to-centre fibril spacing was lower in the first ~10µm of stroma, compared to the overlying ~20µm, indicating that collagen is more closely packed in the pre Descemet's layer, potentially resulting in increased biomechanical strength. Interestingly, this difference was only detected in the central cornea and could therefore explain the "type 1" and "type 2" bubbles observed by Dua and colleagues, making the stroma more difficult to separate from Descemet's membrane in the centre.

Pre-Descemet's layer of stroma was further analysed using SBF SEM in chapter 4, with human corneas processed using a tannic acid based protocol, known to stain elastic fibres as well as collagen (Simmons and Avery, 1980, Kageyama *et al*., 1985). Three-dimensional reconstructions revealed an extensive elastic fibre system concentrated in the first ~8µm of stroma adjacent to Descemet's membrane, running parallel to the surface of the cornea. TPF and orcein staining confirmed their presence in the stroma, and these fibres were discovered in human foetal cornea, proving that they are not a product of ageing or disease. Important quantitative data was provided by imaging the entire depth of the corneal stroma, from epithelium to Descemet's membrane, revealing that elastic fibres are abundant in the posterior stroma, whereas their levels are significantly reduced in the middle and anterior stroma. Furthermore, the fibres were highly concentrated immediately

above Descemet's membrane. The elastic fibre system in represented schematically in Figure 7.1. Given that these structures are known to be stiff reinforcing fibres (Sherratt *et al*., 2003) in addition to providing resiliency (Wess *et al*., 1998), this region of stroma would be biomechanically strengthened, and in combination with closer packed collagen fibrils, could be responsible for the variable cleavage plane created when air is injected. Furthermore, these bubbles required high pressure to cause them to burst (Dua *et al*., 2013), demonstrating the biomechanical strength that is likely provided by the elastic fibres.

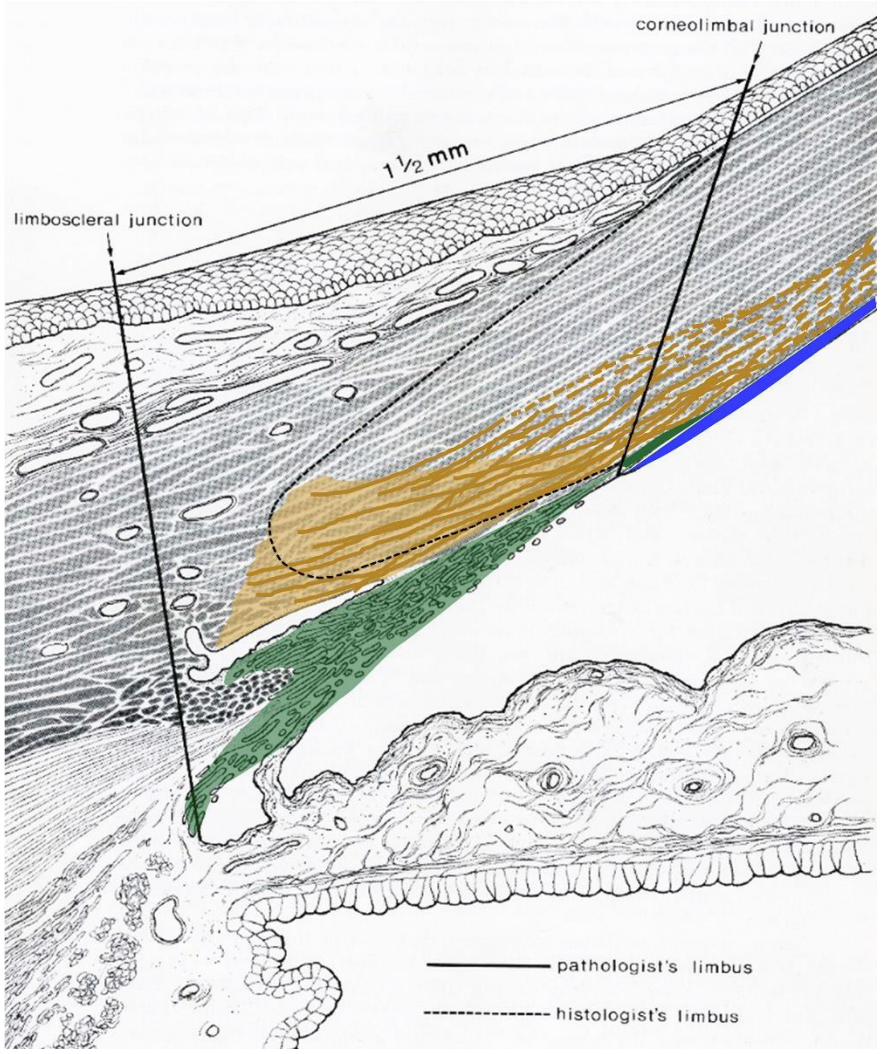


**Figure 7.1. Proposed elastic fibre organisation at the limbus.** Elastic sheets (solid gold lines) seem to originate from the limbus where they are concentrated (gold), before forming fibres in as they extend into the peripheral cornea (dashed gold lines). Green: trabecular meshwork. Blue: Descemet's membrane. Image taken from (Lewis *et al*., 2016), originally adapted from (Hogan *et al*., 1971).

These elastic fibres which lack an elastin core, provide a scaffold for elastin deposition during development in many tissues (Haust *et al*., 1965). It is likely that the elastic fibres play a similar role in the development cornea, guiding keratocytes and assisting in the deposition of collagen fibrils. Moreover, the elastic fibres are continuous with the trabecular meshwork at the limbus, where they form fenestrated sheets, indicating a potential role in trabecular outflow and glaucoma (Dua *et al*., 2015b), in addition to providing increased resiliency at the corneo-scleral interface. In terms of the pre-Descemet's layer, there is not enough evidence to deem it as a structurally distinct novel layer in the cornea, although there are intra-stromal structural variations, as seen, for example, between the anterior and posterior stroma in terms of collagen organisation. Moreover, the cleavage plane can be explained by the final ~8micons of stroma being biomechanically stronger, in combination with the variable distance of the last row of keratocytes from Descemet's membrane (Schlotzer-Schrehardt *et al*., 2015). Elastic fibres are present and uniformly distributed throughout the stroma in murine (chapter 6) and porcine (unpublished results) cornea. Given that pre-Descemet's layer is not separated from the rest of the stroma using the big bubble technique in porcine cornea (A. Mukherjee and D. O'Brart, personal communications), this suggests that the concentration of elastic fibres immediately above Descemet's membrane in human cornea contributes to the cleavage plane, whereby pre-Descemet's layer remains attached to Descemet's membrane.

Moving forward in chapters 5 and 6, the thesis focused primarily on elastic fibres in the cornea. Theories were put forward in chapter 4 regarding a potential functional role of the fibres in human cornea. Chapter 6 aimed to further elucidate the function of elastic fibres by studying eyes from a mouse model of Marfan syndrome, in which the animals have one of the alleles that produce fibrillin-1, a glycoprotein that is the primary component in the individual microfibrils in elastic fibres, knocked out. In contrast to humans, elastic fibres are present uniformly throughout the mouse corneal stroma. Full-thickness quantification analysis revealed that fibrillin-1 knock out corneas contained about 50% less elastic fibres compared to wild types and furthermore, the fibres that were laid down in the mutant stroma were disorganised. Additionally, fibrillin-1 knock out corneas were significantly thinner with a higher radius of curvature, telling us that they are flattened. This data suggests that elastic fibres play an important role in maintaining the curvature of the

cornea, in which they are continuous with the sclera, keeping the cornea taught whilst enabling slight deformation with variations in intraocular pressure and the pull of extraocular muscles. Centre-centre spacing in the thinner knock-out corneas was higher in comparison to wild types, suggesting that the reduction in stromal thickness is caused by less collagen/lamellae.

A reduction in elastic fibres subsequently affecting corneal curvature implies that the system may play some role in keratoconus, a disease where the cornea loses its precise shaped and becomes conical. Human keratoconic buttons were examined in chapter 5 in an attempt to distinguish any differences to normal healthy cornea. The concentration of elastic fibres was not present above Descemet's membrane in keratoconic cornea, although an abundance of fibres were located below the epithelium, the exact opposite of what was observed in normal cornea. These fibres are potentially being laid down in this weakened coned area to boost mechanical stability. Interestingly, collagen fibril centre-to-centre spacing in keratoconic stroma has been reported to be either the same as in normal cornea (Fullwood *et al*., 1992), or higher (Patey *et al*., 1984), yet the corneas are significantly thinner, indicating that less collagen is present. These findings link with results from chapter 6, where a similar observation was made on thin mouse corneas containing a significant reduction in elastic fibres. Given that keratoconic corneas similarly contain low levels of elastic material in the mid/posterior stroma, this data implies that the fibres potentially play a role in collagen biosynthesis, or even the inhibition of collagen degradation.

Overall, the presence of elastic material in the cornea has been largely overlooked in recent years. Results from this thesis show that the elastic system must play an important, multifunctional, role in the human cornea, with further research required to elucidate these properties. Eyes obtained from the $mg\Delta^{loxPneo}$ mouse model for Marfan syndrome has provided important insights into the role of elastic fibres in the cornea. Another mouse model exists in which mice are homozygous for the mutant allele, resulting in a more severe phenotype than the one observed in chapter 6, caused by a further reduction in elastic fibre production. Biomechanical testing should be carried out on these corneas to determine how much of an impact the lack of fibres has on the strength of the tissue. As the whole genetically modified eye is available, inflation testing could be used to examine the mechanical stiffness of corneas lacking elastic fibres compared to normal wild types.

Furthermore, due to the high elastic content in the trabecular meshwork, which plays an important role in aqueous outflow resistance, and with the continuation of these elastic fibres into the cornea, this region should be further examined in the knock-out corneas to determine if the fibres play a role in aqueous outflow. Another interesting area to explore would be the role of elastic fibres in corneal development. Further SBF SEM data collection from developing cornea could tell us how the fibres are interacting with keratocytes and collagen fibrils. It is likely that elastic fibres play some role in collagen production, where it may be a signalling mechanism, or being involved in the spatial organisation of the fibrils/lamellae.

Overall, the potential multi-functional role of the elastic fibre system in the cornea means that further research in this area could provide additionally knowledge in corneal development, biomechanics, and diseases such as keratoconus, Marfan syndrome and glaucoma, as well as having surgical implications.

# 8. References


Abahussin, M., Hayes, S., Cartwright, N. E. K., Kamma-Lorger, C. S., Khan, Y., Marshall, J. & Meek, K. M. 2009. 3D Collagen Orientation Study of the Human Cornea Using X-ray Diffraction and Femtosecond Laser Technology. *Investigative ophthalmology & visual science,* 50**,** 5159-5164.

Abass, A., Hayes, S., White, N., Sorensen, T. & Meek, K. M. 2015. Transverse depth-dependent changes in corneal collagen lamellar orientation and distribution. *Journal of the Royal Society Interface,* 12**,** 13.

Aghamohammadzadeh, H., Newton, R. H. & Meek, K. M. 2004. X-ray scattering used to map the preferred collagen orientation in the human cornea and limbus. *Structure,* 12**,** 249-256.

Akhtar, S., Bron, A. J., Salvi, S. M., Hawksworth, N. R., Tuft, S. J. & Meek, K. M. 2008. Ultrastructural analysis of collagen fibrils and proteoglycans in keratoconus. *Acta Ophthalmol,* 86**,** 764-772.

Akhtar, S., Bron, A. J., Hawksworth, N. R., Bonshek, R. E. & Meek, K. M. 2001. Ultrastructural morphology and expression of proteoglycans, beta ig-h3, tenascin-C, fibrillin-1, and fibronectin in bullous keratopathy. *British Journal of Ophthalmology,* 85**,** 720-731

Alexander, R. A., Clayton, D. C., Howes, R. C. & Garner, A. 1981a. Effect of oxidation upon demonstration of corneal oxytalan fibers - a light and electron microscopical study. *Medical Laboratory Sciences,* 38**,** 91-101.

Alexander, R. A., Grierson, I. & Garner, A. 1981b. Oxytalan fibers in fuchs endothelial dystrophy. *Archives of Ophthalmology,* 99**,** 1622-1627.

Alexander, R. A. & Garner, A. 1983. Elastic and precursor fibers in the normal human eye. *Experimental Eye Research,* 36**,** 305-315.

Alm, A. & Nilsson, S. F. E. 2009. Uveoscleral outflow - A review. *Experimental Eye Research,* 88**,** 760-768.

Al-Mahmood, A. M., Al-Swailem, S. A. & Edward, D. P. 2012. Glaucoma and Corneal Transplant Procedures. *Journal of Ophthalmology***,** 9.

Andres, B., Koethe, U., Kroeger, T., Helmstaedter, M., Briggman, K. L., Denk, W. & Hamprecht, F. A. 2012. 3D segmentation of SBFSEM images of neuropil by a graphical model over supervoxel boundaries. *Medical Image Analysis,* 16**,** 796-805.

Anwar, M. & Teichmann, K. D. 2002. Big-bubble technique to bare Descemet's membrane in anterior lamellar keratoplasty. *Journal of Cataract and Refractive Surgery,* 28**,** 398-403.

Ashworth, J. L., Kielty, C. M. & Mcleod, D. 2000. Fibrillin and the eye. *British Journal of Ophthalmology,* 84**,** 1312-1317.

Baccaranicontri, M., Vincenzi, D., Cicchetti, F., Mori, G. & Pasqualironchetti, I. 1990. Immunocytochemical localization of proteoglycans within normal elastin fibers. *European Journal of Cell Biology,* 53**,** 305-312.

Balasubramanian, S. A., Pye, D. C. & Willcox, M. D. P. 2010. Are Proteinases the Reason for Keratoconus? *Current Eye Research,* 35**,** 185-191.

Baldock, C., Gilpin, C. J., Koster, A. J., Ziese, U., Kadler, K. E., Kielty, C. M. & Holmes, D. F. 2002. Three-dimensional reconstructions of extracellular matrix polymers using automated electron tomography. *Journal of Structural Biology,* 138**,** 130-136.

Baldock, C., Koster, A. J., Ziese, U., Rock, M. J., Sherratt, M. J., Kadler, K. E., Shuttleworth, C. A. & Kielty, C. M. 2001. The supramolecular organization of fibrillin-rich microfibrils. *Journal of Cell Biology,* 152**,** 1045-1056.

Baldock, C., Siegler, V., Bax, D. V., Cain, S. A., Mellody, K. T., Marson, A., Haston, J. L., Berry, R., Wang, M. C., Grossmann, J. G., Roessle, M., Kielty, C. M. & Wess, T. J. 2006. Nanostructure of fibrillin-1 reveals compact conformation of EGF arrays and mechanism for extensibility. *Proceedings of the National Academy of Sciences of the United States of America,* 103**,** 11922-11927.

Basu, S., Hertsenberg, A. J., Funderburgh, M. L., Burrow, M. K., Mann, M. M., Du, Y. Q., Lathrop, K. L., Syed-Picard, F. N., Adams, S. M., Birk, D. E. & Funderburgh, J. L. 2014. Human limbal biopsy-derived stromal stem cells prevent corneal scarring. *Science Translational Medicine,* 6**,** 10.

Beales, M. P., Funderburgh, J. L., Jester, J. V. & Hassell, J. R. 1999. Proteoglycan synthesis by bovine keratocytes and corneal fibroblasts: Maintenance of the keratocyte phenotype in culture. *Investigative ophthalmology & visual science,* 40**,** 1658-1663.

Beecher, N., Carlson, C., Allen, B. R., Kipchumba, R., Conrad, G. W., Meek, K. M. & Quantock, A. J. 2005. An X-Ray Diffraction Study of Corneal Structure in Mimecan-Deficient Mice. *Investigative Ophthalmology & Visual Science,* 46**,** 4046-4049.

Beene, L. C., Wang, L. W., Hubmacher, D., Keene, D. R., Reinhardt, D. P., Annis, D. S., Mosher, D. F., Mecham, R. P., Traboulsi, E. I. & Apte, S. S. 2013. Nonselective assembly of fibrillin 1 and fibrillin 2 in the rodent ocular zonule and in cultured cells: implications for Marfan syndrome. *Investigative Ophthalmol & Visual Science,* 54**,** 8337-8344.

Beene, L. C., Traboulsi, E. I., Seven, I., Ford, M. R., Roy, A. S., Butler, R. S. & Dupps, W. J. 2016. Corneal Deformation Response and Ocular Geometry: A Noninvasive Diagnostic Strategy in Marfan Syndrome. *American Journal of Ophthalmology,* 161**,** 56-64.

Bell, J. S., Christmas, J., Mansfield, J. C., Everson, R. M. & Winlove, C. P. 2014. Micromechanical response of articular cartilage to tensile load measured using nonlinear microscopy. *Acta Biomaterialia,* 10**,** 2574-2581

Benedek, G. B. 1971. Theory of transparency of the eye. *Appl Opt,* 10**,** 459-473.

Benke, K., Agg, B., Szilveszter, B., Tarr, F., Nagy, Z. B., Polos, M., Daroczi, L., Merkely, B. & Szabolcs, Z. 2013. The role of transforming growth factor-beta in Marfan syndrome. *Cardiology Journal,* 20**,** 227-234.

Bergmanson, J. P. G., Horne, J., Doughty, M. J., Garcia, M. & Gondo, M. 2005. Assessment of the number of lamellae in the central region of the normal human corneal stroma at the resolution of the transmission electron microscope. *Eye & contact lens,* 31**,** 281-287.

Bettelheim, F. A. & Plessy, B. 1975. The hydration of proteoglycans of bovine cornea. *Biochim Biophys Acta,* 381**,** 203-214.

Biery, N. J., Eldadah, Z. A., Moore, C. S., Stetten, G., Spencer, F. & Dietz, H. C. 1999. Revised genomic organization of FBN1 and significance for regulated gene expression. *Genomics,* 56**,** 70-77.

Bill, A. 1975. Blood circulation and fluid dynamics in the eye. *Physiol Rev,* 55**,** 383-417.

Binder, P. S., Rock, M. E., Schmidt, K. C. & Anderson, J. A. 1991. High-voltage electron-microscopy of normal human cornea. *Investigative ophthalmology & visual science,* 32**,** 2234-2243.

Birk, D. E., Fitch, J. M., Babiarz, J. P., Doane, K. J. & Linsenmayer, T. F. 1990. Collagen fibrillogenesis in vitro – Interaction of type I and type V collagen regulates fibril diamter. *Journal of Cell Science,* 95**,** 649-657.

Birk, D. E., Fitch, J. M., Babiarz, J. P. & Linsenmayer, T. F. 1988. Collagen type I and type V are present in the same fibril in the avian corneal stroma. *Journal of Cell Biology,* 106**,** 999-1008.

Birk, D. E., Fitch, J. M. & Linsenmayer, T. F. 1986. Organization of collagen type I and type V in the embryonic chicken cornea. *Investigative ophthalmology & visual science,* 27**,** 1470-1477.

Blochberger, T. C., Vergnes, J. P., Hempel, J. & Hassell, J. R. 1992. CDNA to chick lumican (corneal keratan sulphate proteoglycan) reveals homology to the small interstitial proteoglycan gene family and expression in muscle and intestine. *Journal of Biological Chemistry,* 267**,** 347-352.

Bonanno, J. A. 2012. Molecular mechanisms underlying the corneal endothelial pump. *Experimental Eye Research,* 95**,** 2-7.

Boote, C., Dennis, S., Huang, Y. F., Quantock, A. J. & Meek, K. M. 2005. Lamellar orientation in human cornea in relation to mechanical properties. *Journal of Structural Biology,* 149**,** 1-6.

Boote, C., Dennis, S., Newton, R. H., Puri, H. & Meek, K. M. 2003. Collagen fibrils appear more closely packed in the prepupillary cornea: Optical and biomechanical implications. *Investigative ophthalmology & visual science,* 44**,** 2941-2948.

Boote, C., Hayes, S., Abahussin, M. & Meek, K. M. 2006. Mapping collagen organization in the human cornea: Left and right eyes are structurally distinct. *Investigative ophthalmology & visual science,* 47**,** 901-908.

Boote, C., Kamma-Lorger, C. S., Hayes, S., Harris, J., Burghammer, M., Hiller, J., Terrill, N. J. & Meek, K. M. 2011. Quantification of Collagen Organization in the Peripheral Human Cornea at Micron-Scale Resolution. *Biophysical Journal,* 101**,** 33-42.

Boote, C., Hayes, S., Young, R. D., Kamma-Lorger, C. S., Hocking, P. M., Elsheikh, A., Inglehearn, C. F., Ali, M. & Meek, K. M. 2009. Ultrastructural changes in the retinopathy, globe enlarged (rge) chick cornea. *Journal of Structural Biology,* 166**,** 195-204.

Borcherding, M. S., Blacik, L. J., Sittig, R. A., Bizzell, J. W., Breen, M. & Weinstein, H. G. 1975. Proteoglycans and collagen fibre organization in human corneoscleral tissue. *Experimental Eye Research,* 21**,** 59-70.

Boulesteix, T., Pena, A. M., Pages, N., Godeau, G., Sauviat, M. P., Beaurepaire, E. & Schanne-Klein, M. C. 2006. Micrometer scale ex vivo multiphoton imaging of unstained arterial wall structure. *Cytometry Part A,* 69A**,** 20-26.

Bourne, W. M. 2003. Biology of the corneal endothelium in health and disease. *Eye,* 17**,** 912-918.

Bourne, W. M., Nelson, L. R. & Hodge, D. O. 1997. Central corneal endothelial cell changes over a ten-year period. *Investigative ophthalmology & visual science,* 38**,** 779-782.

Boyce, B.L., Grazier, J.M., Jones, R.E., and Nguyen, T.D. (2008) Full-field deformation of bovine cornea under constrained inflation conditions. Biomaterials *29*, 3896-3904.

Branch, M. J., Hashmani, K., Dhillon, P., Jones, D. R. E., Dua, H. S. & Hopkinson, A. 2012. Mesenchymal Stem Cells in the Human Corneal Limbal Stroma. *Investigative ophthalmology & visual science,* 53**,** 5109-5116.

Bruns, R. R., Press, W. & Gross, J. 1987. A large-scale, orthogonal network of microfibril bundles in the corneal stroma. *Investigative ophthalmology & visual science,* 28**,** 1939-1946.

Carlson, E. C. & Waring, G. O. 1988. Ultrastructural analyses of enzyme-treated microfibrils in rabbit corneal stroma. *Investigative ophthalmology & visual science,* 29**,** 578-585.

Carlson, E. C., Liu, C. Y., Chikama, T. I., Hayashi, Y., Kao, C. W. C., Birk, D. E., Funderburgh, J. L., Jester, J. V. & Kao, W. W. Y. 2005. Keratocan, a cornea-specific keratan sulfate proteoglycan, is regulated by lumican. *Journal of Biological Chemistry,* 280**,** 25541-25547.

Carrington, S. D., Alexander, R. A. & Grierson, I. 1984. Elastic and related fibers in the normal cornea and limbus of the domestic cat. *Journal of Anatomy,* 139**,** 319-332.

Castoro, J. A., Bettelheim, A. A. & Bettelheim, F. A. 1988. Water gradients across bovine cornea. *Investigative ophthalmology & visual science,* 29**,** 963-968.

Castro-Munozledo, F. 2013. Review: Corneal epithelial stem cells, their niche and wound healing. *Molecular Vision,* 19**,** 1600-1613.

Chan, F. L. & Choi, H. L. 1995. Proteoglycans associated with the ciliary zonule of the rat eye - a histochemical and immunocytochemical study. *Histochemistry and Cell Biology,* 104**,** 369-381

Chakravarti, S., Magnuson, T., Lass, J. H., Jepsen, K. J., Lamantia, C. & Carroll, H. 1998. Lumican regulates collagen fibril assembly: Skin fragility and corneal opacity in the absence of lumican. *Journal of Cell Biology,* 141**,** 1277-1286.

Chakravarti, S., Petroll, W. M., Hassell, J. R., Jester, J. V., Lass, J. H., Paul, J. & Birk, D. E. 2000. Corneal opacity in lumican-null mice: Defects in collagen fibril structure and packing in the posterior stroma. *Investigative ophthalmology & visual science,* 41**,** 3365-3373.

Chapman, J. A. 1961. Morphological and chemical studies of collagen formation: I. The Fine Structure of Guinea Pig Granulomata. *The Journal of Biophysical and Biochemical Cytology,* 9**,** 639-651.

Charbonneau, N. L., Dzamba, B. J., Ono, R. N., Keene, D. R., Corson, G. M., Reinhardt, D. P. & Sakai, L. Y. 2003. Fibrillins can co-assemble in fibrils, but fibrillin fibril composition displays cell-specific differences. *Journal of Biological Chemistry,* 278**,** 2740-2749.

Chaudhry, S. S., Cain, S. A., Morgan, A., Dallas, S. L., Shuttleworth, C. A. & Kielty, C. M. 2007. Fibrillin-1 regulates the bioavailability of TGF beta 1. *Journal of Cell Biology,* 176**,** 355-367.

Cheng, X. & Pinsky, P. M. 2013. Mechanisms of self-organization for the collagen fibril lattice in the human cornea. *J R Soc Interface,* 10**,** 20130512.

Corpuz, L. M., Funderburgh, J. L., Funderburgh, M. L., Bottomley, G. S., Prakash, S. & Conrad, G. W. 1996. Molecular cloning and tissue distribution of keratocan - Bovine corneal keratan sulfate proteoglycan 37A. *Journal of Biological Chemistry,* 271**,** 9759-9763.

Corson, G. M., Chalberg, S. C., Dietz, H. C., Charbonneau, N. L. & Sakai, L. Y. 1993. Fibrillin binds calcium and is coded by cdnas that reveal a multidomain structure and alternatively spliced exons at the 5' end. *Genomics,* 17**,** 476-484.

Cottapereira, G., Rodrigo, F. G. & Bittencourtsampaio, S. 1976. Oxytalan, elaunin, and elastic fibers in human skin. *Journal of Investigative Dermatology,* 66**,** 143-148.

Cui, J. Z., Tehrani, A. Y., Jett, K. A., Bernatchez, P., Van Breemen, C. & Esfandiarei, M. 2014. Quantification of aortic and cutaneous elastin and collagen morphology in Marfan syndrome by multiphoton microscopy. *Journal of Structural Biology,* 187**,** 242-253.

Dada, T., Aggarwal, A., Minudath, K. B., Vanathi, M., Choudhary, S., Gupta, V., Sihota, R. & Panda, A. 2008. Post-penetrating keratoplasty glaucoma. *Indian Journal of Ophthalmology,* 56**,** 269-277.

Daga Gordini, D., Castellani, I., Volpin, D. & Bressan, G. M. 1990. Ultrastructural immuno-localization of tropoelastin in the chick eye. *Cell and tissue research,* 260**,** 137-146.

Davison, P. F., Hong, B. S. & Cannon, D. J. 1979. Quantitative-analysis of the collagens in the bovine cornea. *Experimental Eye Research,* 29**,** 97-107.

Daxer, A. & Fratzl, P. 1997. Collagen fibril orientation in the human corneal stroma and its implication in keratoconus. *Investigative ophthalmology & visual science,* 38**,** 121-129.

Daxer, A., Misof, K., Grabner, B., Ettl, A. & Fratzl, P. 1998. Collagen fibrils in the human corneal stroma: Structure and aging. *Investigative ophthalmology & visual science,* 39**,** 644-648.

Delmonte, D. W. & Kim, T. 2011. Anatomy and physiology of the cornea. *Journal of Cataract and Refractive Surgery,* 37**,** 588-598.

Denk, W. & Horstmann, H. 2004. Serial block-face scanning electron microscopy to reconstruct three-dimensional tissue nanostructure. *Plos Biology,* 2**,** 1900-1909.

Dietz, H. C., Cutting, G. R., Pyeritz, R. E., Maslen, C. L., Sakai, L. Y., Corson, G. M., Puffenberger, E. G., Hamosh, A., Nanthakumar, E. J., Curristin, S. M., Stetten, G., Meyers, D. A. & Francomano, C. A. 1991. Marfan-syndrome caused by a recurrent denovo missense mutation in the fibrillin gene. *Nature,* 352**,** 337-339.

Drolsum, L., Rand-Hendriksen, S., Paus, B., Geiran, O. R. & Semb, S. O. 2015. Ocular findings in 87 adults with Ghent-1 verified Marfan syndrome. *Acta Ophthalmologica,* 93**,** 46-53.

Dudakova, L., Liskova, P., Trojek, T., Palos, M., Kalasova, S. & Jirsova, K. 2012. Changes in lysyl oxidase (LOX) distribution and its decreased activity in keratoconus corneas. *Experimental Eye Research,* 104**,** 74-81.

Du, Y. D., Funderburgh, M. L., Sundarraj, N. & Funderburgh, J. L. 2005. Multipotent stem cells in human corneal stroma. *Stem Cells,* 23**,** 1266-1275.

Du, Y. Q., Carlson, E. C., Funderburgh, M. L., Birk, D. E., Pearlman, E., Guo, N. X., Kao, W. W. Y. & Funderburgh, J. L. 2009. Stem Cell Therapy Restores Transparency to Defective Murine Corneas. *Stem Cells,* 27**,** 1635-1642.

Dua, H. S., Faraj, L. A., Branch, M. J., Yeung, A. M., Elalfy, M. S., Said, D. G., Gray, T. & Lowe, J. 2014. The collagen matrix of the human trabecular meshwork is an extension of the novel pre-Descemet's layer (Dua's layer). *British Journal of Ophthalmology,* 98**,** 691-697.

Dua, H. S., Faraj, L. A., Said, D. G., Gray, T. & Lowe, J. 2013. Human Corneal Anatomy Redefined A Novel Pre-Descemet's Layer (Dua's Layer). *Ophthalmology,* 120**,** 1778-1785.

Dua, H. S., Mastropasqua, L., Faraj, L., Nubile, M., Elalfy, M. S., Lanzini, M., Calienno, R. & Said, D. G. 2015a. Big bubble deep anterior lamellar keratoplasty: the collagen layer in the wall of the big bubble is unique. *Acta Ophthalmologica,* 93**,** 427-430.

Dua, H. S., Faraj, L. A. & Said, D. G. 2015b. Dua's layer: discovery, characteristics, clinical applications, controversy and potential relevance to glaucoma. *Expert Review of Ophthalmology,* 10**,** 531-547.

Dua, H. S., Shanmuganathan, V. A., Powell-Richards, A. O., Tighe, P. J. & Joseph, A. 2005. Limbal epithelial crypts: a novel anatomical structure and a putative limbal stem cell niche. *British Journal of Ophthalmology,* 89**,** 529-532

Duane, T. D., Jaeger, E. A. & Tasman, W. 1998. *Duane's Foundations of Clinical Ophthalmology*, Lippincott Williams & Wilkins.

Ehlers, N., Heegaard, S., Hjortdal, J., Ivarsen, A., Nielsen, K. & Prause, J. U. 2010. Morphological evaluation of normal human corneal epithelium. *Acta Ophthalmologica,* 88**,** 858-861.

Elliott, G. F. & Hodson, S. A. 1998. Cornea, and the swelling of polyelectrolyte gels of biological interest. *Reports on Progress in Physics,* 61**,** 1325-1365.

Elliott, G. F., Sayers, Z. & Timmins, P. A. 1982. Neutron diffraction studies of the corneal stroma. *Journal of Molecular Biology,* 155**,** 389-393.

Elsheikh, A., Whitford, C., Joda, A., Bao, F., Ibrahim, I., and Rama, P. 2013. Regional variation of biomechanical properties of intact eye globes. ARVO Abstract. *Investigative ophthalmology & visual science 54*, 1631.

Eriksen, T. A., Wright, D. M., Purslow, P. P. & Duance, V. C. 2001. Role of Ca2+ for the mechanical properties of fibrillin. *Proteins-Structure Function and Genetics,* 45**,** 90-95.

Everts, V., Niehof, A., Jansen, D. & Beertsen, W. 1998. Type VI collagen is associated with microfibrils and oxytalan fibers in the extracellular matrix of periodontium, mesenterium and periosteum. *Journal of Periodontal Research,* 33**,** 118-125.

Farjo, A., M, M. & Soong, H. K. 2008. Corneal anatomy, physiology, and wound healing. *In:* M, Y. & J.S, D. (eds.) *Opthalmology.* 3 ed. St. Louis: Mosby.

Finnis, M. L. & Gibson, M. A. 1997. Microfibril-associated glycoprotein-1 (MAGP-1) binds to the pepsin-resistant domain of the alpha 3(VI) chain of type VI collagen. *Journal of Biological Chemistry,* 272**,** 22817-22823.

Fraser, R. D. B., Macrae, T. P. & Suzuki, E. 1979. Chain conformation in the collagen molecule. *Journal of Molecular Biology,* 129**,** 463-481.

Fratzl, P. & Daxer, A. 1993. Structural transformation of collagen fibrils in corneal stroma during drying - an x-ray-scattering study. *Biophysical Journal,* 64**,** 1210-1214.

Freund, D. E., Mccally, R. L., Farrell, R. A., Cristol, S. M., Lhernault, N. L. & Edelhauser, H. F. 1995. Ultrastructure in anterior and posterior stroma of perfused human and rabbit corneas – relation to transparency. *Investigative ophthalmology & visual science,* 36**,** 1508-1523.

Fullmer, H. M. & Lillie, R. D. 1958. The oxytalan fiber - a previously undescribed connective tissue fiber. *Journal of Histochemistry & Cytochemistry,* 6**,** 425-430.

Fullwood, N. J. & Meek, K. M. 1993. A synchrotron x-ray study of the changes occurring in the corneal stroma during processing for electron-microscopy. *Journal of Microscopy-Oxford,* 169**,** 53-60.

Fullwood, N. J., Tuft, S. J., Malik, N. S., Meek, K. M., Ridgway, A. E. A. & Harrison, R. J. 1992. Synchrotron x-ray-diffraction studies of keratoconus corneal stroma. *Investigative ophthalmology & visual science,* 33**,** 1734-1741.

Funderburgh, J. L., Corpuz, L. M., Roth, M. R., Funderburgh, M. L., Tasheva, E. S. & Conrad, G. W. 1997. Mimecan, the 25-kDa corneal keratan sulfate proteoglycan, is a product of the gene producing osteoglycin. *Journal of Biological Chemistry,* 272**,** 28089-28095.

Funderburgh, J. L., Funderburgh, M. L. & Du, Y. Q. 2016. Stem Cells in the Limbal Stroma. *Ocular Surface,* 14**,** 113-120.

Funderburgh, J. L., Funderburgh, M. L., Mann, M. M., Corpuz, L. & Roth, M. R. 2001. Proteoglycan expression during transforming growth factor beta-induced keratocyte-myofibroblast transdifferentiation. *Journal of Biological Chemistry,* 276**,** 44173-44178.

Funderburgh, J. L., Mann, M. M. & Funderburgh, M. L. 2003. Keratocyte phenotype mediates proteoglycan structure - A role for fibroblasts in corneal fibrosis. *Journal of Biological Chemistry,* 278**,** 45629-45637.

Funderburgh, M. L., Du, Y. Q., Mann, M. M., Sundarraj, N. & Funderburgh, J. L. 2005. PAX6 expression identifies progenitor cells for corneal keratocytes. *Faseb Journal,* 19**,** 1371-+.

Gardner, S. J., White, N., Albon, J., Knupp, C., Kamma-Lorger, C. S. & Meek, K. M. 2015. Measuring the Refractive Index of Bovine Corneal Stromal Cells Using Quantitative Phase Imaging. *Biophysical Journal,* 109**,** 1592-1599.

Gawlik, Z. 1965. Morphological and morphochemical properties of the elastic system in the motor organ of man. *Folia Histochem Cytochem (Krakow),* 3**,** 233-251.

Gelse, K., Poschl, E. & Aigner, T. 2003. Collagens - structure, function, and biosynthesis. *Advanced Drug Delivery Reviews,* 55**,** 1531-1546.

Germundsson, J., Karanis, G., Fagerholm, P. & Lagali, N. 2013. Age-Related Thinning of Bowman's Layer in the Human Cornea In Vivo. *Investigative ophthalmology & visual science,* 54**,** 6143-6149.

Gong, H. Y., Trinkausrandall, V. & Freddo, T. F. 1989. Ultrastructural immunocytochemical localization of elastin in normal human trabecular meshwork. *Current Eye Research,* 8**,** 1071-1082.

Goodfellow, J. M., Elliott, G. F. & Woolgar, A. E. 1978. X-ray diffraction studies of the corneal stroma. *Journal of Molecular Biology,* 119**,** 237-252.

Gordon, M. K., Foley, J. W., Birk, D. E., Fitch, J. M. & Linsenmayer, T. F. 1994. Type V collagen and Bowmans membrane – quantitation of messenger-RNA in corneal epithelium and stroma. *Journal of Biological Chemistry,* 269**,** 24959-24966.

Gordon, M. K., Foley, J. W., Linsenmayer, T. F. & Fitch, J. M. 1996. Temporal expression of types XII and XIV collagen mRNA and protein during avian corneal development. *Developmental Dynamics,* 206**,** 49-58.

Gordon, M. K., Gerecke, D. R. & Olsen, B. R. 1987. Type XII collagen – distinct extracullular matrix component discovered by CDNA cloning. *Proceedings of the National Academy of Sciences of the United States of America,* 84**,** 6040-6044.

Gray, J. R., Bridges, A. B., West, R. R., Mcleish, L., Stuart, A. G., Dean, J. C. S., Porteous, M. E. M., Boxer, M. & Davies, S. J. 1998. Life expectancy in British Marfan syndrome populations. *Clinical Genetics,* 54**,** 124-128.

Green, E.M., Mansfield, J.C., Bell, J.S., and Winlove, C.P. (2014) The structure and micromechanics of elastic issue. Interface Focus 20130058. http://dx.doi.org/10.1098/rsfs.2013.0058

Greenlee, T. K., Jr., Ross, R. & Hartman, J. L. 1966. The fine structure of elastic fibers. *J Cell Biol,* 30**,** 59-71.

Gyi, T. J., Meek, K. M. & Elliott, G. F. 1988. Collagen interfibrillar distances in corneal stroma using synchrotron X-ray diffraction – a species study. *International Journal of Biological Macromolecules,* 10**,** 265-269.

Hahnel, C., Somodi, S., Weiss, D. G. & Guthoff, R. F. 2000. The keratocyte network of human cornea: A three-dimensional study using confocal laser scanning fluorescence microscopy. *Cornea,* 19**,** 185-193.

Handford, P. A. 2000. Fibrillin-1, a calcium binding protein of extracellular matrix. *Biochimica Et Biophysica Acta-Molecular Cell Research,* 1498**,** 84-90.

Hanlon, S. D., Behzad, A. R., Sakai, L. Y. & Burns, A. R. 2015. Corneal stroma microfibrils. *Experimental Eye Research,* 132**,** 198-207.

Hann, C. R. & Fautsch, M. P. 2011. The Elastin Fiber System between and Adjacent to Collector Channels in the Human Juxtacanalicular Tissue. *Investigative Ophthalmology & Visual Science,* 52**,** 45-50.

Hart, R. W. & Farrell, R. A. 1969. Light Scattering in the Cornea*. *Journal of the Optical Society of America,* 59**,** 766-774.

Hassell, J. R. & Birk, D. E. 2010. The molecular basis of corneal transparency. *Experimental Eye Research,* 91**,** 326-335.

Hassell, J. R., Newsome, D. A., Krachmer, J. H. & Rodrigues, M. M. 1980. Macular corneal dystrophy – failure to synthesize a mature keratan sulfate proteoglycan. *Proceedings of the National Academy of Sciences of the United States of America-Biological Sciences,* 77**,** 3705-3709.

Hatami-Marbini, H., Etebu, E. & Rahimi, A. 2013. Swelling Pressure and Hydration Behavior of Porcine Corneal Stroma. *Current Eye Research,* 38**,** 1124-1132.

Haust, M. D. 1965. Fine fibrils of extracellular space (microfibrils). Their structure and role in connective tissue organization. *American Journal of Pathology,* 47**,** 1113-1137.

Haust, M. D., More, R. H., Bencosme, S. A. & Balis, J. U. 1965. Elastogenesis in human aorta - an electron microscopic study. *Experimental and Molecular Pathology,* 4**,** 508-511.

Heur, M., Costin, B., Crowe, S., Grimm, R. A., Moran, R., Svensson, L. G. & Traboulsi, E. I. 2008. The value of keratometry and central corneal thickness measurements in the clinical diagnosis of Marfan syndrome. *American Journal of Ophthalmology,* 145**,** 997-1001.

Hirano, K., Kobayashi, M., Kobayashi, K., Hoshino, T. & Awaya, S. 1991. Age-related-changes of microfibrils in the cornea and trabecular meshwork of the human eye. *Japanese Journal of Ophthalmology,* 35**,** 166-174.

Hirsch, M., Prenant, G. & Renard, G. 2001. Three-dimensional supramolecular organization of the extracellular matrix in human and rabbit corneal stroma, as revealed by ultrarapid-freezing and deep-etching methods. *Experimental Eye Research,* 72**,** 123-135.

Hedbys, B. O. & Mishima, S. 1966. The thickness-hydration relationship of the cornea. *Experimental Eye Research,* 5**,** 221-228.

Ho, L. T. Y., Harris, A. M., Tanioka, H., Yagi, N., Kinoshita, S., Caterson, B., Quantock, A. J., Young, R. D. & Meek, K. M. 2014. A comparison of glycosaminoglycan distributions, keratan sulphate sulphation patterns and collagen fibril architecture from central to peripheral regions of the bovine cornea. *Matrix Biology,* 38**,** 59-68.

Hodson, S. A. 1997. Corneal stromal swelling. *Progress in Retinal and Eye Research,* 16**,** 99-116.

Hogan, M. J., Alvarado, J. A., and Weddell, J. E. 1971. *Histology of the Human eye: an Atlas and Textbook,* Philadelphia WB Saunders.

Hollister, D. W., Godfrey, M., Sakai, L. Y. & Pyeritz, R. E. 1990. Immunohistologic abnormalities of the microfibrillar-fiber system in the marfan-syndrome. *New England Journal of Medicine,* 323**,** 152-159.

Holmes, D. F., Gilpin, C. J., Baldock, C., Ziese, U., Koster, A. J. & Kadler, K. E. 2001. Corneal collagen fibril structure in three dimensions: Structural insights into fibril assembly, mechanical properties, and tissue organization. *Proceedings of the National Academy of Sciences of the United States of America,* 98**,** 7307-7312.

Holmes, D. F. & Kadler, K. E. 2005. The precision of lateral size control in the assembly of corneal collagen fibrils. *Journal of Molecular Biology,* 345**,** 773-784.

Howell, S. J. & Doane, K. J. 1998. Type VI collagen increases cell survival and prevents anti-beta(1) integrin-mediated apoptosis. *Experimental Cell Research,* 241**,** 230-241.

Huang, A. J. W. & Tseng, S. C. G. 1991. Corneal epithelial wound healing in the absence of limbal epithelium. *Investigative ophthalmology & visual science,* 32**,** 96-105.

Huang, Y. F. & Meek, K. M. 1999. Swelling studies on the cornea and sclera: The effects of pH and ionic strength. *Biophysical Journal,* 77**,** 1655-1665.

Iordanidou, V., Sultan, G., Boileau, C., Raphael, M., Baudouin, C. & Marfan Study, G. 2007. In vivo corneal confocal microscopy in Marfan syndrome. *Cornea,* 26**,** 787-792.

Jacobsen, I. E., Jensen, O. A. & Prause, J. U. 1984. Structurr and composition of Bowman membrane – study by frozen resin cracking. *Acta Ophthalmologica,* 62**,** 39-53.

Jafarinasab, M. R., Rahmati-Kamel, M., Kanavi, M. R. & Feizi, S. 2010. Dissection Plane in Deep Anterior Lamellar Keratoplasty Using the Big-Bubble Technique. *Cornea,* 29**,** 388-391.

Jefferies, L. W. & Alexander, R. A. 1995. Connective-tissue fiber production in keratoconus. *British Journal of Biomedical Science,* 52**,** 14-18.

Jensen, S. A. & Handford, P. A. 2016. New insights into the structure, assembly and biological roles of 10-12 nm connective tissue microfibrils from fibrillin-1 studies. *The Biochemical journal,* 473**,** 827-838.

Jensen, S. A., Robertson, I. B. & Handford, P. A. 2012. Dissecting the Fibrillin Microfibril: Structural Insights into Organization and Function. *Structure,* 20**,** 215-225.

Jester, J. V. 2008. Corneal crystallins and the development of cellular transparency. *Seminars in Cell & Developmental Biology,* 19**,** 82-93.

Jester, J. V., Barrylane, P. A., Cavanagh, H. D. & Petroll, W. M. 1996. Induction of alpha-smooth muscle actin expression and myofibroblast transformation in cultured corneal keratocytes. *Cornea,* 15**,** 505-516.

Jester, J. V., Moller-Pedersen, T., Huang, J. Y., Sax, C. M., Kays, W. T., Cavangh, H. D., Petroll, W. M. & Piatigorsky, J. 1999a. The cellular basis of corneal transparency: evidence for 'corneal crystallins'. *Journal of Cell Science,* 112**,** 613-622.

Jester, J. V., Murphy, C. J., Winkler, M., Bergmanson, J. P. G., Brown, D., Steinert, R. F. & Mannis, M. J. 2013. Lessons in Corneal Structure and Mechanics to Guide the Corneal Surgeon. *Ophthalmology,* 120**,** 1715-1717.

Jester, J. V., Petroll, W. M. & Cavanagh, H. D. 1999b. Corneal stromal wound healing in refractive surgery: the role of myofibroblasts. *Progress in Retinal and Eye Research,* 18**,** 311-356.

Jester, J. V., Winkler, M., Jester, B. E., Nien, C., Chai, D. & Brown, D. J. 2010. Evaluating Corneal Collagen Organization Using High-Resolution Nonlinear Optical Macroscopy. *Eye & Contact Lens-Science and Clinical Practice,* 36**,** 260-264.

Johnson, D. H., Bourne, W. M. & Campbell, J. 1982. The ultrastructure of Descemet's membrane – changes with age in normal corneas. *Archives of Ophthalmology,* 100**,** 1942-1947.

Jones, C. J. P., Sear, C. H. J. & Grant, M. E. 1980. An ultrastructural-study of fibroblasts derived from bovine ligamentum nuchae and their capacity for elastogenesis in culture. *Journal of Pathology,* 131**,** 35-53.

Jones, K. B., Myers, L., Judge, D. P., Kirby, P. A., Dietz, H. C. & Sponseller, P. D. 2005. Toward an understanding of dural ectasia: A light microscopy study in a murine model of Marfan syndrome. *Spine,* 30**,** 291-293.

Joyce, N. C. 2003. Proliferative capacity of the corneal endothelium. *Progress in Retinal and Eye Research,* 22**,** 359-389.

Judge, D. P. & Dietz, H. C. 2005. Marfan's syndrome. *Lancet,* 366**,** 1965-1976.

Kadler, K. E., Baldock, C., Bella, J. & Boot-Handford, R. P. 2007. Collagens at a glance. *Journal of Cell Science,* 120**,** 1955-1958.

Kadler, K. E., Holmes, D. F., Trotter, J. A. & Chapman, J. A. 1996. Collagen fibril formation. *Biochemical Journal,* 316**,** 1-11.

Kageyama, M., Takagi, M., Parmley, R. T., Toda, M., Hirayama, H. & Toda, Y. 1985. Ultrastructural visualization of elastic fibers with a tannate metal salt method. *Histochemical Journal,* 17**,** 93-103.

Kamma-Lorger, C. S., Boote, C., Hayes, S., Moger, J., Burghammer, M., Knupp, C., Quantock, A. J., Sorensen, T., Di Cola, E., White, N., Young, R. D. & Meek, K. M. 2010. Collagen and mature elastic fibre organisation as a function of depth in the human cornea and limbus. *Journal of Structural Biology,* 169**,** 424-430.

Kanai, A. & Kaufman, H. E. 1973. Electron microscopic studies of corneal stroma aging changes of collagen fibers. *Annals of Ophthalmology,* 5**,** 285-292.

Kao, W. W. Y. & Liu, C. Y. 2003. Roles of lumican and keratocan on corneal transparency. *Glycoconjugate Journal,* 19**,** 275-285.

Keene, D. R., Lunstrum, G. P., Morris, N. P., Stoddard, D. W. & Burgeson, R. E. 1991a. 2 type XII-like collagen localize to the surface of banded collagen fibrils. *Journal of Cell Biology,* 113**,** 971-978.

Keene, D. R., Maddox, B. K., Kuo, H. J., Sakai, L. Y. & Glanville, R. W. 1991b. Extraction of extendable beaded structures and their identification as fibrillin-containing extracellular-matrix microfibrils. *Journal of Histochemistry & Cytochemistry,* 39**,** 441-449

Kenney, M. C., Nesburn, A. B., Burgeson, R. E., Butkowski, R. J. & Ljubimov, A. V. 1997. Abnormalities of the extracellular matrix in keratoconus corneas. *Cornea,* 16**,** 345-351.

Kewley, M. A., Williams, G. & Steven, F. S. 1978. Studies of elastic tissue formation in developing bovine ligamentum nuchae. *Journal of Pathology,* 124**,** 95-97.

Kielty, C. M., Sherratt, M. J. & Shuttleworth, C. A. 2002. Elastic fibres. *Journal of Cell Science,* 115**,** 2817-2828.

Kielty, C. M., Baldock, C., Lee, D., Rock, M. J., Ashworth, J. L. & Shuttleworth, C. A. 2002. Fibrillin: from microfibril assembly to biomechanical function. *Philosophical Transactions of the Royal Society of London Series B-Biological Sciences,* 357**,** 207-217.

Kielty, C. M., Whittaker, S. P., Grant, M. E. & Shuttleworth, C. A. 1992. Type-VI collagen microfibrils - evidence for a structural association with hyaluronan. *Journal of Cell Biology,* 118**,** 979-990.

Kielty, C. M. & Shuttleworth, C. A. 1995. Fibrillin-containing microfibrils - structure and function in health and disease. *International Journal of Biochemistry & Cell Biology,* 27**,** 747-760.

Kielty, C. M., Phillips, J. E., Child, A. H., Pope, F. M. & Shuttleworth, C. A. 1994. Fibrillin secretion and microfibril assembly by marfan dermal fibroblasts. *Matrix Biology,* 14**,** 191-199.

Kielty, C. M. & Shuttleworth, C. A. 1994. Abnormal fibrillin assembly by dermal fibroblasts from 2 patients with marfan-syndrome. *Journal of Cell Biology,* 124**,** 997-1004.

Kielty, C. M., Whittaker, S. P. & Shuttleworth, C. A. 1996. Fibrillin: Evidence that chondroitin sulphate proteoglycans are components of microfibrils and associate with newly synthesised monomers. *Febs Letters,* 386**,** 169-173.

Kikkawa, Y. & Hirayama, K. 1970. Uneven Swelling of the Corneal Stroma. *Investigative ophthalmology & visual science,* 9**,** 735-741.

Knappe, S., Stachs, O., Zhivov, A., Hovakimyan, M. & Guthoff, R. 2011. Results of Confocal Microscopy Examinations after Collagen Cross-Linking with Riboflavin and UVA Light in Patients with Progressive Keratoconus. *Ophthalmologica,* 225**,** 95-104.

Kolliker, A. 1860. *Manual of human microscopic anatomy,* London, J.W. Parker.

Komai, Y. & Ushiki, T. 1991. The 3-dimensional organization of collagen fibrils in the human cornea and sclera. *Investigative ophthalmology & visual science,* 32**,** 2244-2258.

Konradsen, T. R., Koivula, A., Kugelberg, M. & Zetterstrom, C. 2012. Corneal curvature, pachymetry, and endothelial cell density in Marfan syndrome. *Acta Ophthalmologica,* 90**,** 375-379.

Konradsen, T. R. & Zetterstrom, C. 2013. A descriptive study of ocular characteristics in Marfan syndrome. *Acta Ophthalmologica,* 91**,** 751-755.

Kushida, H. 1966. Staining of thin sections with lead acetate. *Journal of electron microscopy,* 15**,** 93-94.

Kuo, C. L., Isogai, Z., Keene, D. R., Hazeki, N., Ono, R. N., Sengle, G., Bachinger, H. P. & Sakai, L. Y. 2007. Effects of fibrillin-1 degradation on microfibril ultrastructure. *Journal of Biological Chemistry,* 282**,** 4007-4020.

Lagali, N., Germundsson, J. & Fagerholm, P. 2009. The Role of Bowman's Layer in Corneal Regeneration after Phototherapeutic Keratectomy: A Prospective Study Using In Vivo Confocal Microscopy. *Investigative ophthalmology & visual science,* 50**,** 4192-4198.

Lee, D. & Wilson, G. 1981. Non-uniform swelling properties of the corneal stroma. *Current Eye Research,* 1**,** 457-461.

Lewis, P. N., Pinali, C., Young, R. D., Meek, K. M., Quantock, A. J. & Knupp, C. 2010. Structural Interactions between Collagen and Proteoglycans Are Elucidated by Three-Dimensional Electron Tomography of Bovine Cornea. *Structure,* 18**,** 239-245.

Lewis, P. N., White, T. L., Young, R. D., Bell, J. S., Winlove, C. P. & Meek, K. M. 2016. Three-dimensional arrangement of elastic fibers in the human corneal stroma. *Experimental Eye Research,* 146**,** 43-53.

Li, W., Vergnes, J. P., Cornuet, P. K. & Hassell, J. R. 1992. CDNA clone to chick corneal chondroitin dermatan sulfate proteoglycans reveals identity to decorin. *Archives of Biochemistry and Biophysics,* 296**,** 190-197.

Lima, B. L., Santos, E. J. C., Fernandes, G. R., Merkel, C., Mello, M. R. B., Gomes, J. P. A., Soukoyan, M., Kerkis, A., Massironi, S. M. G., Visintin, J. A. & Pereira, L. V. 2010. A New Mouse Model for Marfan Syndrome Presents Phenotypic Variability Associated with the Genetic Background and Overall Levels of Fbn1 Expression. *Plos One,* 5**,** 9.

Liu, C. Y., Birk, D. E., Hassell, J. R., Kane, B. & Kao, W. W. Y. 2003. Keratocan-deficient mice display alterations in corneal structure. *Journal of Biological Chemistry,* 278**,** 21672-21677.

Liu, X., Wang, L., Ji, J., Yao, W., Wei, W., Fan, J., Joshi, S., Li, D., and Fan, Y. 2014. A mechanical model of the cornea considering the crimping morphology of collagen fibrils. *Investigative ophthalmology & visual science. 55*, 2739-2746.

Ljubimov, A. V., Alba, S. A., Burgeson, R. E., Ninomiya, Y., Sado, Y., Sun, T. T., Nesburn, A. B., Kenney, M. C. & Maguen, E. 1998a. Extracellular matrix changes in human corneas after radial keratotomy. *Experimental Eye Research,* 67**,** 265-272.

Ljubimov, A. V., Saghizadeh, M., Spirin, K. S., Mecham, R. P., Sakai, L. Y. & Kenney, M. C. 1998b. Increased expression of fibrillin-1 in human corneas with bullous keratopathy. *Cornea,* 17**,** 309-314.

Llobet, A., Gasull, X. & Gual, A. 2003. Understanding trabecular meshwork physiology: A key to the control of intraocular pressure? *News in Physiological Sciences,* 18**,** 205-209.

Lodish H, Berk A, Zipursky SL, et al. Molecular Cell Biology. 4th edition. New York: W. H. Freeman; 2000. Section 22.3, Collagen: The Fibrous Proteins of the Matrix. Available from: http://www.ncbi.nlm.nih.gov/books/NBK21582/

Long, C. J., Roth, M. R., Tasheva, E. S., Funderburgh, M., Smit, R., Conrad, G. W. & Funderburgh, J. L. 2000. Fibroblast growth factor-2 promotes keratan sulfate proteoglycan expression by keratocytes in vitro. *Journal of Biological Chemistry,* 275**,** 13918-13923.

Low, F. N. 1962. Microfibrils - fine filamentous components of tissue space. *Anatomical Record,* 142**,** 131-134.

Lutjendrecoll, E., Futa, R. & Rohen, J. W. 1981. Ultrahistochemical studies on tangential sections of the trabecular meshwork in normal and glaucomatous eyes. *Investigative ophthalmology & visual science,* 21**,** 563-573.

Lutjendrecoll, E., Rittig, M., Rauterberg, J., Jander, R. & Mollenhauer, J. 1989. Immunomicroscopical study of type VI collagen in the trabecular meshwork of normal and glaucomatous eyes. *Experimental Eye Research,* 48**,** 139-147.

Malik, N. S., Moss, S. J., Ahmed, N., Furth, A. J., Wall, R. S. & Meek, K. M. 1992. Aging of the human corneal stroma – structural and biochemical changes. *Biochimica Et Biophysica Acta,* 1138**,** 222-228.

Malik, N. S. & Meek, K. M. 1994. The inhibition of sugar-induced structural alterations in collagen by aspirin and other compounds. *Biochem Biophys Res Commun,* 199**,** 683-686.

Mansfield, J., Yu, J., Attenburrow, D., Moger, J., Tirlapur, U., Urban, J., Cui, Z. F. & Winlove, P. 2009. The elastin network: its relationship with collagen and cells in articular cartilage as visualized by multiphoton microscopy. *Journal of Anatomy,* 215**,** 682-691.

Marchant, J. K., Hahn, R. A., Linsenmayer, T. F. & Birk, D. E. 1996. Reduction of type V collagen using a dominant-negative strategy alters the regulation of fibrillogenesis and results in the loss of corneal-specific fibril morphology. *Journal of Cell Biology,* 135**,** 1415-1426.

Marshall, G. E., Konstas, A. G. & Lee, W. R. 1991a. Immunogold fine-structural localization of extracellular-matrix components in aged human cornea - types-I-IV collagen and laminin. *Graefes Archive for Clinical and Experimental Ophthalmology,* 229**,** 157-163.

Marshall, G. E., Konstas, A. G. P. & Lee, W. R. 1991b. Immunogold ultrastructural-localization of collagens in the aged human outflow system. *Ophthalmology,* 98**,** 692-700.

Marshall, G. E. 1995. Human scleral elastic system - an immunoelectron microscopic study. *British Journal of Ophthalmology,* 79**,** 57-64.

Mathew, J. H., Goosey, J. D. & Bergmanson, J. P. 2011. Quantified histopathology of the keratoconic cornea. *Optom Vis Sci,* 88**,** 988-997.

Mathew, J. H., Goosey, J. D., Soderberg, P. G. & Bergmanson, J. P. 2015. Lamellar changes in the keratoconic cornea. *Acta Ophthalmol,* 93**,** 767-773.

Maumenee, I. H. 1981. The eye in the Marfan syndrome. *Transactions of the American Ophthalmological Society,* 79**,** 684-733.

Maumenee, I. H. 1982. The eye in the Marfan-syndrome. *Birth Defects-Original Article Series,* 18**,** 515-524.

Maurice, D. M. 1957. The structure and transparency of the cornea. *Journal of Physiology-London,* 136**,** 263-269.

Mcbrien, N. A. & Gentle, A. 2003. Role of the sclera in the development and pathological complications of myopia. *Progress in Retinal and Eye Research,* 22**,** 307-338.

Mckee, H. D., Irion, L. C. D., Carley, F. M., Brahma, A. K., Jafarinasab, M. R., Rahmati-Kamel, M., Kanavi, M. R. & Feizi, S. 2014. Re: Dua et al.: Human corneal anatomy redefined: a novel pre-Descemet layer (Dua's layer) (Ophthalmology 2013;120:1778-85). *Ophthalmology,* 121**,** E24-E25.

Mckee, H. D., Irion, L. C. D., Carley, F. M., Jhanji, V. & Brahma, A. K. 2011. Residual corneal stroma in big-bubble deep anterior lamellar keratoplasty: a histological study in eye-bank corneas. *British Journal of Ophthalmology,* 95**,** 1463-1465.

Mckee, H. D., Irion, L. C. D., Carley, F. M., Jhanji, V. & Brahma, A. K. 2012. Donor Preparation Using Pneumatic Dissection in Endothelial Keratoplasty: DMEK or DSEK? *Cornea,* 31**,** 798-800.

McPhee, T.J., Bourne, W., and Brubaker, R.F. 1984. Location of the stress-bearing layers of the cornea. Invest. *Investigative ophthalmology & visual science*. *26,* 869-872.

Meek, K. M., Blamires, T., Elliott, G. F., Gyi, T. J. & Nave, C. 1987. The organization of collagen fibrils in the human corneal stroma - a synchrotron x-ray-diffraction study. *Current Eye Research,* 6**,** 841-846.

Meek, K. M. & Boote, C. 2004. The organization of collagen in the corneal stroma. *Experimental Eye Research,* 78**,** 503-512.

Meek, K. M. & Boote, C. 2009. The use of X-ray scattering techniques to quantify the orientation and distribution of collagen in the corneal stroma. *Progress in Retinal and Eye Research,* 28**,** 369-392.

Meek, K. M., Elliott, G. F., Sayers, Z., Whitburn, S. B. & Koch, M. H. J. 1981. Interpretation of the meridional x-ray-diffraction pattern from collagen fibrils in corneal stroma. *Journal of Molecular Biology,* 149**,** 477-488.

Meek, K. M. & Fullwood, N. J. 2001. Corneal and scleral collagens - a microscopist's perspective. *Micron,* 32**,** 261-272.

Meek, K. M., Fullwood, N. J., Cooke, P. H., Elliott, G. F., Maurice, D. M., Quantock, A. J., Wall, R. S. & Worthington, C. R. 1991. Synchrotron x-ray-diffraction studies of the cornea, with implications for stromal hydration. *Biophysical Journal,* 60**,** 467-474.

Meek, K. M. & Holmes, D. F. 1983. Interpretation of the electron microscopical appearance of collagen fibrils from corneal stroma. *International Journal of Biological Macromolecules,* 5**,** 17-25.

Meek, K. M. & Knupp, C. 2015. Corneal structure and transparency. *Progress in Retinal and Eye Research,* 49**,** 1-16.

Meek, K. M. & Leonard, D. W. 1993. Ultrastructure of the corneal stroma - a comparative-study. *Biophysical Journal,* 64**,** 273-280.

Meek, K. M., Leonard, D. W., Connon, C. J., Dennis, S. & Khan, S. 2003. Transparency, swelling and scarring in the corneal stroma. *Eye,* 17**,** 927-936.

Meek, K. M. & Newton, R. H. 1999. Organization of collagen fibrils in the corneal stroma in relation to mechanical properties and surgical practice. *Journal of Refractive Surgery,* 15**,** 695-699.

Meek, K. M. & Quantock, A. J. 2001. The use of X-ray scattering techniques to determine corneal ultrastructure. *Progress in Retinal and Eye Research,* 20**,** 95-137.

Meek, K. M., Dennis, S. & Khan, S. 2003. Changes in the refractive index of the stroma and its extrafibrillar matrix when the cornea swells. *Biophysical Journal,* 85**,** 2205-2212.

Meek, K. M., Tuft, S. J., Huang, Y. F., Gill, P. S., Hayes, S., Newton, R. H. & Bron, A. J. 2005. Changes in collagen orientation and distribution in keratoconus corneas. *Investigative ophthalmology & visual science,* 46**,** 1948-1956

Michelacci, Y. M. 2003. Collagens and proteoglycans of the corneal extracellular matrix. *Brazilian Journal of Medical and Biological Research,* 36**,** 1037-1046.

Milewicz, D. M., Pyeritz, R. E., Crawford, E. S. & Byers, P. H. 1992. Marfan-syndrome - defective synthesis, secretion, and extracellular-matrix formation of fibrillin by cultured dermal fibroblasts. *Journal of Clinical Investigation,* 89**,** 79-86.

M'ilroy, J. H. 1906. On the Presence of Elastic Fibres in the Cornea. *Journal of anatomy and physiology,* 40**,** 282-291.

Moller-Pedersen, T., Hartmann, U., Moller, H. J., Ehlers, N. & Engelmann, K. 2001. Evaluation of potential organ culture media for eye banking using human donor corneas. *British Journal of Ophthalmology,* 85**,** 1075-1079.

Moller-Pedersen, T. & Moller, H. J. 1996. Viability of human corneal keratocytes during organ culture. *Acta Ophthalmologica Scandinavica,* 74**,** 449-455.

Morishige, N., Petroll, W. M., Nishida, T., Kenney, M. C. & Jester, J. V. 2006. Noninvasive corneal stromal collagen imaging using two-photon-generated second-harmonic signals. *Journal of Cataract and Refractive Surgery,* 32**,** 1784-1791.

Morishige, N., Wahlert, A. J., Kenney, M. C., Brown, D. J., Kawamoto, K., Chikama, T., Nishida, T. & Jester, J. V. 2007. Second-harmonic imaging microscopy of normal human and keratoconus cornea. *Invest Ophthalmol Vis Sci,* 48**,** 1087-1094.

Morishige, N., Takagi, Y., Chikama, T., Takahara, A. & Nishida, T. 2011. Three-Dimensional Analysis of Collagen Lamellae in the Anterior Stroma of the Human Cornea Visualized by Second Harmonic Generation Imaging Microscopy. *Investigative ophthalmology & visual science,* 52**,** 911-915.

Morishige, N., Wahlert, A. J., Kenney, M. C., Brown, D. J., Kawamoto, K., Chikama, T.-I., Nishida, T. & Jester, J. V. 2007. Second-harmonic imaging microscopy of normal human and keratoconus cornea. *Investigative ophthalmology & visual science,* 48**,** 1087-1094.

Morishige, N., Shin-Gyou-Uchi, R., Azumi, H., Ohta, H., Morita, Y., Yamada, N., Kimura, K., Takahara, A. & Sonoda, K. H. 2014. Quantitative analysis of collagen lamellae in the normal and keratoconic human cornea by second harmonic generation imaging microscopy. *Invest Ophthalmol Vis Sci,* 55**,** 8377-8385.

Morris, J. K. 1965. A formaldehyde glutaraldehyde fixative of high osmolality for use in electron microscopy. *J. cell. Biol,* 27**,** 137.

Muller, L. J., Pels, E. & Vrensen, G. 2001. The specific architecture of the anterior stroma accounts for maintenance of corneal curvature. *British Journal of Ophthalmology,* 85**,** 437-443.

Muller, L. J., Pels, L. & Vrensen, G. 1995. Novel aspects of the ultrastructural organization of human corneal keratocytes. *Investigative ophthalmology & visual science,* 36**,** 2557-2567.

Nakamura, H., Kanai, C. & Mizuhira, V. 1977. Electron stain for elastic fibers using orcein. *Journal of Histochemistry & Cytochemistry,* 25**,** 306-308.

Nakamura, M., Kimura, S., Kobayashi, M., Hirano, K., Hoshino, T. & Awaya, S. 1997. Type VI collagen bound to collagen fibrils by chondroitin/dermatan sulfate glycosaminoglycan in mouse corneal stroma. *Japanese Journal of Ophthalmology,* 41**,** 71-76.

Nakamura, M., Kobayashi, M., Hanaichi, T., Hirano, K., Kobayashi, K., Hoshino, T. & Awaya, S. 1993. Observation of 100 nm periodic fibrils in mouse corneal stroma by cryoultramicrotomy. *Journal of Electron Microscopy,* 42**,** 185-188.

Nakamura, T., Inatomi, T., Sotozono, C., Koizumi, N. & Kinoshita, S. 2016. Ocular surface reconstruction using stem cell and tissue engineering. *Progress in Retinal and Eye Research,* 51**,** 187-207.

Neptune, E. R., Frischmeyer, P. A., Arking, D. E., Myers, L., Bunton, T. E., Gayraud, B., Ramirez, F., Sakai, L. Y. & Dietz, H. C. 2003. Dysregulation of TGF-beta activation contributes to pathogenesis in Marfan syndrome. *Nature Genetics,* 33**,** 407-411.

Newsome, D. A., Gross, J. & Hassell, J. R. 1982. Human corneal stroma contains 3 distinct collagens. *Investigative ophthalmology & visual science,* 22**,** 376-381.

Newton, R. H. & Meek, K. M. 1998a. Circumcorneal annulus of collagen fibrils in the human limbus. *Investigative ophthalmology & visual science,* 39**,** 1125-1134.

Newton, R. H. & Meek, K. M. 1998b. The integration of the corneal and limbal fibrils in the human eye. *Biophysical Journal,* 75**,** 2508-2512.

Notara, M., Alatza, A., Gilfillan, J., Harris, A. R., Levis, H. J., Schrader, S., Vernon, A. & Daniels, J. T. 2010. In sickness and in health: Corneal epithelial stem cell biology, pathology and therapy. *Experimental Eye Research,* 90**,** 188-195.

Nucci, P., Brancato, R., Mets, M. B. & Shevell, S. K. 1990. Normal endothelial-cell density range in childhood. *Archives of Ophthalmology,* 108**,** 247-248.

Parfitt, G. J., Pinali, C., Young, R. D., Quantock, A. J. & Knupp, C. 2010. Three-dimensional reconstruction of collagen-proteoglycan interactions in the mouse corneal stroma by electron tomography. *Journal of Structural Biology,* 170**,** 392-397.

Park, C. Y., Lee, J. K., Kahook, M. Y., Schultz, J. S., Zhang, C. & Chuck, R. S. 2016. Revisiting Ciliary Muscle Tendons and Their Connections With the Trabecular Meshwork by Two Photon Excitation Microscopic Imaging. *Investagative Ophthalmology & Visual Science,* 57**,** 1096-1105.

Patel, S. V., Mclaren, J. W., Hodge, D. O. & Bourne, W. M. 2001. Normal human keratocyte density and corneal thickness measurement by using confocal microscopy in vivo. *Investigative ophthalmology & visual science,* 42**,** 333-339.

Patey, A., Savoldelli, M. & Pouliquen, Y. 1984. Keratoconus and normal cornea: a comparative study of the collagenous fibers of the corneal stroma by image analysis. *Cornea,* 3**,** 119-124.

Pellegrini, G., Golisano, O., Paterna, P., Lambiase, A., Bonini, S., Rama, P. & De Luca, M. 1999. Location and clonal analysis of stem cells and their differentiated progeny in the human ocular surface. *Journal of Cell Biology,* 145**,** 769-782.

Pereira, L., Andrikopoulos, K., Tian, J., Lee, S. Y., Keene, D. R., Ono, R., Reinhardt, D. P., Sakai, L. Y., Biery, N. J., Bunton, T., Dietz, H. C. & Ramirez, F. 1997. Targetting of the gene encoding fibrillin-1 recapitulates the vascular aspect of Marfan syndrome. *Nature Genetics,* 17**,** 218-222.

Pereira, L., Lee, S. Y., Gayraud, B., Andrikopoulos, K., Shapiro, S. D., Bunton, T., Biery, N. J., Dietz, H. C., Sakai, L. Y. & Ramirez, F. 1999. Pathogenetic sequence for aneurysm revealed in mice underexpressing fibrillin-l. *Proceedings of the National Academy of Sciences of the United States of America,* 96**,** 3819-3823.

Pinnamaneni, N. & Funderburgh, J. L. 2012. Concise Review: Stem Cells in the Corneal Stroma. *Stem Cells,* 30**,** 1059-1063.

Poole, C. A., Brookes, N. H. & Clover, G. M. 1993. Keratocyte networks visualized in the living cornea using vital dyes. *Journal of Cell Science,* 106**,** 685-692.

Pouliquen, Y. 1987. Doyne lecture - keratoconus. *Eye-Transactions of the Ophthalmological Societies of the United Kingdom,* 1**,** 1-14.

Putnam, E. A., Zhang, H., Ramirez, F. & Milewicz, D. M. 1995. Fibrillin-2 (fbn2) mutations result in the marfan-like disorder, congenital contractural arachnodactyly. *Nature Genetics,* 11**,** 456-458.

Quantock, A. J., Boote, C., Young, R. D., Hayes, S., Tanioka, H., Kawasaki, S., Ohta, N., Iida, T., Yagi, N., Kinoshita, S. & Meek, K. M. 2007. Small-angle fibre diffraction studies of corneal matrix structure: a depth-profiled investigation of the human eye-bank cornea. *Journal of Applied Crystallography,* 40**,** S335-S340.

Quantock, A. J., Meek, K. M. & Chakravarti, S. 2001. An X-ray diffraction investigation of corneal structure in lumican-deficient mice. *Investigative ophthalmology & visual science,* 42**,** 1750-1756.

Quantock, A. J., Winkler, M., Parfitt, G. J., Young, R. D., Brown, D. J., Boote, C. & Jester, J. V. 2015. From nano to macro: studying the hierarchical structure of the corneal extracellular matrix. *Experimental Eye Research,* 133**,** 81-99.

Quantock, A. J., Meek, K. M., Ridgway, A. E., Bron, A. J. & Thonar, E. J. 1990. Macular corneal dystrophy: reduction in both corneal thickness and collagen interfibrillar spacing. *Current Eye Research,* 9**,** 393-398.

Rada, J. A., Cornuet, P. K. & Hassell, J. R. 1993. Regulation of corneal collagen fibrillogenesis invitro by corneal proteoglycan (lumican and decorin) core proteins. *Experimental Eye Research,* 56**,** 635-648.

Radner, W. & Mallinger, R. 2002. Interlacing of collagen lamellae in the midstroma of the human cornea. *Cornea,* 21**,** 598-601.

Radner, W., Zehetmayer, M., Aufreiter, R. & Mallinger, R. 1998a. Interlacing and cross-angle distribution of collagen lamellae in the human cornea. *Cornea,* 17**,** 537-543.

Radner, W., Zehetmayer, M., Skorpik, C. & Mallinger, R. 1998b. Altered organization of collagen in the apex of keratoconus corneas. *Ophthalmic Research,* 30**,** 327-332.

Raghunath, M., Supertifurga, A., Godfrey, M. & Steinmann, B. 1993. Decreased extracellular deposition of fibrillin and decorin in neonatal marfan-syndrome fibroblasts. *Human Genetics,* 90**,** 511-515.

Reinhardt, D. P., Ono, R. N. & Sakai, L. Y. 1997. Calcium stabilizes fibrillin-1 against proteolytic degradation. *Journal of Biological Chemistry,* 272**,** 1231-1236.

Rezakhaniha, R., Fonck, E., Genoud, C. & Stergiopulos, N. 2011. Role of elastin anisotropy in structural strain energy functions of arterial tissue. *Biomechanics and Modeling in Mechanobiology,* 10**,** 599-611.

Robinson, P. N. & Godfrey, M. 2000. The molecular genetics of Marfan syndrome and related microfibrillopathies. *Journal of Medical Genetics,* 37**,** 9-25.

Ross, R. & Bornstein, P. 1969. The elastic fiber. I. The separation and partial characterization of its macromolecular components. *Journal of Cell Biology,* 40**,** 366-381.

Roten, S. V., Bhat, S. & Bhawan, J. 1996. Elastic fibers in scar tissue. *Journal of Cutaneous Pathology,* 23**,** 37-42.

Ruberti, J. W., Roy, A. S. & Roberts, C. J. 2011a. Corneal Biomechanics and Biomaterials. *In:* Yarmush, M. L., Duncan, J. S. & Gray, M. L. (eds.) *Annual Review of Biomedical Engineering, Vol 13.*

Ruberti, J. W., Roy, A. S. & Roberts, C. J. 2011b. Corneal Structure and Function. *In:* Yarmush, M. L., Duncan, J. S. & Gray, M. L. (eds.) *Annual Review of Biomedical Engineering, Vol 13.*

Rufer, F., Schroder, A. & Erb, C. 2005. White-to-white corneal diameter - Normal values in healthy humans obtained with the orbscan II topography system. *Cornea,* 24**,** 259-261.

Sabet, M. D. & Gordon, S. R. 1989. Ultrastructural immunocytochemical localization of fibronectin deposition during corneal endothelial wound repair - evidence for cytoskeletal involvement. *Biology of the Cell,* 65**,** 171-179.

Sakai, L. Y., Keene, D. R., Morris, N. P. & Burgeson, R. E. 1986a. Type VII collagen is a major structural component of anchoring fibrils. *J Cell Biol,* 103**,** 1577-1586.

Sakai, L. Y., Keene, D. R. & Engvall, E. 1986b. Fibrillin, a new 350-kd glycoprotein, is a component of extracellular microfibrils. *Journal of Cell Biology,* 103**,** 2499-2509.

Sakai, L. Y., Keene, D. R., Glanville, R. W. & Bachinger, H. P. 1991. Purification and partial characterization of fibrillin, a cysteine-rich structural component of connective-tissue microfibrils. *Journal of Biological Chemistry,* 266**,** 14763-14770.

Sayers, Z., Koch, M. H. J., Whitburn, S. B., Meek, K. M., Elliott, G. F. & Harmsen, A. 1982. Synchrotron x-ray-diffraction study of corneal stroma. *Journal of Molecular Biology,* 160**,** 593-607.

Scott, J. E. & Bosworth, T. R. 1990. A comparative biochemical and ultrastructural-study of proteoglycan collagen interactions in corneal stroma - functional and metabolic implications. *Biochemical Journal,* 270**,** 491-497.

Scott, J. E. & Haigh, M. 1985. 'Small'-proteoglycan:collagen interactions: keratan sulphate proteoglycan associates with rabbit corneal collagen fibrils at the 'a' and 'c' bands. *Biosci Rep,* 5**,** 765-774

Scott, J. E. & Haigh, M. 1988. Keratan sulfate and the ultrastructure of cornea and cartilage - a stand-in for chondroitin sulfate in conditions of oxygen lack. *Journal of Anatomy,* 158**,** 95-108.

Schermer, A., Galvin, S. & Sun, T. T. 1986. Differentiation-related expression of a major 64k corneal keratin invivo and in culture suggests limbal location of corneal epithelial stem-cells. *Journal of Cell Biology,* 103**,** 49-62.

Schlotzer-Schrehardt, U., Bachmann, B. O., Tourtas, T., Torricelli, A. a. M., Singh, A., Gonzalez, S., Mei, H., Deng, S. X., Wilson, S. E. & Kruse, F. E. 2015. Ultrastructure of the Posterior Corneal Stroma. *Ophthalmology,* 122**,** 693-699.

Schlotzer-Schrehardt, U. & Kruse, F. E. 2005. Identification and characterization of limbal stem cells. *Experimental Eye Research,* 81**,** 247-264.

Schmoll, T., Unterhuber, A., Kolbitsch, C., Le, T., Stingl, A. & Leitgeb, R. 2012. Precise Thickness Measurements of Bowman's Layer, Epithelium, and Tear Film. *Optometry and Vision Science,* 89**,** E795-E802.

Sengle, G., Charbonneau, N. L., Ono, R. N., Sasaki, T., Alvarez, J., Keene, D. R., Bachinger, H. P. & Sakai, L. Y. 2008. Targeting of bone morphogenetic protein growth factor complexes to fibrillin. *J Biol Chem,* 283**,** 13874-13888

Shanmuganathan, V. A., Foster, T., Kulkarni, B. B., Hopkinson, A., Gray, T., Powe, D. G., Lowe, J. & Dua, H. S. 2007. Morphological characteristics of the limbal epithelial crypt. *British Journal of Ophthalmology,* 91**,** 514-519.

Shaw, L. M. & Olsen, B. R. 1991. Facit collagens - diverse molecular bridges in extracellular matrices. *Trends in Biochemical Sciences,* 16**,** 191-194.

Shawky, J. H. & Davidson, L. A. 2015. Tissue mechanics and adhesion during embryo development. *Developmental Biology,* 401**,** 152-164.

Sherratt, M. J. 2009. Tissue elasticity and the ageing elastic fibre. *Age,* 31**,** 305-325.

Sherratt, M. J., Baldock, C., Haston, J. L., Holmes, D. F., Jones, C. J. P., Shuttleworth, C. A., Wess, T. J. & Kielty, C. M. 2003. Fibrillin microfibrils are stiff reinforcing fibres in compliant tissues. *Journal of Molecular Biology,* 332**,** 183-193.

Simmons, T. A. & Avery, J. K. 1980. Electron dense staining affinities of mouse oxytalan and elastic fibers. *Journal of Oral Pathology & Medicine,* 9**,** 183-188.

Smith, J. W., The transparency of the corneal stroma. 1969. *Vision Research,* 9, 393-396.

Starborg, T., Kalson, N. S., Lu, Y. H., Mironov, A., Cootes, T. F., Holmes, D. F. & Kadler, K. E. 2013. Using transmission electron microscopy and 3View to determine collagen fibril size and three-dimensional organization. *Nature Protocols,* 8**,** 1433-1448.

Sugrue, S. P., Gordon, M. K., Seyer, J., Dublet, B., Vanderrest, M. & Olsen, B. R. 1989. Immunoidentification of type-xii collagen in embryonic-tissues. *Journal of Cell Biology,* 109**,** 939-945.

Sultan, G., Baudouin, C., Auzerie, O., De Saint Jean, M., Goldschild, M., Pisella, J. P. & Marfan Study, G. 2002. Cornea in Marfan disease: Orbscan and in vivo confocal microscopy analysis. *Investigative Ophthalmology & Visual Science,* 43**,** 1757-1764.

Takaoka, A., Babar, N., Hogan, J., Kim, M., Price, M. O., Price, F. W., Trokel, S. L. & Paik, D. C. 2016. An Evaluation of Lysyl Oxidase-Derived Cross-Linking in Keratoconus by Liquid Chromatography/Mass Spectrometry. *Investigative ophthalmology & visual science,* 57**,** 126-136.

Tamm, E. R. 2009. The trabecular meshwork outflow pathways: Structural and functional aspects. *Experimental Eye Research,* 88**,** 648-655.

Tandon, A., Tovey, J. C. K., Sharma, A., Gupta, R. & Mohan, R. R. 2010. Role of Transforming Growth Factor Beta in Corneal Function, Biology and Pathology. *Current Molecular Medicine,* 10**,** 565-578.

Tao, A., Wang, J., Chen, Q., Shen, M., Lu, F., Dubovy, S. R. & Abou Shousha, M. 2011. Topographic Thickness of Bowman's Layer Determined by Ultra-High Resolution Spectral Domain-Optical Coherence Tomography. *Investigative ophthalmology & visual science,* 52**,** 3901-3907.

Teng, C. C. 1963. Electron microscope study of the pathology of keratoconus: I. *Am J Ophthalmol,* 55**,** 18-47.

Torricelli, A. a. M., Singh, V., Santhiago, M. R. & Wilson, S. E. 2013. The Corneal Epithelial Basement Membrane: Structure, Function, and Disease. *Investigative ophthalmology & visual science,* 54**,** 6390-6400.

Traboulsi, E., Whittum-Hudson, J.A., Maumenee, I.H. 2000. Microfibril abnormalities of the lens capsule in patients with Marfan syndrome and ectopia lentis. *Ophthalmic Genetics*, 21, 9-15.

Trask, B. C., Trask, T. M., Broekelmann, T. & Mechame, R. P. 2000. The microfibrillar proteins MAGP-1 and fibrillin-1 form a ternary complex with the chondroitin sulfate proteoglycan decorin. *Molecular Biology of the Cell,* 11**,** 1499-1507.

Tsai, R. J., Li, L. M. & Chen, J. K. 2000. Reconstruction of damaged corneas by transplantation of autologous limbal epithelial cells. *New England Journal of Medicine,* 343**,** 86-93.

Tsuji, T. & Sawabe, M. 1987. Elastic fibers in scar tissue - scanning and transmission electron-microscopic studies. *Journal of Cutaneous Pathology,* 14**,** 106-113.

Wachtel, E. & Maroudas, A. 1998. The effects of pH and ionic strength on intrafibrillar hydration in articular cartilage. *Biochim Biophys Acta,* 1381**,** 37-48.

Wess, T. J., Purslow, P. P. & Kielty, C. M. 1998. X-ray diffraction studies of fibrillin-rich microfibrils: Effects of tissue extension on axial and lateral packing. *Journal of Structural Biology,* 122**,** 123-127.

Wessel, H., Anderson, S., Fite, D., Halvas, E., Hempel, J. & Sundarraj, N. 1997. Type XII collagen contributes to diversities in human corneal and limbal extracellular matrices. *Investigative ophthalmology & visual science,* 38**,** 2408-2422.

West-Mays, J. A. & Dwivedi, D. J. 2006. The keratocyte: Corneal stromal cell with variable repair phenotypes. *International Journal of Biochemistry & Cell Biology,* 38**,** 1625-1631.

Wheatley, H. M., Traboulsi, E. I., Flowers, B. E., Maumenee, I. H., Azar, D., Pyeritz, R. E. & Whittumhudson, J. A. 1995. Immunohistochemical localization of fibrillin in human ocular-tissues - relevance to the marfan-syndrome. *Archives of Ophthalmology,* 113**,** 103-109.

Whitford, C., Studer, H., Boote, C., Meek, K. M. & Elsheikh, A. 2015. Biomechanical model of the human cornea: Considering shear stiffness and regional variation of collagen anisotropy and density. *Journal of the Mechanical Behavior of Biomedical Materials,* 42**,** 76-87.

Wilson, S. E., He, Y. G., Weng, J., Li, Q., Mcdowall, A. W., Vital, M. & Chwang, E. L. 1996. Epithelial injury induces keratocyte apoptosis: Hypothesized role for the interleukin-1 system in the modulation of corneal tissue organization and wound healing. *Experimental Eye Research,* 62**,** 325-337.

Wilson, S. E. & Hong, J. W. 2000. Bowman's layer structure and function - Critical or dispensable to corneal function? A hypothesis. *Cornea,* 19**,** 417-420.

Wilson, S. E., Netto, M. & Ambrosio, R. 2003. Corneal cells: Chatty in development, homeostasis, wound healing, and disease. *American Journal of Ophthalmology,* 136**,** 530-536.

Wingate, K., Bonani, W., Tan, Y., Bryant, S. J. & Tan, W. 2012. Compressive elasticity of three-dimensional nanofiber matrix directs mesenchymal stem cell differentiation to vascular cells with endothelial or smooth muscle cell markers. *Acta Biomaterialia,* 8**,** 1440-1449.

Winkler, M., Shoa, G., Xie, Y. L., Petsche, S. J., Pinsky, P. M., Juhasz, T., Brown, D. J. & Jester, J. V. 2013. Three-Dimensional Distribution of Transverse Collagen Fibers in the Anterior Human Corneal Stroma. *Investigative ophthalmology & visual science,* 54**,** 7293-7301.

Worthington, C. R. & Inouye, H. 1985. X-ray-diffraction study of the cornea. *International Journal of Biological Macromolecules,* 7**,** 2-8.

Wright, D. M., Duance, V. C., Wess, T. J., Kielty, C. M. & Purslow, P. P. 1999. The supramolecular organisation of fibrillin-rich microfibrils determines the mechanical properties of bovine zonular filaments. *Journal of Experimental Biology,* 202**,** 3011-3020.

Wu, J., Du, Y. Q., Mann, M. M., Funderburgh, J. L. & Wagner, W. R. 2014. Corneal stromal stem cells versus corneal fibroblasts in generating structurally appropriate corneal stromal tissue. *Experimental Eye Research,* 120**,** 71-81.

Wu, J., Du, Y. Q., Mann, M. M., Yang, E. Z., Funderburgh, J. L. & Wagner, W. R. 2013. Bioengineering Organized, Multilamellar Human Corneal Stromal Tissue by Growth Factor Supplementation on Highly Aligned Synthetic Substrates. *Tissue Engineering Part A,* 19**,** 2063-2075.

Yeh, A. T., Hammer-Wilson, M. J., Van Sickle, D. C., Benton, H. P., Zoumi, A., Tromberg, B. J. & Peavy, G. M. 2005. Nonlinear optical microscopy of articular cartilage. *Osteoarthritis and Cartilage,* 13**,** 345-352.

Yoshida, S., Shimmura, S., Nagoshi, N., Fukuda, K., Matsuzaki, Y., Okano, H. & Tsubota, K. 2006. Isolation of multipotent neural crest-derived stem cells from the adult mouse cornea. *Stem Cells,* 24**,** 2714-2722.

Young, R. D., Knupp, C., Pinali, C., Png, K. M., Ralphs, J. R., Bushby, A. J., Starborg, T., Kadler, K. E. & Quantock, A. J. 2014. Three-dimensional aspects of matrix assembly by cells in the developing cornea. *Proc Natl Acad Sci U S A,* 111**,** 687-692.

Zaki, A. A., Elalfy, M. S., Said, D. G. & Dua, H. S. 2015. Deep anterior lamellar keratoplasty--triple procedure: a useful clinical application of the pre-Descemet's layer (Dua's layer). *Eye (Lond),* 29**,** 323-326.

Zhang, H., Apfelroth, S. D., Hu, W., Davis, E. C., Sanguineti, C., Bonadio, J., Mecham, R. P. & Ramirez, F. 1994. Structure and expression of fibrillin-2, a novel microfibrillar component preferentially located in elastic matrices. *Journal of Cell Biology,* 124**,** 855-863.

Zhang, H., Hu, W., Ramirez, F. 1995. Developmental expression of fibrillin genes suggests heterogeneity of extracellular microfibrils. *Journal of Cell Biology*, 129, 1165-1176.

Zimmermann, D. R., Trueb, B., Winterhalter, K. H., Witmer, R. & Fischer, R. W. 1986. Type-VI collagen is a major component of the human cornea. *Febs Letters,* 197**,** 55-58.

## Appendix 1. Depth correction

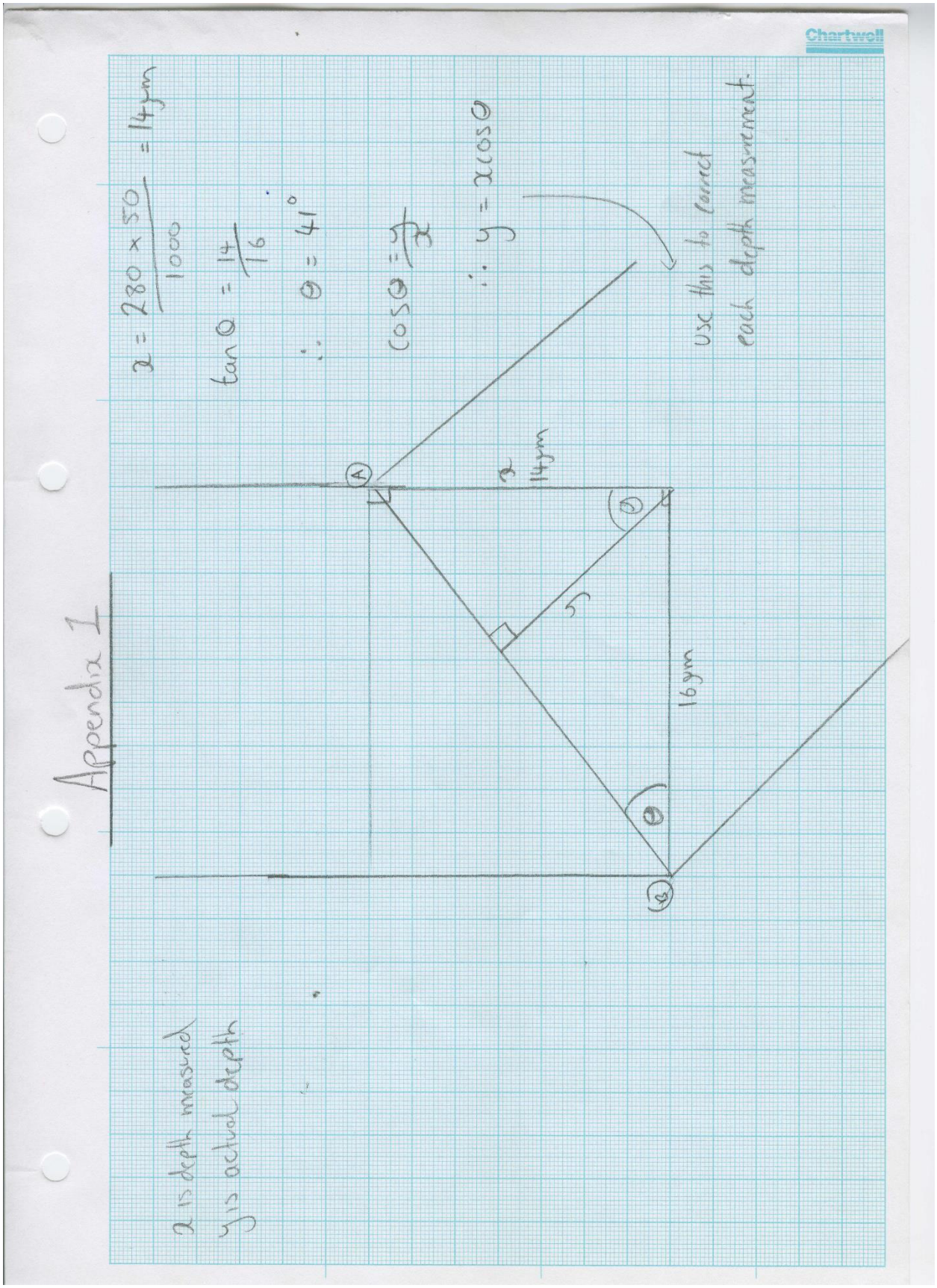

When scrolling through full-thickness data sets, it was evident that the en face sections were not being cut directly parallel to the surface of the corneal samples, meaning that depth measurements were inaccurate. To correct for this, the number of 50nm sections between where Descemet's membrane was just visible in the cornea of the image (which would be position A in the diagram), down to a depth where there stroma was just not visible (position B) was used to make a geometrical calculation of the offset angle and hence correct the depth measurements. The number of sections between positions A and B would theoretically be 1 if the block was being cut perfectly parallel to the surface.

The diagram represents the geometrical calculation used for the human data in chapter 4, with the same method being used for the mouse cornea in chapter 6. There were 280 sections between positions A and B, therefore $x = 280 \times 50/1000 = 14\mu m$. This value was used with the imaging area (16 x 16μm) to calculate θ (the offset angle). Once θ is known, the equation $y = x\cos\theta$ can be used to correct each depth measurement.